
CHARACTERIZATION OF YB-1 AS A NOVEL STRESS BIOMARKER AND PARACRINE SIGNALING POLYPEPTIDE

Andrea Maria Guarino

Dottorato in Biotecnologie – 31° ciclo

Università di Napoli Federico II



Dottorato in Biotecnologie – 31° ciclo

Università di Napoli Federico II



CHARACTERIZATION OF YB-1 AS A NOVEL STRESS BIOMARKER AND PARACRINE SIGNALING POLYPEPTIDE

Andrea Maria Guarino

Dottorando: Andrea Maria Guarino

Relatore: Prof. Viola Calabrò

Coordinatore: Prof. Giovanni Sannia

A mio padre, il primo eroe.

A mia madre, che è me.

A mia sorella, il guerriero della luce.

A te, che sei magma,

*And in the winter cold with open eyes, you will find the strength to fight
and stay upright.*

Gojira – Born in Winter,

INDEX

RIASSUNTO	1
ABSTRACT	8
CHAPTER I	9
1. Cell signalling and biotechnological applications	9
2. Protein secretion	10
3. YB-1 protein	11
3.1 Structure and functions	11
3.2 YB-1 as Stress Granules (SGs) nucleator	13
3.3 YB-1 secretion	13
4. Aim of the work	14
CHAPTER II	15
1. HEK293T cell line characterization	15
1.1 HEK293T response to stress	16
1.2 YB-1 secretion under stress stimuli	19
1.3 TCA precipitation	21
2. HEK293T YB-1-GFP stable clone	23
2.1 Lack of functionality of the clone (paper 1)	24
3. Conclusions	26
CHAPTER III	27
1. Extracellular YB-1 (exYB-1)	27
1.1 Production of human recombinant YB-1 (rYB-1) in bacterial host	27
1.2 Production of Culture Medium derived YB-1 (CCM-YB-1)	29
1.3 Mass Spectrometry analysis	30
2. Functional analysis of exYB-1	31
2.1 Extracellular YB-1 exerts anti-proliferative effects on receiving cell (paper 2)	31
2.2 Extracellular YB-1 induces TNF α	33
3. Conclusions	35
CHAPTER IV	36
1. <i>D. Rerio</i> as good model for <i>in vivo</i> studies	36
1.2 YB-1 positive aggregates in PAC2 cells	36
1.3 Heat Shock induced YB-1 aggregates represent <i>bona fide</i> SGs	42
1.4 Differential response to ROS	44
1.5 YB-1 positive aggregates in adult caudal fins (manuscript 1)	47
2. Conclusions and biotechnological implications	49
CHAPTER V	50
Collaborations	
1. Exploring molecular cell response to oxidative stress	50
1.1 Plant extracts are an important source of bioactive compounds for many drug discovery programs (papers 3,4)	50
1.2 Protective and therapeutic effects of <i>Bacillus megaterium</i> spores on gut oxidative stress (manuscript 2)	51

2. Study on <i>D. Rerio</i> and <i>P. Andruzzii</i>	51
2.1 The tumor-associated YB-1 protein: new player in the circadian control of cell proliferation (paper 5)	51
2.2 Modulation of DNA Repair Systems in Blind Cavefish during Evolution in Constant Darkness (paper 6)	51
3. A novel approach to quantify Wound Healing closure dynamic (paper 7)	52

CONCLUDING REMARKS	53
REFERENCES	55

APPENDIX I – Materials and Methods	59
APPENDIX II – Supplementary material	67
APPENDIX III – Publications and communications	78
APPENDIX IV – Experience in foreign laboratory	183

RIASSUNTO

Segnalazione cellulare

È noto che tutte le cellule ricevono ed emettono segnali di differente natura. Dalla più semplice cellula procariotica fino ai più complessi organismi pluricellulari, dove i meccanismi di segnalazione raggiungono l'apice della complessità.

La segnalazione cellulare è parte integrante dei processi di comunicazione che governano le attività basali delle cellule. Si tratta di meccanismi interconnessi, straordinariamente complessi, che sono oggetto di attiva ricerca da parte del mondo scientifico.

Le cellule eucariotiche, utilizzando svariati meccanismi, sono in grado di trasferire informazioni alle cellule ed all'ambiente circostante, sotto forma di segnali biochimici o meccanici. Tali segnali influenzano il comportamento delle cellule circostanti e per questo si prestano a svariate applicazioni biotecnologiche. Pertanto, l'analisi degli effetti di questi segnali in condizioni fisiologiche o in risposta a precisi stimoli è basilare ai fini della determinazione dei possibili settori di applicazione delle "molecole segnale" individuate.

Secrezione convenzionale e non convenzionale

Il rilascio di sostanze nell'ambiente extracellulare risponde alla necessità di gestire diversi processi biologici come la crescita cellulare, il differenziamento, la neurotrasmissione, i processi infiammatori e le infezioni.

Tutte le cellule eucariotiche dispongono di sistemi di secrezione costitutiva, mentre solo alcuni tipi specializzati di cellule, come neuroni, cellule epiteliali e cellule endocrine, in aggiunta alla secrezione costitutiva hanno sistemi regolati che dipendono da precisi stimoli extracellulari. Entrambi i processi rientrano nella "Secrezione Proteica Convenzionale", nota anche come via classica o canonica di secrezione. La Secrezione Proteica Convenzionale riguarda proteine che hanno una sequenza segnale che ne causa l'indirizzamento dal sito di traduzione al Reticolo Endoplasmatico (RE); da qui il rilascio tramite vescicole rivestite dalla proteina COPII che consente il raggiungimento del Golgi ed in seguito la membrana plasmatica. Molte molecole, utilizzano meccanismi indipendenti dal RE e dal Golgi e rientrano nella Secrezione Proteica definita "Non Convenzionale". Si tratta di proteine che non dispongono della sequenza segnale per l'indirizzamento al Reticolo Endoplasmatico e che tramite tre differenti sistemi attraversano la membrana plasmatica per essere rilasciate nello spazio extracellulare. Tra i sistemi non canonici si distinguono: Tipo 1 o translocazione mediata da pori, in cui il cargo attraversa la membrana plasmatica a seguito della formazione di pori; Tipo 2 o sistema basato su cassette ABC, specifico per la secrezione di proteine acetilate; Tipo 3 sistema basato su autofagosoma/endosoma.

Interessante notare che alcune proteine, pur disponendo di una sequenza segnale di indirizzamento al RE, eludono i sistemi di secrezione convenzionale, dando luogo ad una seconda tipologia di secrezione non convenzionale che non utilizza, di fatto, i tre sistemi precedentemente descritti.

In linea generale questa tipologia di secrezione è innescata dallo stress cellulare. Sostanze come FGF-1 (Fattore di crescita dei Fibroblasti), LPS (lipopolisaccaride) o stress meccanici, inducono il rilascio di citochine e altre molecole come risposta cellulare, da intendersi come segnalazione a beneficio delle cellule che si trovano nell'ambiente circostante.

YB-1 come nuovo player

YB-1, acronimo di *Y box binding protein 1*, è una proteina pleiotropica, coinvolta in numerosi processi cellulari come proliferazione, apoptosi e risposta allo stress. Grazie alla dinamicità della sua struttura tridimensionale in grado di modificarsi adattandosi ai differenti *partner* cellulari, YB-1 svolge funzioni differenti a seconda delle specifiche condizioni e del distretto cellulare in cui si trova. La proteina *full length* del peso di 45-50 kDa è prevalentemente citoplasmatica, mentre la forma proteolizzata da 37 kDa, è nucleare. La forma citoplasmatica interagisce con RNA di diversa tipologia, in modo particolare con gli RNA messaggeri, gestendone il destino sia in condizioni fisiologiche, sia in condizione di stress cellulare. YB-1, infatti, in condizioni fisiologiche è in parte localizzata in particelle ribonucleoproteiche (mRNPs), polisomi o nei corpi-P, deputata al controllo traduzionale degli mRNA 5'-cap dipendente ed indipendente. In condizioni di stress, YB-1, insieme ad altre proteine, sequestra gli RNA messaggeri nei Granuli da Stress, foci citoplasmatici composti da RNA e proteine che gestiscono la traduzione degli mRNA evitando che la cellula sprechi energie ed ottimizzando la risposta cellulare al particolare tipo di stress.

In caso di danno al DNA, YB-1 trasloca nel nucleo dove partecipa ai meccanismi di riparazione del DNA.

Recentemente la proteina è stata ritrovata nei fluidi corporei umani di pazienti affetti da tumore, processi infiammatori e sepsi. Sebbene il ruolo della forma secreta di YB-1 come biomarcatore tumorale sia sempre più accreditato, il ruolo della sua forma extracellulare è pressoché ignoto. È stato dimostrato che la proteina è secreta da cellule eucariotiche in coltura sia in condizioni fisiologiche sia in seguito al trattamento con LPS (lipopolisaccaride) o stimoli pro-infiammatori. Evidenze sperimentali mostrano che la proteina è secreta con meccanismo non convenzionale; ossia, YB-1 viene prima poli-ubiquitinata dalla ubiquitin ligasi HACE1, tale modifica consente l'interazione tra YB-1 e la proteina TSG101, componente del Corpi Multivescicolari, che si traduce nella secrezione della proteina.

Le proteine secrete si prestano a molte applicazioni biotecnologiche per la loro capacità di modulare la risposta cellulare. I sistemi batterici, al pari di alcuni lieviti, sono ampiamente applicati come piattaforme di produzione di proteine secrete. Un esempio è costituito dai cosiddetti *Protein Transduction Domains* (PTD) o *Cell Penetrating Peptides* (CPP), corte sequenze di aminoacidi derivanti da proteine secrete che vengono opportunamente ingegnerizzate e prodotte in batteri per poi essere aggiunte a macromolecole impiegate dal punto di vista farmaceutico e clinico. Tuttavia, esistono ad oggi molti peptidi di interesse farmacologico che non vengono espressi correttamente in procarioti; di qui, il crescente interesse dell'industria biotecnologica nell'impiego della secrezione di molecole solubili nelle cellule eucariotiche. Ciò premesso è importante, effettuare analisi comparative fra la proteina ricombinante prodotta in batteri e quella secreta dalle cellule eucariotiche per evidenziarne le similitudini strutturali e le eventuali differenze funzionali.

Nel presente progetto di dottorato ho condotto uno studio sulla proteina YB-1 secreta in condizioni fisiologiche ed in risposta allo stress, con l'intento di caratterizzarne le proprietà per potenziali applicazioni biotecnologiche nel settore farmaceutico e cosmeceutico e validarne l'utilizzo come biomarcatore associato allo stress cellulare.

Analisi preliminari sulla secrezione

1. YB-1 nella linea cellulare HEK293T in condizioni fisiologiche ed in condizioni di stress

La gran parte degli studi sulla secrezione della proteina YB-1 è stata condotta in HEK293T, una linea cellulare embrionale umana derivante da rene. Questa linea è considerata un ottimo modello cellulare per studiare la secrezione perché in grado di secernere attivamente proteine in risposta a stimoli esterni.

Il primo passo è stato analizzare il comportamento della proteina in condizioni fisiologiche; la proteina è principalmente diffusa nel citoplasma dove, come già suggerito dalla letteratura, esplica il suo ruolo principale di gestione degli RNA messaggeri (mRNA); si localizza, infatti, anche all'interno dei corpi-P, sede in cui si verifica il *sorting* degli mRNA.

Mediante tecniche di immunofluorescenza e microscopia confocale ho verificato l'assemblaggio di YB-1 nei granuli da stress, insieme ad altri marcatori canonici dei granuli come PABP-1, G3BP1, TIA1 e TIAR, a seguito di trattamento con sostanze chimiche in grado di indurre stress ossidativo, come sodio arsenite (Na Ars) o perossido di idrogeno (H₂O₂). Esperimenti di co-immunoprecipitazione hanno rivelato che l'interazione fisica fra YB-1 e PABP1, è evidente solo in presenza di stress ossidativo. Inoltre, esperimenti di silenziamento dell'mRNA di YB-1 (siRNA) hanno mostrato che la formazione di granuli da stress PABP1 positivi è compromessa da una sostanziale riduzione (almeno 50%) dei livelli intracellulari della proteina YB-1.

Simultaneamente alla formazione dei granuli da stress, ho osservato però la diminuzione della quantità totale della proteina ed in particolare della componente citoplasmatica mediante *western blot* e relative analisi densitometriche.

L'ipotesi di lavoro da me formulata era che la diminuzione della componente citoplasmatica della proteina fosse associata alla sua secrezione da parte della cellula, in risposta allo stress. Pertanto, ho estratto con acido tricloroacetico (TCA) al 25% le proteine dal mezzo di coltura delle HEK293T in condizioni normali o dopo stress ossidativo.

Analisi mediante SDS-PAGE ed *immunoblot* mi hanno permesso di concludere che la secrezione di YB-1, che si verifica anche in condizioni fisiologiche, incrementa significativamente in seguito a stress ossidativo.

Le bande elettroforetiche dell'estratto in TCA, immunoreattive all'anticorpo diretto contro YB-1, sono state escisse manualmente, processate e sottoposte ad analisi per Spettrometria di Massa per verificarne l'identità. Anticorpi diretti contro le proteine citoplasmatiche GAPDH e RHN1, sono stati utilizzati per dimostrare che il rilascio di YB-1 fosse specifico e non ascrivibile a danno cellulare. Le due proteine, infatti, sono espresse in quantità paragonabili a quelle di YB-1 nel citoplasma e non sono secrete nel mezzo di coltura sia in condizioni normali sia in seguito a stress ossidativo. Le analisi di spettrometria di massa, hanno rivelato la presenza di peptidi che coprono l'intera sequenza della proteina, alcuni di questi con modifiche post-traduzionali, tra cui l'acetilazione, in accordo con quanto riportato in letteratura e cioè che YB-1 subisce modifiche post-traduzionali per poter essere indirizzata ai sistemi di secrezione.

Questa parte del progetto è stata condotta in collaborazione con il gruppo della Prof.ssa Angela Amoresano dell'Università degli Studi di Napoli *Federico II*.

La secrezione della proteina in condizioni fisiologiche, ma anche e soprattutto in risposta a stress cellulare, pone l'interrogativo sulle funzioni svolte dalla proteina una

volta secreta nel mezzo extracellulare.

2. Produzione di un clone stabile per seguire la secrezione e l'acquisizione della proteina

Per investigare sulle funzioni della proteina secreta si è proceduto alla creazione di una linea cellulare che esprimesse stabilmente la proteina di fusione YB-1-GFP. Una volta caratterizzata, la linea cellulare stabile avrebbe potuto rappresentare un utile sensore di stress cellulare, *in vitro*.

L'impiego di linee cellulari di mammifero che esprimono stabilmente un prodotto genico (cloni stabili), costituiscono una risorsa permanente e riutilizzabile, che consente di superare alcune problematiche della espressione transitoria di prodotti genici esogeni come l'omogeneità dei livelli di espressione intracellulare e la necessità di dover ritrasfettare le cellule ad ogni esperimento.

La produzione di linee stabili prevede la selezione con antibiotico delle cellule che esprimono il plasmide con il gene. Nel mio caso la linea cellulare HEK293T trasfettata in transiente mediante lipofezione con il plasmide pcDNA6/V5-HisA-YB-1-GFP è stata selezionata con blasticidina.

L'intera procedura è stata anche eseguita per un clone controllo esprime in maniera stabile la sola GFP. I livelli di espressione della YB-1 endogena e esogena sono stati analizzati mediante SDS-PAGE. La proteina di fusione è espressa ad elevati livelli nel clone stabile e non influenza i livelli di espressione della proteina endogena. Attraverso microscopia a fluorescenza in *time lapse* ho eseguito esperimenti per monitorare, sfruttando il segnale della GFP, la secrezione della proteina e l'acquisizione della stessa da parte di cellule HaCaT, che non secernono YB-1 né in condizioni fisiologiche né in condizioni di stress. Dati preliminari suggerivano un accumulo della proteina YB-1 taggata sulla membrana esterna delle cellule riceventi. L'ulteriore caratterizzazione delle proprietà del clone stabile ha però messo in evidenza un comportamento anomalo del clone in risposta a stimoli di stress. I granuli assemblati dalla YB-1-GFP avevano morfologia e dimensioni alterate somigliando ad autofagosomi piuttosto che a granuli da stress. Inoltre, il clone presentava un considerevole aumento della mortalità cellulare in risposta allo stress ossidativo che facilitava il rilascio passivo della proteina nel mezzo. Si è deciso quindi di abbandonare l'utilizzo di questo clone stabile. Ulteriori tentativi sono stati eseguiti con altri costrutti aventi tag di più piccole dimensioni come YB-1-myc, che si è rivelato essere promettente dal punto di vista applicativo.

Produzione di YB-1 extracellulare (exYB-1)

Confermata la secrezione specifica della proteina YB-1, l'attenzione è stata focalizzata sulla sua potenziale funzione di segnalazione paracrina in risposta allo stress ossidativo. Per poter analizzare a fondo questi fenomeni si è proceduto alla produzione e purificazione di due forme della proteina YB-1: (1) YB-1 ricombinante (rYB-1) prodotta in batteri e (2) YB-1 dal mezzo di coltura delle cellule HEK293T (CCM-YB-1). L'attività delle due forme è stata confrontata mediante diversi saggi funzionali. Entrambe le procedure di espressione della proteina ricombinante e di purificazione

della frazione arricchita della YB-1 nel mezzo di coltura sono state eseguite in collaborazione con il laboratorio del Dr. Elio Pizzo dell'Università degli Studi di Napoli Federico II.

1. Produzione di YB-1 ricombinante (rYB-1)

La proteina YB-1 umana ricombinante è stata prodotta in *E. Coli*. La scelta di *E. Coli* per la produzione di YB-1 è da ricercarsi nel fatto che si tratta di un ospite relativamente semplice da manipolare e propagare e la cui genetica è ben nota. L'induzione dell'espressione di YB-1 dal vettore plasmidico è stata effettuata con aggiunta di IPTG (isopropil-1-tio-d-galattopiranoside).

Il cDNA codificante la proteina umana YB-1 è stato ottenuto mediante PCR dal vettore umano pEX-A2. Il cDNA ottenuto, opportunamente purificato è stato inserito nel vettore pET22b (+). L'inserimento è stato effettuato a monte di una sequenza di istidine (His-tag), mediante digestione enzimatica con gli enzimi *NdeI* e *HindIII*, per facilitare i successivi passaggi di purificazione.

Il vettore di espressione così ottenuto è stato utilizzato per trasformare ceppi di *Escherichia Coli* competenti BL21 (DE3).

Analisi di *western blot* hanno dato conferma che la proteina YB-1 veniva espressa in maniera inducibile e che si accumulava a seguito di induzione con IPTG nella frazione citosolica solubile. La frazione solubile è stata, quindi, separata dai corpi di inclusione ed i prodotti ottenuti sono stati purificati mediante cromatografia di affinità (IMAC) seguita da cromatografia a fase inversa. Le frazioni YB-1 positive, analizzate mediante WB, sono state dializzate e la loro identità controllata mediante analisi di Spettrometria di Massa.

2. Purificazione di YB-1 dal mezzo di coltura (CCM-YB-1)

Parallelamente alla produzione della proteina ricombinante è stata preparata una frazione arricchita della proteina YB-1 secreta dalle cellule HEK293T in coltura. Terreni di coltura di cellule HEK293T (*conditioning culture media* – CCM) privi di siero sono stati estratti con ammonio solfato (*salting out*). In particolare sono state ottenute 3 frazioni a concentrazioni crescenti di ammonio solfato (30, 70 e 100%). Le tre frazioni sono state analizzate mediante SDS-PAGE ed *immunoblot* con anticorpo diretto contro la proteina YB-1. L'estrazione più efficace è stata quella al 70% di ammonio solfato. Analisi di spettrometria di massa hanno confermato l'arricchimento di YB-1 nelle frazioni estratte con ammonio solfato.

Analisi funzionale della YB-1 extracellulare (exYB-1)

Per comprendere le funzioni della proteina YB-1 secreta dalle cellule HEK293T su cellule riceventi, la proteina ricombinante rYB-1 e la CCM-YB-1 sono state addizionate al terreno di coltura di cellule HaCaT per ottenere una concentrazione di 5.0, 7.5 e 10 µg/ml.

L'utilizzo dei cheratinociti umani immortalizzati (HaCaT) come cellule riceventi non è stato dettato solo dal fatto che le cellule HaCaT non secernono la proteina, ma anche dalla considerazione che esse rappresentano un buon modello cellulare per lo studio del tessuto cutaneo nel cui differenziamento YB-1 svolge un ruolo rilevante. Entrambe le proteine hanno causato una riduzione del tasso proliferativo delle cellule, in maniera

dose-dipendente.

Per verificare se l'effetto di rallentamento della proliferazione fosse dipendente dal contesto cellulare, la stessa tipologia di esperimento è stata eseguita sulle cellule di adenocarcinoma colon-rettale umano CaCo2 e sulle stesse cellule secernenti HEK293T. Anche in questo caso è stato osservato un blocco della proliferazione cellulare.

Interessante notare che la CCM-YB-1, se paragonata alla rYB-1, mostrava un effetto molto più pronunciato su tutte e tre le linee cellulari. Analisi al citofluorimetro di flusso hanno rivelato che le cellule trattate con la YB-1 extracellulare (rYB-1 e CCMYB-1) mostravano un incremento di cellule nella fase G2/M del ciclo cellulare. L'analisi dei livelli di espressione dei marcatori del ciclo cellulare p21WAF e di $\Delta Np63\alpha$ in cellule HaCaT trattate e non con la YB-1 extracellulare ha confermato quanto osservato per citofluorimetria.

Dati di letteratura suggeriscono un possibile ruolo di YB-1 nel controllo dei processi infiammatori. Questo mi ha indotto a valutare un possibile coinvolgimento del *pathway* di NF- κ B in risposta alla YB-1 secreta. Un sistema reporter GFP sotto il controllo del promotore attivato dal fattore trascrizionale NF- κ B è stato trasferito in cellule HaCaT in maniera transiente. Il trattamento con rYB-1 e CCM-YB1 è stato in grado di indurre il sistema reporter in cellule HaCaT. Ho anche osservato in seguito al trattamento un incremento dei livelli di TNF α sia a livello di trascritto che di proteina. Sebbene preliminari, questi dati mi sono parsi incoraggianti. Ulteriori studi potranno far luce sul ruolo della proteina YB-1 secreta nei processi infiammatori. Questo aspetto potrebbe avere potenzialità applicative nel settore farmacologico del controllo dell'infiammazione.

Trasferimento conoscenze su Danio rerio (KIT)

Ho trascorso parte del mio PhD presso il laboratorio del Prof. Dr. N. S. Foulkes dell'Istituto di Tossicologia e Genetica (ITG) del *Karlsruher Institut für Technologies* (KIT), Eggstein-Leopoldshafen, Germania, dove ho effettuato esperimenti volti a comprendere il ruolo di YB-1 quale *stress sensor* nel modello *zebrafish*. YB-1 potrebbe rappresentare un marcatore di stress negli organismi acquatici che sono soggetti a grossi cambiamenti climatici e ambientali. L'impiego dello *zebrafish* come organismo modello è dovuto non solo alla facilità di allevamento degli individui e alla nota trasparenza della progenie, ma anche alla semplicità di manipolazione genetica e cellulare e alla possibilità di allestire screening genetici su larga scala, cosa più impegnativa sia a livello economico che a livello etico se si considerano gli organismi convenzionali come topi e ratti.

Il gruppo di ricerca presso il quale ho svolto parte del mio progetto di dottorato, aveva precedentemente dimostrato che la distribuzione subcellulare della proteina YB-1 in *zebrafish* (zfYB-1) è regolata dal ritmo circadiano. La zfYB-1 ha una identità di sequenza del 69% con la proteina YB-1 umana, e, come questa, è composta da tre domini: dominio N-terminale ricco in alanina e prolina; dominio centrale *Cold Shock*; dominio c-terminale costituito da amminoacidi carichi negativamente e positivamente.

Gli anticorpi contro la YB-1 umana riconoscono zfYB-1 grazie ad una regione N-terminale estremamente conservata. Sorprendentemente, ho osservato che le cellule di *zebrafish*, al contrario delle cellule di mammifero, non assemblano granuli da stress YB-1 positivi in condizioni di stress

ossidativo anche se l'attivazione dei geni della risposta allo stress indicavano chiaramente che le cellule di zebrafish sono sensibili a questo tipo di stress. Una possibile spiegazione è da ricercare nel fatto che *zebrafish* è un animale abituato a gestire variazioni ambientali anche piuttosto repentine come cambi di salinità, concentrazione di nutrienti, ecc., ed è possibile dunque che sia dotato di vie alternative di risposta allo stress.

Al contrario, uno stress fisico come lo shock termico, portava alla formazione di aggregati YB-1 positivi, visualizzati per immunofluorescenza e microscopia confocale. La conferma che gli aggregati ottenuti fossero Granuli da Stress è stata ottenuta mediante trattamenti con cicloesimide, un inibitore della formazione dei granuli, ed esperimenti di immunofluorescenza e microscopia confocale con anticorpi diretti contro G3BP1, marker canonico dei Granuli da Stress.

Il silenziamento di zfYB-1 mediante *RNA interference* ha confermato il ruolo cruciale di questa proteina nell'assemblaggio dei granuli da stress.

Simili analisi eseguite su pinne caudali di esemplari di *zebrafish* (Tübingen) hanno confermato i dati precedentemente ottenuti in un contesto tessutale. In particolare il numero dei granuli era maggiore se il campionamento delle pinne caudali avveniva nelle ore di luce, sottolineando come la luce fosse di per sé fonte di danno ossidativo.

Applicazioni di YB-1 come stress sensor

La capacità di YB-1 di accumularsi nel nucleo in seguito a danno genomico ed il suo ruolo nei granuli da stress, ne sottolineano l'importanza come marcatore dello stress cellulare. Ho potuto osservare che il trattamento di cellule di carcinoma squamoso cutaneo (SCC) con estratti della corteccia della pianta *Uncaria Tomentosa*, induce morte cellulare. L'estratto di *Uncaria Tomentosa* induce nelle cellule di carcinoma squamoso un incremento dei valori di ROS. Nel contempo inibisce l'accumulo della forma da 37 kDa di YB-1 fortemente implicata nei processi di riparo del danno genomico. È stata formulata l'ipotesi che l'azione accoppiata di un agente pro-ossidante ed un potenziale inibitore del proteasoma 20 S contenuti nell'estratto vegetale possa spiegare l'efficacia dell'estratto su questo tipo di cellule cancerose. Esperimenti simili con Argento Colloidale ed altri fitoestratti sono tutt'ora in corso.

Collaborazioni

Durante il mio percorso di dottorato ho avuto la possibilità di svolgere piccole parti in altri progetti in collaborazione con docenti e ricercatori dell'Università degli Studi di Napoli
Napoli Federico II.

In particolare, ho contribuito allo studio delle proprietà antiossidanti delle spore del ceppo SF185 di *Bacillus Megaterium* su cellule umane, con il gruppo della Prof.ssa Istickato, ed ho contribuito nella messa a punto di un nuovo approccio metodologico per la quantificazione del Wound Healing in collaborazione con il Prof. Caserta. Presso l'Istituto di Tossicologia e Genetica (ITG) presso il quale ho svolto il mio periodo all'estero ho contribuito allo studio della perdita del sistema di riparo del DNA mediato da fotoriattivazione nel pesce *P. Andruzzii*.

ABSTRACT

Cell signalling is the complex network of connections between cells and inside the single cell. Protein trafficking is deeply involved in cell signalling. Different proteins are ordered in clusters of receptors of extracellular signals, transducers, sensors and biological response effectors. Together, they are arranged in molecular pathways that are relevant for maintenance of cell homeostasis.

Protein secretion is a relevant component of eukaryotic cell signalling. The prototype cold-shock Y-box binding protein 1 (YB-1) is a multifunctional protein which regulates a variety of fundamental biological processes. Recently YB-1 has been found in human extracellular fluids and shown to be secreted by different cell types. This PhD project is focused on YB-1 protein secretion to investigate on its role as a potential paracrine signal to elicit changes or responses in nearby cells, altering their behaviour.

During the first part of the project I focused on stimuli and conditions triggering YB-1 secretion. Low amounts of extracellular YB-1 are released by HEK293T cells in physiological condition. Interestingly, I found that YB-1 secretion was enhanced following oxidative insults. Secreted YB-1 protein was purified and analysed by mass spectrometry to confirm its identity. In parallel, I verified the assembly of YB-1 in stress granules (SGs), cytoplasmic foci where untranslated mRNAs are sorted or processed for reinitiation, degradation, or packaging into mRNPs.

To understand the mechanism beneath YB-1 secretion and uptake by receiving cells, I tried several experimental approaches; among them the production and characterization of a stable HEK293T cell line expressing a YB-1-GFP fusion protein. The properties of this cell line as a stress biosensor were evaluated.

The second part of the project was devoted to the production of purified recombinant human YB-1 (rYB-1) in bacterial host. In parallel I produced enriched fractions of YB-1 from HEK293T cell culture medium (CCM-YB-1). I found that both CCM-YB-1 and rYB-1 have anti-proliferative activity on receiving cells. Both forms of YB-1 protein were effective on different recipient cell lines, including HaCaT cells. In particular, inhibition of human keratinocytes proliferation by extracellular YB-1 was associated to a G2/M cell cycle arrest, induction of p21WAF and reduction of Δ Np63 α protein level. The obtained results suggest that sustained release of full length YB-1 protein or YB-1 derived peptides, by stress stimuli acts as paracrine/autocrine signal stimulating cell cycle arrest.

Finally, I spent six months of my PhD at the Institute of Toxicology and Genetics (ITG-KIT), in Karlsruhe, Germany, where I had the opportunity to study the behaviour of the evolutionarily conserved YB-1 in zebrafish (*Danio rerio*), one of the most versatile genetic models for environmental studies. Unexpectedly, I found that zebrafish cells assemble YB-1 positive aggregates only in response to heat, but not oxidative stress or copper treatment. YB-1-positive aggregates were confirmed as SGs as they contained the G3BP1 protein, a well assessed SG marker in mammalian. I found that zfYB-1 gene silencing compromised cell viability under heat shock, but not in normal conditions highlighting the essential role played by YB-1 in cell survival following heat shock. My findings point to a fundamental role of YB-1 as a valuable biomarker for thermal stress.

CHAPTER I

1. Cell signalling and biotechnological applications

Cell signalling is at the basis of cellular homeostasis and has to be intended as a complex network of connections between cells and inside the single cell. Simplifying, signalling machineries act as highly dynamic two-components system, composed by a sensor, which sense the internal or external change, and an effector, which execute the best response to the variation experienced. All cells communicate with each other and with the surroundings. Eukaryotic cell communication takes places basically thanks to the trafficking and exchange of soluble molecules, proteins, lipids and also through mechanical contacts (Figure 1). Understanding how the signalling circuitry of eukaryotic cells can be engineered to construct cells, or part of them with designed behaviours is of deep interest of biotech industries. Targeted immunosuppression or design of anti-cancer cells are indeed good examples of how manipulation and reprogramming of cellular signalling systems can be applied [1].

Signalling can adopt different mechanisms, protein secretion among them plays a major role. Accordingly, the analysis of protein secretory pathways has been the focus of many research fields throughout the years.

Although they have a sophisticated information processing capacity, bacterial systems are already widely applied as production platforms of secreted proteins because they are less complex than eukaryotic cells [2]. There are countless examples in literature of engineering of microbial and yeast secretion machineries to refine recombinant protein expression or to create Protein Delivery Systems for mammalian cells [3]. For instance, Protein Transduction Domains (PTDs) or Cell Penetrating Peptides (CPPs), short amino-acids sequences that added to specific cargos facilitate their delivery into recipient cells, have opened new frontiers in the control of intracellular cell functions by macromolecules [4]. Recently, the study and application of eukaryotic secretion itself has gained interest; in particular great progresses have been made in expanding the categories of characterized biological components that can be used for cell signal manipulation.

This PhD project was focused on YB-1 protein secretion to investigate on its role as a potential paracrine signal to elicit changes or responses in nearby cells, altering their behaviour.

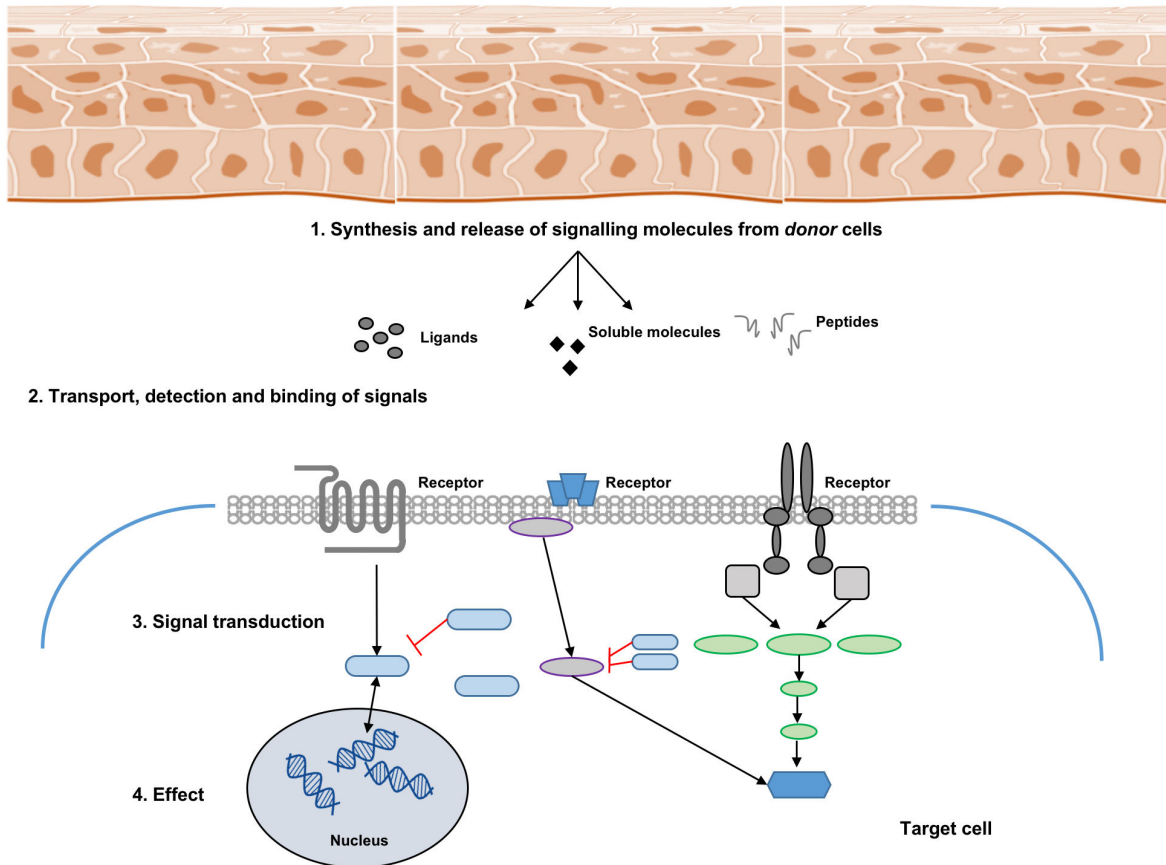


Figure 1. Representation of eukaryotic cells signalling. Eukaryotic cell signalling can be summarized in four passages: 1. the synthesis and production of different type of signal molecules; 2. the transport until the target cell and the uptake of the signal by this one; 3. the transduction of signals; 4. the trigger one or more cellular responses which led to an effect.

2. Protein secretion

Trafficking and secretion of soluble proteins containing typical N-terminal signal peptide in eukaryotes has been extensively studied. These proteins follow what is usually referred to as the Conventional Protein Secretion (CPS) pathway [5]. This trafficking route is a linear movement of cargoes, which traverse distinct organelles in a membrane-bound way [6]; starting from the rough endoplasmic reticulum (RER), where newly synthesized proteins are concentrated in transport vesicles which travel along the cell to the Golgi Apparatus (GA), then to the trans-Golgi network (TGN) and then fuse with the plasma membrane [7]. A first definition of the collection of proteins secreted through CPS was *secretome*; nowadays the definition encompasses proteins shed from the cell surface and intracellular proteins released through non-classical (or unconventional) secretion pathway or exosomes. Less, indeed, is known about Unconventional Protein Secretion, also known as ER/Golgi-independent protein secretion [8] although it was discovered more than 10 years ago (Figure 2).

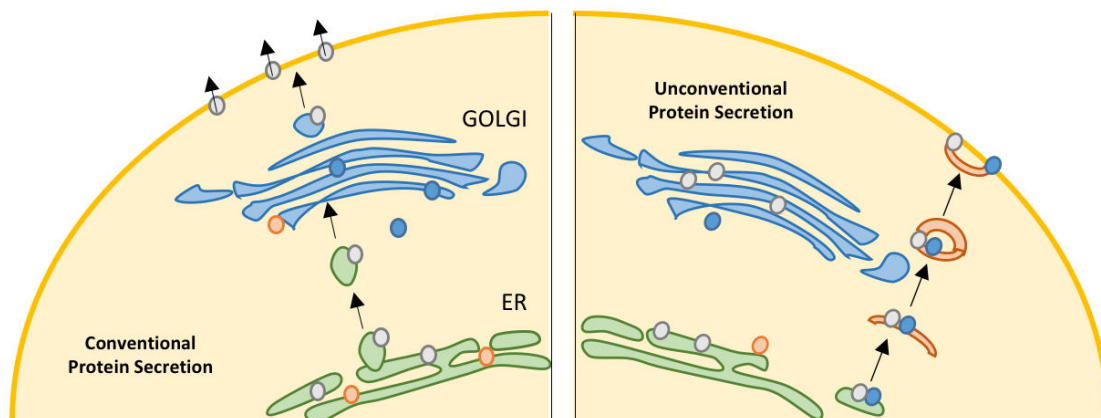


Figure 2. Representation of Conventional and Unconventional Protein secretion. Two different major mechanisms of protein secretion in eukaryotic cells.

Beyond solving a fundamental problem in current cell biology, the molecular analysis of these processes is of major importance as these export routes are taken by viral proteins, angiogenic growth factors, inflammatory cytokines and components of the extracellular matrix. These factors can regulate cell differentiation, proliferation, apoptosis, parasite infection and inflammatory processes, being of tremendous interest of biotechnological industries.

3. YB-1 protein

3.1 Structure and functions

YB-1 (Y-box binding protein 1) is a member of the evolutionarily conserved cold shock domain (CSD) proteins and was first identified as a DNA/RNA binding protein [9] involved in the control of gene expression both at transcriptional and translational level [10,11].

Human YB-1 is made up of three domains: A/P rich N- terminal domain (amino acids 1-51); a highly conserved CSD domain (amino acids 52-129) and a large C-terminus (amino acids 130-324) [12] (Figure 3). The Cold Shock Domain is composed by five β -barrel strands connected by a long flexible loop; it contains the RNA binding motifs *RNP1* and *RNP2*, which mediate the interaction with nucleic acids, both specific and unspecific [10]. The Alanine/Proline domain is involved in protein-protein interaction and, according to the literature, enhances and stabilizes the CTD specific binding with RNAs. The CTD domain includes alternating basic and acid clusters and is implicated in DNA/RNA binding and protein-protein interaction. Except the CSD, which owns a precise secondary structure, the protein shows no ordered three-dimensional structure (Figure 3); this gives YB-1 the possibility to modulate its structure gaining different fixed organizations through the interaction with several distinct partners [13]. YB-1 subcellular localization is finely regulated. Specific nuclear localization (NLS) and

cytoplasmic retention signals (CRS), all localized in the CTD domain, contribute and direct the multifunctional tasking of YB-1 [14].

Combining its structural flexibility and the possibility to move from a cellular district to another, derives that YB-1 is involved in the control of several biological processes including cell proliferation, migration, DNA damage, RNA sorting and many others.

In normal resting cells, YB-1 localizes to cytoplasm where it is a major component of P-body and messenger ribonucleoproteins (mRNPs) acting, predominantly, as a RNA binding protein [15; 16]. Furthermore, YB-1 activates translation of specific transcripts via its ability to bind UTRs of target mRNAs (low YB-1/mRNA ratio); at high YB-1/mRNA ratio, instead, it functions as a component of translationally inactive mRNPs, and directly blocks the initiation of translation inhibiting mRNA degradation [17]. YB-1 is also able to bind specific miRNAs, snoRNAs and tRNA-derived fragments and regulate the expression of miRNA biogenesis and processing machinery [18]. This function of YB-1 is particularly attractive because of the interest on microRNA (miRNA)-based technology for therapeutic applications. In this regard RNA-binding proteins and microvesicle-dependent trafficking systems are actively studied to set up miRNAs-loaded systems which can be delivered into recipient cells simultaneously regulating multiple target genes or signalling pathways [19].

Mitogens and stress stimuli can trigger YB-1 nuclear translocation where it acts as a transcription factor, at the G1-S transition of the cell cycle, for instance [20,21]. Moreover, IR-induced DNA damage activates the DNA-repair activity of YB-1 in the nuclear compartment.

Recent studies link YB-1 to the cellular response to oxidative stress and DNA repair mechanisms, leading to the concept of YB-1 as a stress sensor. Indeed, following acute oxidative stress, YB-1 localizes to cytoplasmic Stress Granules (SGs), organelle-like structures devoid of membranes, engaged in mRNA sorting and pro-survival translational reprogramming [22,23].

In particular, YB-1 is recruited in TIA-containing Stress Granules (SGs) where it functions as a component of translationally inactive mRNPs to directly block translational initiation of highly expressed transcripts [24].

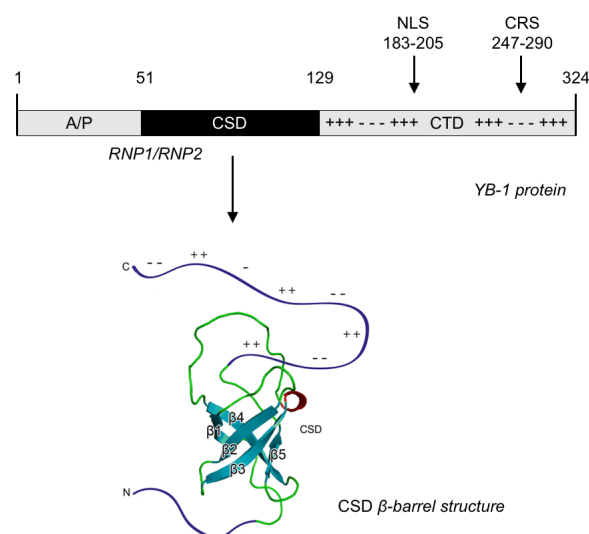


Figure 3. Schematic representation of human YB-1 protein. YB-1 is composed by three domains; only the CSD has a 3-dimensional structure.

3.2 YB-1 as Stress Granules (SGs) nucleator

Stress caused by environmental insults or disease can disrupt cellular, tissue and organ homeostasis. Stress-induced DNA damage may culminate in cell or even organismal death [25]. Eukaryotes respond to detrimental conditions by activating a set of conserved processes that aim to re-establish cellular homeostasis. This multifaceted response is critical for cell survival [25]. It is characterized by stress-dependent changes in the transcriptome and down-regulation of global translation [26]. At the same time, the production of molecular chaperones is enhanced to promote the refolding or degradation of damaged proteins [27].

After exposure to distinct environmental insults, such as oxidative stress, hypothermia or extreme heat, eukaryotic cells relocate proteins and messenger RNA into transient, dynamic structures known as Stress Granules (SGs). Stress granules, directly respond to the protein synthesis status of cells; contain mRNAs, small ribosomal subunits and factors such as G3BP1 and YB-1 as their core components [28].

Stress granules are dynamic cytosolic aggregates composed by ribonucleoproteins that are induced during cellular stress when protein synthesis is inhibited [29]. In response to environmental stress such as oxidative stress or heat shock, cells respond by shutting down overall protein synthesis. This results in the disassembly of polyribosomes, leading to stalled initiation complexes that are dynamically recruited to cytoplasmic foci called, hence, stress granules. Stress granules biology is very complex; they somehow evolve from Processing Bodies (PBs) which are linked to exosomes, by sharing proteins and RNAs [29,30]. Following this concept, it has been proposed a model wherein mRNAs released from polysomes during stress are routed to SGs for triage, sorting, and mRNP remodelling, after which certain transcripts are selectively exported to associated PBs for degradation, while other transcripts, specifically those deadenylated, are degraded by the 3'–5' exonucleases present in the exosomes [31].

YB-1 performs a role in SGs formation, in particular in sodium arsenite response, by activating translation of HSP70 and G3BP1 protein, which is a well characterized SGs nucleator and recruiting tiRNAs generated by angiogenin cleavage [24].

3.3 YB-1 secretion

A newly identified YB-1 feature is its ability to be secreted in cell culture media and human body fluids [32]. YB-1 secretion is particularly active in association with malignancies, bacterial infections and inflammatory diseases [33].

The precise molecular mechanisms through which YB-1 is secreted is still under investigation, but it is generally accepted that YB-1 is secreted through non canonical pathways [34] and there are evidences about different proteins and molecular machineries involved. One of the more recently mechanism proposed, indicates that YB-1 is secreted via exosome vesicles following a specific ubiquitination process [35]; this seems to be in contrast with other mechanisms proposed so far, for instance acetylation-dependent secretion [36]. In exosomes YB-1 is believed to sort RNA by type and quantity in a cell specific manner [37].

Moreover, it is still not clear if YB-1 protein is secreted as a sum of multiple fragments and what are the effects of secreted YB-1 on distinct target cells. As a matter of fact,

bioinformatic analysis of YB-1 amino acid sequence predict that it may represent a precursor for bioactive paracrine molecules; interactions between secreted YB-1 and some extracellular receptor domains, for instance Notch 3, have been proposed [38]. Due to its simultaneous presence in P-bodies, Stress Granules (SGs) and exosomes YB-1 is thought to function as a regulator of peptides/RNAs trafficking in and outside the cell.

4. Aim of the work

In the last decade and half the scientific community has investigated numerous features of the YB-1 protein, ranging from its involvement in mRNA control in the cytoplasm, leading to its function as transcription factor in the nucleus. Different authors have pointed out the extraordinary versatility of the protein, which is mostly based on its molecular structure. Until a few years ago YB-1 was considered a relevant *passive* player of such processes. More recently, with the discoveries that YB-1 is involved in vesicles trafficking routes, for example loading cargos on vesicles or participating in their formation and release, a new approach has emerged, the one that considers YB-1 an *active* player. It is not exaggerated to intend YB-1 as *molecular supervisor* of (some) cellular processes.

Accordingly, the idea behind this PhD project was to evaluate the rationality of this concept, focusing on YB-1 response to stress. As reported above, based on its structural organization, YB-1 is predicted to be a potential precursor of signal peptides, and considering its ability to respond to stress by assembling SGs, I speculated that YB-1 can act as a sensitive stress sensor being secreted to propagate stress signals and by so inducing adaptive response in neighbouring cells.

Starting from this hypothesis I have explored in detail YB-1 response to stress stimuli and, finally, I concentrated my studies on the potential role of YB-1 as paracrine signalling molecule on receiving cells.

YB-1 roles and functions are currently being investigated not only in mammals, but also in other organisms such as fish. In zebrafish YB-1 is involved in circadian rhythm and DNA damage response.

For those reasons I have also conducted comparative studies on mammalian and zebrafish cells to evaluate the sensitivity and relevance of YB-1 as an environmental stress biomarker and a water toxicity biosensor in fish for aquaculture optimization.

CHAPTER II

1. HEK293T cell line characterization

Human embryonic kidney 293T (HEK293T) cell line is a popular, heterologous expression system for producing recombinant proteins in mammalian cells [39]; it is also widely used for production of secreted proteins [40]. For these reasons it has been chosen as a good cell model system to analyse YB-1 response to stress.

First, I analysed YB-1 subcellular distribution in normal conditions: I set up immunofluorescence experiments in HEK293T using anti-YB-1 antibodies raised against the region 1 to 100 of YB-1 protein (abcam 12148). Given that HEK293T adhesion to glass/plastic surfaces was weak, plates and slips for immunofluorescence were treated with Poly-D-lysine 0.1mg/ml (Sigma-Aldrich, St Louis) before seeding cells. Poly-D-lysine increases HEK293T adhesion to plating surfaces by increasing electrostatic interaction between negatively-charged ions of cell membrane and culture surface.

In normal condition, immunofluorescence and confocal microscopy revealed that YB-1 was abundant and almost exclusively cytoplasmic. Interestingly, I observed small cytoplasmic aggregates that appeared to be randomly distributed throughout the cell (Figure 4, white arrows).

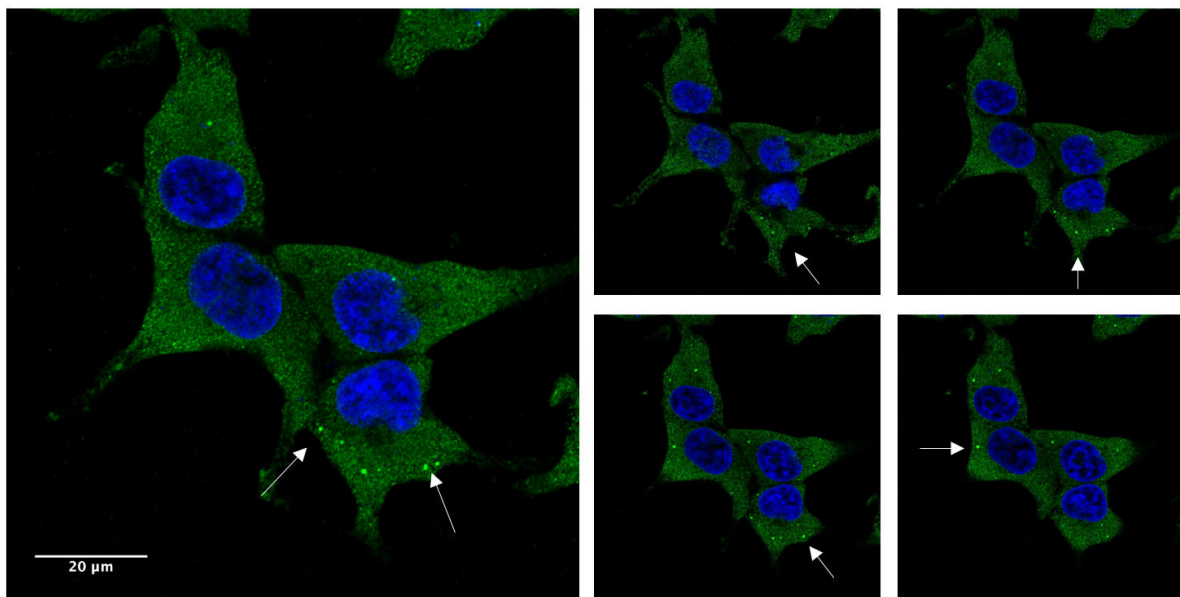


Figure 4. Confocal immunofluorescence of HEK293T stained with α -YB-1 (green), nuclei are stained with DAPI (blue); arrows indicate YB-1 aggregates.

Knowing that YB-1 has been found in P-bodies in many mammalian cell lines, for example in Hep-2 and Hela cells [15,41], I evaluated the possibility that also HEK293T have YB-1 positive P-bodies.

Therefore, I performed double immunofluorescence with antibodies against YB-1 (abcam) and GW182 (Santa Cruz Biotechnology), and as shown in Figure 5, YB-1 and GW182 co-localize in cytoplasmic aggregates, confirming that they are P-bodies, or at

least GW bodies, which are often associated with the P-bodies of higher eukaryotic organisms [42].

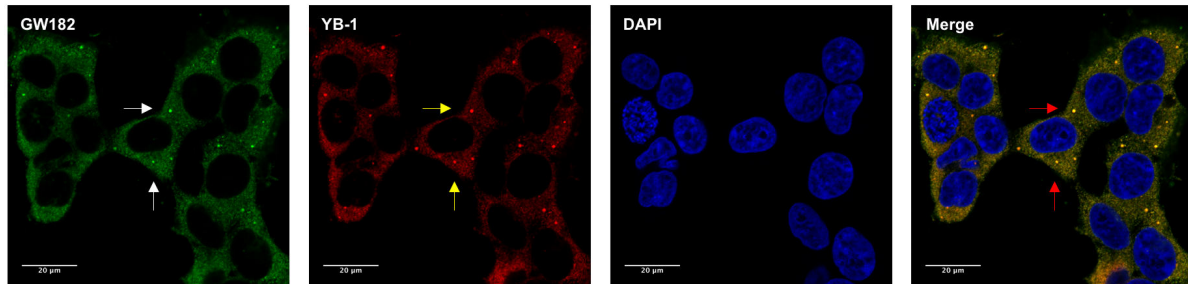


Figure 5. YB-1 co-localizes with GW182.

Confocal immunofluorescence of HEK293T stained with α -GW182 (green) and α -YB-1 (red), nuclei are stained with DAPI (blue); white, yellow and red arrows indicate respectively, YB-1, GW182 and YB-1/GW182 aggregates.

1.1 HEK293T response to stress

Once defined the subcellular distribution of YB-1 protein in normal conditions I treated cells with different stressors. Following heat shock or treatment with 250 μ M sodium arsenite (Na Ars) or 500 μ M hydrogen peroxide (H_2O_2), YB-1 was found to co-localize with PABP1, a canonical SGs marker [43], in cytoplasmic stress granules (Figure 6). Interestingly, SGs size and overall number per cell were different depending on the type of stimulus applied confirming previous finding indicating stress-specific differences in composition and assembly of stress granules [44].

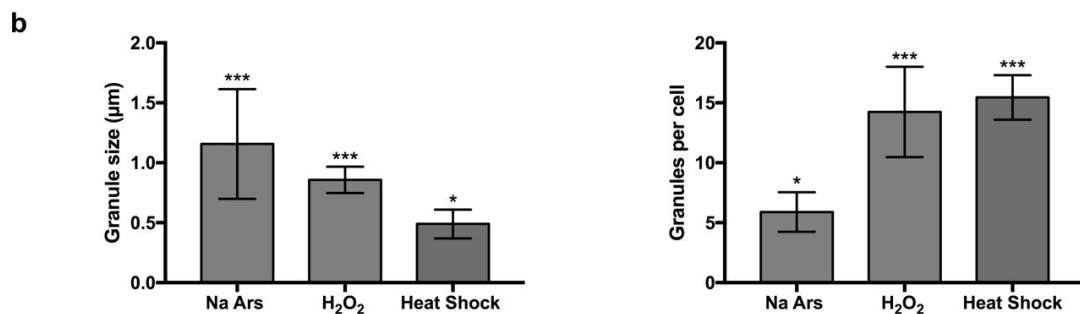
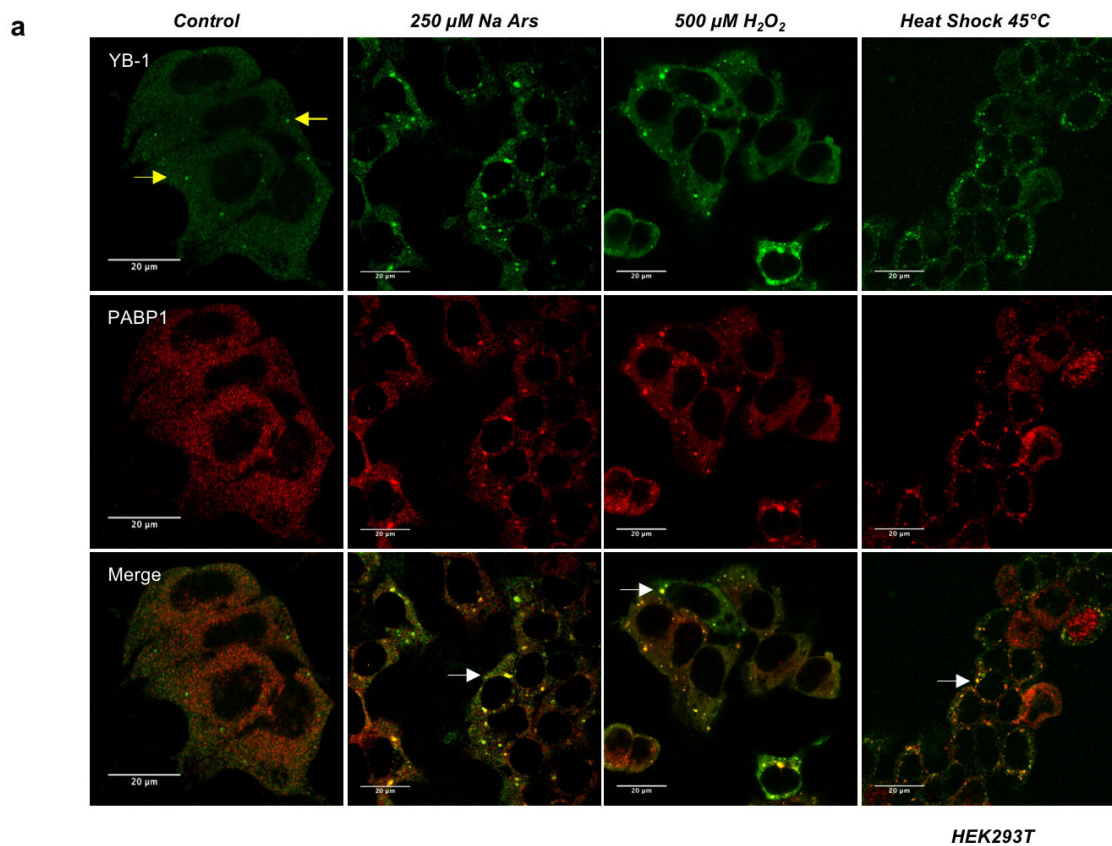


Figure 6. YB-1 co-localizes with PABP1 under stress conditions.

a) confocal immunofluorescence of un-treated (control) HEK293T and treated with different stressors, stained with α -YB-1 (green) and α -PABP1 (red), nuclei are stained with DAPI (blue); yellow arrows indicate YB-1 positive P-bodies; white arrows indicate YB-1 and PABP1 positive stress granules; **b) (left panel)** size of granules and **(right panel)** number of granules after treatments compared to control; statistical analysis was performed using 1-way ANOVA followed by Dunnett's multiple comparisons test. Levels of significance are indicated (***) $p < 0.001$, * $p = 0.001$; see also Appendix II, table 1).

Next, I immunoprecipitated YB-1 protein from extracts of untreated or sodium arsenite treated HEK293T cells. As shown in Figure 7 PABP1 was detectable in YB-1 immunocomplexes exclusively from cells treated with arsenite thereby indicating that YB-1 and PABP1 association occurs predominantly in SGs (Figure 7).

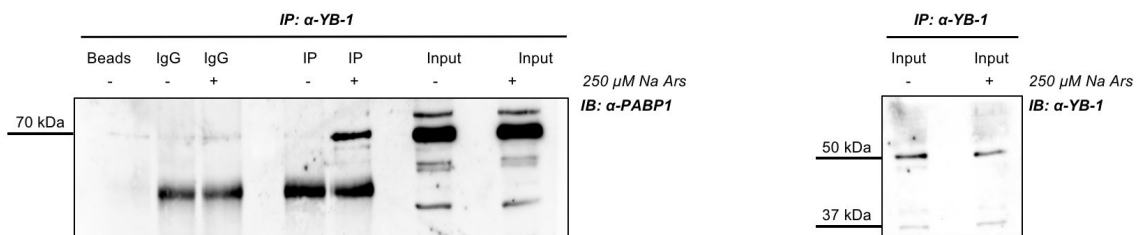


Figure 7. YB-1 and PABP1 physically interact under sodium arsenite stimulation. Co-immunoprecipitation of HEK293T total protein extracts treated (+) or not (-) with 250 μ M Na Ars for 30'; extracts were immunoprecipitated for YB-1 and immunorevealed for PABP1. YB-1 physically interacts with PABP1 only in the presence of Na Ars. Input samples immunorevealed with α -PABP1 and α -YB-1 are shown.

To assess the relevance of YB-1 in SGs assembly, I depleted HEK293T cells of YB-1 using a specific siRNA pool against endogenous YB-1 mRNA (siYB1). By immunoblot and densitometric analysis I found that the expression level of YB-1 protein was reduced to 55% of control (Figure 8a). YB-1 knock-down consistently impaired the assembly of arsenite-induced PABP1-positive stress granules by reducing their size and number (Figure 8b and c). Interestingly, in YB-1 depleted cells, PABP1 showed a more nuclear localization both in resting condition and under stress stimuli (Figure 8c) suggesting that YB-1 can influence PABP1 subcellular distribution.

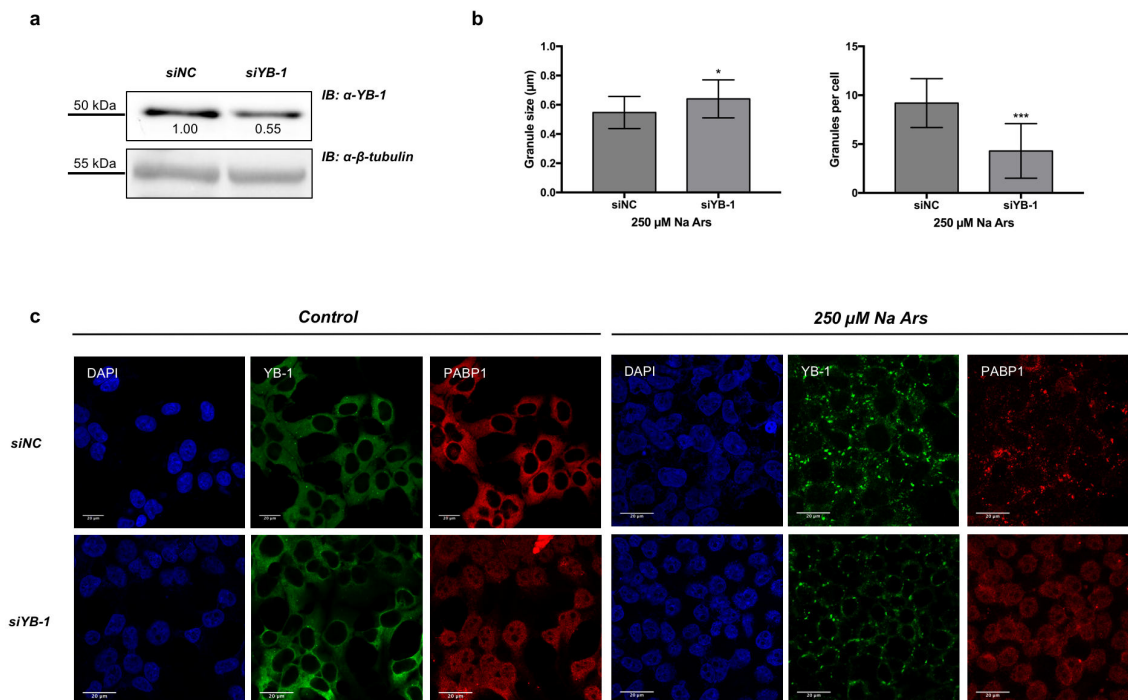


Figure 8. Silencing of YB-1 affects PABP1 positive SGs formation.

a) western blot of total extract from control (siNC) or 100 nM YB-1 silenced (siYB-1) HEK293T; the degree of reduction of YB-1 protein levels in YB-1 siRNA-treated cells compared with control is indicated beneath each band in the western blot (where the relative unit 1.0 represents YB-1 levels in cells transfected with the control siRNA). β -tubulin was used as loading control. Each panel is assembled from cropped western blotting images. **b**) (*left panel*) size of granules and (*right panel*) number of granules in YB-1 silenced cells treated with Na Ars compared to siNC (control) cells; statistical analysis was performed using unpaired t-test with Welch's correction (**p = 0.010 and *p = 0.02; see also Appendix II, table 1). **c**) confocal immunofluorescence of control (siNC) and silenced (siYB-1) HEK293T cells, treated or not with 250 μ M Na Ars for 30', stained with α -YB-1 (green) and α -PABP1 (red), nuclei are stained with DAPI (blue).

1.2 YB-1 secretion under stress stimuli.

Despite the apparent enrichment of YB-1 in SGs, I observed a significant reduction of intracellular YB-1 protein level in total extracts of Na Ars and H₂O₂-treated HEK293T (Figure 9a and b). The observed decrease of YB-1 was not caused by cell death and subsequent leakage of cell contents as the level of GAPDH and actinin proteins, used as control, remained unaffected (Figure 9a and b). By immunoblot analysis of nuclear and cytoplasmic subcellular fractions I found that the reduction of YB-1 protein level induced by sodium arsenite was exclusively at the expense of the cytoplasmic pool, while nuclear YB-1 was totally unaffected (Figure 9c).

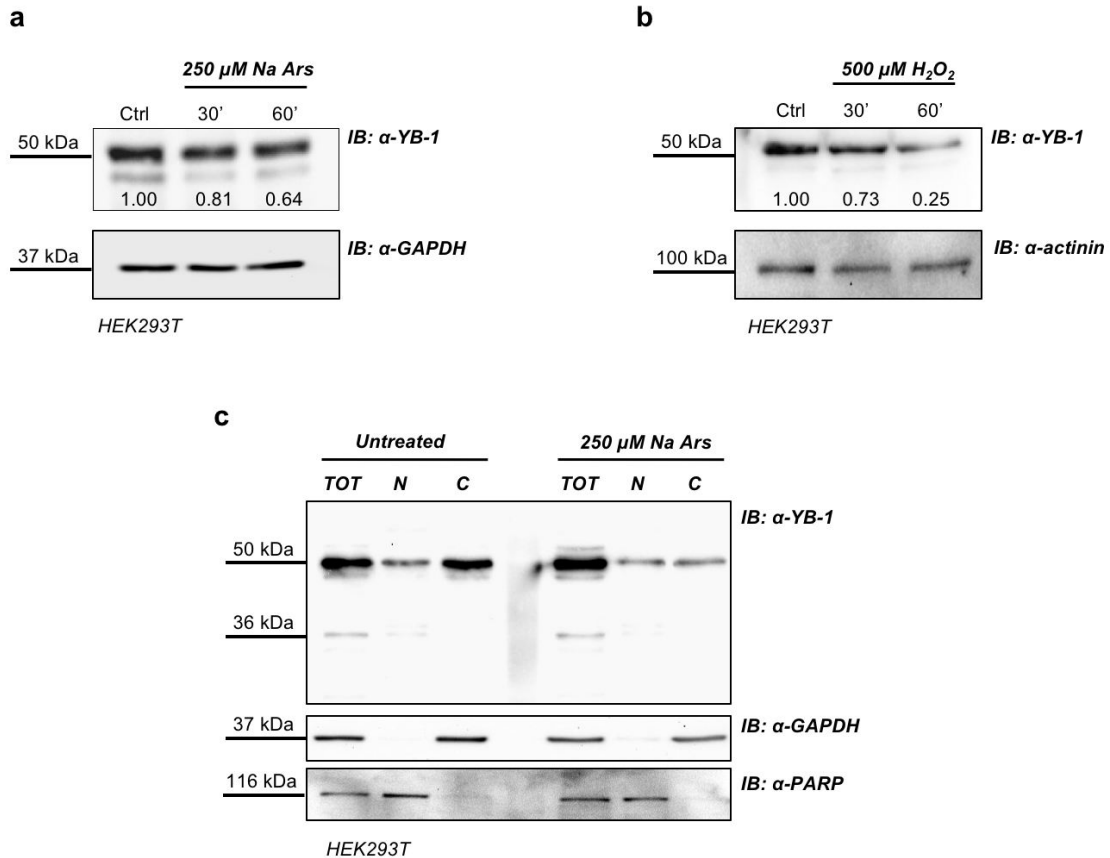


Figure 9. Sodium arsenite and hydrogen peroxide treatments affect cytoplasmic pool of YB-1. Western blot of total protein extracts from HEK293T treated with 250 μ M Na Ars (**a**) or 500 μ M H₂O₂ (**b**) for 30' and 60'; GAPDH and actinin were used as loading control. The degree of reduction of YB-1 protein levels in treated cells compared with controls is indicated beneath each band in the western blot (where the relative unit 1.0 represents YB-1 levels in control cells). **c**) western blot of total extract and nuclear/cytoplasmic fractionation of Na Ars treated and untreated HEK293T. GAPDH and PARP were used as loading control for cytoplasm and nucleus respectively. Each panel is assembled from cropped western blotting images.

Moreover, after 30' and 60' treatment with 250 μ M sodium arsenite or 500 μ M hydrogen peroxide, cell viability was only slightly reduced (90% and 94%, respectively) compared to control cells and the increase of trypan blue positive cells was negligible (Figure 10a and b), further indicating that extracellular accumulation of YB-1 was not due to cell injury.

Thus, I hypothesized that oxidative stress would enhance YB-1 protein secretion.

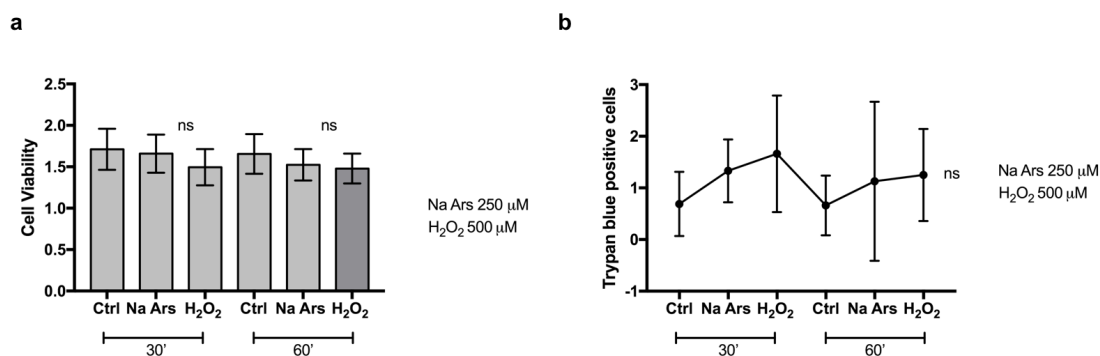


Figure 10. Sodium arsenite and hydrogen peroxide treatments do not affect cell viability.

Cell viability assay (a) and Trypan blue (b) of HEK293T cells treated with 250 μ M Na Ars and 500 μ M H₂O₂ for 30' and 60', ns indicate no statistically significance (ordinary 1-way ANOVA and Dunnett's multiple comparison; ns means no statistical significance; see also Appendix II, table 1).

1.3 TCA precipitation

To detect YB-1 protein in culture medium I performed trichloroacetic acid precipitation (TCA ppt). TCA precipitation is a cost effective and easy to perform method to concentrate proteins from culture medium; if added to an aqueous solution TCA causes aggregation and precipitation of proteins [45]. I performed TCA ppt on culture media of HEK293T treated cells with sodium arsenite at different time intervals (from 30' to 240').

Briefly, media were collected, centrifuged and filtered with 0.22 μ m device to eliminate cells eventually present. Processed media were then extracted with TCA 25% (1:1) (see Appendix I Materials and Methods) and then subjected to immunoblot. As shown in Figure 11, a 50 kDa YB-1 positive signal was detected in all samples; in particular, the amount of secreted YB-1 protein significantly peaked after 60' of treatment. Conversely, the ribonuclease inhibitor (RNH1), a not secreted protein whose abundance in HEK293T cytoplasm is comparable to that of YB-1 [46] was barely detectable (Figure 11, lower panel).

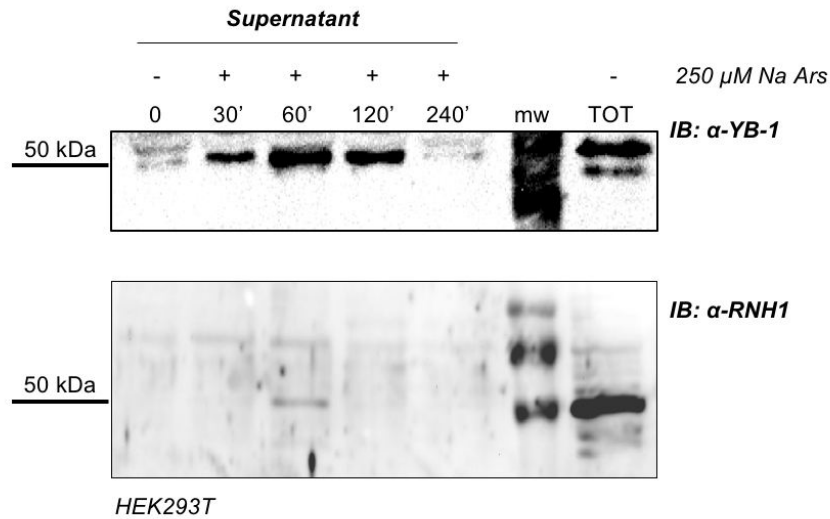


Figure 11. YB-1 is secreted after sodium arsenite stimulation.

Western blot of TCA precipitated supernatants of HEK293T cells. YB-1 secretion peaked at 60' after Na Ars treatment; RNH1 was used as a negative control of cell lysis.

Moreover, I transfected HEK293T cells with Myc-YB-1 expression plasmid and treated them with Na Ars 250 μ M for 30', 60' and 120'. Immunoblotting of TCA-precipitated CCM media showed the presence of Myc-tagged YB-1 only in arsenite-stimulated cells thus indicating that stressed cells can also secrete transfected YB-1 (Figure 12).

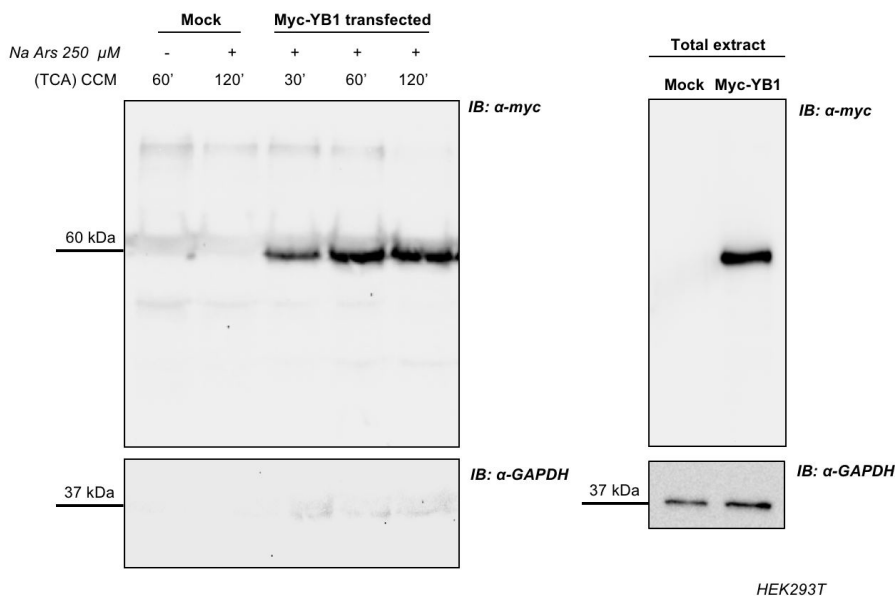


Figure 12. Transfected myc-YB-1 can be secreted by cells.

Western blot of TCA-precipitated CCM of HEK293T cells transfected with Myc-YB-1 and treated or not with 250 μ M Na Ars for 30' up to 120'. The presence of Myc-tagged YB-1 only in arsenite-stimulated cells indicates that stressed cells can also secrete transfected YB-1.

2. HEK293T YB1-GFP stable clone

Once defined the presence of a connection between cellular stress and YB-1 secretion I sought to generate a stable pool of cells constitutively expressing YB-1 as a GFP fusion protein to easily follow secretion and eventually uptake by receiving cells. Stable cell lines represent a permanent resource that can be stored under cryogenic conditions for long periods of time, retrieved, and cultured to provide a consistent and reliable level of sustained gene expression [47]. HEK293T stable clones can be generated to produce high quantity of recombinant proteins. Therefore, I transiently transfected HEK293T cells with YB-1-GFP cDNA cloned in pcDNA6/V5-His, a vector derived from pcDNATM3.1(+) (Invitrogen). Cells (5.0×10^5) were seeded in order to reach 80% confluence the day after; lipofection was performed using pcDNA6/V5-HisA-YB-1-GFP and peGFP-C1 empty vector as control [48]. 48 hours after transfection cells were analysed by immunoblot to evaluate the level of YB-1-GFP exogenous expression. Transfected YB-1-GFP was highly expressed in HEK293T cells (Figure 13a). Direct fluorescence, acquired by Nikon Eclipse 800 microscope, showed a prevalent cytoplasmic localization for YB-1-GFP (Figure 13b).

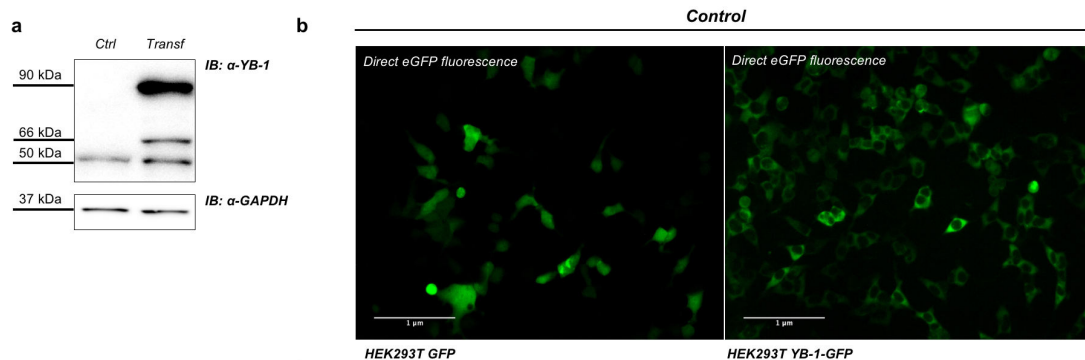


Figure 13. YB-1-GFP fusion protein is cytoplasmic. a) western blot of total extract from HEK293T transfected with mock (Ctrl) and pcDNA6/V5-HisA-YB-1-GFP (transf); GAPDH was used as loading control. b) direct eGFP fluorescence acquisition images.

The next step was to produce a pool of clones of HEK293T stably expressing YB-1-GFP or GFP alone. YB-1-GFP expressing cells were selected with blasticidin while G418 was used for selection of peGFP-C1 stable pool. After 4 weeks, 91% of selected cells were GFP positive. It is known that YB-1 is involved in cell proliferation [49], and total protein amount is crucial for the correct behaviour of cells; for this reason I evaluated the proliferation rate of YB-1-GFP expressing cells, where YB-1 protein amount was increased compared to HEK293T. Compared to the parental cell line, YB-1-GFP expressing cells grew slightly faster, but reach a plateau earlier (Figure 14).

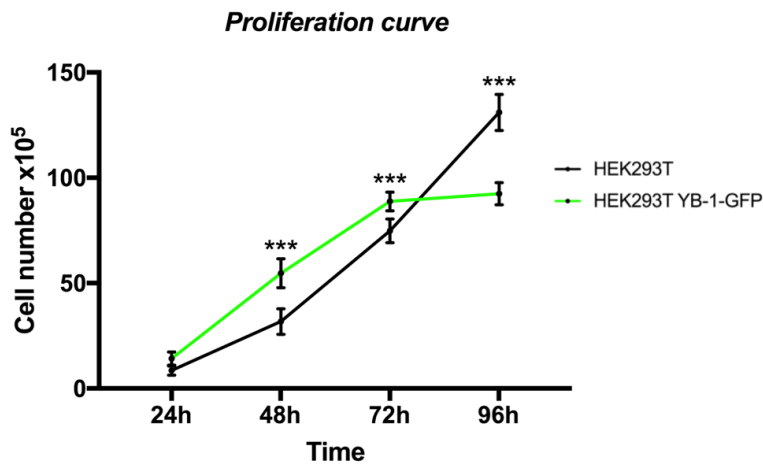


Figure 14. HEK293T YB-1-GFP grow faster than HEK293T.

Cell proliferation profile of HEK293T and HEK293T YB-1-GFP from time 0 (seeding time) to 96 hours (2-way ANOVA and Sidak's multiple comparisons test, $P < 0.001^{***}$; see also Appendix II, table 1).

2.1 Lack of functionality of the clone

To examine YB-1-GFP protein localization under oxidative stress I treated HEK293T YB-1-GFP cells with sodium arsenite, hydrogen peroxide (H_2O_2) and performed heat shock. By direct fluorescence acquisition, I observed that YB-1 fusion protein was detected in unusual GFP-positive aggregates that were abnormal in both dimension and shape (Figure 15).

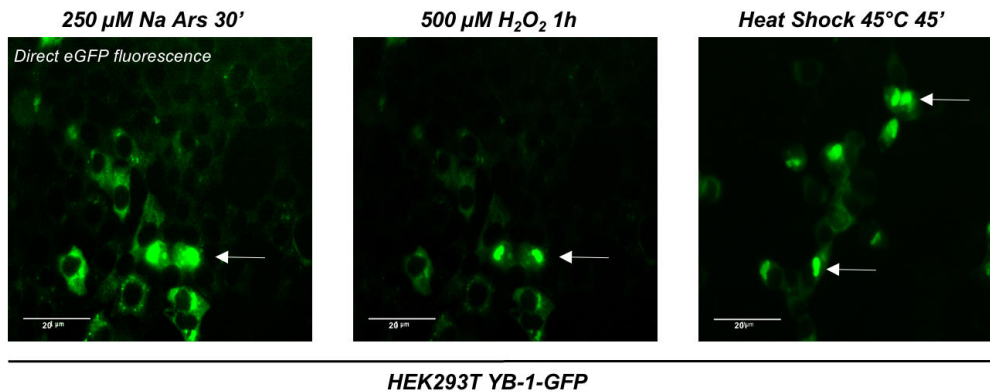


Figure 15. HEK293T YB-1-GFP cells form aberrant SGs after oxidative and physical insults.

Direct eGFP fluorescence acquisition of HEK293T-YB-1-GFP treated with 250 μM sodium arsenite, 500 μM H_2O_2 or subjected to heat shock (45°C for 45'); arrows indicate aberrant SGs.

Even though in normal conditions the GFP fusion protein behaved like the endogenous one and was localized in the right subcellular compartment, I hypothesized that the presence of the huge GFP tag (27 kDa) and the fact that the unstructured YB-1 C-terminus folds depending on the molecular partner [50], may have caused an incorrect folding of YB-1-GFP fusion protein (Figure 16).

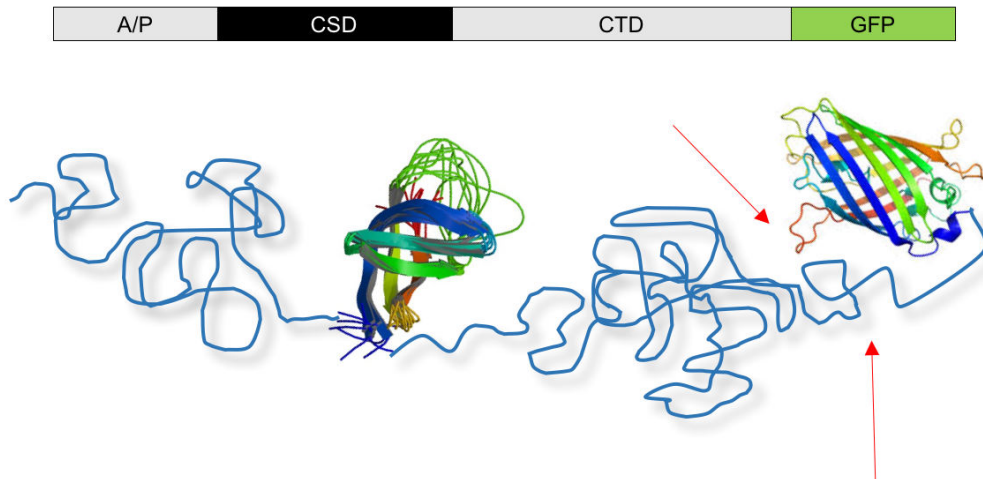


Figure 16. Putative structure of YB-1-GFP protein. The GFP tag could hamper YB-1 correct folding and function (red arrows).

Moreover, as demonstrated by MTT and trypan blue assays (Figure 17a and b) I found an increase sensitivity of YB-1-GFP cells to oxidative stress, suggesting that the overexpression of YB-1 with an incorrect form, alters cells responsiveness to stress stimuli.

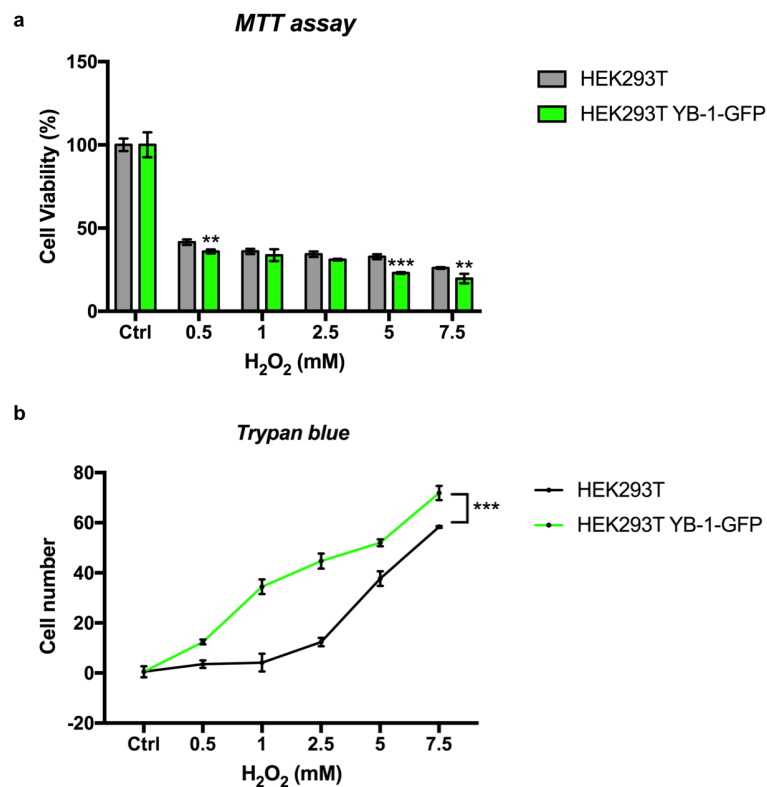


Figure 17. HEK293T YB-1-GFP are more sensitive to hydrogen peroxide. MTT assay (a) and trypan blue count (b) of HEK293T and HEK293T YB-1-GFP after treatment with the indicated concentrations of hydrogen peroxide (2-way ANOVA and Sidak's multiple comparison test, *** $p < 0.001$ and ** $p < 0.002$; see also Appendix II, table 1).

Given that HEK293T YB-1-GFP showed an altered stress response I decided do not adopt this model for further studies on stress-induced secretion.

3. Conclusions

The concept of protein equilibrium for YB-1 is essential. Its deficiency or excess can induce pathological conditions or unhealthy situations [13].

It is well documented, for example, that mRNAs fate in the cytoplasm is dependent also on YB-1/mRNA ratio, which in turn relies on YB-1 expression and amount. The quantity, and also the localization of the protein, is definitely important for many cellular events to happen.

For all those reasons it appeared quite interesting and unexpected that the total YB-1 protein amount decreased after oxidative treatments in HEK293T cells. This was astonishing considering also YB-1 relevance in SGs formation.

One possible explanation was the existence of a mechanism through which cells facing stress release YB-1.

On behalf of the experiments performed, I can postulate that YB-1 secretion is the result of an active mechanism and not a passive release.

These findings could open to the possibility that secreted YB-1 works as molecular signal, perhaps for neighbouring cells, to signal the occurring of unhappy and harmful situation.

Ideally, the possibility to have a modified form of the protein could have been very useful to simplify the observation of the secretion. I attempted to perform live-cell immunofluorescence experiments, using HEK293T YB-1-GFP as *YB-1-donor* cells, but without success. In fact, YB-1-GFP, produced for this purpose, was ineffective, because it led to the formation of aberrant SGs, probably for steric issues. Moreover, YB-1-GFP fusion protein was not secreted, neither in physiological conditions, nor after exposure to oxidative stressors.

On the contrary, other tagged-YB-1 forms, for example myc-YB-1, were successfully secreted after oxidative stimuli. This result was really interesting because underlines the fact that cells are able to secrete also non-endogenous form of YB-1, suggesting that YB-1 bears a sort of signal which makes it *secretable*.

CHAPTER III

1. Extracellular YB-1 (exYB-1)

Once excluded the possibility to use the YB-1-GFP expressing cells to follow the secretion and uptake of YB-1 protein, to analyse the effects of extracellular YB-1 on receiving cells, I prepared a YB-1 enriched fraction from HEK293T conditioned cell culture medium (CCM-YB-1) by ammonium sulphate precipitation followed by HPLC purification. Furthermore, I produced a recombinant YB-1 from *E. coli*, which accumulated mainly in bacterial cytosolic fraction.

The whole procedure of recombinant expression and purification was performed in collaboration with Dr. E Pizzo and Dr. A. Bosso of the University of Naples Federico II.

1. Production of human recombinant YB-1 (rYB-1) in bacterial host

Human YB-1 cDNA sequence was amplified from pEX-A2 plasmid (Eurofins Genomics, Germany) and inserted into the pET22b (+) expression vector upstream to a His-Tag sequence to facilitate the purification of the recombinant protein (for detailed procedure see Appendix I, Materials and Methods). The expression plasmid produced, was used then to transform competent *E. coli* strain BL21(DE3) (New England BioLabs, USA).

I choose *Escherichia coli* as host since it facilitates protein expression by its relative simplicity, its inexpensive and fast high density cultivation and the well-known genetics. Cells were grown at 37 °C to an $A_{600\text{ nm}} = 0.7$, induced with 0.6 mM isopropyl-1-thio-d-galactopyranoside (IPTG) and grown overnight.

By Western blot analysis I found that recombinant YB-1 was successfully expressed upon induction with IPTG and that it accumulated almost completely in bacterial cytosolic fraction (Figure 18), thus avoiding any effort for the redirection from inclusion bodies into the soluble cytoplasmic fraction.

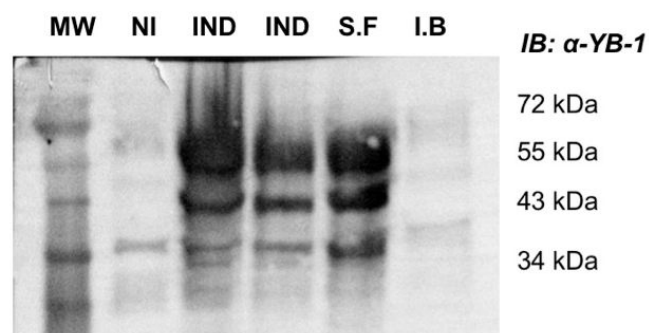


Figure 18. rYB-1 production. Western blot of bacterial lysate revealed with anti-YB-1, before (lane NI not induced) and after induction (lane IND induced) with IPTG; the amount of YB-1 protein is relevant in the soluble fraction (lane SF) and almost absent in inclusion bodies (lane IB).

Bacterial cells were harvested by centrifugation, resuspended in Tris-acetate buffer (pH 8.0) and subjected to sonication in presence of protease inhibitors. After three washes inclusion bodies were separated from cytosolic soluble fraction.

Recombinant YB1 was purified performing a two-step procedure composed by an immobilized metal ion affinity chromatography (IMAC) followed by a reverse phase chromatography.

Figure 19a shows the affinity chromatography elution profile. Fraction 3,5,7,8,9, and 11 were loaded on polyacrylamide gel to check the ongoing purification (Figure 19b).

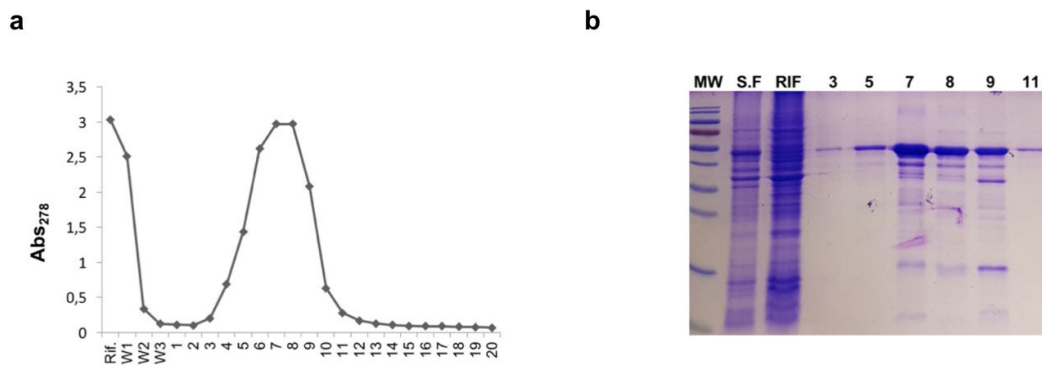


Figure 19. Affinity chromatography.

a) affinity chromatography on HisTrap resin; *Rif* indicates proteins without his-tag, eluted even before the elution buffer; W1-W3 resin washes; 1-20 eluted fractions; **b)** fractions 3-5-7-8-9-11 were loaded on polyacrylamide gel; coomassie stain indicated the presence of putative YB-1.

Then, I performed a step of purification by HPLC reverse phase chromatography (for further details see Appendix I, Materials and Methods).

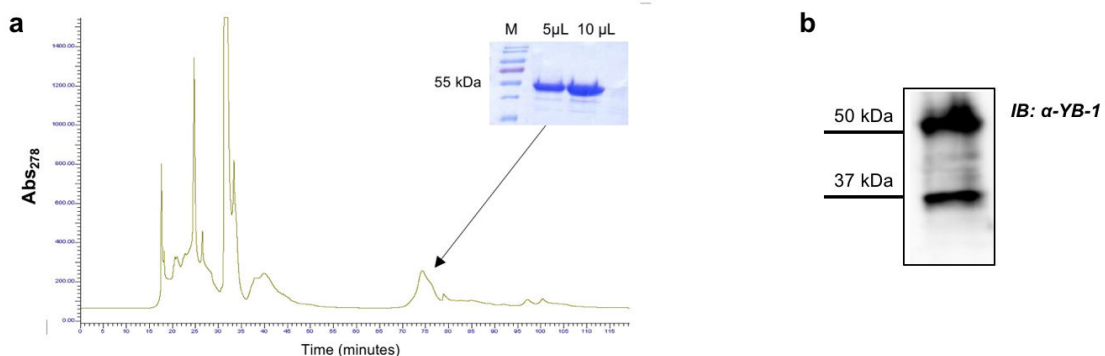


Figure 20. Reverse phase chromatography reveals that two YB-1 major forms are purified.

a) reverse phase chromatography of fractions obtained by the first step of affinity chromatography; two different volumes of the prior elution peak were loaded on gel. **b)** western blot of full purified fractions showing 50 kDa and 37 kDa canonical YB-1 bands.

As shown in Figure 20a the prior elution peak was observed after 75 minutes of elution; aliquots of the elution peak were loaded on polyacrylamide gel to check the process. SDS-PAGE revealed a major 50 kDa band that was consistent with previous purification steps and with YB-1 molecular weight. Next, I dialysed the positive fraction to further purify the protein and performed immunoblot with YB-1 antibodies to finally identify the protein (Figure 20b).

1.2 Production of Culture Medium derived YB-1 (CCM-YB-1)

Conditioned culture medium (CCM) was prepared by seeding HEK293T cells on Poly-D-lysine pre-treated wells in order to minimize cell detachment; the day after the culture medium was collected, and centrifuged to discard any cells and debris that may be present; medium was then sterilized by filtration.

Media were subjected to three subsequent steps of ammonium sulphate (Sigma-Aldrich, St Louis) precipitation, 30%, 70% and 100%, determining proteins salting out. At each step, media were centrifuged and protein precipitated were analysed by SDS-PAGE and immunoblot.

YB-1 positive forms were extracted mostly with 70% of ammonium sulphate. As shown in Figure 21, both 50 and 37 kDa form of YB-1 were detectable in the majority of protein enriched fractions. Moreover, I was also able to detect smaller YB-1-derived peptide bands.

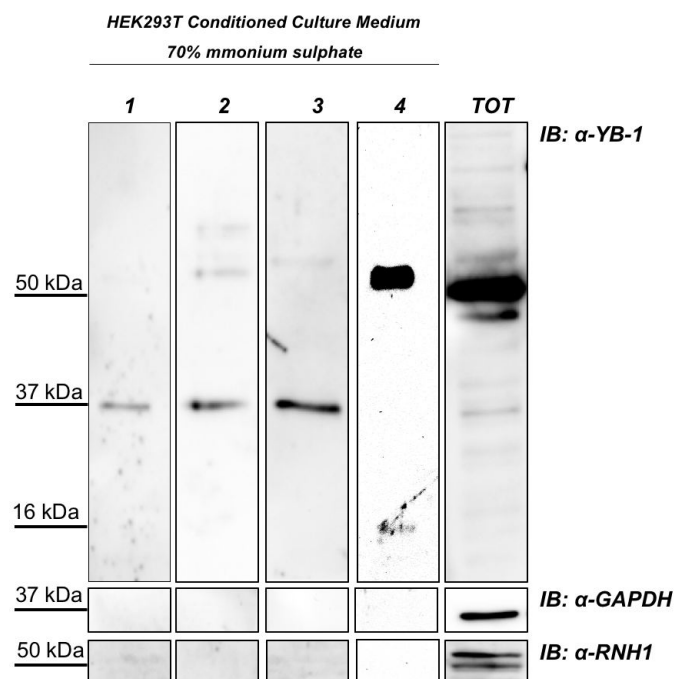


Figure 21. 70% Ammonium sulphate extracted fraction are the most promising. Western blot of different CCMs (from 1 to 4) extracted with 70% of ammonium sulphate and immunorevealed with YB-1. Different signals were detected depending on the samples. In sample 1 only a 37 kDa band was visible; in samples 2 and 3, 37 and 50 kDa bands were detectable; in lane 4 only a huge 50 kDa form was detectable; GAPDH and RNH1 were used to ensure the absence of cytoplasmic protein due to cell lysis. A total protein extract sample is also shown.

As shown in Figure 21, YB-1 pattern in enriched fractions from different CCM samples was different. Given that the 37 kDa form is associated to DNA damage, I postulated

that a higher prevalence of the 37 kDa fragment may be either linked to more damaged cells or to spontaneous limited YB-1 proteolysis [51]. This interpretation could be consistent with the fact that YB-1 secretion is a very dynamic phenomenon, not just a release of proteins by cells. On the other hand, hence, the presence of a huge 50 kDa band in lane 4 could be connected to more healthy cells.

1.3 Mass Spectrometry analysis

To finally confirm the identity of purified YB-1 proteins, I resolved CCM-YB-1 and rYB-1 in a polyacrylamide gel, stained it with colloidal coomassie and excised the YB-1 positive bands for Mass Spectrometry analysis. This part of the project was done in collaboration with Prof. A. Amoresano from University of Naples *Federico II*.

Each band was subjected to *in-situ* tryptic digestion and peptides eluted from the gel were analysed by LTQ-Orbitrap mass spectrometer. By matching MS and MSMS data obtained from the mass spectrometer and peptide sequence databases by Mascot search engine, a high sequence coverage of 79% for R1 band (rYB-1 band 1 in Figure 22), 78% for R2 (rYB-1 band 2 in Figure 22), 60% for S1 and 29% for S2 (CCM-YB-1 band 1 and 2 respectively, in Figure 22), with an error lower than 10 ppm. A list of peptides with relative score, sequence and modifications allowed me to unambiguously identify the YB-1 protein with a high sequence coverage and protein score (Appendix II, Table 2).

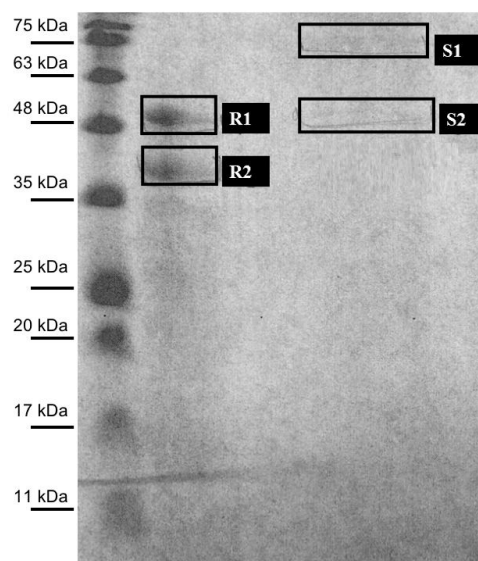


Figure 22. Band excision.

Image of polyacrylamide gel stained with colloidal coomassie blue. Excised YB-1 putative bands are indicated: bands R1 and R2 (recombinant YB-1); band S1 and S2 (Na Ars treated CCM-derived sample).

2. Functional analysis of exYB-1

2.1 Extracellular YB-1 exerts anti-proliferative effects on receiving cell

We have previously demonstrated that intracellular YB-1 is implicated in keratinocyte proliferation and survival to oxidative stress [51,52].

To get an insight into the function of secreted YB-1 I evaluated the proliferative response of HaCaT cells to the addition of recombinant YB-1 and purified YB-1 from HEK293T cell culture medium (CCM-YB-1).

YB-1 is normally released in the culture medium by HEK293T cells but not by HaCaT or CaCo2 cells even though all these cell lines express high level of endogenous YB-1. This may depend on a particular pathway constitutively activated in HEK293T cells or may rely on specific post-translational modifications occurring in HEK293T and possibly other cell contexts facilitating YB-1 extracellular release.

HaCaT cells were incubated for the indicated time with increasing amounts (5.0, 7.5 and 10 µg/ml) of rYB-1 protein, CCM-YB-1 or Bovine Serum Albumin (BSA) as control in serum supplemented culture medium. As shown in Figure 23 (panels a and b), treatment with CCM-YB-1 or rYB-1 reduced the rate of proliferation of HaCaT cells while equivalent amounts of BSA were ineffective (Figure 23c).

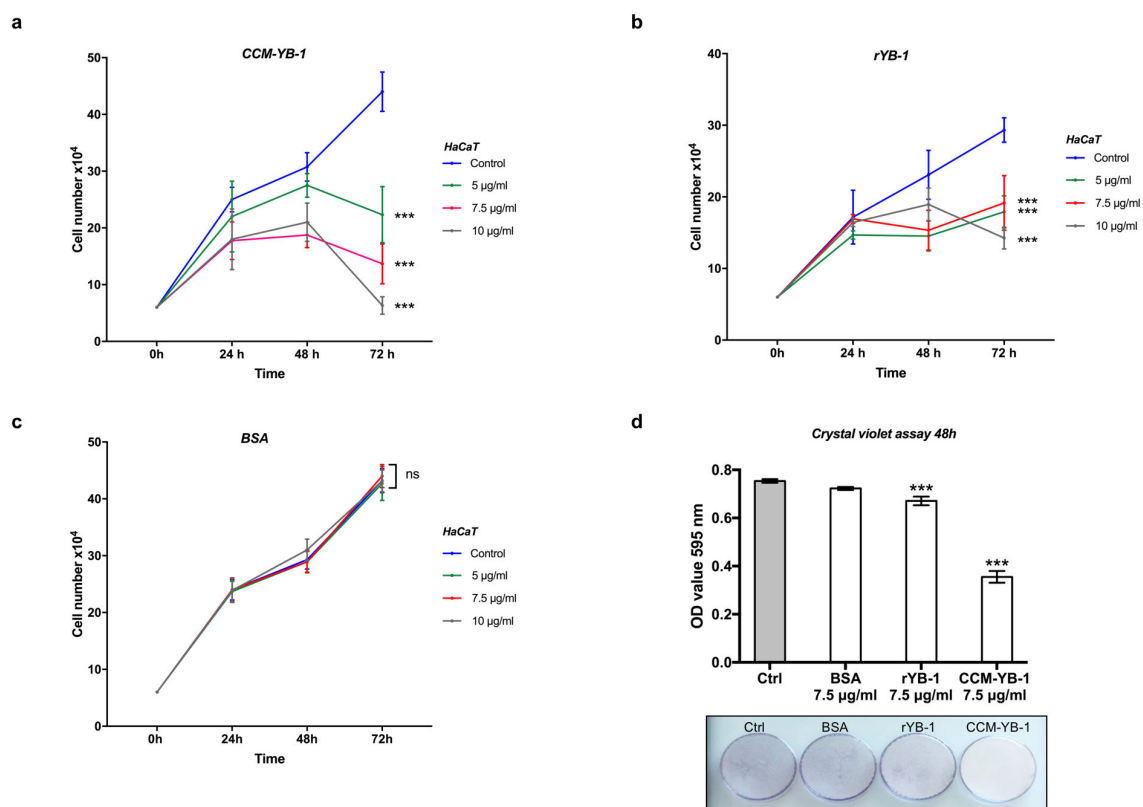


Figure 23. Extracellular YB-1 affects HaCaT cell proliferation.

Cell proliferation profile of HaCaT cells incubated with indicated concentrations of CCM-YB-1 (**a**), rYB-1 (**b**) or BSA (**c**); statistical analysis was performed using 2-way ANOVA followed by Dunnett's multiple comparisons test. Levels of significance are indicated (** $p < 0.001$, ns indicates no statistical significance; see also Appendix II, table 1). **d**) crystal violet assay of HaCaT cells treated with 7.5 µg/ml of CCM-YB-1, rYB-1, BSA or left untreated (Ctrl); (*bars*) optical absorbance at 595 nm is reported on the y-axis; (*image*) representative colorimetric evaluation. Statistical analysis was performed using 1-way ANOVA followed by Dunnett's multiple comparisons test. Levels of significance are indicated (** $p < 0.001$; see also Appendix II, table 1).

This effect was not cell type specific since it was also observed using HEK293T and CaCo2 as receiving cells (Figure 24).

Remarkably, compared to rYB-1, CCM-YB-1 exerted a stronger inhibitory effect on all cell lines tested (Figures 23-24a and b). This was confirmed by Crystal Violet Assay (CVA) where HaCaT cells treated with 7.5 $\mu\text{g/ml}$ of CCM-YB-1 for 48 hours showed a 47% reduction in viable cells compared to a 11% reduction obtained with the same amount of rYB-1 (Figure 23d).

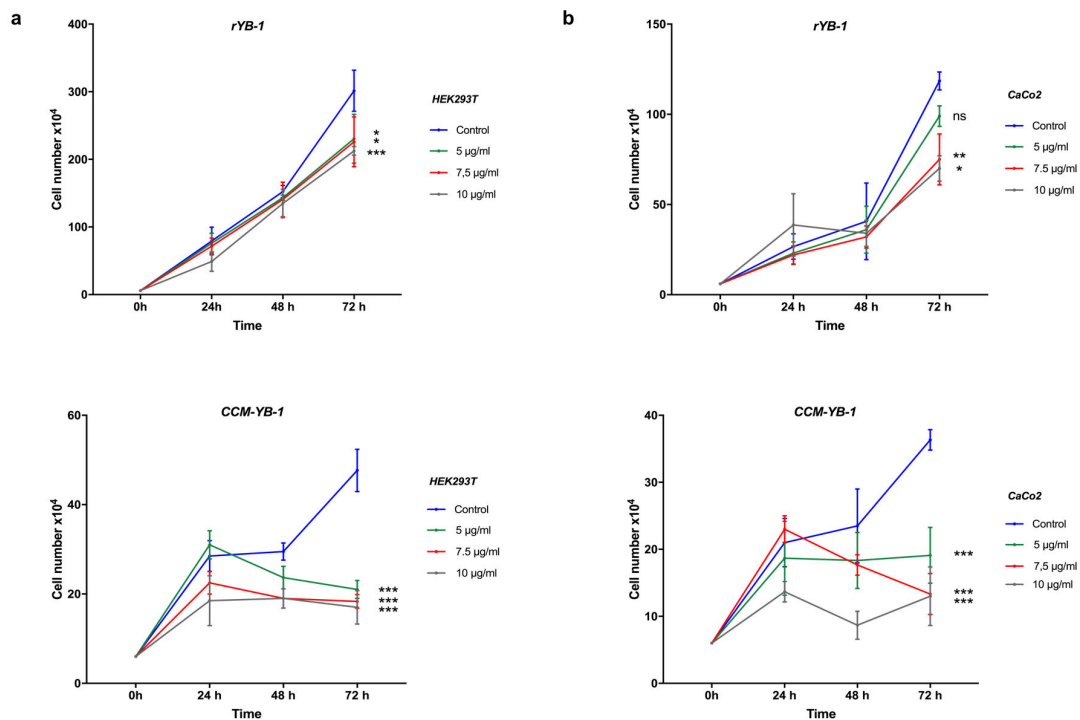


Figure 24. Extracellular YB-1 affects HEK293T and CaCo2 cell proliferation.

Cell proliferation profile of HEK293T (a) and CaCo2 (b) incubated with indicated concentrations of CCM-YB1 (upper panels) and rYB-1 (lower panels). Statistical analysis was performed using 2-way ANOVA followed by Dunnett's multiple comparisons test (** $p < 0.001$, ** $p = 0.003$, * $p = 0.03$, ns indicates no statistical significance; see also Appendix II, table 1).

Flow cytometry analysis of HaCaT cells treated with extracellular YB-1 revealed that cell proliferation slowdown was due to a G2/M cell cycle arrest (Figure 25a). Finally, to explore the molecular mechanism underlying inhibition of cell proliferation by extracellular YB-1, I analysed by quantitative PCR the mRNA level of *p21waf* and $\Delta np63\alpha$ in rYB-1 or CCM-YB-1 treated HaCaT cells. *p21WAF* is a relevant cell cycle marker that induces G1 and G2/M cell cycle arrest by inhibiting the kinase activity of CDK-cyclin complexes [53] while $\Delta Np63\alpha$ maintains the proliferative capacity of keratinocytes [54]. *p21waf* was strongly induced by both rYB-1 and CCM-YB-1 while $\Delta np63\alpha$ was significantly downregulated only by treatment with CCM-YB-1 (Figure 25b upper and lower panels). By western blot analysis we also confirmed reduction of

Δ Np63 α and induction of p21WAF at protein level (Figure 25 c and d). Moreover, according to the observed cell cycle arrest the level of cyclin A2 and cyclin D1 were also reduced (Figure 25c).

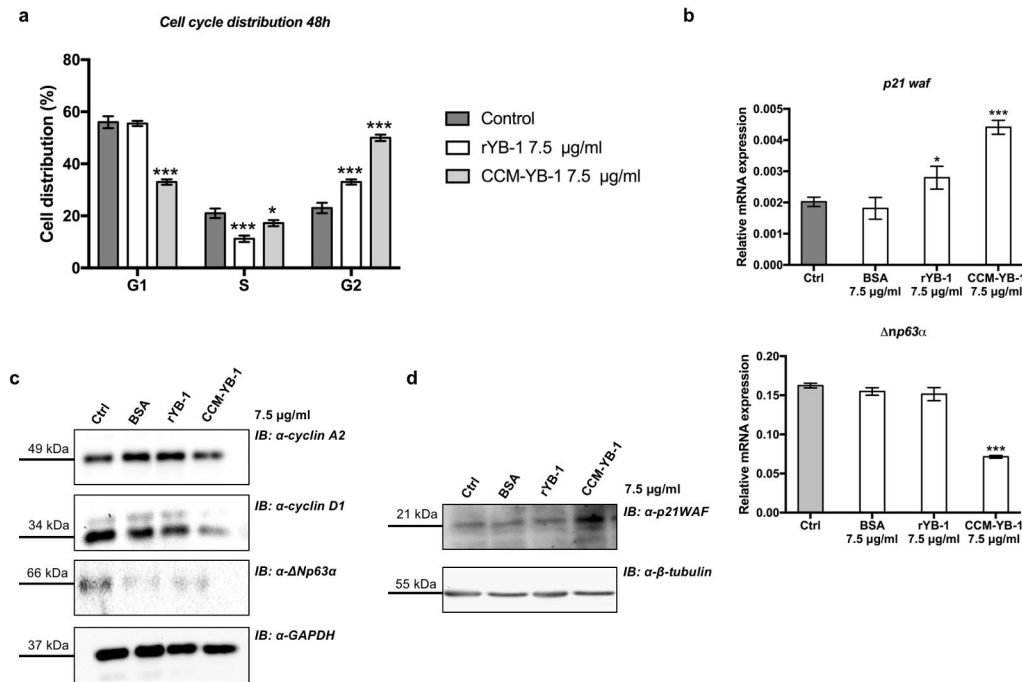


Figure 25. exYB-1 induced G2/M phase arrest.

a) cell cycle profile of HaCaT cells treated with 7.5 μ g/ml of CCM-YB-1, rYB-1, BSA or left untreated for 48 hours. Statistical analysis was performed using 2-way ANOVA followed by Dunnett's multiple comparisons test. Levels of significance are indicated (***) p <0.001, * p = 0.01; see also Appendix II table 1). **b)** RT-qPCR analysis of *p21waf* and Δ *np63 α in HaCaT cells treated with 7.5 μ g/ml of CCM-YB-1, rYB-1, BSA or left untreated (Ctrl) for 48 hours. Statistical analysis was performed using 1-way ANOVA followed by Dunnett's multiple comparisons test. Levels of significance are indicated (***) p <0.001, * p = 0.01; see also Appendix II table 1). **c-d)** western blot analysis of total extracts of HaCaT cell treated with rYB-1 and CCM-YB1 and revealed with the indicated antibodies. GAPDH and β -tubulin were used as loading control.*

2.2 Extracellular YB-1 induces TNF α

YB-1 has been previously described as a mediator of inflammatory processes [34,55]; I explored the possibility of a cross-talk between secreted YB-1 and the NF- κ B signalling pathway. Nuclear factor- κ B (NF- κ B) is a family of highly regulated dimeric transcription factors that play crucial roles in inflammatory responses (Nishikori). I first examined the activity of the NF- κ B promoter in HaCaT cells by transient transfection of a NF- κ B-driven GFP reporter construct. Cells were first transfected with the reporter construct (expressing GFP) and then treated with rYB-1 or CCM-YB1 for 24 hours. Western blot analysis of total extracts from YB-1 treated HaCaT cells showed that both forms of YB-1 protein were able to induce the NF- κ B promoter (Figure 26).

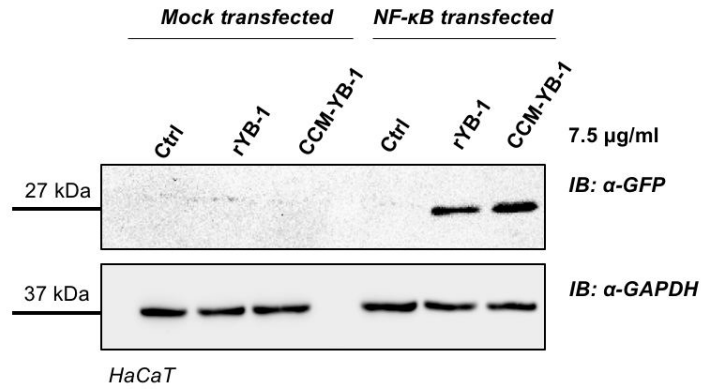


Figure 26. rYB-1 and CCM-YB-1 induce NF-κB-driven GFP expression.

Western blot of total extracts of HaCaT cells transiently transfected with a Mock plasmid or NF-κB-driven GFP reporter construct. GAPDH was used as loading control.

Tumor Necrosis Factor α (TNF α) is one of the most potent physiological inducers of the nuclear transcription factor NF-κB [56]. Therefore, I analysed the effect of rYB-1 and CCM-YB-1 treatments on TNF α protein expression. HaCaT cells were treated with increasing amount of rYB-1 and CCM-YB-1. Then, I performed immunoblot on total cell extracts. As shown in Figure 27, TNF α was induced in a time-dependent way and after 24 hours it was significantly increased in exYB-1 treated cells.

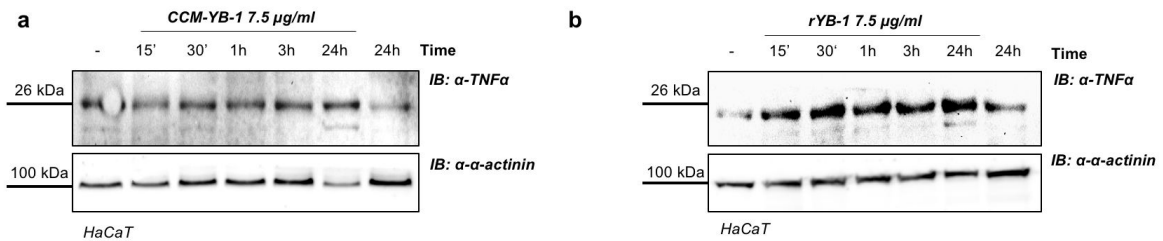


Figure 27. CCM-YB-1 and rYB-1 induce TNF α protein.

Western blot of total protein extract from HEK293T treated with increasing concentrations of CCM-YB-1 (a) or rYB-1 (b). Actinin was used as loading control.

3. Conclusions

During my PhD I have reported evidences that the extracellular release of YB-1 by HEK293T is not the result of a passive mechanism, but follows a rationale. In other cell types, such as CaCo2 and HaCaT cells, even if the general YB-1 behaviour is conserved and the protein is abundant as in HEK293T cells [14,51,52] no YB-1 secretion occurs. Moreover, it was previously reported that LPS induces YB-1 secretion in primary monocytes and in MonoMac-6 (MM6) cells [35] and that YB-1 is secreted from macrophages but not dendritic cells [33]. Based on all these observations I can reasonably conclude that secretion of YB-1 upon oxidative and inflammatory stimuli is cell-type dependent and that enhanced level of YB-1 in the extracellular environment is a clear sign of cellular stress. The production of a recombinant form of the protein and the purification of a fraction from conditioned culture medium, allowed me to have two *tools* to perform functional studies on receiving cells. Conditioned culture medium derived YB-1 (CCM-YB-1) represents the protein (or parts of it) which is secreted by cultured cells, so all the modifications needed for the secretion should be preserved. Instead, recombinant YB-1 (rYB-1), being processed in bacteria, is an unmodified form of the protein. Such differences in concept are also visible in practice, as indicated by Mass Spectrometry analysis and western blot.

Referring to the major molecular pathway in which YB-1 is involved [13] I decided to verify possible effects on cell proliferation and inflammation. As receiving cells, after different preliminary tests, I choose HaCaT cells which offer a well-studied and simplified model of the skin [52]. Treatments were performed mostly with a fixed concentration of exYB-1 (7.5 µg/ml) as indicated in the text, because, among all concentration tested, was the one which gave reproducible and consistent results.

Both extracellular YB-1 forms seem to negatively control cell proliferation inducing a G2/M phase arrest. The effect of CCM-YB-1 is stronger compared to that of rYB-1, perhaps as a consequence of the post-post-translational modifications as discussed above.

As regards the inflammatory response, this is a really complex field which requires great expertise. Classic and alternative inflammation pathway relies on the activity of NF-κB proteins, for this reason I decided to test the activity of NF-κB promoter after treatments with exYB-1, by monitoring GFP expression, as preliminary experiment. Both CCM-YB-1 and rYB-1 had an effect on NF-κB promoter activity and also in this case CCM-YB-1 seemed to be more active. The induction of TNFα was definitely more intense after treatment with rYB-1 rather than CCM-YB-1. Even if the interplay between NF-κB and TNFα is not always clear and linear, I can conclude that there is an involvement of inflammatory pathways. To summarize, it can be said that treatment with exYB-1 produce effect on cell proliferation and trigger inflammation response in immortalized keratinocyte. The same effect on cell proliferation was observed also in HEK293T cells, which have a complex karyotype, with two or more copies of each chromosome, including three copies of the X chromosome, and in CaCo2, cells of human adenocarcinoma. Those findings could represent a starting point to verify if secreted YB-1 could work not only as signal, but also as effector molecule. Further investigations should be extended to un-transformed cell lines, to verify the potential role of YB-1 as anti-proliferative agent for cancer cells.

CHAPTER V

Collaborations

1. Exploring molecular cell response to oxidative stress

Endogenous reactive oxygen species (ROS) are by-products of the aerobic metabolism of cells and have an important signalling role as secondary messengers in various physiological processes, including cell growth and development [71]. However, the excessive production of ROS as well as the exposure to exogenous ROS, originated, for example, from xenobiotics or foods, can cause protein oxidation, lipid peroxidation and DNA damages leading to cell damages and a number of health disorders. ROS accumulation has been associated with diverse pathogenesis, among them, for instance, neurodegenerative diseases, progression of arteriosclerosis and inflammatory bowel diseases. During my PhD I have contributed to various studies aimed to understand the effects of plant extracts and bacterial spores on mammalian cells, monitoring cells response to ROS.

1.1 Plant extracts are an important source of bioactive compounds for many drug discovery programs

Plant extracts are an important source of bioactive compounds for many drug discovery programs. Given the chemical complexity, however, the identification and characterization of bioactive compounds in crude plant extracts still remain a big challenge. Moreover, complex mixtures of phytochemicals generally combine the advantage of targeting multiple molecular pathways so that a desired biological response may be due to a mixture of different bioactive components. *Uncaria tomentosa* (Willd.) DC. (Rubiaceae), also known as *uña de gato*, a plant that grows wild in the upper Amazon region of Peru and Cayenne pepper (*Capsicum*), a spicy staple of many foods, have been widely used in folk medicine to treat several health conditions including cancer. I have contributed to the study of the effects of *Uncaria Tomentosa* and *Capsicum annuum fiesta* on squamous carcinoma cells and immortalized HaCaT keratinocytes, in order to provide molecular evidence supporting its therapeutic use against this type of cancer.

Briefly, we have produced an aqueous extract from *Uncaria tomentosa* (UT-ex) and *Capsicum* and we have evaluated cell proliferation, apoptosis and the level of reactive oxygen species following treatments. UT-ex affected cell cycle progression and reduced cell viability in a dose and time-dependent manner.

We have exploited the activity of the 37 kDa pro-survival YB-1 form, which is involved in DNA damage repair interacting with Mre11 and Rad50 complexes, providing cellular protection from oxidative stress [13,20,23].

Our data indicate that UT-ex-induced cell death can be ascribed, at least in part, to its ability both to induce oxidative DNA damage and antagonize the mechanism of DNA repair relying upon YB-1 activity. *C. annuum fiesta*, instead, exerts a protective role reducing intracellular ROS levels in a dose-dependent manner and stimulating cell viability at low concentrations without affecting cell proliferation.

See Appendix III, papers 3 and 4.

1.2 Protective and therapeutic effects of *Bacillus megaterium* spores on gut oxidative stress

A variety of molecules and live bacteria with antioxidant activity have been proposed as food additives to avoid ROS accumulation.

The research group of Prof. Isticato, from University of Naples *Federico II*, has demonstrated that spores of SF185, a human isolate of *Bacillus megaterium*, have intrinsic antioxidant activity and we analyse their effect *in vitro* and *in vivo*.

The antioxidant effects of SF185 spores were tested *in vitro* on CaCo-2 cells measuring the ability of spores to reduce the toxicity of hydrogen peroxide and *in vivo* in a murine model of dextran sodium sulphate (DSS) -induced oxidative stress.

In vitro, spores have a scavenging action reducing the amount of intracellular ROS and so inducing a protected state in cells. Pre-dosing mice with spores before the treatment with DSS protects the animals from the chemically-induced damages.

The consumption of spores-based products could prevent or reduce the damages caused by oxidative stress. The human origin of SF185, its strong antioxidant activity, and its protective effects both *in vitro* and *in vivo* led to propose the spore of this strain as a new probiotic for gut health.

See Appendix III, manuscript 2.

2. Studies on *D. Rerio* and *P. Andruzzii*

As mentioned before the possibility to analyse YB-1 protein as stress sensor in zebrafish come from previous information obtained during my stay at Institute of Toxicology and Genetics (ITG-KIT) in Germany, investigating the circadian rhythm in zebrafish.

Moreover, I had the possibility to join another research project regarding the different response to DNA damage of blind cavefish *P. Andruzzii*.

2.1 The tumor-associated YB-1 protein: new player in the circadian control of cell proliferation

In this study, using zebrafish as a vertebrate model system, we show that the nuclear localization of the Y-box binding protein 1 (YB-1), a regulator of cyclin expression and a hallmark of certain cancers, is robustly regulated by the circadian clock. We implicate clock-controlled changes in YB-1 SUMOylation as one of the mechanisms regulating its periodic nuclear entry at the beginning of the light phase. Furthermore, we demonstrate that YB-1 nuclear protein is able to downregulate cyclin A2 mRNA expression in zebrafish via its direct interaction with the cyclin A2 promoter. Thus, by acting as a direct target of cyclic posttranslational regulatory mechanisms, YB-1 serves as one bridge between the circadian clock and its cell cycle control. See Appendix III, paper 5.

2.2 Modulation of DNA Repair Systems in Blind Cavefish during Evolution in Constant Darkness

In a comparative study using zebrafish and the Somalian blind cavefish, *Phreatichthys andruzzii*, we reveal that during evolution for millions of years in continuous darkness, photoreactivation DNA repair function has been lost in *P. andruzzii*. We demonstrate that this loss results in part from loss-of-function mutations in pivotal DNA-

repair genes. Specifically, C-terminal truncations in *P. andrussii* DASH and 6-4 photolyase render these proteins predominantly cytoplasmic, with consequent loss in their functionality. In addition, we reveal a general absence of light-, UV-, and ROS-induced expression of *P. andrussii* DNA-repair genes. This results from a loss of function of the D-box enhancer element, which coordinates and enhances DNA repair in response to sunlight. Our results point to *P. andrussii* being the only species described, apart from placental mammals, that lacks the highly evolutionary conserved photoreactivation function. We predict that in the DNA repair systems of *P. andrussii*, we may be witnessing the first stages in a process that previously occurred in the ancestors of placental mammals during the Mesozoic era.

See Appendix III, paper 6.

3. A novel approach to quantify Wound Healing closure dynamic

The Wound Healing (WH) assay is widely used to investigate cell migration in vitro, in order to reach a better understanding of many physiological and pathological phenomena. Several experimental factors, such as uneven cell density among different samples, can affect the reproducibility and reliability of this assay, leading to a discrepancy in the wound closure kinetics among data sets corresponding to the same cell sample. Together with the group of Prof. S. Caserta from University of Naples *Federico II*, we observed a linear relationship between the wound closure velocity and cell density, and suggested a novel methodological approach, based on transport phenomena concepts, to overcome this source of error on the analysis of the Wound Healing assay. In particular, we propose a simple scaling of the experimental data, based on the interpretation of the wound closure as a diffusion-reaction process. We applied our methodology to the MDA-MB-231 breast cancer cells, whose motility was perturbed by silencing or over-expressing genes involved in the control of cell migration. Our methodological approach leads to a significant improvement in the reproducibility and reliability in the in vitro WH assay.

See Appendix III, paper 7.

CONCLUDING REMARKS

YB-1 protein is biotechnologically relevant because is involved in different cellular processes both in physiological and in pathological conditions; for this reason the spectrum of applications is potentially unlimited. With the proper manipulation the protein could be used for many purposes, ranging from pharmaceutical drugs production to the creation of biomarkers and biosensors.

In this PhD project I have evaluated the connections between YB-1 protein secretion and cellular stress response in human cells.

My data point out that YB-1 protein secretion is enhanced as a direct consequence of oxidative stress. YB-1 secretion has to be intended as one of the signalling processes that cells set up while facing unhealthy or dangerous conditions. Cells experience stress as they are put into culture dishes, not only when are treated with stress-inducing chemicals or reagents. *In vitro* system constitutes an exemplification of a living organism, but they give the not trivial possibility to understand the basis of a specific phenomenon, and in the end, the possibility to create applications.

There is no accordance in literature about the precise mechanism by which YB-1 is secreted; as a matter of fact, different publications suggest the involvement of different machineries [10,37]. In my experience I have observed that YB-1 can undergo different post-translational modifications such as ubiquitination, SUMOylation, phosphorylation and acetylation [10,60,51]. Thus, is generally accepted that upon different stimuli, YB-1 is modified, processed accordingly and secreted. This would be in accordance with Mass Spectrometry data, (see Appendix II, table 2), which report modifications on the secreted forms I analysed.

The most followed hypothesis is the one which states that YB-1 is engulfed in exosome-like vesicles, which on turn, take contact with plasmatic membrane of receiving cells releasing their cargoes. On the other hand, this assumption would be a little in contrast with other publications which report that secreted YB-1 is internalized after the interaction with a receptor (i.e. Notch3) [34].

Understanding the precise secretion mechanism would be really interesting for developing proper delivery strategies using YB-1 or YB-1 derived peptides as therapeutic agent.

Beside the not yet completely understood secretion modality, once released the protein triggers a response in receiving cells.

During my investigations, I reported data on YB-1 induced cell cycle arrest in receiving cells, when treated with extracellular YB-1.

An effect on the cell cycle was somehow expected, because it is well known that endogenous YB-1 plays a role in controlling cell proliferation [10].

It is well reported, in fact, that YB-1 protein over-expression or down-expression can alter proliferation rates, inducing either complete cell cycle arrest or an increase of duplication rates depending on cell lines and cellular context.

Although data are still preliminary, I observed also a potential effect on NF- κ B pathway activation, highlighting that there is not only a single response to exogenous YB-1 treatment.

Moreover, it should be investigated if YB-1 works only as a signal molecule, so after secretion and uptake by neighbouring cells other molecules do trigger pathways, or if the protein itself directly induces a response. Clues would be indicated by understanding *how* YB-1 is secreted.

REFERENCES

1. Lim, W. A. Designing customized cell signalling circuits. *Nature Reviews Molecular Cell Biology* (2010). doi:10.1038/nrm2904
2. Zerbs, S., Frank, A. M. & Collart, F. R. *Bacterial systems for production of heterologous proteins. Methods in Enzymology* (2009). doi:10.1016/S0076-6879(09)63012-3
3. Reeves, A. Z. *et al.* Engineering Escherichia coli into a Protein Delivery System for Mammalian Cells. *ACS Synth. Biol.* (2015). doi:10.1021/acssynbio.5b00002
4. Zahid, M. & D. Robbins, P. Protein Transduction Domains: Applications for Molecular Medicine. *Curr. Gene Ther.* (2012). doi:10.2174/156652312802762527
5. Viotti, C. ER to golgi-dependent protein secretion: The conventional pathway. in *Methods in Molecular Biology* (2016). doi:10.1007/978-1-4939-3804-9_1
6. Szul, T. & Sztul, E. COPII and COPI Traffic at the ER-Golgi Interface. *Physiology* (2011). doi:10.1152/physiol.00017.2011
7. Tartakoff, a, Vassalli, P. & Détraz, M. Comparative studies of intracellular transport of secretory proteins. *J. Cell Biol.* (1978). doi:10.1083/jcb.79.3.694
8. Cleves, A. E. Protein transport: The nonclassical ins and outs. *Curr. Biol.* (1997). doi:10.1016/S0960-9822(06)00148-5
9. Kohno, K., Izumi, H., Uchiumi, T., Ashizuka, M. & Kuwano, M. The pleiotropic functions of the Y-box-binding protein, YB-1. *BioEssays* (2003). doi:10.1002/bies.10300
10. Eliseeva, I. A., Kim, E. R., Guryanov, S. G., Ovchinnikov, L. P. & Lyabin, D. N. Y-box-binding protein 1 (YB-1) and its functions. *Biochem.* (2011). doi:10.1134/S0006297911130049
11. Matsumoto, S. *et al.* Ribonucleoprotein Y-box-binding protein-1 regulates mitochondrial oxidative phosphorylation (OXPHOS) protein expression after serum stimulation through binding to OXPHOS mRNA. *Biochem. J.* (2012). doi:10.1042/BJ20111728
12. Matsumoto, K. & Wolffe, A. P. Gene regulation by Y-box proteins: Coupling control of transcription and translation. *Trends in Cell Biology* (1998). doi:10.1016/S0962-8924(98)01300-2
13. Lyabin, D. N., Eliseeva, I. A. & Ovchinnikov, L. P. YB-1 protein: Functions and regulation. *Wiley Interdisciplinary Reviews: RNA* (2014). doi:10.1002/wrna.1200
14. Di Costanzo, A. *et al.* The p63 protein isoform $\Delta Np63\alpha$ modulates Y-box binding protein 1 in its subcellular distribution and regulation of cell survival and motility genes. *J. Biol. Chem.* (2012). doi:10.1074/jbc.M112.349951
15. Yang, W. H. & Bloch, D. B. Probing the mRNA processing body using protein macroarrays and 'autoantigenomics'. *RNA* (2007). doi:10.1261/rna.411907
16. Guarino, A. M. *et al.* Oxidative Stress Causes Enhanced Secretion of YB-1 Protein that Restrains Proliferation of Receiving Cells. *Genes (Basel)*. (2018). doi:10.3390/genes9100513
17. Evdokimova, V. *et al.* The major mRNA-associated protein YB-1 is a potent 5' cap-dependent mRNA stabilizer. *EMBO J.* (2001). doi:10.1093/emboj/20.19.5491
18. Blenkiron, C., Hurley, D. G., Fitzgerald, S., Print, C. G. & Lasham, A. Links between the oncoprotein YB-1 and small non-coding RNAs in breast cancer. *PLoS One* (2013). doi:10.1371/journal.pone.0080171

19. Yang, M. *et al.* Microvesicles secreted by macrophages shuttle invasion-potentiating microRNAs into breast cancer cells. *Mol. Cancer* (2011). doi:10.1186/1476-4598-10-117
20. Kim, E. R. *et al.* The proteolytic YB-1 fragment interacts with DNA repair machinery and enhances survival during DNA damaging stress. *Cell Cycle* (2013). doi:10.4161/cc.26670
21. Ohga, T. *et al.* Direct involvement of the Y-box binding protein YB-1 in genotoxic stress-induced activation of the human multidrug resistance 1 gene. *J. Biol. Chem.* (1998). doi:10.1074/jbc.273.11.5997
22. Anderson, P. & Kedersha, N. Stress granules: the Tao of RNA triage. *Trends in Biochemical Sciences* (2008). doi:10.1016/j.tibs.2007.12.003
23. Somasekharan, S. P. *et al.* YB-1 regulates stress granule formation and tumor progression by translationally activating G3BP1. *J. Cell Biol.* (2015). doi:10.1083/jcb.201411047
24. Lyons, S. M., Achorn, C., Kedersha, N. L., Anderson, P. J. & Ivanov, P. YB-1 regulates tiRNA-induced Stress Granule formation but not translational repression. *Nucleic Acids Res.* (2016). doi:10.1093/nar/gkw418
25. Mahboubi, H. & Stochaj, U. Cytoplasmic stress granules: Dynamic modulators of cell signaling and disease. *Biochimica et Biophysica Acta - Molecular Basis of Disease* (2017). doi:10.1016/j.bbadis.2016.12.022
26. Thomas, M. G., Loschi, M., Desbats, M. A. & Boccaccio, G. L. RNA granules: The good, the bad and the ugly. *Cellular Signalling* (2011). doi:10.1016/j.cellsig.2010.08.011
27. Morimoto, R. I. The heat shock response: Systems biology of proteotoxic stress in aging and disease. *Cold Spring Harb. Symp. Quant. Biol.* (2011). doi:10.1101/sqb.2012.76.010637
28. Protter, D. S. W. & Parker, R. Principles and Properties of Stress Granules. *Trends in Cell Biology* (2016). doi:10.1016/j.tcb.2016.05.004
29. Khong, A. & Jan, E. Modulation of Stress Granules and P Bodies during Dicrostovirus Infection. *J. Virol.* (2011). doi:10.1128/JVI.02220-10
30. Kedersha, N. *et al.* Stress granules and processing bodies are dynamically linked sites of mRNP remodeling. *J. Cell Biol.* (2005). doi:10.1083/jcb.200502088
31. Mukherjee, D. *et al.* The mammalian exosome mediates the efficient degradation of mRNAs that contain AU-rich elements. *EMBO J.* (2002). doi:10.1093/emboj/21.1.165
32. Hanssen, L. *et al.* YB-1 Is an Early and Central Mediator of Bacterial and Sterile Inflammation In Vivo. *J. Immunol.* (2013). doi:10.4049/jimmunol.1300416
33. Kang, S. *et al.* Differential control of interleukin-6 mRNA levels by cellular distribution of YB-1. *PLoS One* (2014). doi:10.1371/journal.pone.0112754
34. Frye, B. C. *et al.* Y-box protein-1 is actively secreted through a non-classical pathway and acts as an extracellular mitogen. *EMBO Rep.* (2009). doi:10.1038/embor.2009.81
35. Palicharla, V. R. & Maddika, S. HACE1 mediated K27 ubiquitin linkage leads to YB-1 protein secretion. *Cell. Signal.* (2015). doi:10.1016/j.cellsig.2015.09.001
36. Brandt, S. *et al.* Cold shock Y-box protein-1 participates in signaling circuits with auto-regulatory activities. *European Journal of Cell Biology* (2012). doi:10.1016/j.ejcb.2011.07.002
37. Shurtleff, M. J., Temoche-Diaz, M. M., Karfilis, K. V., Ri, S. & Schekman, R. Y-

- box protein 1 is required to sort microRNAs into exosomes in cells and in a cell-free reaction. *Elife* (2016). doi:10.7554/eLife.19276
38. Rauen, T. *et al.* YB-1 acts as a ligand for notch-3 receptors and modulates receptor activation. *J. Biol. Chem.* (2009). doi:10.1074/jbc.M109.046599
 39. Thomas, P. & Smart, T. G. HEK293 cell line: A vehicle for the expression of recombinant proteins. *J. Pharmacol. Toxicol. Methods* (2005). doi:10.1016/j.vascn.2004.08.014
 40. Aydin, H., Azimi, F. C., Cook, J. D. & Lee, J. E. A Convenient and General Expression Platform for the Production of Secreted Proteins from Human Cells. *J. Vis. Exp.* (2012). doi:10.3791/4041
 41. Anderson, P., Kedersha, N. & Ivanov, P. Stress granules, P-bodies and cancer. *Biochimica et Biophysica Acta - Gene Regulatory Mechanisms* (2015). doi:10.1016/j.bbagr.2014.11.009
 42. Patel, P. H., Barbee, S. A. & Blankenship, J. T. GW-bodies and P-bodies constitute two separate pools of sequestered non-translating RNAs. *PLoS One* (2016). doi:10.1371/journal.pone.0150291
 43. Kedersha, N. & Anderson, P. Mammalian Stress Granules and Processing Bodies. *Methods in Enzymology* (2007). doi:10.1016/S0076-6879(07)31005-7
 44. Aulas, A. *et al.* Stress-specific differences in assembly and composition of stress granules and related foci. *J. Cell Sci.* (2017). doi:10.1242/jcs.199240
 45. Budavari, S.; Smith, A.; Heckelman, P. E.; Assistant, E. The Merck index. *An Encycl. Chem. Drugs Biol.* (1989). doi:10.1126/science.226.4680.1250
 46. Haigis, M. C., Kurten, E. L. & Raines, R. T. Ribonuclease inhibitor as an intracellular sentry. *Nucleic Acids Research* (2003). doi:10.1093/nar/gkg163
 47. Saifudin, N., Ibrahim, N. & Anuar, N. Optimization in transfection and stable production of p-galactosidase in chinese hamster ovary cells. *Biotechnology* (2011). doi:10.3923/biotech.2011.86.93
 48. Troiano, A. *et al.* Y-box Binding Protein-1 Is Part of a Complex Molecular Network Linking Δ Np63 α to the PI3K/akt Pathway in Cutaneous Squamous Cell Carcinoma. *J. Cell. Physiol.* (2015). doi:10.1002/jcp.24934
 49. Miao, X. *et al.* Y-box-binding protein-1 (YB-1) promotes cell proliferation, adhesion and drug resistance in diffuse large B-cell lymphoma. *Exp. Cell Res.* (2016). doi:10.1016/j.yexcr.2016.07.003
 50. Kreto, D. A. *et al.* mRNA and DNA selection via protein multimerization: YB-1 as a case study. *Nucleic Acids Res.* (2015). doi:10.1093/nar/gkv822
 51. Ciani, F. *et al.* Anti-proliferative and pro-apoptotic effects of *Uncaria tomentosa* aqueous extract in squamous carcinoma cells. *J. Ethnopharmacol.* (2018). doi:10.1016/j.jep.2017.09.031
 52. di Martino, O. *et al.* Δ Np63 α controls YB-1 protein stability: evidence on YB-1 as a new player in keratinocyte differentiation. *Genes to Cells* (2016). doi:10.1111/gtc.12373
 53. Abbas, T. & Dutta, A. P21 in cancer: Intricate networks and multiple activities. *Nature Reviews Cancer* (2009). doi:10.1038/nrc2657
 54. McDade, S. S., Patel, D. & McCance, D. J. p63 maintains keratinocyte proliferative capacity through regulation of Skp2-p130 levels. *J. Cell Sci.* (2011). doi:10.1242/jcs.084723
 55. Raffetseder, U., Liehn, E. A., Weber, C. & Mertens, P. R. Role of cold shock Y-box protein-1 in inflammation, atherosclerosis and organ transplant rejection. *European Journal of Cell Biology* (2012). doi:10.1016/j.ejcb.2011.07.001
 56. Martin, a G. & Fresno, M. Tumor necrosis factor-alpha activation of NF-kappa

- B requires the phosphorylation of Ser-471 in the transactivation domain of c-Rel. *J. Biol. Chem.* (2000). doi:10.1074/jbc.M909396199
57. Beliaeva, N. F. *et al.* [Zebrafish as a model organism for biomedical studies]. *Biomeditsinskaia Khimiia* (2010). doi:10.1134/S1990750809040039
 58. Bradford, Y. M. *et al.* Zebrafish models of human disease: Gaining insight into human disease at ZFIN. *ILAR J.* (2017). doi:10.1093/ilar/ilw040
 59. Best, J. D. & Alderton, W. K. Zebrafish: An in vivo model for the study of neurological diseases. *Neuropsychiatric Disease and Treatment* (2008). doi:10.1006/dbio.2001.0201
 60. Pagano, C. *et al.* The tumor-associated YB-1 protein: new player in the circadian control of cell proliferation. *Oncotarget* (2016). doi:10.18632/oncotarget.14051
 61. Scott, G. R. & Johnston, I. A. Temperature during embryonic development has persistent effects on thermal acclimation capacity in zebrafish. *Proc. Natl. Acad. Sci.* (2012). doi:10.1073/pnas.1205012109
 62. Sfakianakis, D. G., Leris, I. & Kentouri, M. Effect of developmental temperature on swimming performance of zebrafish (*Danio rerio*) juveniles. *Environ. Biol. Fishes* (2011). doi:10.1007/s10641-010-9751-5
 63. McClelland, G. B., Craig, P. M., Dhekney, K. & Dipardo, S. Temperature- and exercise-induced gene expression and metabolic enzyme changes in skeletal muscle of adult zebrafish (*Danio rerio*). *J. Physiol.* (2006). doi:10.1113/jphysiol.2006.119032
 64. Moutaoufik, M. T. *et al.* UVC-induced stress granules in mammalian cells. *PLoS One* (2014). doi:10.1371/journal.pone.0112742
 65. Matsuki, H. *et al.* Both G3BP1 and G3BP2 contribute to stress granule formation. *Genes to Cells* (2013). doi:10.1111/gtc.12023
 66. Wilczynska, A. The translational regulator CPEB1 provides a link between dcp1 bodies and stress granules. *J. Cell Sci.* (2005). doi:10.1242/jcs.01692
 67. Kedersha, N. Evidence That Ternary Complex (eIF2-GTP-tRNA^{iMet})-Deficient Preinitiation Complexes Are Core Constituents of Mammalian Stress Granules. *Mol. Biol. Cell* (2002). doi:10.1091/mbc.01-05-0221
 68. Lefauve, M. K. & Connaughton, V. P. Developmental exposure to heavy metals alters visually-guided behaviors in zebrafish. *Curr. Zool.* (2017). doi:10.1093/cz/zox017
 69. Arunachalam, M., Raja, M., Vijayakumar, C., Malaiammal, P. & Mayden, R. L. Natural history of zebrafish (*Danio rerio*) in India. *Zebrafish* (2013). doi:10.1089/zeb.2012.0803
 70. Spence, R., Gerlach, G., Lawrence, C. & Smith, C. The behaviour and ecology of the zebrafish, *Danio rerio*. *Biological Reviews* (2008). doi:10.1111/j.1469-185X.2007.00030.x
 71. Schieber, M. & Chandel, N. S. ROS function in redox signaling and oxidative stress. *Current Biology* (2014). doi:10.1016/j.cub.2014.03.034
 72. Lin, S. *et al.* Integration and germ-line transmission of a pseudotyped retroviral vector in zebrafish. *Science* (80-.). (1994). doi:10.1126/science.8036514
 73. Avdesh, A. *et al.* Regular care and maintenance of a zebrafish (*Danio rerio*) laboratory: an introduction. *J. Vis. Exp.* (2012). doi:10.3791/4196

APPENDIX I

Materials and Methods

Plasmids and chemicals

The expression construct 5xMyc-YB-1 was previously described [60]. pcDNA 3.1B, used as control, was purchased by ThermoFisher Scientific (USA). pcDNA6/V5-His derived from pcDNATM3.1(+) (Invitrogen).

Sodium (meta)arsenite (NaAsO₂) (Sigma-Aldrich, St Louis, S7400); hydrogen peroxide (Sigma-Aldrich, St Louis, H1009); trichloroacetic acid (TCA) (Sigma-Aldrich, St Louis, T4885); Poly-D-lysine (Sigma-Aldrich, St Louis, P7405); cycloheximide (Sigma-Aldrich, St Louis, C7698).

Cell culture

HEK293T, human embryonic kidney cells, HaCaT, spontaneously immortalized keratinocytes from adult skin, and Caco-2 human colorectal adenocarcinoma cells, were purchased from Cell Line Service (CLS, Germany), cultured in humidified incubator at 37°C and 5% CO₂, and maintained in DMEM High Glucose (Gibco) supplemented with 10% Fetal Bovine Serum (Gibco), 1% L-Glutamine (Gibco) and 1% Pen-Strep solution (Gibco).

To increase HEK293T adhesion to glass/plastic surfaces, all plates and slips for immunofluorescence were treated with Poly-D-lysine 0.1mg/ml (Sigma-Aldrich, St Louis) before seeding cells.

The zebrafish PAC2 cell line [72] was propagated at 26°C in an atmospheric CO₂, non-humidified cell culture incubator; cells were cultured in L-15 (Leibovitz) medium (Gibco BRL) supplemented with 15% Fetal Bovine Serum (Sigma-Aldrich, St Louis), 100 units/ml penicillin, 100 µg/ml streptomycin and 50 µg/ml gentamicin (Gibco BRL). Cells were routinely checked for mycoplasma contamination, using a mycoplasma detection kit (abm, Canada).

Fish care, treatment and ethical statements

All husbandry and experimental procedures were performed in accordance with European Legislation for the Protection of Animals used for Scientific Purposes (Directive 2010/63/EU), the German (Animal Protection Law, BGBI. I, 1934, 2010). Research was also approved by the Local Government of Baden-Württemberg, Karlsruhe, Germany (35-9185.81/G-131/16). General license for fish maintenance and breeding: Az.: 35-9185.64.

Zebrafish (*Danio rerio*, Tubingen strain) were maintained according to standard procedures [73] in a re-circulating water system at 26°C and under 14:10 light:dark cycles. For each experiment 6 –12 months old zebrafish males or females were used. The caudal fins were amputated using razor blades following anesthesia with 0.02% w/v MS222 (3-aminobenzoate methanesulfonic acid, Sigma-Aldrich, St Louis).

Stereo-image of caudal fins were acquired using a Zeiss Stemi 305 microscope.

Heat Shock treatments in cells and adult zebrafish caudal fins

Cells cultured in petri dishes were abruptly placed on the surface of a pre-heated water bath at the indicated time points and temperatures by floating the Petri dishes on a water bath floater (Promega).

Following heat shock treatment, cells were processed for immunofluorescence analysis. For the heat shock recovery experiment, cells were returned to a 26°C incubator for the designated time.

For the analysis of mRNA expression during heat shock treatment, for the time points harvested at 3 and 6 hours from the onset of heat shock, the cells were exposed for 1 hour to heat shock and then returned to a 26 °C incubator for the remainder of the time course in order to avoid mortality due to prolonged exposure to the higher temperature.

Fins were gently placed in 2ml Eppendorf filled with complete cell culture medium (Leibovitz's L-15, Gibco BRL) and placed in a pre-warmed water bath at 45°C for the designated time or in a cell culture incubator at 26°C as a control.

Immunofluorescence microscopy in zebrafish cells and mammalian cells

6.0×10^4 PAC2 cells were seeded on coverslips and maintained in constant darkness for the subsequent 48 hours prior to receive the treatment. 3×10^4 HEK293T cells were seeded on Poly-D-lysine pre-treated coverslips, HaCaT and Caco-2 cells were seeded on not pre-treated surfaces; the day after cells were treated or left untreated. Following treatment, both mammalian and zebrafish cells were gently rinsed with 1X PBS and then fixed in PFA 3.7% for 10 and 15', respectively. After 3 washes with 1X PBS (10 minutes each), cells were washed twice with 0.01% Tween-PBS and blocked for 1 hour with a 1% BSA-0.01% Tween-PBS solution for PAC2 and with a 3% BSA solution for mammalian cells to avoid unspecific binding of antibodies. PAC2 cells were then incubated overnight at 4°C with the primary antibodies. Primary antibody incubation for mammalian cells was performed for 1 hour in dark at room temperature. After incubation with primary antibodies, cells were washed three times with 0.01% Tween-PBS (10 minutes each) and incubated with secondary antibodies for 45 minutes in darkness. Then, both PAC2 and HaCaT cells were incubated for 5 minutes in a DAPI solution (1:50000) (Sigma-Aldrich, St Louis) followed by 3 washes in 0.01% Tween PBS. Coverslips were immersed in a Dako mounting medium (Agilent).

All images were acquired using a Leica SPE confocal microscopy (63x oil immersion objective) or Carl Zeiss LSM 700 (63x oil immersion objective) microscope. Image processing and analysis were performed with Fiji (ImageJ) software.

Immunofluorescence microscopy in zebrafish adult caudal fins

After an overnight fixation of the fin-clips in Carnoy's solution (60% ethanol, 30% chloroform, 10% acetic acid) at 4°C, fins were incubated overnight in 100% Methanol and then subjected to sequential rehydration steps of 10' in 100%, 66% and 33% methanol in PBTX (1XPBS, 0.3% Triton X100). At this stage, fins were pre-incubated in PBTX plus 1% BSA blocking solution for 3 hours. Then the primary antibody was added and the samples were incubated at 4°C overnight. After several washes, samples were incubated at 4°C with the secondary fluorescent antibody overnight. DAPI staining was used for visualization of nuclei. The samples were mounting on glass slides.

All images were acquired using a Leica SPE confocal microscopy (63x oil immersion objective). Image processing and analysis were performed with Fiji (ImageJ) software.

Cell Viability assays

Cell viability was determined by the crystal violet assay (CVA) method, through a (3-(4,5-dimethylthiazol-2-yl)-2,5-diphenyl-tetrazolium bromide) MTT based assay, or through trypan blue count.

Cells were seeded in 96-well plate for MTT (8×10^3 cells), in 35mm dishes (2.5×10^5 cells) for CVA and in 12-well plates (1.5×10^5 cells) for trypan blue.

The day after plating, cells were treated or not. For crystal violet, dye uptake was measured at 570 nm using a spectrophotometer. Cell viability was calculated as dye intensity and compared with untreated samples.

For MTT, the optical absorbance was determined at 570 nm using an iMark microplate reader (Bio-Rad, USA). For trypan blue count, after treatment cells were gently rinsed with 1X PBS, trypsinized and collected. An aliquot was diluted 1:1 with trypan blue (Sigma-Aldrich, St Louis, MO).

Cell cycle analysis

3×10^5 cells were seeded and let grow for 24 hours; then cells were serum starved for 24 hours to achieve synchronization; the day after cells were treated with recombinant YB-1 or CCM-derived-YB-1 or left untreated for 24 hours. Cells were then trypsinized, collected in FACS Buffer (1% FBS, 0.25 mM EDTA in PBS) and centrifuged at 1200 rpm, 4 minutes, 4°C; for each sample the same number of cells (1×10^5) was processed. The cell pellet was resuspended in methanol, incubated on ice for 20 minutes and centrifuged at 1200 rpm, 5 minutes, 4°C. After a wash in FACS Buffer PBS, the pellet was incubated in FACS Buffer PBS, containing RNase A (Thermo-Fisher Scientific) 100 µg/ml for 20 minutes at RT. Propidium iodide (Sigma-Aldrich, St Louis, MO) was then added at a concentration of 50 µg/ml for 30 minutes at 4°C. Cell cycle analysis was performed on the BD Accuri C6 flow cytometer (BD Biosciences).

Cell proliferation analysis

6×10^4 HaCaT and Caco-2 cells were seeded in 12-well plate while HEK293T were seeded on pre-treated 12-well; cells were serum starved for 24 hours; after starvation recombinant or CCM-derived YB-1 were added at different concentrations. Every 24 hour cells were gently rinsed with 1X PBS, trypsinized and counted. The count was confirmed by Scepter 2.0 analysis (Millipore).

RNA silencing (siRNA) and transfections

Mammalian cells were transfected using Lipofectamine 2000 (Life Technology) according to the manufacturer's recommendations. Briefly, cells were seeded at 70-80% confluence (1.5×10^6) in 100-mm dishes and transiently transfected with different concentrations of plasmid (from 800 ng up to 1.5 µg).

YB-1 transient silencing was carried out with IBONI YB-1siRNA pool (RIBOXX GmbH, Germany) and RNAiMAX reagent (Life Technologies, CA, USA), according to the manufacturer's recommendations. Cells were seeded at 70-80% confluence (1.5×10^6) in 100-mm dishes and transiently silenced with IBONI YB1-siRNA at 100 nM final concentration.

All Star Negative Control siRNA, provided by Quiagen (Hilden, Germany), was used as negative control.

PAC2 cells were transfected using Fugene HD (Promega) according to the manufacturer's recommendations. A 4:1 ratio (4 μ l of Fugene HD reagent for each μ g of siRNA) was used. Briefly, cells were seeded at 70-80% confluence (1.5×10^6) in 100-mm dishes; after 48 hours of incubation in darkness, cells were transiently transfected with siRNA (100 nM final concentration). 24 hours after siRNA transfection, cells were treated or left untreated. All Star Negative Control siRNA, provided by Quiagen (Hilden, Germany), was used as negative control. Predesigned siRNAs for YB-1 were purchased from Riboxx (Germany) and listed below:

<i>zf YB-1_1</i>	<i>guide 5'-3'</i> AUUCUGUCACAUCUCUCCCC	<i>passenger 5'-3'</i> GGGGGAGAGAUGUGACAGAAUA
<i>zf YB-1_2</i>	<i>guide 5'-3'</i> UUCUCCUUAUCCUCCUCUCCCC	<i>passenger 5'-3'</i> GGGGGAGAGGAGGAUAAGGAGA
<i>zf YB-1_3</i>	<i>guide 5'-3'</i> UUUGCAAGCUUAGACGAUCCCC	<i>passenger 5'-3'</i> GGGGGAGAGGAGGAUAAGGAGAA
<i>h YB-1(pool)</i>	<i>guide 5'-3'</i> UUUAUCUUCUUCUUGCCGCCCCC	<i>passenger 5'-3'</i> UUAUUCUUCUUAUGGCAGCCCC
<i>h YB-1(pool)</i>	<i>guide 5'-3'</i> UUCAACAACAUCAAACUCCCC	<i>passenger 5'-3'</i> UCAUAUUUCUUCUUGUUGGCCCCC

Antibodies

Primary antibodies: anti-YB-1 raised against the region 1 to 100 of YB-1 protein (12148 Abcam); anti-YB-1 raised against amino acids 307-324 of hYB-1 (Sigma-Aldrich, St Louis, MO, Y0396 C-ter); anti-PABP1 (Sigma-Aldrich, St Louis, MO, clone 10E10); anti-Myc (Sigma-Aldrich, St Louis, MO, SAB21084786); anti-cyclin D1 (GT8912, Genetex); anti-cyclin A2 (GT2547, Genetex); anti-GAPDH (6C5 Santa Cruz Biotechnology); anti-PARP1 (Cell Signaling); anti-RNH1 (Sigma-Aldrich, St Louis, MO 436-450) anti- β -tubulin (H-235, Santa Cruz Biotechnology); anti-actinin (AT6/172, Abcam); anti-p21 WAF (1D21 Cell Signaling); anti- Δ Np63 α (4A4) (sc-8431 Santa Cruz Biotechnology); anti-vinculin (Sigma-Aldrich, St Louis, MO, V9131); anti-G3BP1 (611127 BD transduction Laboratories, BD Biosciences); anti-Histone H3 (9715 Cell Signaling).

Secondary fluorescent antibodies: Alexa Fluor 488 anti-rabbit (ThermoFisher Scientific); Alexa Fluor 647 anti-goat (ThermoFisher Scientific); Cy3 anti-mouse (Jackson ImmunoResearch); DAPI (Sigma-Aldrich, St Louis, MO D9542).

Immunoblot analysis

For total protein extraction cells were seeded at 1.5×10^6 in 100-mm petri dishes. After 48 hours the cells were harvested in Lysis Buffer (50 mM Tris-HCl pH 7.5, 5 mM EDTA, 150 mM NaCl, 1% NP-40, 0.5% sodium deoxycholate) with the addition of 1 mM phenylmethylsulfonyl fluoride and protease inhibitor cocktail (Sigma-Aldrich,

St Louis, MO). Cells were dislodged with a scraper and left on ice for 30'. Then extracts were clarified by centrifugation at 13200 rpm for 30' at 4°C. For nuclear-cytoplasmic fractionation, cells were seeded 1.5×10^6 in 100-mm dishes. 24 hours after seeding, cell lysates were fractionated to obtain cytoplasmic and nuclear fractions as previously reported [24]. The amount of protein in the samples was determined by the Bio-Rad protein assay (Bio-Rad, Milan, Italy). After the addition of Laemmli buffer (Sigma-Aldrich, St Louis, MO) the samples were boiled at 100°C for 5 min and resolved by SDS- polyacrylamide gel electrophoresis (SDS-PAGE). About 10µg of nuclear and 30µg of cytoplasmic or total extracts (1:3 rate) were separated by SDS-PAGE. The proteins were then transferred to a polyvinylidene difluoride membrane (PDVF, Millipore) using a Mini trans-blot apparatus (Bio-Rad, Milan, Italy) according to the manufacturer's instructions. The PVDF membrane was blocked in 5% w/v milk buffer (5% w/v non-fat dried milk, 50 mM Tris, 200 mM NaCl, 0.2% Tween 20) and incubated overnight at 4°C with primary antibodies diluted in 5% w/v milk or bovine serum albumin (BSA) buffer according to the manufacturer's instructions. Following three washes with TTBS (Tris-buffered saline, 0.1 % Tween), the blots were incubated for 1 hour at RT with HRP-conjugated secondary antibodies (Sigma-Aldrich, St Louis, MO). Proteins were visualized by an enhanced chemiluminescence method (ECL, Bio-rad) and analysed by Quantity One W software of ChemiDoc TM XRS system (Bio-Rad, Milan, Italy).

Co-immunoprecipitation.

For co-immunoprecipitations (Co-IP) 2×10^6 HEK293T cells were seeded in Poly-D-lysine pre-treated 100-mm dishes; the day after cells were treated with Na Ars (Sigma-Aldrich, St Louis) 250 µM for 30 minutes; cells extracts were incubated with an anti-PABP1 antibody (Sigma-Aldrich, St Louis, MO), 3 µg for 1mg of protein extract overnight at 4 °C. The day after Dynabeads Protein G (Invitrogen) were added to samples for 4 hrs at 4°C in rotation. Immunoglobulin G (IgG) 3 µg for 1mg of protein extract was used as a negative control. Immunocomplexes were resolved with SDS-PAGE; immunoblot was performed with anti-YB-1 antibody (bcam).

Trichloroacetic acid precipitation

HEK293T cells were grown as previously described; 24 hours after seeding cells were gently rinsed twice with 1xPBS, and serum starved for 2 hours. After treatments, the cell culture medium was filtered through 0.22 µm filters to remove floating cells and debris. Scepter 2.0 (Merck, Millipore) was used to determine if cells were still present in the collected medium. TCA (Trichloroacetic acid, Sigma-Aldrich, St Louis) 25% was added to culture medium in 1:1 ratio, tubes were placed on ice for 30 min. Samples were then centrifuged at maximum speed at 4°C for 30 min. Supernatant was discarded and cold acetone 100% (200 µl per sample), was added to tubes, samples were then centrifuged at maximum speed, for 15 minutes, at 4°C. This passage was done twice. Acetone was gently removed and 200uL of diethyl ether was added to tubes for 15 minutes on ice. After a centrifuge at maximum speed at 4°C for 15 minutes, samples were placed on the block heater in order to evaporate diethyl ether. After addition of sample buffer. Samples were denatured in sample buffer (Sigma-Aldrich, St Louis, USA) and loaded on the gel.

Quantitative Real Time-PCR

3x10⁵ cells were seeded and let grow for 24 hours; the day after were treated with rYB-1 or CCM-YB-1 or left untreated.

For RT-PCR cells analysis total RNA was isolated using the RNA Extraction Kit from Qiagen (Hilden, Germany) according to the manufacturer's instructions. RNA (2-5µg) was treated with DNase I (Promega, Madison USA) and used to generate reverse transcribed cDNA using SuperScript III (Life Technologies, CA, USA), according to the manufacturer's instructions. Real Time PCR with SYBR green (Promega) detection was performed with a 7500 RT-PCR Thermo Cycler (Applied Biosystem, Foster City, USA).

Expression levels were normalized using *g6pd* mRNA expression. Expression levels were normalized using *zf β-actin* and *gapdh* mRNA expression for zebrafish PAC2 and human HaCaT cells, respectively. The relative levels of mRNA were calculated using the 2^{-ΔΔCT} method. For each gene, primer sequences are presented below:

<i>zf β-actin</i>	F: GCCTGACGGACAGGTCAT	R: ACCGCAAGATTCCATACCC
<i>zf yb-1</i>	F: TACCCACCATACTTCGTGCG	R: GCGGTAGTTGAAGTTGCGAC
<i>hyYb-1</i>	F: CGCAGTGTAGGAGATGGAGAG	R: GAACACCACCAGGACCTGTAA
<i>zf hsp70</i>	F: AGAGCATTACCTGATGAAGC	R: TAAGTGGTGAAGGTCTGGGTCT
<i>zfcry1a</i>	F: TCCGCTGTGTGTACATCCTC	R: CAAACACTGCAGCAAAAACC
<i>Zfcry5</i>	F: ATGAGCCATAACACCATTCA	R: TTATCTCTTTGCCTTCTTCTG:
<i>zf c-fos</i>	F: GCTCCATCTCAGTCCCAGAG	R: AGAGTGGGCTCCAGATCAGA
<i>zf junB</i>	F: GCTTCGTCAAGGCTCTGGAT	R: GTATGTGGGACGGCAGGTAG
<i>zf junD</i>	F: TTACACGAACTTGAGCGCCT	R: CGGTTACGCAGCTTCTTCTCT
<i>zf gapdh</i>	F: CGACCACTTTGTCAAGCTCA	R: TTCCTCTTGTGCTCTTGCTG
<i>h p21waf</i>	F: GCTAAGGTTTACCTGGGGTCTTA	R: GTGGCTCTGATTGGCTTTCTG
<i>h Δnp63α</i>	F: GGTTGGCAAATCCTGGAG	R: GGTTTCGTGTACTGTGGCTCA
<i>h gapdh</i>	F: ACCCAGAAGACTGTGGATGG	R: TTCTAGACGGCAGGTCAGGT

Preparation of bacterial expression vector pET22b⁽⁺⁾/YB-1

Human YB-1 cDNA sequence was amplified with a PCR reaction from recombinant vector pEX-A2 (Eurofins Genomics, Edersberg, Germany). PCR has been carried out using following primers: forward 5'- CCCATATGAGCAGCGAGGCCGAGACCC-3'; reverse 5'- GGAAGCTTGCCTCGGGAGCGGGAA-3'. Bold and underlined sequences refer to restriction sites (*NdeI* and *HindIII*), designed to permit the insertion of YB-1 coding sequence upstream to a His-Tag sequence to facilitate the purification of the recombinant protein. The PCR reaction was carried out in a total volume of 50 µl containing 60 ng of each primer, 20 ng of template, deoxyribonucleotides (dNTPs) containing 0.2 mM of each dNTP, 5 µl 10X Taq buffer and 1.5 units of Taq DNA polymerase (EuroClone, Milan, Italy). PCR was performed under the following conditions: an initial denaturation step at 98°C for 5 minutes, followed by 38 cycles of 30 seconds at 98 °C, 1 minute at 65 °C, and 2 minute at 72

°C. PCR products were then isolated by electrophoresis on 1% agarose gel, and purified using the Product Purification Kit (Roche Applied Science, Monza, Italy). Purified DNA, treated with *NdeI* and *HindIII* restriction enzymes, was inserted into the pET22b (+) expression vector by ligation reaction catalysed by T4 DNA ligase (ThermoFisher Scientific). All cloned, purified DNAs were certified through sequencing (Eurofins Genomics Edersberg, Germany) before processing. The recombinant expression plasmid, was used then to transform competent *E. coli* strain BL21(DE3) (New England BioLabs, Ipswich, Massachusetts, United States).

Recombinant YB-1 protein preparation

The expression plasmid pET22b(+)/YB-1 was used to transform competent *E. coli* strain BL21(DE3) cells. Cells were grown at 37 °C to an $A_{600\text{ nm}} = 0.7$, and then induced with 0.6 mM isopropyl-1-thio-d-galactopyranoside (IPTG) and grown overnight. The expression level of recombinant YB-1 (rYB-1) was estimated performing a western blot on two bacterial aliquots collected before the addition of IPTG and after 16 hrs respectively. Bacterial cells were then harvested by centrifugation (7000 rpm, 4°C, 15 min), re-suspended in 100 mM Tris acetate buffer (pH 8.0) and subjected to sonication in presence of protease inhibitors. Cell debris and precipitated proteins were removed by centrifugation (17500 g, 1 hour) whereas the supernatant was subjected to at least three washes in 100 mM Tris acetate pH 8.0 and finally centrifuged to separate inclusion bodies and cytosolic soluble fraction, the latter containing rYB-1.

Chromatographic procedures

rYB1 was purified performing a two-step procedure composed by an affinity chromatography followed by a reverse phase chromatography. Affinity chromatography was carried out on HisTrap resin (GE Healthcare) equilibrated with 100 mM Tris acetate pH 8.0 containing 20 mM imidazole. Elution was carried out by using 100 mM Tris acetate pH 8.0 containing 500 mM imidazole and spectrophotometrically monitored at 280 nm. Reverse phase chromatography was performed on a HPLC device Series 200 (Perkin Elmer, Waltham, Massachusetts, United States) by using a C4 column (Dr. Maisch GmbH, Ammerbuch-Entringen Germany), 0.1% TFA in 5% acetonitrile as buffer A and 0.1% TFA in 95% acetonitrile as buffer B. Elution was performed by setting a linear gradient 5-95% buffer B in 60 min and spectrophotometrically monitored at 278 nm.

Protein separation by SDS-PAGE and in situ digestion

Proteins precipitated from culture medium were separated by 12% SDS-PAGE, under reducing conditions. Proteins were visualized by colloidal Coomassie brilliant blue and the immunopositive bands were excised, also depending on the visualization of bands at expected molecular weight. Each band was subjected to in situ digestion protocol by reducing proteins by 10 mM DTT and alkylation with 55 mM iodoacetamide, according to the established protocol. Finally, each dry gel piece was rehydrated in 40 μ L of 10 mM ammonium bicarbonate solution containing 200 ng of Trypsin Gold, Mass Spectrometry grade (Promega, Madison, USA), and incubated at 37 °C overnight. The trypsinolysis was stopped with 0.1% formic acid (FA), and tryptic peptides were eluted, vacuum dried, and dissolved in 0.1% formic acid for LC-MS/MS analysis.

LTQ-Orbitrap analysis

Peptides were separated on a 1.7- μ m BEH C18 column (Waters Corporation, USA) at a flow rate of 280 nL/min by using as mobile phase solution A: 95% water, 5% Acetonitrile, 0.1% acetic acid; solution B: 95% Acetonitrile, 5% water, 0.1% acetic acid. Peptide elution was achieved along a linear gradient of B from 20% to 90% over 53 min. MS and MS/MS data were acquired on an Orbitrap LTQ XL high-performance liquid chromatography MS system (Thermo-Scientific, Waltham, MA, USA) equipped with an electrospray source (ESI). The full scan precursor MS spectra (400–1600 m/z) were acquired in the Velos-Orbitrap analyser with a resolution of $r = 60000$. This was followed by data dependent MS/MS fragmentation in centroid mode of the most intense ion from the survey scan using collision-induced dissociation (CID) in the linear ion trap: normalized collision energy 35%; activation Q 0.25; electrospray voltage 1.4 kV; capillary temperature 200 °C; and isolation width 2.00. The targeted ions were dynamically excluded for 30 s, and this MS/MS scan event was repeated for the top 20 peaks in the MS survey scan. The five most intense doubly and triply charged peptide ions were selected and fragmented. The resulting MS data were processed by MS Converter General User Interface software (ProteoWizard) to generate peak lists for protein identifications. Database searches were carried out on the Mascot Deamon version 4.1 by Matrix Science (London, UK). The SwissProt database (release January 2017, 547599 sequences; 195014757 residues) was employed (settings: two missed cleavages; carbamidomethyl (C) as fixed modification and Oxidation (M), Phospho (ST), Phospho (Y), Acetyl (K), Gln->pyro-Glu (N-term Q), Glu->pyro-Glu (N-term E) as variable modifications; peptide tolerance of 10 ppm and fragment mass tolerance of ± 0.6 Da).

Statistical Analysis

Statistical analyses were performed using GraphPad Prism7 (GraphPad Software Inc). Statistical significance of difference in measured variables between control and treated groups was determined by *t*-test or analysis of variance (ANOVA) followed by Tukey's or Dunnett's multiple comparisons post-test. To report p-values, the NEJM (New England Journal of Medicine) decimal format was used; differences were considered statistically significant at * $P < 0.033$, ** $P < 0.002$ and *** $P < 0.001$. Detailed statistical information are shown in Appendix II, Table 1.

APPENDIX II

Supplementary material

Table 1. Statistical analysis.

Figure/experiment	Test method	Significance	n
Figure 6b - Granules size (left panel)	1 way ANOVA, $\alpha = 0.05$	F = 21.12; P <0.001***	5
Ctrl. vs Na Ars	Dunnett's multiple comparisons test	P <0.001***	
Ctrl. vs H ₂ O ₂	-	P <0.001***	
Ctrl. vs Heat Shock	-	P = 0.01*	
Figure 6b - Granules per cell (right panel)	1 way ANOVA, $\alpha = 0.05$	F = 31.3; P <0.001***	3
Na Ars vs. Ctrl.	Dunnett's multiple comparisons test	P = 0.03*	
H ₂ O ₂ vs. Ctrl.	-	P <0.001***	
Heat Shock vs. Ctrl.	-	P <0.001***	
Figure 8b - Granules size (left panel)	Unpaired t-test with Welch's correction	F = 1.397; P = 0.02*	20
siYB-1 vs. siNC (control)	Two-tailed, $\alpha = 0.05$		
Figure 8b - Granules per cell (right panel)	Unpaired t-test with Welch's correction	F = 1.254; P = 0.01**	6
siYB-1 vs. siNC (control)	Two-tailed, $\alpha = 0.05$		
Figure 10a - MTT assay 30'	1 way ANOVA, $\alpha = 0.05$	F = 1.409; P = 0.27 ns	6
Ctrl. vs. 250 μ M Na Ars	Dunnett's multiple comparisons test	P = 0.90 ns	
Ctr. vs. 500 μ M H ₂ O ₂	-	P = 0.22 ns	
Figure 10a - MTT assay 60'	1 way ANOVA, $\alpha = 0.05$	F = 1.198; P = 0.33 ns	6
Ctrl. vs. 250 μ M Na Ars	Dunnett's multiple comparisons test	P = 0.45 ns	
Ctr. vs. 500 μ M H ₂ O ₂	-	P = 0.26 ns	
Figure 10b - Trypan blue 30'	1 way ANOVA, $\alpha = 0.05$	F = 1.079; P = 0.40 ns	3
Ctrl. vs. 250 μ M Na Ars	Dunnett's multiple comparisons test	P = 0.57 ns	
Ctr. vs. 500 μ M H ₂ O ₂	-	P = 0.32 ns	
Figure 10b - Trypan blue 60'	1 way ANOVA, $\alpha = 0.05$	F = 0.2497; P = 0.79 ns	3

Ctrl. vs. 250 μ M Na Ars	Dunnett's multiple comparisons test	P = 0.82 ns
Ctrl. vs. 500 μ M H ₂ O ₂	-	P = 0.74 ns
Figure 14 - HEK293T/HEK239T YB-1-GFP proliferation curve	2 way ANOVA, α = 0.05	6
Time (h)		F = 1031; P <0.001***
Cell line		F = 0.3737; P =0.54 ns
Interaction (Time vs. Cell line)		F = 67.97; P <0.001***
HEK293T vs. HEK293T YB-1-GFP	Sidak's multiple comparison test	
0 h	-	P >0.99 ns
24 h	-	P = 0.25 ns
48 h	-	P <0.001***
72 h	-	P <0.001***
96 h	-	P <0.001***
Figure 17a - HEK293T/HEK239T YB-1-GFP MTT assay	2 way ANOVA, α = 0.05	6
Treatment (H ₂ O ₂)		F = 1136; P <0.001***
Cell line		F = 43.62; P <0.001***
Interaction (Treatment vs. Cell line)		F = 4.174; P = 0.003**
HEK293T vs. HEK293T YB-1-GFP	Sidak's multiple comparison test	
Ctrl.	-	P >0.99 ns
H ₂ O ₂ 0.5 mM	-	P = 0.010**
H ₂ O ₂ 1 mM	-	P = 0.71 ns
H ₂ O ₂ 2.5 mM	-	P = 0.29 ns
H ₂ O ₂ 5 mM	-	P <0.001***
H ₂ O ₂ 7.5 mM	-	P = 0.002**
Figure 17b - HEK293T/HEK239T YB-1-GFP Trypan Blue	2 way ANOVA, α = 0.05	6
Treatment (H ₂ O ₂)		F = 695.1; P <0.001***
Cell line		F = 493.3; P <0.001***
Interaction (Treatment vs. Cell line)		F = 47.13; P <0.001***
HEK293T vs. HEK293T YB-1-GFP	Sidak's multiple comparison test	
Ctrl.	-	P >0.99 ns
H ₂ O ₂ 0.5 mM	-	P <0.001***
H ₂ O ₂ 1 mM	-	P <0.001***

H ₂ O ₂ 2.5 mM	-	P <0.001***
H ₂ O ₂ 5 mM	-	P <0.001***
H ₂ O ₂ 7.5 mM	-	P <0.001***
Figure 23a - HaCaT proliferation curve	2 way ANOVA, $\alpha = 0.05$	3
Time (h)		F = 3.56; P = 0.04*
Treatment (CCM-YB-1)		F = 46; P <0.001***
Interaction (Time vs. CCM-YB-1)		F = 11.63; P <0.001***
Ctrl. vs. 5 μ g/ml	Dunnett's multiple comparisons test	P <0.001***
Ctrl. vs. 7.5 μ g/ml	-	P <0.001***
Ctrl. vs. 10 μ g/ml	-	P <0.001***
Figure 23b - HaCaT proliferation curve	2 way ANOVA, $\alpha = 0.05$	3
Time (h)		F = 7.866; P = 0.002**
Treatment (rYB-1)		F = 18.34; P <0.001***
Interaction (Time vs. rYB-1)		F = 6.075; P <0.001***
Ctrl. vs. 5 μ g/ml	Dunnett's multiple comparisons test	P <0.001***
Ctrl. vs. 7.5 μ g/ml	-	P <0.001***
Ctrl. vs. 10 μ g/ml	-	P <0.001***
Figure 23c - HaCaT proliferation curve	2 way ANOVA, $\alpha = 0.05$	3
Time (h)		F = 286.9; P <0.001***
Treatment (BSA)		F = 0.3106; P = 0.82 ns
Interaction (Time vs. BSA)		F = 0.3227; P = 0.92 ns
Ctrl. vs. 5 μ g/ml	Dunnett's multiple comparisons test	P = 0.96 ns
Ctrl. vs. 7.5 μ g/ml	-	P >0.99 ns
Ctrl. vs. 10 μ g/ml	-	P = 0.91 ns
Figure 23d - Crystal Violet Assay (48)	1 way ANOVA, $\alpha = 0.05$	F = 400.9; P <0.001***
Ctrl. vs. BSA 7.5 μ g/ml	Dunnett's multiple comparisons test	P = 0.10 ns

Ctrl. vs. rYB-1 7.5 µg/ml	-	P <0.001***
Ctrl. vs. CCM-YB-1 7.5 µg/ml	-	P <0.001***
Figure 24a - HEK293T prol. curve (upper panel)	2 way ANOVA, $\alpha = 0.05$	3
Time (h)		F = 188.8; P <0.001***
Treatment (rYB-1)		F = 6.809; P = 0.002**
Interaction (Time vs rYB-1)		F = 2.314; P = 0.07 ns
Ctrl. vs. 5 µg/ml	Dunnett's multiple comparisons test	P = 0.03*
Ctrl. vs. 7.5 µg/ml	-	P = 0.01*
Ctrl. vs. 10 µg/ml	-	P <0.001***
Figure 24a - HEK293T prol. curve (lower panel)	2 way ANOVA, $\alpha = 0.05$	3
Time (h)		F = 3.273; P = 0.06 ns
Treatment (CCM-YB-1)		F = 52.45; P <0.001***
Interaction (Time vs CCM-YB-1)		F = 13.72; P <0.001***
Ctrl. vs. 5 µg/ml	Dunnett's multiple comparisons test	P <0.001***
Ctrl. vs. 7.5 µg/ml	-	P <0.001***
Ctrl. vs. 10 µg/ml	-	P <0.001***
Figure 24b - CaCo2 prol. curve (upper panel)	2 way ANOVA, $\alpha = 0.05$	3
Time (h)		F = 118.8; P <0.001***
Treatment (rYB-1)		F = 5.012; P = 0.008**
Interaction (Time vs rYB-1)		F = 4.796; P = 0.002**
Ctrl. vs. 5 µg/ml	Dunnett's multiple comparisons test	P = 0.20 ns
Ctrl. vs. 7.5 µg/ml	-	P = 0.003**
Ctrl. vs. 10 µg/ml	-	P = 0.03*
Figure 24b - CaCo2 prol. curve (lower panel)	2 way ANOVA, $\alpha = 0.05$	3
Time (h)		F = 2.775; P = 0.08 ns
Treatment (CCM-YB-1)		F = 27.54; P <0.001***

Interaction (Time vs CCM-YB-1)		F = 6.682; P <0.001***	
Ctrl. vs. 5 µg/ml	Dunnett's multiple comparisons test	P <0.001***	
Ctrl. vs. 7.5 µg/ml	-	P <0.001***	
Ctrl. vs. 10 µg/ml	-	P <0.001***	
Figure 25a - HaCaT cell cycle distribution (48h)	2 way ANOVA, α = 0.05		3
Cell phase		F = 1025; P <0.001***	
Treatment		F = 0.02836; P = 0.97 ns	
Interaction (Cell phase vs. Treatment)		F = 257.4; P <0.001***	
G1 - Ctrl. vs. rYB-1 7.5 µg/ml	Dunnett's multiple comparisons test	P = 0.89 ns	
G1 - Ctrl. vs. CCM-YB-1 7.5 µg/ml	-	P <0.001***	
S - Ctrl. vs. rYB-1 7.5 µg/ml	-	P <0.001***	
S - Ctrl. vs. CCM-YB-1 7.5 µg/ml	-	P = 0.01*	
G2 - Ctrl. vs. rYB-1 7.5 µg/ml	-	P <0.001***	
G2 - Ctrl. vs. CCM-YB-1 7.5 µg/ml	-	P <0.001***	
Figure 25b - RT-qPCR <i>p21waf</i> (upper panel)	1 way ANOVA, α = 0.05	F = 50.98; P <0.001***	3
Ctrl. vs. BSA 7.5 µg/ml	Dunnett's multiple comparisons test	P = 0.71 ns	
Ctrl. vs. rYB-1 7.5 µg/ml	-	P = 0.03*	
Ctrl. vs. CCM-YB-1 7.5 µg/ml	-	P <0.001***	
Figure 25b - RT-qPCR $\Delta Np63\alpha$ (lower panel)	1 way ANOVA, α = 0.05	F = 210.6; P <0.001***	3
Ctrl. vs. BSA 7.5 µg/ml	Dunnett's multiple comparisons test	P = 0.23 ns	
Ctrl. vs. rYB-1 7.5 µg/ml	-	P = 0.07 ns	
Ctrl. vs. CCM-YB-1 7.5 µg/ml	-	P <0.001***	
Figure 30a – PAC2 MTT assay	1 way ANOVA, α = 0.05	F = 0.7438; P = 0.57 ns	6
Ctrl 26°C vs. 45°C 30'	Dunnett's multiple comparison test	P >0.99 ns	
Ctrl 26°C vs. 45°C 45'	-	P = 0.95 ns	
Ctrl 26°C vs. 45°C 60'	-	P = 0.73 ns	
Ctrl 26°C vs. 45°C 90'	-	P = 0.46 ns	
Figure 30b – RT-qPCR (<i>zf hsp70</i>)	2-way ANOVA, α = 0.05		3

Interaction		F = 54.61; P <0.001***	
Time (h)		F = 345.2; P <0.001***	
Temperature °C		F = 186; P <0.001***	
0' - 26°C vs. 37°C	Dunnett's multiple comparison test	P >0.99 ns	
0' - 26°C vs. 42°C	-	P = 0.96 ns	
0' - 26°C vs. 45°C	-	P = 0.96 ns	
30' - 26°C vs. 37°C	-	P <0.001***	
30' - 26°C vs. 42°C	-	P <0.001***	
30' - 26°C vs. 45°C	-	P = 0.005**	
1h' - 26°C vs. 37°C	-	P <0.001***	
1h' - 26°C vs. 42°C	-	P <0.001***	
1h' - 26°C vs. 45°C	-	P <0.001***	
Figure 30c – RT-qPCR (<i>zf yb-1</i>)	2-way ANOVA, $\alpha = 0.05$		3
Interaction		F = 16.54; P <0.001***	
Time (h)		F = 25.61; P <0.001***	
Temperature °C		F = 90.44; P <0.001***	
26°C vs. 45°C	Sidak's multiple comparison test		
0'	-	P >0.99 ns	
30'	-	P = 0.45 ns	
1h	-	P = 0.1 ns	
3h	-	P <0.001***	
6h	-	P <0.001***	
Figure 30d – RT-qPCR (<i>h yb-1</i>)	2-way ANOVA, $\alpha = 0.05$		3
Interaction		F = 2.995; P <0.04*	
Time (h)		F = 2.792; P <0.05 ns	
Temperature °C		F = 14.53; P <0.001**	
37°C vs. 45°C	Sidak's multiple comparison test		
0'	-	P = 0.92 ns	
30'	-	P = 0.01*	
1h	-	P = 0.03*	

3h	-	P = 0.38 ns	
6h	-	P = 0.82 ns	
Figure 31b – Aggregate size (μm)	Unpaired t-test with Welch's correction Two-tailed, $\alpha = 0.05$	P = 0.007**	3
Figure 32c – Aggregate size (μm)	1 way ANOVA, $\alpha = 0.05$	F = 52.54; P <0.001***	3
26°C vs. 37°C	Dunnett's multiple comparisons test	P >0.99 ns	
26°C vs. 40°C	-	P >0.99 ns	
26°C vs. 42°C	-	P = 0.50 ns	
26°C vs. 45°C	-	P <0.001***	
Figure 33c – left part (white bars)	1 way ANOVA, $\alpha = 0.05$	F = 87.27; P <0.001***	3
Ctrl 26°C vs 45°C 30'	Dunnett's multiple comparisons test	P = 0.30 ns	
Ctrl 26°C vs 45°C 45'	-	P <0.001***	
Ctrl 26°C vs 45°C 60'	-	P <0.001***	
Ctrl 26°C vs 45°C 90'	-	P <0.001***	
Figure 33c – right part (black bars)	1 way ANOVA, $\alpha = 0.05$	F = 45.77; P <0.001***	3
Ctrl 45°C 45' vs Rec 26°C 15'	Dunnett's multiple comparison test	P <0.001***	
Ctrl 45°C 45' vs Rec 26°C 30'	-	P <0.001***	
Ctrl 45°C 45' vs Rec 26°C 60'	-	P <0.001***	
Figure 35d – Aggregate size (μm)	1 way ANOVA, $\alpha = 0.05$	F = 157.7; P <0.001***	3
Ctrl 45°C 45' vs Rec 26°C 15'	Dunnett's multiple comparisons test	P <0.001***	
Ctrl 45°C 45' vs Rec 26°C 30'	-	P <0.001***	
Ctrl 45°C 45' vs Rec 26°C 60'	-	P <0.001***	
Figure 35c – Aggregate size (μm)	1 way ANOVA, $\alpha = 0.05$	F = 60.78; P <0.001***	3
Ctrl vs. CHX	Tukey's multiple comparison test	P = 0.46 ns	
Ctrl vs. HS 45°C 45'	-	P <0.001***	
Ctrl vs. CHX + HS	-	P = 0.005**	
CHX vs. HS 45°C 45'	-	P = 0.002**	
CHX 20 $\mu\text{g}/\text{mL}$ vs. CHX + HS	-	P = 0.01*	
HS 45°C 45' vs. CHX + HS	-	P = 0.05*	

Figure 36c – MTT assay	1 way ANOVA, $\alpha = 0.05$	F = 17.19; P <0.001***	3
Ctrl 26°C vs. siYB-1 26°C	Tukey's multiple comparison test	P = 0.38 ns	
Ctrl 26°C vs. Ctrl 45°C	-	P = 0.85 ns	
Ctrl 26°C vs. siYB-1 45°C	-	P <0.001***	
siYB-1 26°C vs. Ctrl 45°C	-	P = 0.84 ns	
siYB-1 26°C vs. siYB-1 45°C	-	P <0.001***	
Ctrl 45°C vs. siYB-1 45°C	-	P <0.001***	
Figure 38b – RT-qPCR (<i>zf c-fos</i>)	1 way ANOVA, $\alpha = 0.05$	F = 13.24; P <0.001***	3
0 vs. 30'	Dunnett's multiple comparison test	P = 0.01*	
0 vs. 1h	-	P = 0.02*	
0 vs. 3h	-	P = 0.46 ns	
0 vs. 6h	-	P = 0.42 ns	
0 vs. 9h	-	P = 0.33 ns	
Figure 38b – RT-qPCR (<i>zf jun-B</i>)	1 way ANOVA, $\alpha = 0.05$	F = 93.63; P <0.001***	3
0 vs. 30'	Dunnett's multiple comparison test	P <0.001***	
0 vs. 1h	-	P <0.001***	
0 vs. 3h	-	P = 0.54 ns	
0 vs. 6h	-	P = 0.91 ns	
0 vs. 9h	-	P >0.99 ns	
Figure 38b – RT-qPCR (<i>zf jun-D</i>)	1 way ANOVA, $\alpha = 0.05$	F = 114.9; P <0.001***	3
0 vs. 30'	Dunnett's multiple comparison test	P <0.001***	
0 vs. 1h	-	P <0.001***	
0 vs. 3h	-	P = 0.01*	
0 vs. 6h	-	P = 0.02*	
0 vs. 9h	-	P = 0.04*	
Figure 38b – RT-qPCR (<i>zf cry1a</i>)	1 way ANOVA, $\alpha = 0.05$	F = 90.13; P <0.001***	3
0 vs. 30'	Dunnett's multiple comparison test	P = 0.99 ns	
0 vs. 1h	-	P <0.001***	
0 vs. 3h	-	P <0.001***	
0 vs. 6h	-	P <0.001***	

Figure 38b – RT-qPCR (<i>zf cry5</i>)	1 way ANOVA, $\alpha = 0.05$	F = 16.53; P <0.001***	3
0 vs. 30'	Dunnett's multiple comparison test	P = 0.85 ns	
0 vs. 1h	-	P = 0.002**	
0 vs. 3h	-	P = 0.001**	
0 vs. 6h	-	P <0.001***	

Table 2. MSMs analysis on rYB-1 and CCM-YB-1.

Peptides with relative score, sequence and modifications obtained after MS and MSMS analysis on YB-1 putative bands. Rec1 and Rec2 correspond to rYB-1; S1 and S2 correspond to CCM-YB-1 (see Figure 22 in the text).

Gel band	Gene Name	Protein name	Protein score	Sequence coverage
Rec1	YBX1	YB-1	1553	79%
ppm	Peptide score	Unique*	Peptide sequence	Modification
4.94	24	U	R.RNFNYR.R	-
4.89	53		R.NGYGFINR.N	-
3.44	11	U	K.YAADRNHYYR.Y	-
5.52	13	U	K.YAADRNHYYR.R	-
5.38	14	U	R.RRPENPKPQDGK.E	-
8.10	15	U	R.SVGDGETVEFDVVEGEKGAEAAANVTGPGGV PVQGSK.Y	+ Phospho (ST)
3.87	20	U	R.RPENPKPQDGK.E	-
5.92	22	U	K.NEGSESAPEGQAQQR.R	-
4.94	24	U	R.RNFNYR.R	-
4.54	25	U	R.RRFPYYMR.R + Oxidation (M)	-
2.87	26		R.NGYGFINRNDTK.E	-
3.43	31	U	R.FPPYYMR.R + Oxidation (M)	-
4.92	32	U	R.RRPENPKPQDGK.E	-
6.31	32	U	R.GPPRNYQQNYQNSGEGKNEGSESAPEGQAQ QR.R	-
5.84	33	U	R.RPENPKPQDGKETK.A	-
3.22	35	U	R.RRFPYYMR.R + Oxidation (M)	-
4.47	39	U	R.EDGNEEDKENQGDETQGQPPQR.R	+ Glu->pyro-Glu (N-term E)
5.62	47	U	R.QPREDGNEEDKENQGDETQGQPPQR.R	+ Gln->pyro-Glu (N-term Q)
2.79	48	U	M.SSEAETQPPAAPPAPALSAADTKPGTTGS GAGSGGPGGLTSAAPAGGDKK.V	-
5.83	49	U	R.RRPENPKPQDGKETK.A	-
4.89	53		R.NGYGFINR.N	-
3.33	53	U	K.VIATKVLGTVK.W + Acetyl (K)	-
2.29	53		K.EDVVFVHQTAIKK.N + Glu->pyro-Glu (N-term E)	-
1.52	58		R.NDTKEDVVFVHQTAIKK.N	-
4.38	60		K.EDVVFVHQTAIKK + Glu->pyro-Glu (N-term E)	-
6.60	61	U	R.QRQPREDGNEEDKENQGDETQGQPPQR.R	+ Gln->pyro-Glu (N-term Q)
5.13	66	U	R.NYQQNYQNSGEGKNEGSESAPEGQAQQR.R	-
4.98	80		R.NDTKEDVVFVHQTAIKK.K	-
-0.64	80	U	M.SSEAETQPPAAPPAPALSAADTKPGTTGS GAGSGGPGGLTSAAPAGGDKK.K	-
4.79	86	U	R.NYQQNYQNSGEGK.N	-
7.27	90	U	R.EDGNEEDKENQGDETQGQPPQR.R	-
6.32	90	U	R.QPREDGNEEDKENQGDETQGQPPQR.R	+ Gln->pyro-Glu (N-term Q)

Gel band	Gene Name	Protein name	Protein score	Sequence coverage
S1	YBX1	YB-1	394	60%
ppm	Peptide score	Unique*	Peptide sequence	Modification
6.52	13	U	R.SVGDGETVEFDVVEGEKGAEAAANVTGPGGV VQGSK.Y + Phospho (ST)	+ Phospho (ST)
2.26	13	U	M.SSEAETQPPAAPPAPALSAADTKPGTTGS AGSGGPGGLTSAAPAGGDKK.V	-
7.98	19	U	R.EDGNEEDKENQGDETQGQPPQR.R	-
6.63	20	U	R.EDGNEEDKENQGDETQGQPPQR.R	-
3.83	26		R.NGYGFINR.N	-
3.93	33	U	R.NYQQNYQNSGEGKNEGSESAPEGQAQQR.R	-
2.81	44	U	R.NDTKEDVVFVHQTAIKK.N	-
3.16	66		R.SVGDGETVEFDVVEGEK.G	-
3.04	74		R.NDTKEDVVFVHQTAIKK.K	-
4.67	85	U	R.RPQYSNPPVQGEVMEGADNQGAGEQGRPVR. Q + Oxidation (M)	+ Oxidation (M)

Gel band	Gene Name	Protein name	Protein score	Sequence coverage
Rec2	YBX1	YB-1	1446	78%
ppm	Peptide score	Unique*	Peptide sequence	Modification
4.50	10	U	R.RPENPKPQDGKETK.A	-
3.86	116	U	M.SSEAETQPPAAPPAPALSAADTKPGTTGSGA GSGGPGGLTSAAPAGGDK.K	-
6.09	117	U	R.RPQYSNPPVQGEVMEGADNQGAGEQGRPV.R.Q	-
4.61	129		R.SVGDGETVEFDVVEGEK.G	-
4.13	13	U	K.YAADRNHYRR.Y	-
4.80	15	U	R.EDGNEEDK.E	-
3.30	16	U	R.RRPENPKPQDGKETK.A	-
5.35	18	U	K.YAADRNHYR.R	-
4.11	20		K.VLGTVKWFNVR.N	-
9.68	21	U	R.SVGDGETVEFDVVEGEKGAAANVIGPGGVPV QGSK.Y	+ Phospho (ST)
4.28	21	U	R.RPQYSNPPVQGEVMEGADNQGAGEQGRPV.R.Q NM.YR.G	+ 2 Oxidation (M)
2.26	24		R.NGYGFINRNDTKEDVFVHQTAIK.K	-
7.75	25	U	R.RGPPRNYQQNYQNSGESGEKNEGESAPEGQAQ QR.R	-
2.23	26		R.NGYGFINRNDTK.E	-
4.80	32	U	R.QPREDGNEEDKENQGETQGQPPQRR.Y	+ Gln->pyro-Glu (N-term Q)
6.10	33	U	R.EDGNEEDKENQGETQGQPPQRR.Y	+ Glu->pyro-Glu (N-term E)
2.52	35	U	R.RFPYYMR.R + Oxidation (M)	-
2.51	35	U	K.NEGSESAPGQAQQR.R	-
3.40	38	U	R.FPPYYMR.R	-
2.35	38	U	R.RRFPYYMR.R	-
3.71	41	U	R.QPREDGNEEDKENQGETQGQPPQRR.R	+ Gln->pyro-Glu (N-term Q)
4.93	43	U	R.QRQPREDGNEEDKENQGETQGQPPQRR.R	+ Gln->pyro-Glu (N-term Q)
2.34	55		R.NGYGFINR.N	-
2.00	56		K.EDVFVHQTAIK.N	+ Glu->pyro-Glu (N-term E)
3.88	59		K.EDVFVHQTAIK.K	-
7.16	59	U	R.NYQQNYQNSGESGEKNEGESAPEGQAQQR.R	-
6.68	63	U	R.NYQQNYQNSGESGEK.N	-
3.70	68		R.NDTKEDVFVHQTAIK.N	-
6.12	78	U	R.EDGNEEDKENQGETQGQPPQRR.R	+ Glu->pyro-Glu (N-term E)
4.41	81		R.NDTKEDVFVHQTAIK.K	-
-0.89	81	U	M.SSEAETQPPAAPPAPALSAADTKPGTTGSGA GSGGPGGLTSAAPAGGDKK.V	-

Gel band	Gene Name	Protein name	Protein score	Sequence coverage
S2	YBX1	YB-1	88	29%
ppm	Peptide score	Unique*	Peptide sequence	Modification
6.33	46	U	R.NYQQNYQNSGESGEKNEGESAPEGQAQQR.R	-
3.73	17		R.NDTKEDVFVHQTAIK.K	-
2.55	15	U	R.NDTKEDVFVHQTAIK.N	-
7.48	10	U	M.SSEAETQPPAAPPAPALSAADTKPGTTGSGA GSGGPGGLTSAAPAGGDKK.V	-

APPENDIX III

Publications

1. O. di Martino, A. Troiano, L. Addi, **A. M. Guarino**, S. Calabrò, R. Tudisco, N. Murru, M. I. Cutrignelli, F. Infascelli & V. Calabrò. *Regulation of Stearoyl Coenzyme A Desaturase 1 Gene Promoter in Bovine Mammary Cells*. *Animal Biotechnology*. **2015** October, 26:4, 251-259. doi:10.1080/10495398.2015.1022182
2. Orsola Di Martino, Annaelena Troiano, **Andrea Maria Guarino**, Alessandra Pollice, Maria Vivo, Girolama La Mantia, Viola Calabrò. *$\Delta Np63a$ controls YB-1 protein stability: evidence on YB-1 as a new player in keratinocyte differentiation*. *Genes to Cells* **2016** May. Doi:10.1111/gtc.12373.
3. Cristina Pagano, Orsola di Martino, Nathalie Muller, **Andrea Maria Guarino**, Rima Siauciunaite, Markus Reischl, Nickolas Simon Foulkes, Daniela Vallone and Viola Calabrò. *The tumor-associated YB-1 protein: New player in the circadian control of cell proliferation*. *Oncotarget* **2017** Jan 24;8(4):6193-6205. doi:10.18632/oncotarget.14051.
4. Flora Ascione, **Andrea Maria Guarino**, Viola Calabrò, Stefano Guido, Sergio Caserta. *A novel approach to quantify the wound closure dynamic*. *Exp Cell Res*. **2017** Mar 15;352(2):175-183. doi: 10.1016/j.yexcr.2017.01.005.
5. Francesca Ciani, Simona Tafuri, Annaelena Troiano, Alessio Cimmino, Bianca Saveria Fioretto, **Andrea Maria Guarino**, Alessandra Pollice, Maria Vivo, Antonio Evidente, Domenico Carotenuto, Viola Calabrò. *Anti-proliferative and pro-apoptotic effects of *Uncaria tomentosa* aqueous extract in carcinoma cells*. *Journal of Ethnopharmacology*. **2017** Sep 28; 211:285-294. doi: 10.1016/j.jep.2017.09.031.
6. Viola Calabrò, Domenico Carotenuto, Francesca Ciani, Marilena De Lillo, **Andrea Maria Guarino**, Federico Infascelli, Pietro Lombardi, Vincenzo Mastellone, Alessandra Pollice, Simona Tafuri, Annaelena Troiano, and Rosa Tundis. *Molecular and Cellular Approaches to evaluate biological properties of higher plant extracts*. *J. Nutr. Ecol. Food Res*. **2017** 4, 86-88.
7. Giuliana Donadio, Arianna Mazzoli, Mariamichela Lanzilli, **Andrea Maria Guarino**, Miriam Rivetti, Raffaella Crescenzo, Ezio Ricca, Susanna Iossa, Alessandra Pollice, Rachele Isticato. *Protective and therapeutic effects of *Bacillus megaterium* spores on gut oxidative stress*. *European Journal of Nutrition*. **2018**. Under revision.
8. **Andrea Maria Guarino**, Alessandra Pollice and Viola Calabro. *GFP Fusion Proteins: A Solution or a Problem?* **2018**. *Biomedical Journal of Scientific & Technical Research (BJSTR)*. doi:10.26717/BJSTR.2018.05.001258.
9. Haiyu Zhao, Giuseppe Di Mauro, Sebastian Lungu-Mitea, Pietro Negrini, **Andrea Maria Guarino**, Elena Frigato, Thomas Braunbeck, Honju Ma, Tilman

Lamparter, Daniela Vallone, Cristiano Bertolucci and Nicholas S. Foulkes. *Modulation of DNA repair systems in blind cavefish during evolution in constant darkness*. *Current Biology*. **2018**.
Doi:<https://doi.org/10.106/j.cub.2018.08.039>

10. Andrea Maria Guarino, Giuseppe Di Mauro, Gennaro Ruggiero, Nicholas Simon Foulkes, Daniela Vallone and Viola Calabrò. *YB-1 recruitment to stress granules reveals a differential adaptive response to stress in Zebrafish*. *Scientific Reports*. **2018. Under revision**.

11. Andrea Maria Guarino, Annaelena Troiano, Elio Pizzo, Andrea Bosso, Maria Vivo, Gabriella Pinto, Angela Amoresano, Alessandra Pollice, Girolama La Mantia and Viola Calabrò. *Oxidative stress causes enhanced secretion of YB-1 protein that restrains proliferation of receiving cells*. *Genes*. **2018**.
Doi: [10.3390/genes9100513](https://doi.org/10.3390/genes9100513).

Communications and activities

XV FISV Congress September 18-21, 2018. Sapienza University of Rome, Italy.
Abstract presentation.

Title: Secreted YB-1 regulates NF- κ B signaling pathway.

Authors: **Andrea Maria Guarino**, Felicia Sangermano, Andrea Bosso, Elio Pizzo, Alessandra Pollice, Girolama La Mantia and Viola Calabrò.

XV FISV Congress September 18-21, 2018. Sapienza University of Rome, Italy.
Oral presentation.

Title: YB-1 recruitment to stress granules reveals a differential adaptive response to stress in Zebrafish.

Authors: **Andrea Maria Guarino**, Giuseppe Di Mauro, Gennaro Ruggiero, Concetta Sozio, Antonella Delicato, Nicholas Simon Foulkes, Daniela Vallone and Viola Calabrò.

XV FISV Congress September 18-21, 2018. Sapienza University of Rome, Italy.
Poster session.

Title: Antibacterial and wound healing effects of colloidal silver on human keratinocytes.

Authors: Elena Montano, Maria Vivo, **Andrea Maria Guarino**, Sergio Caserta, Viola Calabrò and Alessandra Pollice.

SIBBM 2016 *From single cell analysis to precision medicine*. June 16-18, 2016, Naples, Italy.
Poster session.

Title: *The emerging relationship between Y box binding protein 1 and the cellular stress response*.

Authors: **Andrea Maria Guarino**, Orsola di Martino and Viola Calabrò.

IBSA Foundation: *the thyroid in the periphery*. April 15, 2016, Naples, Italy.

Abstract contest.

Title: *YB-1 plays a double role in stress response acting as stress granules nucleator and secreted signaling molecule.*

Authors: **Andrea Maria Guarino**, Orsola di Martino and Viola Calabrò.

XXX Futuro Remoto *Un viaggio tra scienza e fantascienza, una festa di Arte Scienza e Tecnologia*. 7-10 October 2015, Naples.

Biology stand and theatrical Representation.

XXXI Futuro Remoto *Connessioni*. 24 May 2017, Naples.

Biology stand.

Biotechnology Open day 22-23 February 2016, University of Naples *Federico II*.

PhD student coordinator.

Biotechnology Open day 13-14 February 2017, University of Naples *Federico II*.

PhD student coordinator.

PLS (Progetto Lauree Scientifiche) DNA detection

University of Naples *Federico II*.

3 February 2017, theoretical lesson; 14, 16, 17, 24 February 2017, laboratory experience (3h each).

GFP Fusion Proteins: A Solution or a Problem?



Andrea Maria Guarino, Alessandra Pollice and Viola Calabro*

Dipartimento di Biologia, Università degli Studi di Napoli, Italy

Received: May 31, 2018; Published: June 20, 2018

*Corresponding author: Viola Calabro, Dipartimento di Biologia, Italy, Tel: 39081679233; Fax 39081679233; Email: vcalabro@unina.it

Abstract

Using fluorescent proteins as imaging probes is a wide spread and versatile technique in microscopy. GFP tagged proteins can be used to track and examine real time localization, interactions and translocation of proteins of interest as well as to investigate several aspects of cell biology. The Y-box binding protein 1 (YB-1) is a pleiotropic protein involved in a wide number of cellular processes and a substantial amount of knowledge on YB-1 localization and function was produced using YB-1-GFP constructs. Recently, it has been shown that YB-1 plays a critical role in cell stress response, playing an important role in the formation of stress granules (SG). To deeply investigate on this subject, we produced a stable HEK293T cell line constitutively expressing YB-1-GFP. In physiological conditions YB-1-GFP expressing cells behaved like the parental cells and YB-1-GFP protein properly localized to the cytoplasmic compartment. However, upon oxidative insult we observed a strong reduction in cell viability along with the occurrence of unusual GFP positive aggregates. Taken together, our findings suggest to critically revise existing insights obtained with YB-1-GFP construct and, more in general, to beware and be critical in interpreting data obtained with functionally uncharacterized GFP fusion proteins.

Keywords: GFP; Stress Granules; Oxidative Stress; Stable Cell Line

Abbreviations: CSD: Cold Shock Domain; NES: Specific Nuclear Export; NLS: Nuclear Localization; CRS: Cytoplasmic Retention Signals; SG: Stress Granules; RNP: Ribonucleoproteins; CLS: Cell Line Service; mRNPs: Messenger Ribonucleoproteins

Introduction

Y-box binding protein 1 (YB-1) is a member of the evolutionarily conserved cold shock domain (CSD) proteins and was first identified as a DNA/RNA binding protein [1] involved in the control of gene expression at both transcriptional and translational level [2-4]. Given its multiple cellular functions, YB-1 is involved in the control of several biological processes including cell proliferation and migration. To properly perform its functions, YB-1 subcellular localization has to be finely regulated. Specific nuclear export (NES), nuclear localization (NLS) and cytoplasmic retention signals (CRS) contribute and direct the multifunctional tasking of YB-1 [5]. In normal resting cells, YB-1 localizes to cytoplasm where it is a major component of P-bodies and messenger ribonucleoproteins (mRNPs) [6]. Recent studies link YB-1 to the cellular response to oxidative stress and DNA repair mechanisms. Indeed, following acute oxidative stress, YB-1 localizes to cytoplasmic Stress Granules (SGs), organelle-like structures devoid of membranes engaged in mRNA sorting and pro-survival translational reprogramming [7,8]. In particular, YB-1 is recruited in TIA-containing Stress Granules (SGs) where it functions as a component of translationally inactive mRNPs to directly block translational initiation of highly expressed [9]. Following DNA damage, YB-1 translocates to the nucleus and associates with DNA repair protein complexes. Here we report the characterization of a stable pool of HEK293T cells constitutively ex-

pressing YB-1 as a GFP fusion protein enabling sensitive analysis of YB-subcellular localization by confocal microscopy.

Methodology

Cell Culture: HEK293T, human embryonic kidney cells were purchased from Cell Line Service (CLS, Germany). Cells were cultured in humidified incubator at 37°C and 5% CO₂ and maintained in DMEM High Glucose (Gibco) supplemented with 10% Fetal Bovine Serum (Gibco), 1% L-Glutamine (Gibco) and 1% Pen-Strep solution (Gibco). For HEK293T YB-1-GFP and HEK293T GFP, blasticidin (Sigma-Aldrich, St Louis, MO) and G418 (Sigma-Aldrich, St Louis, MO) antibiotics were added in the medium to a final concentration of 5 µg/ml.

Plasmids: The expression construct pcDNA6V5/HIS-A-YB-1-GFP derived from pcDNATM3.1(+) (Invitrogen); pcDNA 3.1HIS-C was purchased from Thermo Fischer Scientific (USA). pGFP-C1 was purchased from Clontech (USA).

Transfections: Cells were transfected using Lipofectamine 2000 (Life Technology) according to the manufacturer's instructions. Briefly, cells were seeded at 70-80% confluence (1.5×10^6) in 100mm dishes and transiently transfected with different concentrations of plasmid (from 800ng up to 1,5 µg).

Generation of YB1-GFP Stable Clones: HEK293T cells were tested for their sensitivity to blasticidin in order to determine the best concentration for a correct selection. Concentrations of 2,5, 8, 10 and 12mg/ml were tested. Controls start to die from the day after the addition of the higher blasticidin concentration up to 3 days for the lower antibiotic concentration. The concentration chosen for selection was 5mg/ml. HEK293T cells were seeded in 100mm dishes (Corning) and let grow to reach 80% confluence. Cells were transfected by lipofectamine with pcDNA6/V5-HISA encoding human YB-1-GFP bearing the gene for blasticidin resistance or with pcDNA3.1/His C control plasmid. After 48 hours from transfection, blasticidin was added to plates at a final concentration of 5mg/ml. As previously observed, pcDNA3.1/His C transfected cells start to die after 3 days of selection. After one week of selection cells were trypsinized and replated and after two weeks of selection stable clones were obtained.

Immunofluorescence Microscopy: 3×10^4 HEK293T, HEK293T GFP and HEK293T YB-1-GFP cells were seeded on poly-D-lysine pre-treated coverslips (12mm thickness); the day after, cells were treated or not with H_2O_2 (Sigma-Aldrich, St Louis, MO). At the end of treatment cells were gently rinsed with 1X PBS before adding PFA at 3,4% for 10 minutes to fix cells; after 3 washes with 1X PBS cells were permeabilized by adding 0.5% Triton X-100-PBS for five minutes; then, after 3 washes with 1X PBS, cells were blocked to avoid unspecific binding of antibodies with a 3% BSA solution for 20 minutes. Primary antibodies were added for 1hour (dilution range 1:200); after incubation, three washes with 0.05% Tween PBS were performed; then Alexa Fluor 488 (Life Technologies) and Cy3 (Jackson Immuno Research, USA) secondary antibodies were added for 45 minutes in dark; after 3 washes in 0.05% Tween PBS coverslips were immersed in a glycerol PBS solution and fixed. Direct eGFP signal was acquired without the addition of fluorescent dyes. Images were acquired using a Carl Zeiss LSM700 equipped with an axio Observer Z1 or with a Nikon TE Eclipse 2000. Image processing and analysis were performed with Fiji (ImageJ) software.

Cell Viability Assay: Cell viability was determined by the MTT 3-(4,5-dimethylthiazol-2-yl)-2,5-diphenyl tetrazolium bromide assay (Sigma-Aldrich, St Louis, MO) as previously described [10]. Cells were seeded in 96-well plate at the cell density of 2×10^3 ; the day after cells were treated or not with H_2O_2 . After treatment, cell medium was substituted with DMEM without phenol-red (GIBCO) and without supplements; MTT solution was added to cells to produce formazan crystals. After 2hrs MTT solution was substituted by acidic isopropanol to solubilize the formazan crystals. The optical

absorbance was determined at 570nm using an iMark microplate reader (Bio-Rad, USA). The experiments were carried out in triplicate for each experimental point and reported as percentage of the untreated control set at 1.0.

Trypan Blue Assay: Cells were seeded on poly-D-lysine pre-treated 12 well plates at $2,5 \times 10^5$. The day after plating, cells were treated or not; after treatment cells were gently rinsed with 1X PBS, trypsinized and collected. An aliquot was diluted 1:1 with trypan blue (Sigma-Aldrich, St Louis, MO). The experiments were carried out in triplicate for each experimental point.

Cell Proliferation Analysis: Cells were seeded on poly-D-lysine pre-treated 12-well plates at $2,5 \times 10^5$. Every 24 hours cells were gently rinsed with 1X PBS, trypsinized and counted in a Burkert chamber. The count was confirmed with analysis by a Scepter 2.0 (Millipore). The experiments were carried out in triplicate for each experimental point.

Immunoblot Analysis: Cells were seeded at 60% confluence (1.5×10^6) in 100mm plates; the day after, plates were gently rinsed with 1X PBS, and collected in Lysis Buffer (50mM Tris-HCl pH 7.5, 5mM EDTA, 150mM NaCl, 1% NP-40, 1Mm phenylmethylsulphonyl fluoride, 0.5% sodium deoxycholate, and protease inhibitors). Cells were then left on ice for 30 minutes, and crude extracts were obtained following centrifugation at 13200rpm for 30 minutes at 4°C. The amount of protein in the samples was determined by the Bio-Rad protein assay (Bio-Rad, Milan, Italy). After the addition of Laemmli buffer (Sigma Chemical Co, St. Louis, MO, USA) the samples were boiled at 100°C for 5min and resolved by SDS- polyacrylamide gel electrophoresis (SDS-PAGE). The proteins were then transferred to a polyvinylidene difluoride membrane (PDVF, Millipore) using a Mini trans-blot apparatus (Bio-Rad, Milan, Italy) according to the manufacturer's instructions. The PVDF membrane was blocked in 5% w/v milk buffer (5% w/v non-fat dried milk, 50mM Tris, 200mM NaCl, 0.2% Tween 20) and incubated with primary antibodies diluted in 5% w/v milk or bovine serum albumin (BSA) buffer overnight at 4°C. The blots, washed three times with TTBS (Tris-buffered saline, 0.1% Tween), were incubated for 1 hour at RT with HRP-conjugated secondary antibodies (SigmaAldrich). Proteins were visualized by an enhanced chemi luminescence method (ECL, GE-Healthcare) and analyzed by Quantity One W software of ChemiDoc TM XRS system (Bio-Rad, Milan, Italy).

Primary Antibodies: Anti-YB-1 (Abcam, UK); anti-PABP (Sigma-Aldrich, St Louis, MO); anti-GAPDH (Santa Cruz Biotechnology, USA) (Table 1).

Table 1: Statistical analysis.

Panel Experiment	Test Method	Significance	n
Panel c (proliferation curve)	Cell line vs. time		
	2 way ANOVA Time(h)		
	Cell line Interaction Sidak's multiple comparison test	F = 1031; p < 0,00*** F = 0,3737; p = 0,54 ns F = 67,97; p < 0,001***	6

	HEK293T vs. HEK293T YB-1-GFP			
	0 h	-	P>0,99 ns	
	24h	-	P=0,25 ns	
	48h	-	P<0.001***	
	72h	-	P<0,001***	
	96h	-	P<0,001***	
Panel E (Trypan blue count)		2-way ANOVA Time(h) Cell line Interaction Sidak's multiple comparison test	F=695,1; P<0,001*** F=493,3; P<0,001*** F=47,13; P<0,001***	3
	HEK293T vs. HEK293T YB-1-GFP			
	Control	-	P>0,99 ns	
	Hydrogen Peroxide 0,5 mM	-	P<0,001***	
	Hydrogen Peroxide 1 mM	-	P<0,001***	
	Hydrogen Peroxide 2,5 mM	-	P<0,001***	
	Hydrogen Peroxide 5 mM	-	P<0,001***	
	Hydrogen Peroxide 7,5 mM	-	P<0,001***	
Panel F (MTT assay)		2-way ANOVA Time(h) Cell line Interaction Sidak's multiple comparison test	F=1136; P <0,001*** F=43,62; P<0,001*** F=4,174; P=0,003***	6
	HEK293T vs. HEK293T YB-1-GFP			
	Control	-	p>0,99 ns	
	Hydrogen Peroxide 0,5 mM	-	P=0,010**	
	Hydrogen Peroxide 1 mM	-	P=0,71 ns	
	Hydrogen Peroxide 2,5 mM	-	P=0,29 ns	
	Hydrogen Peroxide 5 mM	-	P<0,001***	
	Hydrogen Peroxide 7,5 mM	-	P<0,002***	

Statistical analyses were performed using GraphPad Prism7 (GraphPad Software Inc). Statistical significance of difference in measured variables between control and treated groups was determined by the two-way analysis of variance (ANOVA) followed by Sidak's multiple comparisons post-test. Difference were considered significant at $P < 0.033$ (*), $P < 0.002$ (**) and $P < 0.001$ (***)

Conclusion

Stable cell lines represent a permanent resource that can be stored under cryogenic conditions for long periods of time, retrieved, and cultured to provide a consistent and reliable level of sustained gene expression. To explore the role of YB-1 localization upon stress stimuli we sought to generate a stable pool of cells constitutively expressing YB-1 as a GFP fusion protein. Preliminarily, we transiently transfected HEK293T cells with YB-1-GFP cDNA cloned in pcDNA6/V5-His, a vector derived from pcDNATM3.1(+) (Invitrogen). 5.0×10^5 cells were seeded in order to reach 80% confluence the day after; lipofection was performed using pcDNA6/V5-HisA-YB-1GFP and pEGFP-C1 empty vector as control [10]. 48 hours after transfection cells were analyzed by immuno blot to evaluate the level of YB-1-GFP fusion GFP exogenous expression. Transfected YB-1-GFP was highly expressed in HEK293T cells (Figure 1). Direct fluorescence, acquired by Nikon Eclipse 800 microscope,

showed a prevalent cytoplasmic localization for YB1-GFP (Figure 2). Moreover, viability of YB-1-GFP cells, as assessed by MTT assay, was undistinguishable from HEK293T parental cells and cells expressing GFP alone (data not shown). Next, we produced pools of clones of HEK293T stably expressing YB-1-GFP or GFP alone. YB-1-GFP expressing cells were selected by blasticidin in while G418 was used for selection of pEGFP-C1 stable pool. After 4 weeks, 91% of selected cells were GFP positive. Next, we analyzed the proliferation rate of YB-1-GFP expressing pool. Compared to the parental cell line, YB-1-GFP expressing cells grew slightly faster (Figure 3). To examine YB-1 protein localization under oxidative stress we treated HEK293T YB-1-GFP cells with hydrogen peroxide (H₂O₂). By immunofluorescence, we could observe typical stress granules (SGs) in control and GFP expressing cells, using a canonical SGs marker, PABP-1 Figure 4 left panel. Unexpectedly, YB-1 fusion protein was detected in unusual GFP positive aggregates that were ab-

normal in both dimension and shape (Figure 5 right panel arrows). Remarkably, although YB-1-GFP cells grew faster than control cells, their sensitivity to oxidative stress was increased as demonstrated by MTT and trypan blue assays (Figure 6). Taken together, our data show that, even though the GFP fusion protein behaved like the endogenous one and is localized in the right sub cellular compart-

ment, the presence of the huge GFP tag causes a lack in functionality that can be observed only in particular experimental conditions. Therefore, insights obtained so far with YB-1-GFP construct should be critically revised and, more in general, we should beware and be careful in interpreting data obtained with functionally uncharacterized GFP fusion proteins.

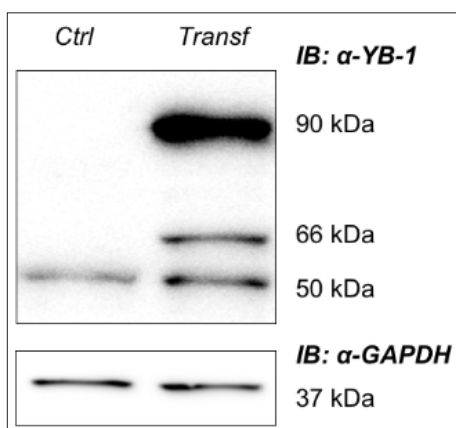


Figure 1: Western blot of total extracts from HEK293T YB-1-GFP and control (untransfected) HEK293T cells, showing the full length endogenous 50 kDa YB-1 band and the YB-1-GFP bands (66-90 kDa); GAPDH was used as loading control.

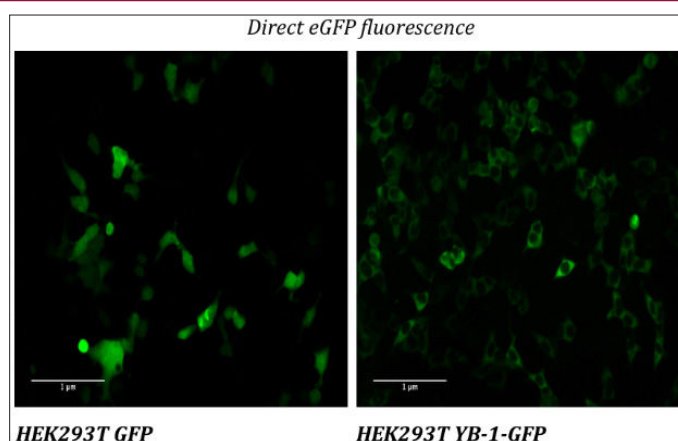


Figure 2: Direct eGFP fluorescence of HEK293T YB-1-GFP and HEK293T GFP in physiological conditions; images were acquired using a Nikon TE Eclipse 2000 (20x objective).

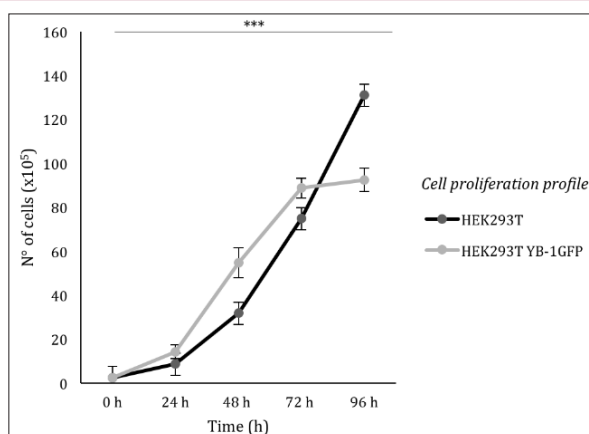


Figure 3: Cell proliferation profile of HEK293T and HEK293T YB-1-GFP from time 0 (seeding time) to 96 hours (2-way ANOVA $P < 0,001^{***}$, for post-hoc tests see Table 1).

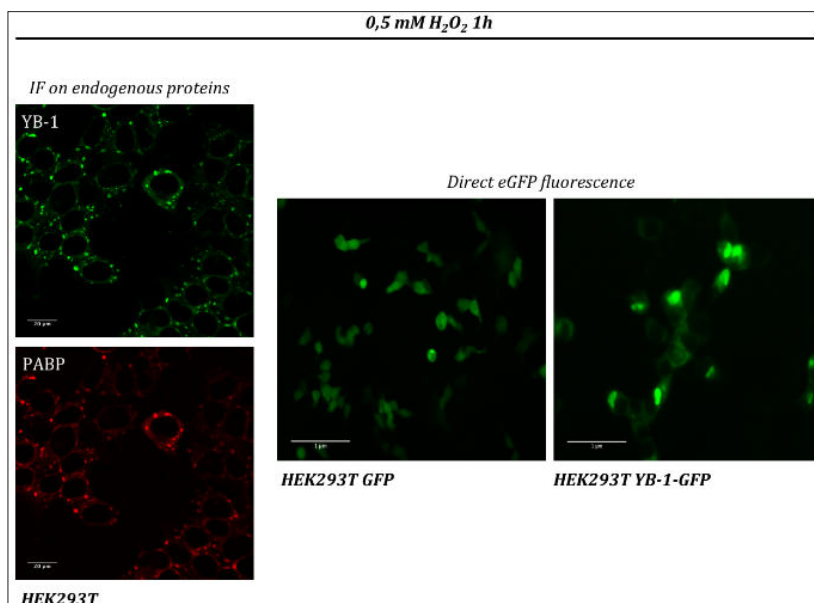


Figure 4: (left panel) confocal immunofluorescence of HEK293T treated with 0,5 mM hydrogen peroxide (H₂O₂) for 1 hour; PABP (red) and YB-1 (green) mark Stress Granules; (right panel) direct eGFP fluorescence of HEK293T, HEK293T GFP and HEK293T YB-1GFP treated with 0,5 mM hydrogen peroxide (H₂O₂) for 1 hour; images acquired using a Carl Zeiss LSM 700 (40x oil objective) (left panel) and Nikon TE Eclipse 2000 (20x objective) (right panel).

MTT assay	HEK293T	SD	HEK293T YB-1-GFP	SD	***
Control	100%	3,75	100%	7,5	
H ₂ O ₂ 0,5 mM	41,55%	1,59	39,95%	1,2	
H ₂ O ₂ 1 mM	36%	1,62	33,73%	3,54	
H ₂ O ₂ 2,5 mM	34,33%	1,66	31,03%	0,5	
H ₂ O ₂ 5 mM	32,86%	1,5	23,03%	0,5	
H ₂ O ₂ 7,5 mM	26,06%	0,5	19,67%	2,83	

Figure 5: Cell viability assay (MTT) of HEK293T and HEK293T YB-1-GFP cells treated with indicated concentrations of hydrogen peroxide (H₂O₂) for 1 hour (2-way ANOVA P<0,001***, for post-hoc tests see Table 1).

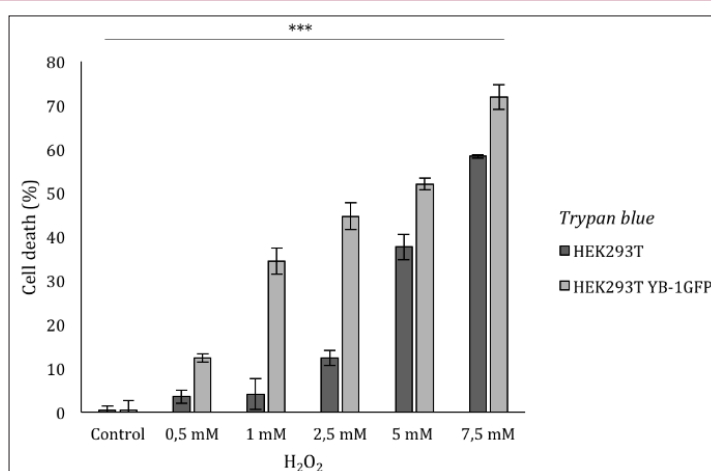


Figure 6: Trypan blue count; representation of the increasing number of dead cells after hydrogen peroxide (H₂O₂) treatments (2-way ANOVA P<0,001***, for post-hoc tests see Table 1).

References

1. Kohno K, H Izumi, Uchiumi T, Ashizuka M, Kuwano M (2003) The pleiotropic functions of the Y-box-binding protein, YB-1. *Bio Essays* 25(7): 691-698.
2. Ohga, T, Uchiumi T, Makino Y, Koike K, Wada M, et al. (1998) Direct involvement of the Y-box binding protein YB-1 in genotoxic stress induced activation of the human multi drug resistance 1 gene. *J Biol Chem* 273(11): 5997-6000.
3. Eliseeva IA, Kim ER, Guryanov SG, Ovchinnikov LP, Lyabin DN (2011) Y-boxbindingprotein 1 (YB-1) and its functions. *Biochemistry (Mosc)* 76(13): 1402-1433.
4. Matsumoto K, Tanaka KJ, Tsujimoto M (2005) An Acidic Protein, YBAP1, Mediates the Release of YB-1 from m-RNA and Relieves the Translational Repression Activity of YB-1. *Mol Cell Biol* 25(5): 1779-1792.
5. Di Costanzo A, Troiano A, Di Martino O, Cacace A, Calabro V, et al. (2012) The p63 protein isoforms $\Delta Np63\alpha$ modulates Y-box binding protein-1 in its subcellular distribution and regulation of cell survival and motility genes. *J Biol Chem* 287(36): 30170-3080.
6. Wei-Hong Yang, Donald B. Bloch (2007) Probing the mRNA processing body using protein macroarrays and "autoantigenomics". *RNA* 13(5): 704-712.
7. Kedersha N, Anderson P (2007) Mammalian Stress Granules and Processing Bodies. *Methods in Enzymology* 431: 61-81.
8. Somasekharan SP, El Naggat A, Leprivier G, Cheng H, Hajee S, et al. (2015) YB-1 regulates stress granule formation and tumor progression by translationally activating G3BP1. *J Cell Biol* 208(7): 913-929.
9. Lyons Shawn M, Achorn C, Kedersha NL, Anderson PJ, Ivanov P (2016) YB-regulates tiRNA-induced Stress Granule formation but not translational repression. *Nucl Acids Res* 44(14): 6949-6960.
10. Troiano A, Schiano Lomoriello I, Di Martino O, Fusco S, Pollice A, et al. (2015) Y-box Binding Protein-1 Is Part of a Complex Molecular Network Linking DNP63a to the PI3K/akt Pathway in Cutaneous Squamous Cell Carcinoma. *J Cell Physiol* 230: 2067-2074.



This work is licensed under Creative Commons Attribution 4.0 License

Submission Link: <https://biomedres.us/submit-manuscript.php>








Assets of Publishing with us

- Global archiving of articles
- Immediate, unrestricted online access
- Rigorous Peer Review Process
- Authors Retain Copyrights
- Unique DOI for all articles

<https://biomedres.us/>

Article

Oxidative Stress Causes Enhanced Secretion of YB-1 Protein that Restrains Proliferation of Receiving Cells

Andrea Maria Guarino ¹, Annaelena Troiano ¹, Elio Pizzo ¹, Andrea Bosso ¹, Maria Vivo ¹, Gabriella Pinto ², Angela Amoresano ², Alessandra Pollice ¹, Girolama La Mantia ¹ and Viola Calabrò ^{1,*}

¹ Dipartimento di Biologia, Università degli Studi di Napoli, Federico II, 80126 Napoli, Italy; andreamaria.guarino@unina.it (A.M.G.); annaelena.troiano@unina.it (A.T.); elipizzo@unina.it (E.P.); andrea.bosso@unina.it (A.B.); maria.vivo@unina.it (M.V.); apollice@unina.it (A.P.); lamantia@unina.it (G.L.M.)

² Dipartimento di Scienze Chimiche, Università degli Studi di Napoli, Federico II, 80126 Napoli, Italy; gabriella.pinto@unina.it (G.P.); angamor@unina.it (A.A.)

* Correspondence: vcalabro@unina.it; Tel.: +39-081-679-069

Received: 2 October 2018; Accepted: 18 October 2018; Published: 22 October 2018



Abstract: The prototype cold-shock Y-box binding protein 1 (YB-1) is a multifunctional protein that regulates a variety of fundamental biological processes including cell proliferation and migration, DNA damage, matrix protein synthesis and chemotaxis. The plethora of functions assigned to YB-1 is strictly dependent on its subcellular localization. In resting cells, YB-1 localizes to cytoplasm where it is a component of messenger ribonucleoprotein particles. Under stress conditions, YB-1 contributes to the formation of stress granules (SGs), cytoplasmic foci where untranslated messenger RNAs (mRNAs) are sorted or processed for reinitiation, degradation, or packaging into ribonucleoprotein particles (mRNPs). Following DNA damage, YB-1 translocates to the nucleus and participates in DNA repair thereby enhancing cell survival. Recent data show that YB-1 can also be secreted and YB-1-derived polypeptides are found in plasma of patients with sepsis and malignancies. Here we show that in response to oxidative insults, YB-1 assembly in SGs is associated with an enhancement of YB-1 protein secretion. An enriched fraction of extracellular YB-1 (exYB-1) significantly inhibited proliferation of receiving cells and such inhibition was associated to a G2/M cell cycle arrest, induction of p21WAF and reduction of $\Delta Np63\alpha$ protein level. All together, these data show that acute oxidative stress causes sustained release of YB-1 as a paracrine/autocrine signal that stimulate cell cycle arrest.

Keywords: cold shock proteins; stress granules; oxidative stress; protein secretion

1. Introduction

Oxidative stress is linked to a number of chronic diseases including diabetes, neurodegenerative and cardiovascular diseases, cancer, and aging [1]. The cold-shock Y-box binding protein 1 (YB-1) is involved in stress response [2] and chronic inflammation [3–5]. YB-1 is a member of the evolutionarily conserved cold shock domain (CSD) proteins and was first identified as a DNA binding protein interacting with the Y-box motif present in the major histocompatibility complex class II gene [6]. YB-1 binds to DNA and RNA [7] and it is involved in the transcriptional and translational control of many biological processes including cell proliferation and migration [8–11]. Moreover, YB-1 protein is upregulated in many types of human cancers including, breast, prostate, ovarian and melanoma [12,13].

Human YB-1 contains 324 amino acids [14]. Its structure can be subdivided into three domains namely N-terminal, cold shock (CS) and C-terminal domain. The short N-terminal domain, named A/P, contains 1–51 residues and is rich in alanine and proline. The central part of YB-1 is a CS

domain conserved from bacteria to human (52–129 residues) [9]. The long C-terminal domain (130–324 residues) contains positive and negative charged clusters of amino acids.

Accumulating evidence links YB-1 to the cell response to oxidative stress [2] and DNA damage [15–17]. More specifically, following acute oxidative stress, YB-1 localizes to cytoplasmic stress granules (SGs) where it participates in a pro-survival mRNA translational reprogramming [2]. Cytosolic YB-1 can also be found in P-bodies [18], TIA-containing SGs, but its precise role in these cytoplasmic structures remains to be defined [2,19–21].

Following DNA damage, YB-1 translocates to the nucleus to oversee DNA damage repair mechanisms [16,17]. Indeed, genotoxic stress triggers a limited cleavage of YB-1 by the 20S proteasome with the consequent accumulation of a 36 kDa truncated form of YB-1 (amino acids 1–219) in the nucleus [22]. Truncated YB-1 associates with Mre11 and Rad50 in DNA repair complexes [16]. Nuclear shuttling of YB-1 also takes place during cancer growth and upon activation of pro-survival signaling cascades such as PI3K/AKT, RSK, Ras/MAPK and PKC and is triggered by phosphorylation at serine 102 of YB-1 [23–27].

Recent data show that YB-1 can also be secreted after cytokine challenge by mesangial and immune cells [28] and is increased in sera from sepsis and tumor patients [29–31]. Here, we focused our studies on secreted YB-1 and found that oxidative stress enhances YB-1 secretion. Finally, using extracellular YB-1 (exYB-1) we provide some evidence of a role of exYB-1 as an autocrine/paracrine signal inducing cell cycle arrest.

2. Materials and Methods

2.1. Plasmids and Chemicals

The expression construct 5xMyc-YB-1 was previously described [32]. Plasmid pcDNA 3.1B, used as a control, was purchased by Thermo-Fisher Scientific (Waltham, MA, USA).

Sodium (meta)arsenite (NaAsO_2) (S7400 Sigma-Aldrich, Saint Louis, MO, USA); hydrogen peroxide (H1009 Sigma-Aldrich, Saint Louis, MO, USA) were used to perform oxidative stress. Trichloroacetic acid (TCA) (T4885 Sigma-Aldrich, Saint Louis, MO, USA) was used to extract proteins from cell culture medium.

2.2. Cell Culture

Human embryonic kidney cells (HEK293T), spontaneously immortalized keratinocytes from adult skin (HaCaT), and human colorectal adenocarcinoma cells (CaCo-2), were purchased from Cell Line Service (CLS, Eppelheim, Germany) and grown as previously described [33].

To increase HEK293T adhesion to glass/plastic surfaces, plates and slips for immunofluorescence were treated with poly-D-lysine 0.1 mg/mL (P7405, Sigma-Aldrich, Saint Louis, MO, USA) before seeding cells.

2.3. Immunofluorescence Microscopy

Confocal immunofluorescence was performed as previously described [34]. All images were acquired using a Carl Zeiss LSM700 (63× oil immersion objective). Image processing and analysis were performed with Fiji (ImageJ version 2.0) software.

2.4. Cell Viability Assays

Cell viability was determined by the crystal violet assay (CVA) method, through a (3-(4,5-dimethylthiazol-2-yl)-2,5-diphenyl-tetrazolium bromide) MTT based assay, or through trypan blue count as previously described [35].

Cells were seeded in 96-well plate for MTT (8×10^3 cells), in 35 mm dishes (2.5×10^5 cells) for CVA and in 12-well plates (1.5×10^5 cells) for trypan blue.

The day after plating, cells were treated or not. For crystal violet, dye uptake was measured at 570 nm using a Beckman Coulter spectrophotometer (DU730). Cell viability was calculated as dye intensity and compared with untreated samples.

For MTT, the optical absorbance was determined at 570 nm using an iMark microplate reader (Bio-Rad, Hercules, CA, USA). For trypan blue count, after treatment cells were gently rinsed with $1 \times$ Phosphate-buffered saline (PBS), trypsinized and collected. An aliquot was diluted 1:1 with trypan blue (Sigma-Aldrich, Saint Louis, MO, USA).

2.5. Cell Cycle Analysis

A total of 3×10^5 cells were seeded and let grow for 24 h; then, cells were serum starved for 24 h to achieve synchronization; the day after, cells were treated with recombinant YB-1 (rYB-1) or Conditioned Culture Medium derived YB-1 (CCM-YB-1) or left untreated for 24 h. Cells were then trypsinized, collected in PBS with the addition of 1% FBS, 0.25 mM ethylenediaminetetraacetic acid (EDTA) in PBS and centrifuged at 1200 rpm, 4 min, 4 °C; for each sample the same number of cells (1×10^5) was processed. The cell pellet was resuspended in methanol, incubated on ice for 20 min and centrifuged at 1200 rpm, 5 min, 4 °C. After a wash in PBS, the pellet was incubated in PBS, containing RNase A (Thermo-Fisher Scientific) 100 µg/mL for 20 min at RT. Propidium iodide (Sigma-Aldrich, Saint Louis, MO, USA) was then added at a concentration of 50 µg/mL for 30 min at 4 °C. Cell cycle analysis was performed on the BD Accuri C6 flow cytometer (BD Biosciences, San Jose, CA, USA).

2.6. Cell Proliferation Analysis

A total of 6×10^4 HaCaT and CaCo-2 cells were seeded in 12-well plate, while HEK293T were seeded on pre-treated 12-well; cells were serum starved for 24 h; after starvation, recombinant or CCM-YB-1 were added at different concentrations. Every 24 h cells were gently rinsed with $1 \times$ PBS, trypsinized and counted. The count was confirmed by Scepter 2.0 analysis (Millipore, Burlington, MI, USA) as previously described [36].

2.7. Transfections

Cells were transfected using Lipofectamine 2000 (Life Technologies, Carlsbad, CA, USA) according to the manufacturer's recommendations. Briefly, cells were seeded at 70–80% confluence (1.5×10^6) in 100-mm dishes and transiently transfected with different concentrations of plasmid (from 800 ng up to 1.5 µg).

YB-1 transient silencing was carried out with IBONI YB-1 small interfering (siRNA) pool (RIBOXX GmbH, Radebeul, Germany) and RNAiMAX reagent (Life Technologies, Carlsbad, CA, USA), according to the manufacturer's recommendations. Cells were seeded at 70–80% confluence (1.5×10^6) in 100-mm dishes and transiently silenced with IBONI YB1-siRNA at 100 nM final concentration.

All Star Negative Control siRNA, provided by Quiagen (Hilden, Germany), was used as negative control. YB-1 guide sequences:

5'-UUUAUCUUCUUCUAUUGCCGCCCCC-3'; 5'-JUUAUUCUUCUUAUGGCAGCCCCC-3';
5'-UUCAACAACAUAACUCCCCC-3'; 5'-UCAUAUUUCUUCUUGUUGGCCCCC-3'.

2.8. Antibodies

Primary antibodies: anti-YB-1 raised against the region 1 to 100 of YB-1 protein (12148 Abcam, Cambridge, UK); anti-PABP1 (poly(A)-binding-protein 1) (clone 10E10, Sigma-Aldrich); anti-Myc (SAB21084786, Sigma-Aldrich, Saint Louis, MI, USA); anti-cyclin D1 (GT8912, Genetex, Irvine, CA, USA); anti-cyclin A2 (GT2547, Genetex, Irvine, CA, USA); anti-GAPDH (6C5 Santa Cruz Biotechnology, Dallas, TX, USA); anti-PARP1 (Cell Signalling, Danvers, MA, USA); anti-RNH1 (436–450, Sigma-Aldrich, Saint Louis, MO, USA) anti-β-tubulin (H-235, Santa Cruz Biotechnology, Dallas, TX, USA); anti-actinin (AT6/172, Abcam, Cambridge, UK); anti-p21 WAF (1D21 Cell Signaling, Danvers, MA, USA); anti-ΔNp63α (4A4) (sc-8431 Santa Cruz Biotechnology, Dallas, TX, USA).

Secondary fluorescent antibodies: Alexa Fluor 488 anti-rabbit (Thermo-Fisher Scientific, Waltham, MA, USA); Cy3 anti-mouse (Jackson ImmunoResearch, Cambridge, UK); DAPI (Sigma-Aldrich, Saint Louis, MO, USA).

2.9. Immunoblot Analysis

Immunoblots were performed as previously described [37,38].

For total protein extraction and nuclear-cytoplasmic fractionation, cells were seeded at 60% confluence (1.5×10^6 cells) in 100-mm dishes. Then, 24 h after seeding, cells were treated or left untreated; cell lysates were fractionated to obtain total, cytoplasmic and nuclear fractions as previously described [38]. About 20 μ g of total extract, 10 μ g of nuclear and 30 μ g of cytoplasmic extracts (1:3 rate) were separated by SDS-PAGE and subjected to immunoblot.

Proteins were visualized by enhanced chemiluminescence (ECL, GE-Healthcare, Chicago, IL, USA) and ChemiDoc TM XRS system and analyzed by Quantity One W software (Bio-Rad, Milan, Italy).

2.10. Co-Immunoprecipitation

For co-immunoprecipitations (Co-IP) 2×10^6 HEK293T cells were seeded in poly-D-lysine pre-treated 100-mm dishes; the day after cells were treated with sodium arsenite (Na Ars) (Sigma-Aldrich, Saint Louis, MO, USA) 250 μ M for 30 min; cells extracts were incubated with an anti-PABP1 antibody (Sigma-Aldrich, Saint Louis, MO, USA), 3 μ g for 1 mg of protein extract overnight at 4 °C. The day after, Dynabeads Protein G (Invitrogen, Carlsbad, CA, USA) were added to samples for 4 h, at 4 °C in rotation. Immunoglobulin G (IgG) 3 μ g for 1 mg of protein extract was used as a negative control. Immunocomplexes were resolved with SDS-PAGE; immunoblot was performed with anti-YB-1 antibody (Abcam, Cambridge, UK).

2.11. Trichloroacetic Acid Precipitation

HEK293T cells were grown as previously described; Then, 24 h after seeding cells were gently rinsed twice with $1 \times$ PBS, and serum starved for 2 h. After treatments, cell culture medium was filtered through 0.22 μ m filters to remove floating cells and debris. Scepter 2.0 (Millipore, Burlington, MA, USA) was used to determine if cells were still present in the collected medium. Trichloroacetic acid 25% was added to culture medium in 1:1 ratio, tubes were placed on ice for 30 min. Samples were then centrifuged at maximum speed at 4 °C for 30 min. Supernatant was discarded and cold acetone 100% was added to tubes (200 μ L per sample), samples were then centrifuged at maximum speed, for 15 min, at 4 °C. This passage was done twice. Acetone was gently removed and 200 μ L of diethyl ether was added to tubes for 15 min on ice. After a centrifuge at maximum speed at 4 °C for 15 min, samples were placed on the block heater in order to evaporate diethyl ether. After addition of sample buffer. Samples were denatured in sample buffer (Sigma Chemical Co, St. Louis, MO, USA) and loaded on the gel.

2.12. Quantitative Real Time-PCR

A total of 3×10^5 cells was seeded and let grow for 24 h; the day after, they were treated with recombinant YB-1 (rYB-1) or CCM-YB-1 for 24 h or left untreated.

For real time (RT)-PCR cells analysis, total RNA was isolated using the RNA Extraction Kit from Qiagen (Hilden, Germany) according to the manufacturer's instructions. RNA (2–5 μ g) was treated with DNase I (Promega, Madison, WI, USA) and used to generate reverse transcribed cDNA using SuperScript III (Life Technologies, CA, USA), according to the manufacturer's instructions. RT-PCR with SYBR green (Promega) detection was performed with a 7500 RT-PCR Thermo Cycler (Applied Biosystem, Foster City, Carlsbad, CA, USA). The relative quantification in gene expression was determined using the $2^{-\Delta\Delta C_t}$ method.

Expression levels were normalized using *g6pd* mRNA expression.

For each gene, primer sequences are presented in Supplementary Materials Table S3.

2.13. Statistical Analysis

Statistical analyses were performed using GraphPad Prism (version 7.0, GraphPad Software Inc., San Diego, CA, USA).

Statistical significance of the difference in measured variables between control and treated groups was determined by *t*-test or analysis of variance (ANOVA) followed by Tukey's or Dunnett's multiple comparisons post-test. Differences were considered significant at $p < 0.033$ (*), $p < 0.002$ (**) and $p < 0.001$ (***). To report *p*-values, the New England Journal of Medicine (NEJM) decimal format was used; differences were considered statistically significant at * $p < 0.033$, ** $p < 0.002$ and *** $p < 0.001$. Detailed statistical information is shown in Table S2.

3. Results

3.1. YB-1 Is Recruited in Stress Granules under Diverse Stress Stimuli

It is documented that the functions played by YB-1 are strictly dependent on its subcellular localization [16,39,40]. Thus, we examined YB-1 subcellular localization in human HEK293T cells in resting conditions and following treatment with Na Ars, a well-known inducer of oxidative stress and translational arrest [41,42]. By double immunofluorescence labelling and confocal microscopy using antibodies against YB-1 and PABP1, another specific SGs marker [43], we found that YB-1 and PABP1 were evenly distributed in the cytoplasm in resting conditions (Figure 1a, control). However, following heat shock or treatment with Na Ars or hydrogen peroxide, YB-1 was found to co-localize with PABP1 in cytoplasmic stress granules (Figure 1a). Interestingly, the size and overall number of SGs per cell were different depending on the type of stimulus applied (Figure 1b, upper and lower panels), thus confirming previous findings indicating stress-specific differences in composition and assembly of stress granules [44].

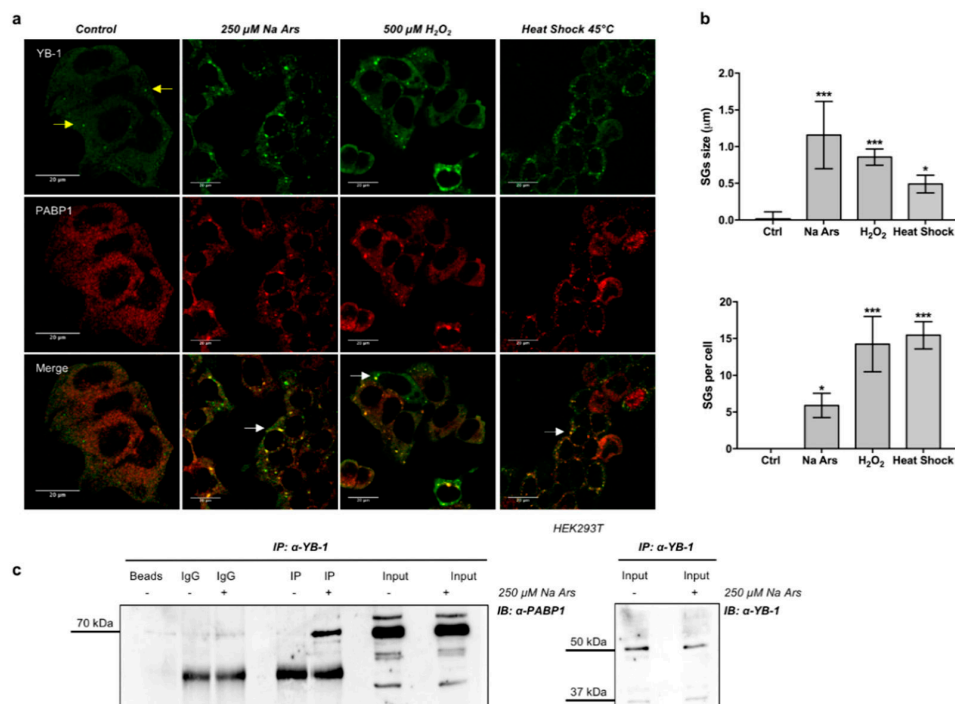


Figure 1. Y-box-binding protein 1 (YB-1) and Poly(A)-binding protein 1 (PABP1) co-localize and interact in stress granules (SGs) under stress conditions. (a) Confocal immunofluorescence of un-treated (control) HEK293T, and treated with 250 μM sodium arsenite (Na Ars) for 30', 500 μM H₂O₂ for 1 h or subjected to heat shock at 45 °C for 1 h, stained with α-YB-1 (green) and α-PABP1 (red); yellow and white arrows indicate P-bodies and stress granules respectively; (b) (Upper panel) size and number (lower panel) of SGs after treatments compared to control; statistical analysis was performed using 1-way ANOVA

followed by Dunnett's multiple comparisons test. Levels of significance are indicated (***) $p < 0.001$, * $p = 0.001$, see also Supplementary Materials Table S2); (c) Co-immunoprecipitation of HEK293T total protein extracts treated (+) or not (–) with 250 μM Na Ars for 30'; extracts were immunoprecipitated for YB-1 and immunorevealed for PABP1. Input samples immunorevealed with α -PABP1 and α -YB-1 are shown. Each panel is assembled from cropped Western blotting images (see original Western blot file for the original images).

Next, we immunoprecipitated YB-1 protein from extracts of HEK293T cells left untreated (–) or treated with 250 μM Na Ars (+). As shown in Figure 1c, PABP1 was detectable in YB-1 immunocomplexes exclusively from Na Ars treated cells, indicating that YB-1 and PABP1 association occurs predominantly in SGs.

To determine the relevance of YB-1 in SGs assembly, we depleted HEK293T cells of YB-1 using a specific siRNA pool against endogenous YB-1 mRNA (siYB1). By immunoblot and densitometric analysis we found that the expression level of YB-1 protein was reduced to 55% of control (Figure 2a). However, YB-1 knock-down consistently impaired the assembly of arsenite-induced PABP1-positive stress granules by reducing their size and number (Figure 2b, upper and lower panels and Figure 2c). Interestingly, in YB-1 depleted cells, PABP1 was located into the nucleus both in resting and under stress condition (Figure 2c), thus suggesting that YB-1 may act as a cytoplasmic anchor for PABP1.

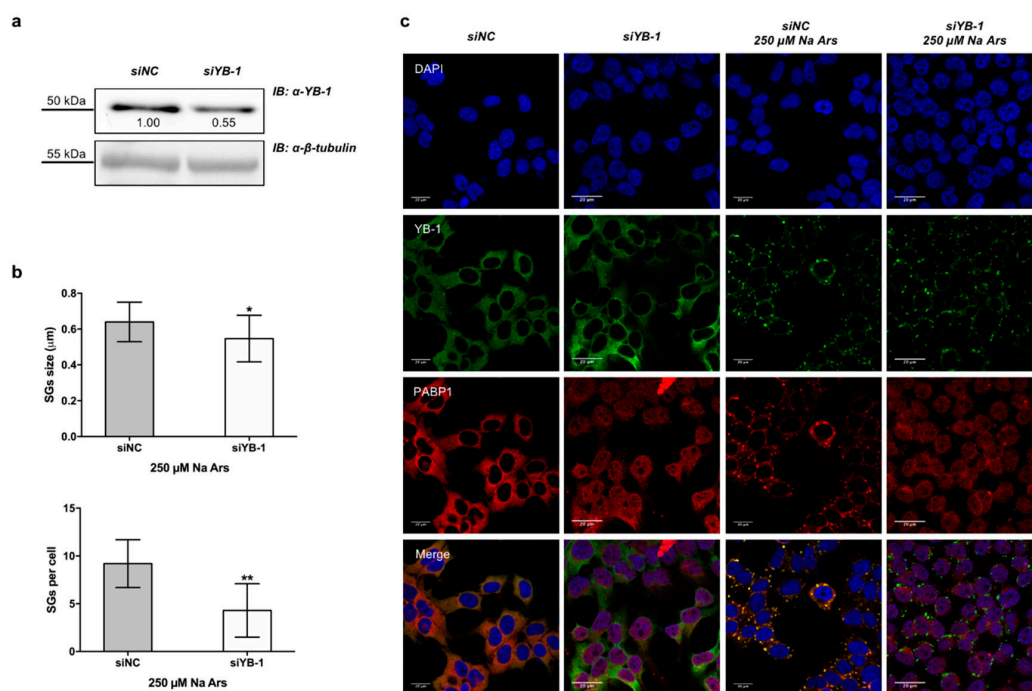


Figure 2. Silencing of YB-1 affects PABP1 positive SGs formation. (a) Western blot of total extract from control (siNC) or 100 nM YB-1 silenced (siYB-1) HEK293T; the degree of reduction of YB-1 protein levels in YB-1 siRNA-treated cells compared with control is indicated beneath each band in the Western blot (where the relative unit 1.0 represents YB-1 levels in cells transfected with the control siRNA). β -tubulin was used as loading control. Each panel is assembled from cropped Western blotting images (see original Western blot file for the original images); (b) (Upper panel) size and number (lower panel) of stress granules (SGs) in YB-1 silenced cells treated with Na Ars compared to siNC (control) cells; statistical analysis was performed using unpaired *t*-test with Welch's correction (** $p = 0.010$ and * $p = 0.02$ see Supplementary Materials Table S2); (c) Confocal immunofluorescence of control (siNC) and silenced (siYB-1) HEK293T cells, treated or not with 250 μM Na Ars for 30', stained with α -YB-1 (green) and α -PABP1 (red), nuclei are stained with DAPI (blue).

3.2. Arsenite-Induced Oxidative Stress Promotes YB-1 Secretion

We performed Western blotting analysis to reveal YB-1 protein in total extracts of Na Ars and H₂O₂-treated HEK293T cells. Despite the apparent enrichment of YB-1 in SGs, we found a significant reduction of the level of intracellular YB-1 protein (Figure 3a,b). By immunoblot analysis of HEK293T nuclear and cytoplasmic fractions we found that the reduction of YB-1 protein level induced by Na Ars was exclusively at the expense of the cytoplasmic pool, while nuclear YB-1 was totally unaffected (Figure 3c). YB-1 was previously found to be secreted [45,46] therefore we hypothesize that the decrease of cytoplasmic YB-1 was due to oxidative stress-enhanced YB-1 secretion. To prove this hypothesis, we treated HEK293T cells with Na Ars and precipitated the supernatant by TCA at different time points (from 30' to 240'). Trichloroacetic acid-precipitated fractions were then subjected to immunoblot and revealed with antibodies against YB-1 and Ribonuclease/Angiogenin Inhibitor 1 (RNH1) a not secreted cytoplasmic ribonuclease inhibitor abundantly expressed in HEK293T [47]. As shown in Figure 3d, in the 240' time course the amount of secreted YB-1 protein upon Na Ars treatment significantly increased and peaked after 60'. RNH1 signal was barely detectable ensuring that the increase of exYB-1 was not due to cell death and passive release (Figure 3d, lane 3, lower panel). Moreover, after 30' and 60' treatment with 250 μ M Na Ars or 500 μ M hydrogen peroxide, cell viability was only slightly reduced (90% and 94%, respectively) compared to control cells and the increase of trypan blue positive cells was negligible (Figure S1a,b, respectively). These data further indicate that extracellular accumulation of YB-1 was not due to cell injury.

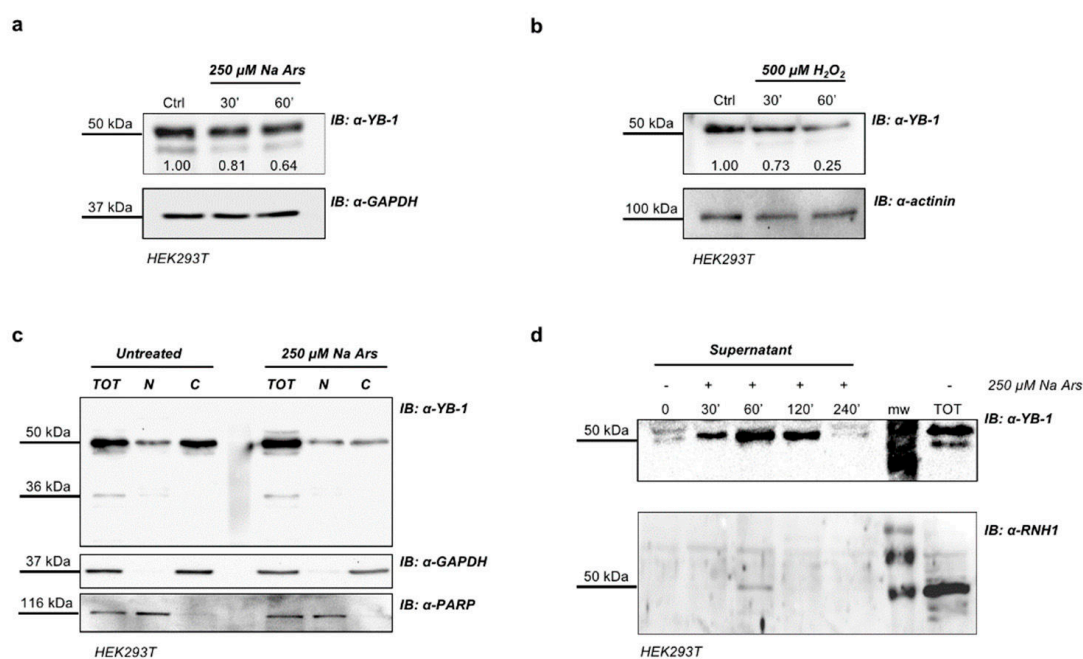


Figure 3. Na Ars induced oxidative stress promotes YB-1 secretion. Western blot of total protein extracts from HEK293T treated with 250 μ M Na Ars (a) or 500 μ M H₂O₂ (b) for 30' and 60'; glyceraldehyde 3-phosphate dehydrogenase (GAPDH) and actinin were used as loading control. The degree of reduction of YB-1 protein levels in treated cells compared with controls is indicated beneath each band in the Western blot (where the relative unit 1.0 represents YB-1 levels in control cells); (c) Western blot of total extract and nuclear/cytoplasmic fractionation of Na Ars treated and untreated HEK293T. GAPDH and PARP were used as loading control for cytoplasm and nucleus, respectively; (d) Western blot of TCA precipitated supernatants of HEK293T cells. Ribonuclease/Angiogenin Inhibitor 1 (RNH1) was used as negative control of cell lysis. Each panel is assembled from cropped Western blotting images (see original Western blot file for the original images).

Similar results were obtained from Western blot analysis of supernatants from HEK293T cells transfected with Myc-YB-1 expression plasmid and treated with Na Ars 250 μ M for 30', 60' and 120'. Immunoblotting of TCA-precipitated CCM media showed the presence of Myc-tagged YB-1 only in arsenite-stimulated cells thus indicating that stressed cells can also secrete transfected YB-1 (Figure S2).

3.3. Extracellular YB-1 Exerts Anti-Proliferative Effects on Receiving Cells

To analyze the effects of exYB-1 on receiving cells we prepared a YB-1 enriched fraction from HEK293T conditioned cell culture medium (CCM-YB-1) by ammonium sulphate precipitation followed by high performance liquid chromatography (HPLC) purification. Furthermore, we produced a recombinant YB-1 from *Escherichia coli*, that was accumulated mainly in bacterial cytosolic fraction. CCM-YB-1 and rYB-1 were analyzed by SDS-PAGE and YB-1 immunopositive bands were manually excised as reported in Figure S3. Each band was subjected to in situ tryptic digestion and peptides eluted from the gel were analyzed by LTQ-Orbitrap mass spectrometer (Thermo-Scientific, Waltham, MA, USA) (see Appendix A). By matching MS and MSMS data obtained from the mass spectrometer and peptide sequence databases by Mascot search engine, a high number of identified peptides was obtained with an error lower than 10 ppm. We obtained a high sequence coverage of 79% for R1 band (rYB-1 band 1 in Figure S3), 78% for R2 (rYB-1 band 2 in Figure S3), 60% for S1 and 29% for S2 (CCM-YB-1 band 1 and 2 respectively, in Figure S3). A list of peptides with relative score, sequence and modification allowed to unambiguously identify the YB-1 protein with a high sequence coverage and protein score (Table S1).

We have previously demonstrated that intracellular YB-1 is implicated in keratinocytes proliferation and survival to oxidative stress [40,48]. To get an insight into the function of secreted YB-1 we evaluated the proliferative response of HaCaT cells to the addition of rYB-1 or HPLC-purified YB-1 from HEK293T cell culture medium (CCM-YB-1).

HaCaT cells were then incubated for the indicated time with increasing amounts (5.0, 7.5 and 10 μ g/mL) of rYB-1 protein, CCM-YB-1 or Bovine Serum Albumin (BSA) as control in serum supplemented culture medium. As shown in Figure 4a,b, treatment with CCM-YB-1 or rYB-1 reduced the rate of proliferation of HaCaT cells while equivalent amounts of BSA were ineffective (Figure 4c). This effect was not cell type specific since it was also observed using HEK293T and CaCo2 as receiving cells (Figure S4). Remarkably, compared to rYB-1, CCM-YB-1 exerted a stronger inhibitory effect on all cell lines tested (Figure 4a,b; Figure S4). This was confirmed by Crystal Violet Assay (CVA) where HaCaT cells treated with 7.5 μ g/mL of CCM-YB-1 for 48 h showed a 47% reduction in viable cells compared to a 11% reduction obtained with the same amount of rYB-1 (Figure 4d).

The effect on the rate of cell proliferation caused by CCM-YB-1 and rYB-1 was associated to a G2/M phase cell cycle arrest, as indicated by flow cytometry analysis of HaCaT cells treated with exYB-1 (Figure 5a). Finally, to explore the molecular mechanism underlying inhibition of cell proliferation by exYB-1 we analyzed by quantitative PCR the mRNA level of *p21waf* and $\Delta np63\alpha$ in rYB-1 or CCM-YB-1 treated HaCaT cells. *p21WAF* is a relevant cell cycle marker that induces G1 and G2/M cell cycle arrest by inhibiting the kinase activity of Cyclin-dependent kinase (CDK)-cyclin complexes [49] while $\Delta Np63\alpha$ maintains the proliferative capacity of keratinocytes [50]. *p21waf* was strongly induced by both rYB-1 and CCM-YB-1 while $\Delta np63\alpha$ was significantly downregulated only by treatment with CCM-YB-1 (Figure 5a,b). By Western blot analysis we also confirmed reduction of $\Delta Np63\alpha$ and induction of *p21WAF* at protein level (Figure 5c,d). Moreover, according to the observed cell cycle arrest the level of cyclin A2 and cyclin D1 were also reduced (Figure 5c).

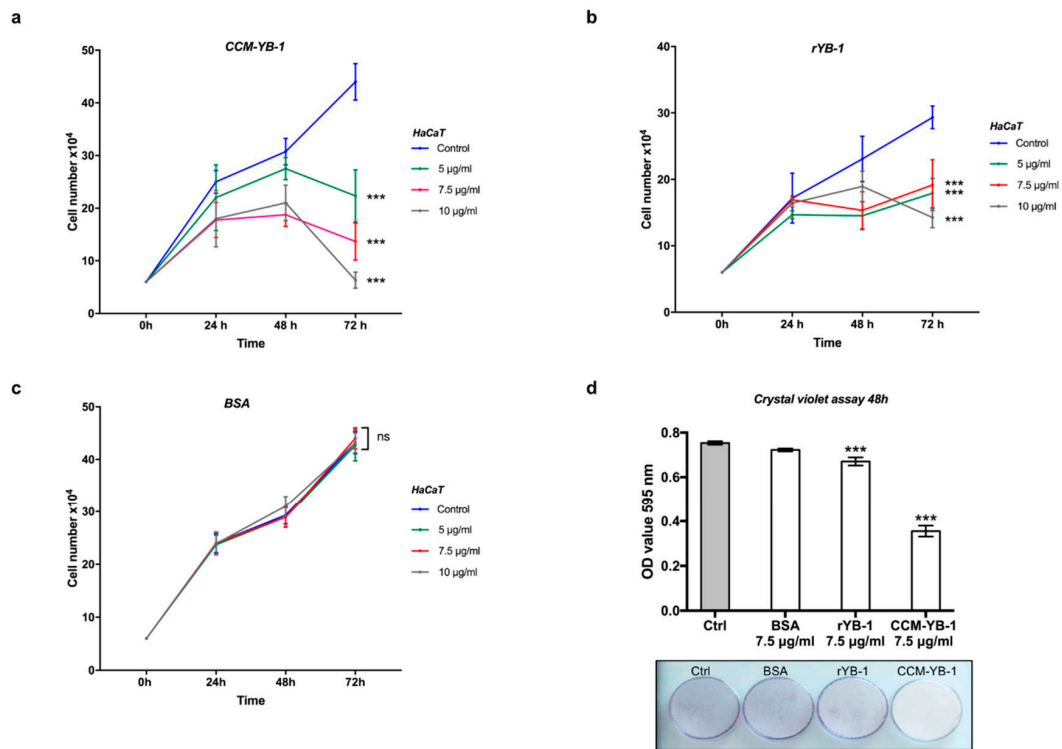


Figure 4. Extracellular YB-1 (exYB-1) affects HaCaT cell proliferation. Cell proliferation profile of HaCaT cells incubated with indicated concentrations of CCM-YB-1 (a), rYB-1 (b) or Bovine Serum Albumin (BSA) (c); statistical analysis was performed using 2-way ANOVA followed by Dunnett’s multiple comparisons test. Levels of significance are indicated (***) $p < 0.001$, see also Supplementary Materials Table S2); (d) Crystal violet assay of HaCaT cells treated with 7.5 µg/mL of CCM-YB-1, rYB-1, BSA or left untreated (Control; (bars) optical absorbance at 595 nm is reported on the y-axis; (image) representative colorimetric evaluation. Statistical analysis was performed using 1-way ANOVA followed by Dunnett’s multiple comparisons test. Levels of significance are indicated (***) $p < 0.001$, see also Supplementary Materials Table S2).

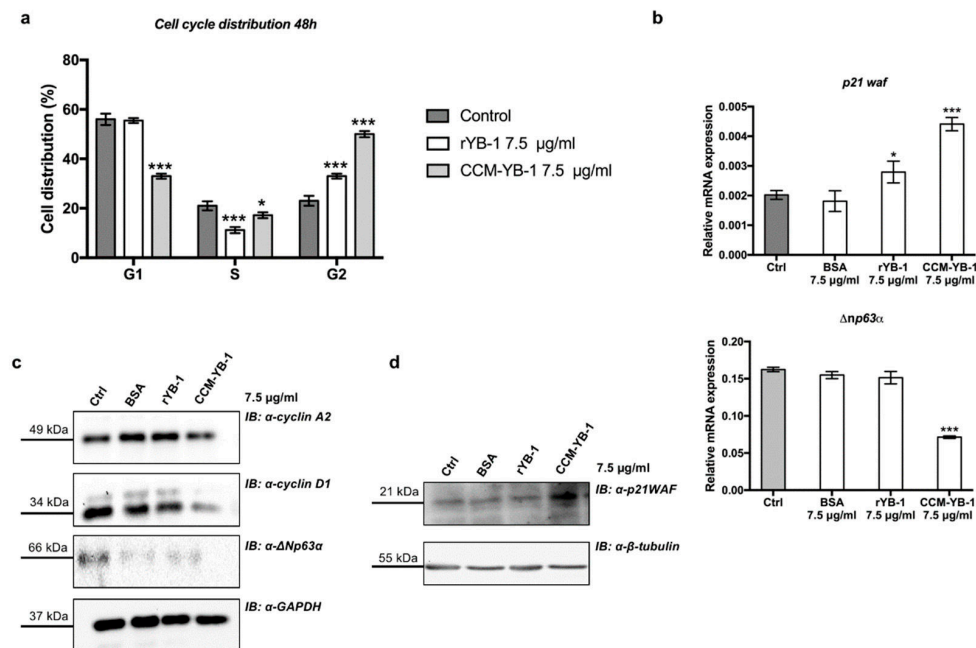


Figure 5. Extracellular YB-1 induced G2/M phase arrest. (a) Cell cycle profile of HaCaT cells treated with 7.5 µg/mL of CCM-YB-1, rYB-1, BSA or left untreated for 48 h. Statistical analysis was performed

using 2-way ANOVA followed by Dunnett's multiple comparisons test. Levels of significance are indicated (** $p < 0.001$, * $p = 0.01$, see also Supplementary Materials Table S2); (b) RT-qPCR analysis of *p21waf* and *Δnp63α* in HaCaT cells treated with 7.5 μg/mL of CCM-YB-1, rYB-1, BSA or left untreated (Control for 48 h. Statistical analysis was performed using 1-way ANOVA followed by Dunnett's multiple comparisons test. Levels of significance are indicated (** $p < 0.001$, * $p = 0.01$, see also Supplementary Materials Table S2); (c,d) Western blot analysis of total extracts of HaCaT cell treated with rYB-1 and CCM-YB1 and revealed with the indicated antibodies. GAPDH and β-tubulin were used as loading control. Each panel is assembled from cropped Western blotting images (see original Western blot file for the original images).

4. Discussion

Although YB-1 was originally identified as a transcription factor belonging to the Y-box binding family, a number of works provide evidence that YB-1 possesses additional functions, independent of its DNA binding activity [7,9,39]. Based on more recent literature, a possible regulatory role of YB-1 in inflammation and stress response has started to emerge [4].

The goal of our study was to investigate the function of YB-1 protein under stress conditions. In unstressed cells, YB-1 was diffusely distributed throughout the cytoplasm. Upon addition Na Ars, H₂O₂ and heat shock at 45 °C, we observed YB-1 protein association to SGs, which constitute a canonical cellular response to stress. In HEK293T cells, YB-1 almost complete co-localizes with the SGs marker PABP1; the co-localization was accompanied by the physical interaction between the two proteins, only in stress conditions.

Moreover, we show that YB-1 silencing impairs the assembly of PABP-1 positive SGs under stress conditions, thus confirming that YB-1 plays a pivotal role in the aggregation of SG components. Interestingly, we also found that PABP1 was mainly nuclear in YB-1 depleted cells, under normal as well as stress conditions, indicating that YB-1 may retain PABP1 protein in the cytoplasmic compartment. This observation raises the question of whether YB-1 silencing, by altering PABP1 localization, also influences the metabolism of PABP1-associated transcripts.

Involvement of YB-1 in SGs formation has potential pathological relevance in vivo, given that SGs formation in cancer cells might protect them against stress-induced cell damage and death [2]. Indeed, because of metabolic and signaling aberrations, cancer cells exhibit elevated ROS levels that can promote tumor formation and progression by inducing DNA mutations and pro-oncogenic signaling pathways [51]. By impairing SGs assembly, YB-1 depletion may weaken the antioxidant capacity of tumor cells, thus sensitizing them to necrosis/apoptosis and may have a therapeutic impact in cancer chemotherapy.

In the process of characterization of YB-1 response to cellular stresses, we observed a decrease of total amount of the protein after Na Ars or hydrogen peroxide treatments. This result sounded unexpected, considering the relevance of YB-1 in SGs.

Remarkably, the decrease of YB-1 protein level was at the expenses of cytoplasmic YB-1, while nuclear YB-1 was totally unaffected.

However, considering that YB-1 is normally released in the culture medium by HEK293T cells [28], we speculated that stress stimuli may function as enhancers of YB-1 protein secretion.

Interestingly, we found a significant increase of exYB-1 level during Na Ars treatment; such increase was clearly detectable after 30 min and peaked at 60 min of treatment. After 4 h of treatment the level of exYB-1 was reduced probably because of protein degradation. It should be noticed that non-specific YB-1 release due to cell death was excluded by cell viability assays (viability of treated cells >95%) and the lack of comparable RNH1 release, a highly abundant cytoplasmic protein.

YB-1 secretion after cell stimulation is not unprecedented. Recently, YB-1 was found to be secreted by Lipopolysaccharide (LPS)-stimulated human monocytes and mesangial cells and acts as an extracellular mitogen by interacting with Notch-3 receptor [45]. YB-1 has been isolated in extracellular vesicles and postulated to play a role in sorting small noncoding RNAs into a subpopulation of

exosomes [52]. However, it has to be noted, that in previous manuscripts neither YB-1 positive SGs formation nor reduction of intracellular YB-1 was observed in stimulated cells [45].

Extracellular occurrence of YB-1 raises the question of its functional relevance. So far, the functional role of exYB-1 and the pathological implications of secreted YB-1 are largely unknown. Data from other laboratories indicated that exYB-1 may be involved in tumor progression since addition of recombinant YB-1 to cancer cell lines revealed pro-mitogenic effects [45].

Intriguingly, we found that exYB-1 exerts an anti-proliferative effect on receiving HaCaT, HEK293T, and CaCo-2 cells. Remarkably, YB-1 is normally released in the culture medium by HEK293T cells but not by HaCaT or CaCo2 cells even though all these cell lines express high levels of endogenous YB-1. This may depend on a particular pathway constitutively activated in HEK293T cells or rely on specific posttranslational modifications occurring in HEK293T and possibly other cell contexts facilitating YB-1 extracellular release.

Treatment of HaCaT cells with exYB-1 induced a G2/M cell cycle arrest associated with p21WAF induction and Δ Np63 α reduction. The effect of CCM-YB-1 was more pronounced compared to that of the rYB-1. We can speculate that specific posttranslational modifications, such as ubiquitination and/or sumoylation, occurring in mammalian cells can explain the different effects showed by CCM-YB1 and rYB-1 proteins on receiving cells. Alternatively, bacterially synthesized rYB-1 may have a different protein folding that partially affect its functions.

It has been reported that intracellular YB-1 activates Notch signalling [53] and acts as a mediator of signals transmitted via the EGFR-RAS-MAPK [54] enhancing Δ Np63 α level in keratinocytes. Therefore, we postulate that exYB-1 may either activate Notch or repress EGFR pathways, thus reducing Δ Np63 α level which is known to support the proliferative potential of normal and transformed keratinocytes [55].

We can presume that upon severe tissue-injury, exYB-1 can signal to neighboring cells that a cell cycle arrest is required to allow cells to recover from stress and/or avoid the propagation of genetic lesions and repair them. However, further studies are needed to define the molecular mechanisms by which YB-1 can signal and regulate this response in receiving cells and the exact cellular source and targets in patients with malignant disorders.

Supplementary Materials: The following are available online at <http://www.mdpi.com/2073-4425/9/10/513/s1>, Figure S1: YB-1 presence in the cell medium is not due to cell death and lysis, Figure S2: Transfected myc-YB-1 can be secreted by cells, Figure S3: Band excision, Figure S4: Extracellular YB-1 affects HEK293T and CaCo2 cell proliferation. Table S1: MS/MS analysis of rYB-1 and CCM-YB-1, Table S2: Statistical analysis, Table S3: RT-qPCR assay PCR primers.

Author Contributions: V.C. designed the research project and prepared the manuscript. A.M.G., A.T. and M.V. performed the experiments. E.P. and A.B. produced recombinant and CCM-purified YB-1 protein. G.P. and A.A. performed Mass Spectrometry analysis. V.C. and A.M.G. analyzed the data; A.M.G. prepared the figures.

Funding: This research received no specific grant from any funding agency in the public, commercial or not-for-profit sectors. Andrea Maria Guarino is supported by 31st PhD program in Biotechnology 2016-2019-MIUR. Viola Calabrò is supported by Ricerca Dipartimentale 2017-2018-MIUR. Viola Calabrò is also supported by the MIUR-DAAD Joint Mobility Program 2018.

Acknowledgments: We thank Daniela Vallone for helpful support and discussion.

Conflicts of Interest: The authors declare no conflicts of interest.

Appendix A.

Appendix A.1. Preparation of Bacterial Expression Vector pET22b⁽⁺⁾/YB-1

Recombinant vector pEX-A2 containing human YB-1 cDNA sequence (purchased from Eurofins Genomics, Edersberg, Germany), has been used as template for a PCR reaction.

PCR has been carried out using following primers: forward 5'-CC**CA**TATGAGCAGCGAGGCCGAGACCC-3'; reverse 5'-GG**AAGCTT**GCCTCGGGAGCGGGAA-3'. Bold and underlined sequences refer to restriction sites (NdeI and HindIII), designed to permit the

insertion of YB-1 coding sequence upstream to a His-Tag sequence to facilitate the purification of the recombinant protein. The PCR reaction was carried out in a total volume of 50 μ L containing 60 ng of each primer, 20 ng of template, deoxyribonucleotides (dNTPs) containing 0.2 mM of each dNTP, 5 μ L 10 \times Taq buffer and 1.5 units of Taq DNA polymerase (EuroClone, Milan, Italy). PCR was performed under the following conditions: An initial denaturation step at 98 $^{\circ}$ C for 5 min, followed by 38 cycles of 30 s at 98 $^{\circ}$ C, 1 min at 65 $^{\circ}$ C, and 2 min at 72 $^{\circ}$ C. PCR products were then isolated by electrophoresis on 1% agarose gel, and purified using the Product Purification Kit (Roche Applied Science, Monza, Italy). Purified DNA, treated with NdeI and HindIII restriction enzymes, was inserted into the pET22b (+) expression vector by ligation reaction catalyzed by T4 DNA ligase (Thermo Fisher Scientific, Waltham, MA, USA). All cloned, purified DNAs were certified through sequencing (Eurofins Genomics, Edersberg, Germany) before processing. The recombinant expression plasmid was used then to transform competent *E. coli* strain BL21(DE3) (New England BioLabs, Ipswich, MA, USA).

Appendix A.2. Recombinant YB-1 Protein Preparation

The expression plasmid pET22b(+)/YB-1 was used to transform competent *E. coli* strain BL21(DE3) cells. Cells were grown at 37 $^{\circ}$ C to an $A_{600\text{ nm}} = 0.7$, and then induced with 0.6 mM isopropyl-1-thio-D-galactopyranoside (IPTG) and grown overnight. The expression level of rYB-1 was estimated performing a Western blot on two bacterial aliquots collected before the addition of IPTG and after 16 h respectively. Bacterial cells were then harvested by centrifugation (7000 rpm, 4 $^{\circ}$ C, 15 min), re-suspended in 100 mM Tris acetate buffer (pH 8.0) and subjected to sonication in presence of protease inhibitors. Cell debris and precipitated proteins were removed by centrifugation (17,500 \times g, 1 h) whereas the supernatant was subjected to at least three washes in 100 mM Tris acetate pH 8.0 and finally centrifuged to separate inclusion bodies and cytosolic soluble fraction, the latter containing rYB-1. Recombinant YB1 was purified performing a two-step procedure composed by an affinity chromatography followed by a reverse phase chromatography.

Appendix A.3. Chromatographic Procedures

Affinity chromatography was carried out on HisTrap resin (GE Healthcare, Chicago, IL, USA) equilibrated with 100 mM Tris acetate pH 8.0 containing 20 mM imidazole. Elution was carried out by using 100 mM Tris acetate pH 8.0 containing 500 mM imidazole and spectrophotometrically monitored at 280 nm. Reverse phase chromatography was performed on a HPLC device Series 200 (Perkin Elmer, Waltham, MA, USA) by using a C4 column (Dr. Maisch GmbH, Ammerbuch-Entringen, Germany), 0.1% TFA in 5% acetonitrile as buffer A and 0.1% TFA in 95% acetonitrile as buffer B. Elution was performed by setting a linear gradient 5–95% buffer B in 60 min and spectrophotometrically monitored at 278 nm.

Appendix A.4. Extraction of Human Secreted YB-1 from HEK293T Cell Culture Medium

All culture media, enriched with secreted YB-1, have been processed with three subsequent steps of protein precipitations by using ammonium sulfate (Sigma Aldrich, Milan, Italy). The concentration of ammonium sulfate was increased from 0 to 30%, 30% to 70% and, finally until 100%, determining proteins salting out. Between each step, media were centrifuged 1 h at 14,000 rpm and 4 $^{\circ}$ C to sediment protein aggregates. All sediments were finally re-suspended in PBS, quantified and then analyzed by SDS-page and Western blotting.

Appendix A.5. Protein Separation by SDS-PAGE and In Situ Digestion

The proteins precipitated from culture medium were separated by 12% SDS-PAGE, under reducing conditions. Proteins were visualized by colloidal Coomassie brilliant blue and the immunopositive bands were excised, also depending on the visualization of bands at expected molecular weight. Each band was subjected to in situ digestion protocol by reducing proteins by 10 mM DTT and alkylation with 55 mM iodoacetamide, according to the established protocol. Finally, each dry gel

piece was rehydrated in 40 μ L of 10 mM ammonium bicarbonate solution containing 200 ng of Trypsin Gold, Mass Spectrometry grade (Promega, Madison, WI, USA), and incubated at 37 °C overnight. The trypsinolysis was stopped with 0.1% formic acid (FA), and tryptic peptides were eluted, vacuum dried, and dissolved in 0.1% formic acid for LC-MS/MS analysis.

Appendix A.6. LTQ-Orbitrap Analysis

Peptides were separated on a 1.7- μ m BEH C18 column (Waters Corporation, Milford, MA, USA) at a flow rate of 280 nL/min by using as mobile phase solution A: 95% water, 5% acetonitrile, 0.1% acetic acid; solution B: 95% acetonitrile, 5% water, 0.1% acetic acid. Peptide elution was achieved along a linear gradient of B from 20% to 90% over 53 min. MS and MS/MS data were acquired on an Orbitrap LTQ XL high-performance liquid chromatography MS system (Thermo-Scientific, Waltham, MA, USA) equipped with an electrospray source (ESI). The full scan precursor MS spectra (400–1600 m/z) were acquired in the Velos-Orbitrap analyzer with a resolution of $r = 60,000$. This was followed by data dependent MS/MS fragmentation in centroid mode of the most intense ion from the survey scan using collision-induced dissociation (CID) in the linear ion trap: Normalized collision energy 35%; activation Q 0.25; electrospray voltage 1.4 kV; capillary temperature 200 °C; and isolation width 2.00. The targeted ions were dynamically excluded for 30 s, and this MS/MS scan event was repeated for the top 20 peaks in the MS survey scan. The five most intense double and triple charged peptide ions were selected and fragmented. The resulting MS data were processed by MS Converter General User Interface software 3.0 (ProteoWizard) to generate peak lists for protein identifications. Database searches were carried out on the Mascot Daemon version 4.1 by Matrix Science (London, UK). The SwissProt database (release January 2017, 547,599 sequences; 195,014,757 residues) was employed (settings: two missed cleavages; carbamidomethyl (C) as fixed modification and Oxidation (M), Phospho (ST), Phospho (Y), Acetyl (K), Gln->pyro-Glu (N-term Q), Glu->pyro-Glu (N-term E) as variable modifications; peptide tolerance of 10 ppm and fragment mass tolerance of ± 0.6 Da).

References

1. Biswas, S.K. Does the interdependence between oxidative stress and inflammation explain the antioxidant paradox? *Oxid. Med. Cell. Longev.* **2016**. [[CrossRef](#)] [[PubMed](#)]
2. Somasekharan, S.P.; El-Naggar, A.; Leprivier, G.; Cheng, H.; Hajee, S.; Grunewald, T.G.P.; Zhang, F.; Ng, T.; Delattre, O.; Evdokimova, V.; et al. YB-1 regulates stress granule formation and tumor progression by translationally activating G3BP1. *J. Cell Biol.* **2015**. [[CrossRef](#)] [[PubMed](#)]
3. Higashi, K.; Tomigahara, Y.; Shiraki, H.; Miyata, K.; Mikami, T.; Kimura, T.; Moro, T.; Inagaki, Y.; Kaneko, H. A novel small compound that promotes nuclear translocation of YB-1 ameliorates experimental hepatic fibrosis in mice. *J. Biol. Chem.* **2011**. [[CrossRef](#)] [[PubMed](#)]
4. Bernhardt, A.; Fehr, A.; Brandt, S.; Jerchel, S.; Ballhause, T.M.; Philipsen, L.; Stolze, S.; Geffers, R.; Weng, H.; Fischer, K.D.; et al. Inflammatory cell infiltration and resolution of kidney inflammation is orchestrated by the cold-shock protein Y-box binding protein-1. *Kidney Int.* **2017**. [[CrossRef](#)] [[PubMed](#)]
5. Wang, J.; Gibbert, L.; Djudjaj, S.; Alidousty, C.; Rauen, T.; Kunter, U.; Rembiak, A.; Enders, D.; Jankowski, V.; Braun, G.S.; et al. Therapeutic nuclear shuttling of YB-1 reduces renal damage and fibrosis. *Kidney Int.* **2016**. [[CrossRef](#)] [[PubMed](#)]
6. Didier, D.K.; Schiffenbauer, J.; Woulfe, S.L.; Zacheis, M.; Schwartz, B.D. Characterization of the cDNA encoding a protein binding to the major histocompatibility complex class II Y box. *Proc. Natl. Acad. Sci. USA* **1988**. [[CrossRef](#)]
7. Kohno, K.; Izumi, H.; Uchiumi, T.; Ashizuka, M.; Kuwano, M. The pleiotropic functions of the Y-box-binding protein, YB-1. *BioEssays* **2003**. [[CrossRef](#)] [[PubMed](#)]
8. Ohga, T.; Uchiumi, T.; Makino, Y.; Koike, K.; Wada, M.; Kuwano, M.; Kohno, K. Direct involvement of the Y-box binding protein YB-1 in genotoxic stress-induced activation of the human multidrug resistance 1 gene. *J. Biol. Chem.* **1998**. [[CrossRef](#)]
9. Eliseeva, I.A.; Kim, E.R.; Guryanov, S.G.; Ovchinnikov, L.P.; Lyabin, D.N. Y-box-binding protein 1 (YB-1) and its functions. *Biochem* **2011**. [[CrossRef](#)] [[PubMed](#)]

10. Matsumoto, S.; Uchiumi, T.; Tanamachi, H.; Saito, T.; Yagi, M.; Takazaki, S.; Kanki, T.; Kang, D. Ribonucleoprotein Y-box-binding protein-1 regulates mitochondrial oxidative phosphorylation (OXPHOS) protein expression after serum stimulation through binding to OXPHOS mRNA. *Biochem. J.* **2012**. [[CrossRef](#)] [[PubMed](#)]
11. Troiano, A.; Lomoriello, I.S.; di Martino, O.; Fusco, S.; Pollice, A.; Vivo, M.; La Mantia, G.; Calabrò, V. Y-box binding protein-1 is part of a complex molecular network linking Δ Np63 α to the PI3K/akt pathway in cutaneous squamous cell carcinoma. *J. Cell. Physiol.* **2015**. [[CrossRef](#)] [[PubMed](#)]
12. Kosnopfel, C.; Sinnberg, T.; Sauer, B.; Busch, C.; Niessner, H.; Schmitt, A.; Forchhammer, S.; Grimm, C.; Mertens, P.R.; Hailfinger, S.; et al. YB-1 expression and phosphorylation regulate tumorigenicity and invasiveness in melanoma by influencing EMT. *Mol. Cancer Res.* **2018**. [[CrossRef](#)] [[PubMed](#)]
13. Sinnberg, T.; Sauer, B.; Holm, P.; Spangler, B.; Kuphal, S.; Bosserhoff, A.; Schitteck, B. MAPK and PI3K/AKT mediated YB-1 activation promotes melanoma cell proliferation which is counteracted by an autoregulatory loop. *Exp. Dermatol.* **2012**. [[CrossRef](#)] [[PubMed](#)]
14. Minich, W.B.; Maidebura, I.P.; Ovchinnikov, L.P. Purification and characterization of the major 50-kDa repressor protein from cytoplasmic mRNP of rabbit reticulocytes. *Eur. J. Biochem.* **1993**. [[CrossRef](#)]
15. De Souza-Pinto, N.C.; Mason, P.A.; Hashiguchi, K.; Weissman, L.; Tian, J.; Guay, D.; Lebel, M.; Stevnsner, T.V.; Rasmussen, L.J.; Bohr, V.A. Novel DNA mismatch-repair activity involving YB-1 in human mitochondria. *DNA Repair. (Amst.)* **2009**. [[CrossRef](#)] [[PubMed](#)]
16. Kim, E.R.; Selyutina, A.A.; Buldakov, I.A.; Evdokimova, V.; Ovchinnikov, L.P.; Sorokin, A.V. The proteolytic YB-1 fragment interacts with DNA repair machinery and enhances survival during DNA damaging stress. *Cell Cycle* **2013**. [[CrossRef](#)] [[PubMed](#)]
17. Fomina, E.E.; Pestryakov, P.E.; Maltseva, E.A.; Petrusheva, I.O. Y-Box binding protein 1 (YB-1) promotes detection of DNA bulky lesions by XPC-HR23B factor. *Biochemistry* **2015**. [[CrossRef](#)] [[PubMed](#)]
18. Yang, W.H.; Bloch, D.B. Probing the mRNA processing body using protein macroarrays and 'autoantigenomics'. *RNA* **2007**. [[CrossRef](#)] [[PubMed](#)]
19. Anderson, P.; Kedersha, N. Stress granules: The Tao of RNA triage. *Trends Biochem. Sci.* **2008**. [[CrossRef](#)] [[PubMed](#)]
20. Kedersha, N.; Anderson, P. Mammalian stress granules and processing bodies. *Methods Enzymol.* **2007**. [[CrossRef](#)]
21. Lyons, S.M.; Achorn, C.; Kedersha, N.L.; Anderson, P.J.; Ivanov, P. YB-1 regulates tiRNA-induced stress granule formation but not translational repression. *Nucleic Acids Res.* **2016**. [[CrossRef](#)] [[PubMed](#)]
22. Orokin, A.V.; Selyutina, A.A.; Skabkin, M.A.; Guryanov, S.G.; Nazimov, I.V.; Richard, C.; Th'Ng, J.; Yau, J.; Sorensen, P.H.B.; Ovchinnikov, L.P.; et al. Proteasome-mediated cleavage of the Y-box-binding protein 1 is linked to DNA-damage stress response. *EMBO J.* **2005**. [[CrossRef](#)]
23. Kyriakis, J.M.J.; Avruch, J.; Adams, R.; Porras, A.; Alonso, G.; Jones, M.; Vintersten, K.; Panelli, S.; Valladares, A.; Perez, L.; et al. Mammalian MAPK signal transduction pathways activated by stress and inflammation: A 10-year update. *Physiol. Rev.* **2012**. [[CrossRef](#)] [[PubMed](#)]
24. Evdokimova, V.; Ruzanov, P.; Anglesio, M.S.; Sorokin, A.V.; Ovchinnikov, L.P.; Buckley, J.; Triche, T.J.; Sonenberg, N.; Sorensen, P.H. Akt-mediated YB-1 phosphorylation activates translation of silent mRNA species. *Mol. Cell. Biol.* **2006**. [[CrossRef](#)] [[PubMed](#)]
25. Fujii, T.; Seki, N.; Namoto-Matsubayashi, R.; Takahashi, H.; Inoue, Y.; Toh, U.; Kage, M.; Shirouzu, K. YB-1 prevents apoptosis via the mTOR/STAT3 pathway in HER-2-overexpressing breast cancer cells. *Future Oncol.* **2009**. [[CrossRef](#)] [[PubMed](#)]
26. Astanehe, A.; Finkbeiner, M.R.; Krzywinski, M.; Fotovati, A.; Dhillon, J.; Berquin, I.M.; Mills, G.B.; Marra, M.A.; Dunn, S.E. MKNK1 is a YB-1 target gene responsible for imparting trastuzumab resistance and can be blocked by RSK inhibition. *Oncogene* **2012**. [[CrossRef](#)] [[PubMed](#)]
27. Van Roeyen, C.R.C.; Scurt, F.G.; Brandt, S.; Kuhl, V.A.; Martinkus, S.; Djudjaj, S.; Raffetseder, U.; Royer, H.D.; Stefanidis, I.; Dunn, S.E.; et al. Cold shock Y-box protein-1 proteolysis autoregulates its transcriptional activities. *Cell Commun. Signal.* **2013**. [[CrossRef](#)] [[PubMed](#)]
28. Rauen, T.; Raffetseder, U.; Frye, B.C.; Djudjaj, S.; Mühlenberg, P.J.T.; Eitner, F.; Lendahl, U.; Bernhagen, J.; Dooley, S.; Mertens, P.R. YB-1 acts as a ligand for notch-3 receptors and modulates receptor activation. *J. Biol. Chem.* **2009**. [[CrossRef](#)] [[PubMed](#)]

29. Hanssen, L.; Alidousty, C.; Djudjaj, S.; Frye, B.C.; Rauen, T.; Boor, P.; Mertens, P.R.; van Roeyen, C.R.; Tacke, F.; Heymann, F.; et al. YB-1 is an early and central mediator of bacterial and sterile inflammation in vivo. *J. Immunol.* **2013**. [[CrossRef](#)] [[PubMed](#)]
30. Tacke, F.; Galm, O.; Kanig, N.; Yagmur, E.; Brandt, S.; Lindquist, J.A.; Eberhardt, C.S.; Raffetseder, U.; Mertens, P.R. High prevalence of Y-box protein-1/p18 fragment in plasma of patients with malignancies of different origin. *BMC Cancer* **2014**. [[CrossRef](#)] [[PubMed](#)]
31. Ferreira, A.R.; Bettencourt, M.; Alho, I.; Costa, A.L.; Sousa, A.R.; Mansinho, A.; Abreu, C.; Pulido, C.; Macedo, D.; Vendrell, I.; et al. Serum YB-1 (Y-box binding protein 1) as a biomarker of bone disease progression in patients with breast cancer and bone metastases. *J. Bone Oncol.* **2017**. [[CrossRef](#)] [[PubMed](#)]
32. Pagano, C.; di Martino, O.; Ruggiero, G.; Maria Guarino, A.; Mueller, N.; Siauciunaite, R.; Reischl, M.; Simon Foulkes, N.; Vallone, D.; Calabro, V. The tumor-associated YB-1 protein: New player in the circadian control of cell proliferation. *Oncotarget* **2016**. [[CrossRef](#)] [[PubMed](#)]
33. Ranieri, M.; Vivo, M.; De Simone, M.; Guerrini, L.; Pollice, A.; La Mantia, G.; Calabrò, V. Sumoylation and ubiquitylation crosstalk in the control of Δ Np63 α protein stability. *Gene* **2018**. [[CrossRef](#)] [[PubMed](#)]
34. Vivo, M.; Ranieri, M.; Sansone, F.; Santoriello, C.; Calogero, R.A.; Calabrò, V.; Pollice, A.; la Mantia, G. Mimicking p14ARF phosphorylation influences its ability to restrain cell proliferation. *PLoS ONE* **2013**. [[CrossRef](#)]
35. Vivo, M.; Fontana, R.; Ranieri, M.; Capasso, G.; Angrisano, T.; Pollice, A.; Calabrò, V.; La Mantia, G. P14ARF interacts with the focal adhesion kinase and protects cells from anoikis. *Oncogene* **2017**. [[CrossRef](#)] [[PubMed](#)]
36. Fontana, R.; Guidone, D.; Sangermano, F.; Calabrò, V.; Pollice, A.; La Mantia, G.; Vivo, M. PKC dependent p14ARF phosphorylation on threonine 8 drives cell proliferation. *Sci. Rep.* **2018**. [[CrossRef](#)] [[PubMed](#)]
37. Vivo, M.; Matarese, M.; Sepe, M.; Di Martino, R.; Festa, L.; Calabrò, V.; La Mantia, G.; Pollice, A. MDM2-mediated degradation of p14ARF: A novel mechanism to control ARF levels in cancer cells. *PLoS ONE* **2015**. [[CrossRef](#)] [[PubMed](#)]
38. Vivo, M.; Di Costanzo, A.; Fortugno, P.; Pollice, A.; Calabrò, V.; La Mantia, G. Downregulation of Δ Np63 α in keratinocytes by p14ARF-mediated SUMO-conjugation and degradation. *Cell Cycle* **2009**. [[CrossRef](#)] [[PubMed](#)]
39. Lyabin, D.N.; Eliseeva, I.A.; Ovchinnikov, L.P. YB-1 protein: Functions and regulation. *Wiley Interdiscip. Rev. RNA* **2014**. [[CrossRef](#)] [[PubMed](#)]
40. di Martino, O.; Troiano, A.; Guarino, A.M.; Pollice, A.; Vivo, M.; La Mantia, G.; Calabrò, V. Δ Np63 α controls YB-1 protein stability: Evidence on YB-1 as a new player in keratinocyte differentiation. *Genes Cells* **2016**. [[CrossRef](#)] [[PubMed](#)]
41. Wheeler, J.R.; Matheny, T.; Jain, S.; Abrisch, R.; Parker, R. Distinct stages in stress granule assembly and disassembly. *eLife* **2016**. [[CrossRef](#)] [[PubMed](#)]
42. Buchan, J.R.; Parker, R. Eukaryotic stress granules: The ins and outs of translation. *Mol. Cell* **2009**. [[CrossRef](#)] [[PubMed](#)]
43. Chen, C.Y.A.; Shyu, A.B. Emerging mechanisms of mRNP remodeling regulation. *Wiley Interdiscip. Rev. RNA* **2014**. [[CrossRef](#)] [[PubMed](#)]
44. Aulas, A.; Fay, M.M.; Lyons, S.M.; Achorn, C.A.; Kedersha, N.; Anderson, P.; Ivanov, P. Stress-specific differences in assembly and composition of stress granules and related foci. *J. Cell Sci.* **2017**. [[CrossRef](#)] [[PubMed](#)]
45. Frye, B.C.; Halfter, S.; Djudjaj, S.; Muehlenberg, P.; Weber, S.; Raffetseder, U.; En-Nia, A.; Knott, H.; Baron, J.M.; Dooley, S.; et al. Y-box protein-1 is actively secreted through a non-classical pathway and acts as an extracellular mitogen. *EMBO Rep.* **2009**. [[CrossRef](#)] [[PubMed](#)]
46. Palicharla, V.R.; Maddika, S. HACE1 mediated K27 ubiquitin linkage leads to YB-1 protein secretion. *Cell Signal.* **2015**. [[CrossRef](#)] [[PubMed](#)]
47. Haigis, M.C.; Kurten, E.L.; Raines, R.T. Ribonuclease inhibitor as an intracellular sentry. *Nucleic Acids Res.* **2003**. [[CrossRef](#)]
48. Ciani, F.; Tafuri, S.; Troiano, A.; Cimmino, A.; Fioretto, B.S.; Guarino, A.M.; Pollice, A.; Vivo, M.; Evidente, A.; Carotenuto, D.; et al. Anti-proliferative and pro-apoptotic effects of *Uncaria tomentosa* aqueous extract in squamous carcinoma cells. *J. Ethnopharmacol.* **2018**. [[CrossRef](#)] [[PubMed](#)]
49. Abbas, T.; Dutta, A. P21 in cancer: Intricate networks and multiple activities. *Nat. Rev. Cancer* **2009**. [[CrossRef](#)] [[PubMed](#)]

50. McDade, S.S.; Patel, D.; McCance, D.J. p63 maintains keratinocyte proliferative capacity through regulation of Skp2-p130 levels. *J. Cell Sci.* **2011**. [[CrossRef](#)] [[PubMed](#)]
51. Kumari, S.; Badana, A.K.; Malla, R. Reactive oxygen species: A key constituent in cancer survival. *Biomark. Insights* **2018**. [[CrossRef](#)] [[PubMed](#)]
52. Shurtleff, M.J.; Yao, J.; Qin, Y.; Nottingham, R.M.; Temoche-Diaz, M.M.; Schekman, R.; Lambowitz, A.M. Broad role for YBX1 in defining the small noncoding RNA composition of exosomes. *Proc. Natl. Acad. Sci. USA* **2017**. [[CrossRef](#)] [[PubMed](#)]
53. Raffetseder, U.; Rauen, T.; Boor, P.; Ostendorf, T.; Hanssen, L.; Floege, J.; En-Nia, A.; Djudjaj, S.; Frye, B.C.; Mertens, P.R. Extracellular YB-1 blockade in experimental nephritis upregulates Notch-3 receptor expression and signaling. *Nephron Exp. Nephrol.* **2011**. [[CrossRef](#)] [[PubMed](#)]
54. Roßner, F.; Gieseler, C.; Morkel, M.; Royer, H.D.; Rivera, M.; Blaker, H.; Dietel, M.; Shafer, R.; Sers, C. Uncoupling of EGFR-RAS signaling and nuclear localization of YBX1 in colorectal cancer. *Oncogenesis* **2016**. [[CrossRef](#)] [[PubMed](#)]
55. Truong, A.B.; Kretz, M.; Ridky, T.W.; Kimmel, R.; Khavari, P.A. p63 regulates proliferation and differentiation of developmentally mature keratinocytes. *Genes Dev.* **2006**. [[CrossRef](#)] [[PubMed](#)]



© 2018 by the authors. Licensee MDPI, Basel, Switzerland. This article is an open access article distributed under the terms and conditions of the Creative Commons Attribution (CC BY) license (<http://creativecommons.org/licenses/by/4.0/>).



Molecular and Cellular Approaches to Evaluate Biological Properties of Higher Plant Extracts

Viola Calabrò^{1,*}, Domenico Carotenuto⁴, Francesca Ciani², Marilena De Lillo¹, Andrea Maria Guarino¹, Federico Infascelli², Pietro Lombardi², Vincenzo Mastellone², Elena Montano¹, Alessandra Pollice^{1,*}, Simona Tafuri², Annaelena Troiano¹, and Rosa Tundis³

¹Dipartimento di Biologia, Università di Napoli Federico II, Complesso Universitario Monte S. Angelo, via Cinthia Napoli, Italy

²Dipartimento di Medicina Veterinaria e Produzioni Animali, Università di Napoli Federico II—via Delpino, 1 Napoli

³Dipartimento di Farmacia e Scienze della Salute e della Nutrizione, Università della Calabria, Arcavacata di Rende (CS)

⁴UNMSM, Universidad Nacional Mayor San Marcos, Lima, Peru

Plant extracts are an important source of bioactive compounds for many drug discovery programs. Given the chemical complexity, however, the identification and characterization of bioactive compounds in crude plant extracts still remain a big challenge. Moreover, complex mixture of phytochemicals generally combine the advantage of targeting multiple molecular pathways so that a desired biological response may be due to a mixture of different bioactive components. Ethno-pharmacology history and available information about the plant to be studied may help to set specific bio-assays that can predict the reputed therapeutic activity and facilitate the isolation of the bioactives responsible for that biological activity. In a collaborative effort, we have analyzed the bioactivities of Cayenne pepper (*Capsicum*) a spicy staple of many foods, largely used in folk medicine for its extensive curative properties. Used either topically or internally, *Capsicum* may help support healthy bone, joint and muscle function by reducing inflammation. It is commonly used as a general stimulant and to heal ulcers, improve circulation and boost immune system. To elucidate the mechanism of action of *Capsicum* at cellular level, we have studied the effects of the variety *Capsicum annum fiesta* on immortalized human keratinocytes. We have analyzed cell viability, intracellular ROS levels, stress granules formation and cell cycle distribution demonstrating that *C. annum fiesta* exerts a protective role reducing intracellular ROS levels in a dose-dependent manner and stimulating cell viability at low concentrations without affecting cell proliferation. Another area of interest in our lab involves the characterization of *Uncaria tomentosa* extract (UT-ex) that has been widely used in folk medicine to treat a variety of health conditions including skin burns and cancer. Cell viability, intracellular ROS levels and cell cycle distribution were evaluated following treatment of immortalized and transformed keratinocytes cells with UT-ex. All cell lines tested showed dose-dependent susceptibility to *Uncaria* cytotoxicity, untransformed HaCaT keratinocytes being, however, less sensitive than squamous carcinoma cells. Interestingly, we found that following UT-ex treatment PARP1 cleavage occurred concomitantly with the reduction of the cleaved form of Y-box binding protein 1 (YB-1), a nuclear prosurvival factor involved in DNA damage repair. Taken together, our observations suggest that *Uncaria* induced cell death can be ascribed to its ability to simultaneously induce oxidative DNA damage and antagonize the mechanism of DNA repair. Our data support the use of *Uncaria* extract as adjuvant therapy for treatment of precancerous and early forms of squamous cell carcinomas.

Keywords: Skin Cancer, ROS, *Uncaria tomentosa*, Apoptosis, *Capsicum annum fiesta*.

1. INTRODUCTION

Given the steady increase in global cancer incidence with its associated morbidity and mortality, together with the

healthcare costs of treatment, there is increasing interest in strategies for cancer prevention. One approach with enormous potential is the administration of phyto-extracts for chemoprevention. Higher plants are an important source of a wide array of bioactive compounds since they can

*Authors to whom correspondence should be addressed.

exert protective effects against the initial phases of carcinogenesis as well as in the progression to an invasive disease.¹ Given the chemical complexity, the identification and characterization of bioactive compounds in crude plant extracts still remain a big challenge. On the other hand, biological effects of a complex mixtures of phytochemicals are hard to predict from chemical analysis of individual constituents because they usually present the advantage of targeting the multiple molecular pathways involved in complex disorders; therefore, a desired biological response may be due to a mixture or to a synergy of different bioactive components in extracts that often results in a considerable reduction of toxic side effects that, conversely, could be lost if single constituents are analyzed.²

Ethno-pharmacology history and available information about the plant to be studied may help to set specific bioassays that can predict the reputed therapeutic activity and eventually facilitate the isolation of the bioactives responsible for an observed biological activity.

Cancer control may benefit from the potential that resides in alternative therapies. Ideally, a phytochemical should possess anti-tumor properties, minimal toxicity and a defined mechanism of action. The knowledge of the mechanism of action and signaling pathway/s that are targeted by natural compounds is a way to understand the molecular mechanisms involved in cancer progression and indicate novel therapeutic approaches.

Induction of apoptosis is considered one of the most important markers of cytotoxicity for antitumor agents. Some natural compounds including plant metabolites are able to induce apoptotic pathways that are usually blocked in cancer cells through various mechanisms.

Another key feature in most chronic diseases, cancer included, is the continued oxidative stress; this lead to chronic inflammation. On the other hand, chronic inflammation is, in turn, associated with an increased risk of cancers.³ Interestingly, phytoextracts have often been described for their extensive antioxidant and anti-inflammatory activities.⁴

Skin is an interesting and versatile model to study the anticancer effects of natural compounds. Skin organotypic cultures as well as immortalized keratinocytes and skin tumor derived carcinoma cells represent good simplified *in vitro* models to study potential antitumoral and antioxidant effects of natural compounds. On the other hand, *in vitro* analysis are fundamental steps in the evaluation of both the efficacy and eventual toxicity of new substances.

In line with this, we have previously published that *Aloe arborescens* Miller crude leaf extract is able to exert an antiproliferative effect on several human cancer cell lines. Furthermore, analyzing several skin markers we could show that *Aloe arborescens* extract is able to exert

a pro-differentiative effect on both primary and immortalized human keratinocyte, Proteomic analysis of whole cell extracts coupled with a cellular biological approach helped us to reveal the presence of proteins with strong antiproliferative and antioxidant activity in the *Aloe arborescens* phytoextract, supporting its application as a therapeutical agent.⁵

Another area of interest in our laboratory involves the characterization of *Uncaria tomentosa* extract (UT-ex) that has been widely used in folk medicine to treat a variety of health conditions including skin burns and cancer. Cell viability, intracellular ROS levels and cell cycle distribution were evaluated following treatment of immortalized and transformed keratinocytes cells with UT-ex. All cell lines tested showed dose-dependent susceptibility to *Uncaria* cytotoxicity, untransformed HaCaT keratinocytes being, however, less sensitive than squamous carcinoma cells. Interestingly, we found that following UT-ex treatment PARP1 cleavage occurred concomitantly with the reduction of the cleaved form of Y-box binding protein 1 (YB-1), a nuclear prosurvival factor involved in DNA damage repair. Taken together, our observations suggest that *Uncaria* induced cell death can be ascribed to its ability to simultaneously induce oxidative DNA damage and antagonize the mechanism of DNA repair. Our data support the use of *Uncaria* extract as adjuvant therapy for treatment of precancerous and early forms of squamous cell carcinomas.

In a collaborative effort, we have analyzed the bioactivities of Cayenne pepper (*Capsicum*) a spicy staple of many foods, largely used in folk medicine for its extensive curative properties. Used either topically or internally, *Capsicum* may help support healthy bone, joint and muscle function by reducing inflammation. It is commonly used as a general stimulant and to heal ulcers, improve circulation and boost immune system. One of the most important actions, although not extensively studied at the molecular level, appear to be *Capsicum annuum* anti-inflammatory activity. To elucidate the mechanism of action of *Capsicum* at the molecular and cellular level, we have studied the effects of the variety *Capsicum annuum fiesta* on immortalized human keratinocytes (*HaCat* cells). Cell viability analysis shows that *C. annuum Fiesta* ethanolic extract is non toxic in the range of concentrations analyzed (up to 300 $\mu\text{g/ml}$) instead, it is slightly stimulating cell viability at low doses (1–10 $\mu\text{g/ml}$) without affecting cell proliferation. We also observed that *C. annuum fiesta* exerts a protective role on *HaCat* cells functioning as antioxidant. Infact we observed that *C. annuum fiesta* can reduce intracellular ROS species of cells subjected to oxidative stress in a dose-dependent manner. Interestingly, also the number of cells that respond to an acute oxidative insult with the formation of Stress Granules (SG) is reduced following incubation with *C. annuum fiesta* extracts.

Conflict of Interest

The authors declare no conflict of interest.

References and Notes

1. W. P. Steward and K. Brown, *Br. J. Cancer* 109, 1 (2013).
2. X. Zhou, S. W. Seto, D. Chang, H. Kiat, V. Razmovski-Naumovski, K. Chan, and A. Bensoussan, *Front Pharmacol.* 7, 201 (2016).
3. S. Reuter, S. C. Gupta, M. M. Chaturvedi, and B. B. Aggarwal, *Free Radic Biol. Med.* 49, 1603 (2010).
4. C. Rice-Evans, N. Miller, and G. Paganga, *Trends in Plant Science* 2, 152 (1997).
5. B. Di Luccia, N. Manzo, M. Vivo, E. Galano, A. Amoresano, E. Crescenzi, A. Pollice, R. Tudisco, F. Infascelli, and V. Calabrò, *Phytother. Res.* 27, 1819 (2013).

Received: 18 April 2017. Accepted 20 May 2017.



Contents lists available at ScienceDirect

Journal of Ethnopharmacology

journal homepage: www.elsevier.com/locate/jethpharm

Anti-proliferative and pro-apoptotic effects of *Uncaria tomentosa* aqueous extract in squamous carcinoma cells



Francesca Ciani^{a,*}, Simona Tafuri^{a,1}, Annaelena Troiano^b, Alessio Cimmino^c, Bianca Saveria Fioretto^b, Andrea Maria Guarino^b, Alessandra Pollice^b, Maria Vivo^b, Antonio Evidente^c, Domenico Carotenuto^d, Viola Calabrò^{b,*}

^a Department of Veterinary Medicine and Animal Productions, University "Federico II", Via Veterinaria 1, Naples 80137, Italy

^b Department of Biology, Complesso Universitario Monte S. Angelo, University "Federico II", Via Cintia, Monte S. Angelo, Naples 80126, Italy

^c Department of Chemical Sciences, University "Federico II", Complesso Universitario Monte S. Angelo, Via Cintia, Monte S. Angelo, Naples 80126, Italy

^d UNMSM, Universidad Nacional Mayor San Marcos, Lima, Peru

ARTICLE INFO

Keywords:

Squamous carcinoma
Cat's claw
Y box binding protein 1
Oxidative stress
Cell death

ABSTRACT

Uncaria tomentosa (Willd.) DC. (Rubiaceae), also known as *uña de gato*, is a plant that grows wild in the upper Amazon region of Peru and has been widely used in folk medicine to treat several health conditions including cancer. We have produced an aqueous extract from *Uncaria tomentosa* (UT-ex) and analyzed its effects on squamous carcinoma cells and immortalized HaCaT keratinocytes. Squamous cell carcinoma (SCC) is an uncontrolled growth of abnormal cells arising in the skin's squamous layer of epidermis. When detected at an early stage, SCCs are almost curable, however, if left untreated, they can penetrate the underlying tissue and become disfiguring. We have evaluated cell proliferation, apoptosis and the level of reactive oxygen species following UT-ex treatment. UT-ex affected cell cycle progression and reduced cell viability in a dose and time-dependent manner. From a mechanistic point of view, this delay in cell growth coincided with the increase of reactive oxygen species (ROS). Furthermore, PARP1 cleavage was associated to the reduction of Y-box binding protein 1 (YB-1) 36 kDa, a nuclear prosurvival factor involved in DNA damage repair. These data indicate that UT-ex-induced cell death can be ascribed, at least in part, to its ability both to induce oxidative DNA damage and antagonize the mechanism of DNA repair relying upon YB-1 activity. They also show that non metastatic SCCs are more susceptible to UT-ex treatment than untransformed keratinocytes supporting the use of UT-ex for the treatment of precancerous and early forms of squamous cell carcinomas. Preliminary chemical investigation of UT-ex revealed the presence of hydrophilic low-medium molecular weight metabolites with anticancer potential towards squamous carcinoma cells.

1. Introduction

Squamous cell carcinoma (SCC) is an uncontrolled growth of abnormal cells arising in the squamous cells, which compose most of the skin's upper layers (Sapijaszko et al., 2015). SCCs may occur on any part of the body, including the mucous membranes and genitals, but are most common in areas frequently exposed to the sun, such as the neck, face, balding scalp, arms and legs. Squamous cell carcinomas detected at an early stage are almost always curable. However, left untreated, they eventually penetrate the underlying tissues and can become disfiguring. A small percentage may even metastasize to local lymph nodes, distant tissues, and organs and can become fatal. Actinic keratoses (AKs) are considered the earliest form of SCC and may be the first

sign of squamous cell carcinoma (Boukamp, 2005); indeed, 40–60% of squamous cell carcinomas begin as untreated AKs.

Though considerable progress has been made in developing effective skin cancer treatments, surgery and radiation are still predominant and it would be beneficial to find new topical treatments for precancerous skin lesions to prevent their progression.

Nowadays, there is an increased demand for alternative concepts or approaches to cancer treatment. Compelling evidence from epidemiological and experimental studies highlight the importance of compounds derived from plants, "phytochemicals", for inhibiting the development and spread of tumors in pre-clinical studies.

Uncaria tomentosa (Willd.) DC., from the Rubiaceae family, is a thorny liana that grows wild in the upper Amazon region of Peru and

* Corresponding authors.

E-mail addresses: francesca.ciani@unina.it (F. Ciani), vcalabro@unina.it (V. Calabrò).

¹ These authors contributed equally to this work.

neighboring countries. In Peru, *Uncaria tomentosa*, also known as *uña de gato*, is believed to have anti-inflammatory and anti-tumoral properties (Heitzman et al., 2005; García Prado et al., 2007). The boiled extract of *Uncaria tomentosa* root/bark has been used over the centuries by the indigenous civilization of the Amazonian rain forest for the treatment of fever, rheumatism, arthritis, gastrointestinal disorders, cirrhosis, neurodegenerative diseases, microbial infections, cancer, skin impurities and inflammation (Keplinger et al., 1998; Ccahuana-Vasquez et al., 2007).

Many active compounds have been isolated from *Uncaria tomentosa* including antioxidants such as tannin, catechins, and procyanidins, sterols, triterpenes, flavonoids, carboxyl alkyl esters, indol and oxindol alkaloids (Heitzman et al., 2005; Wagner et al., 1985a). In particular, alkaloids, the major active components of *Uncaria* species were extensively studied for their potential use as anticancer agents and found to be effective against the proliferation of breast and bladder tumor lineages (Riva et al., 2001; Kaiser et al., 2013). From a mechanistic point of view, *Uncaria tomentosa* was found to affect tumor growth by inhibiting the Wnt or NF- κ B/TNF α signaling pathways (Akesson et al., 2003; Gurrola-Diaz et al., 2011). Moreover, *Uncaria tomentosa* aqueous extract was reported to enhance DNA repair in human skin organ cultures irradiated with UV-B (Mammone et al., 2006) and to abate actinic keratoses and early squamous cell cancer in hairless mice exposed to UV-A radiation thereby suggesting its possible application as a product for skin cancer protection (Mentor et al., 2015).

The aim of the present study was to analyze, the biological effects of *Uncaria tomentosa* extract on human immortalized keratinocytes and squamous carcinoma cells in order to provide molecular evidence supporting its therapeutic use against this type of cancer.

2. Materials and methods

2.1. Cell culture and reagents

HaCaT, spontaneously immortalized keratinocytes from adult skin, were purchased from Service Cell Line (CLS, Germany) and cultured as described (Amoresano et al., 2010); A431, human epidermoid carcinoma cells were from American Type Culture Collection (ATCC, Manassas, VA). Head and neck cancer cell lines SCC011, SCC013 and SCC022 were originally derived from tumors in patients affected by squamous cell carcinoma of the upper aerodigestive tract (Resto et al., 2008). HaCaT and A431 cell lines were cultured in Dulbecco's Modified Eagle's Medium (DMEM, Sigma Chemical Co, St. Louis, MO, USA), while all SCC lines were cultured in Roswell Park Memorial Institute medium (RPMI 1640 Sigma Chemical Co, St. Louis, MO, USA). All cell line cultures were supplemented with 10% fetal bovine serum (FBS, Hyclone Laboratories, Inc., Logan, UT, USA), 1% L-glutamine, and 1% penicillin-streptomycin (ICN Biomedicals, Inc., Aurora, OH, USA) at 37 °C in humidified atmosphere of 5% CO₂.

2.2. Bright-field microscopy

HaCaT, A431, SCC011, SCC013 and SCC022 cells were plated at a density of 2.5×10^5 per well and treated with the indicated doses of *Uncaria tomentosa*. After 24 h of treatment, images were acquired in phase-contrast at Nikon Eclipse TE-2000U.

2.3. Antibodies

The primary antibodies GAPDH (6C5), actin (I-19) and actinin (H-2) were purchased from Santa Cruz Biotechnology, Inc. Santa Cruz, CA, USA). Primary antibodies YB-1 (ab12148), hnRNPA1 (ab177152) were from Abcam (Cambridge, UK). PARP1, p21-WAF (12D1), Bax (D2E11) and H2AX antibodies were from Cell Signaling (Beverly, MA). Anti-Ubiquitin antibodies were purchased from DAKO (Glostrup, Denmark).

2.4. Extract preparation

The water extract of *Uncaria tomentosa* bark (UT-ex) used for the experiments was prepared as follows: 15 g of dried bark were shredded and boiled for 30 min in 500 ml of bi-distilled H₂O, then cooled at room temperature (RT) and filtered through sterile gauze. The concentration (w/v) was estimated by the ratio between the weight of the bark, expressed in grams, and the final volume obtained at the end of the preparation:

$$15 \text{ g}/400\text{ml} = [0.0375 \text{ g/ml}]$$

UT-ex contains 1.28 mg/ml of proteins as determined by Bradford assay, 3.08 mg/ml phenols and 4.05 mg/ml carbohydrates (2.08 pentoses and 1.97 hexoses).

The water extract was filtered through a 0.20 μ m filter before being applied to the cells. An aliquot was lyophilized (SAVANT, SC110 Speed Vac Plus A) and resuspended in the initial volume of sterile H₂O in order to check for loss of properties during the sublimation process (ReUT-ex).

2.5. Cell viability assay

The effect of *Uncaria tomentosa* on cell viability was evaluated by measuring the reduction of 3-(4,5-dimethylthiazol-2) 2,5-diphenyltetrazolium bromide (MTT) to formazan by mitochondrial dehydrogenase. Briefly, 9×10^3 cells were seeded on 96-well plates and exposed to increasing concentrations of UT-ex (from 0.3 to 10 mg/ml) for 24, 48 and 72 h. MTT/PBS solution (0.5 mg/ml) was then added to the wells and incubated for 3 h at 37 °C in a humidified atmosphere. The reaction was stopped by removal of the supernatant followed by dissolving the formazan product in acidic isopropanol. Optical density was measured with an ELISA reader (Bio-Rad) using a 570 nm filter. Under these conditions, undissolved formazan crystals were not observed. Cell viability was assessed comparing optical density of the treated samples compared to the control group.

2.6. Cell growth profile

HaCaT, A431 and SCC022 cells were plated at a density of 2.5×10^5 per well in a Corning 6 well plate and the counts were performed in a Neubauer chamber by Trypan Blue dye exclusion. Briefly, 20 μ L cell suspension was diluted 1:1 with 0.4% solution of trypan blue in phosphate saline buffer pH 7.2. Cell counting was carried out at 24-hr intervals for 3 days.

2.7. Cell cycle analysis

Cells were seeded at 3×10^5 in 35 mm dishes and treated with UT-ex at 0.3 and 1.5 mg/ml for 24 h. Cells were then trypsinized and washed by centrifugation (1200 rpm, 4 min, 4 °C) in Phosphate Buffered Saline (PBS 1x). The cell pellet was resuspended in methanol, incubated in ice for 20 min and centrifuged at 1200 rpm, 5 min, 4 °C. After a wash in PBS, the cell pellet was incubated in PBS 1x, containing RNase 100 μ g/ml for 20 min at RT. Propidium iodide was then added at a concentration of 50 μ g/ml for 30 min at 4 °C. Cell cycle analysis was performed on the BD Accury™ C6 flow cytometer (BD Biosciences). Cell debris and aggregates were excluded from the analysis.

2.8. Western blot and immunoprecipitation analyses

Immunoblots (IB) and immunoprecipitations (Co-IP) were performed as previously described (Calabrò et al., 2004; Di Costanzo et al., 2011). *Uncaria tomentosa* treated and untreated cells were harvested in lysis buffer (50 mM Tris-HCl pH 7.5, 5 mM EDTA, 150 mM NaCl, 1% NP-40, 1 mM phenylmethylsulfonyl fluoride, 0.5% sodium deoxycholate, and protease inhibitors) as previously described (Lo Iacono

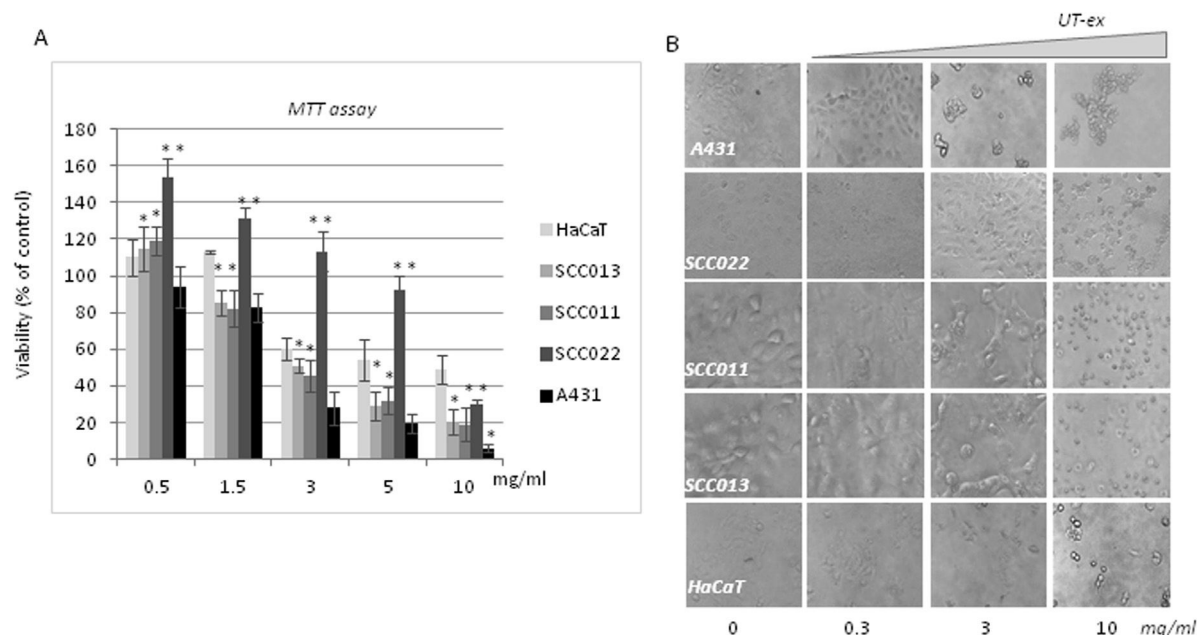


Fig. 1. (A) Percentage of viability of HaCaT, SCC013, SCC011, SCC022 and A431 cell lines after 48 h of incubation with the indicated doses of UT-ex (mg/ml). Cell viability was measured by the chromogenic MTT assay and is expressed as the percentage of viable cells compared to cells in the absence of the plant extract (mean \pm S.D. n = 6 technical replicates). ANOVA * p < 0.05, ** p < 0.005. (B) Bright-field microscopy of representative images of A431, SCC022, SCC011, SCC013 and HaCaT cells after 24 h of incubation with UT-ex at increasing concentrations from 0 to 10 mg/ml (0, 0.3, 3.0 and 10 mg/ml).

et al., 2006). Total cell lysates were incubated on ice for 40 min and clarified by centrifugation at 13,200 rpm for 15 min at 4 °C. The amount of protein in the samples was determined by the Bio-Rad protein assay (Bio-Rad, Milan, Italy). After the addition of Laemmli buffer (Sigma Chemical Co, St. Louis, MO, USA) the samples were boiled at 100 °C for 5 min and resolved by SDS-polyacrylamide gel electrophoresis (SDS-PAGE). The proteins were then transferred to a polyvinylidene difluoride membrane (PDVF, Millipore) using a Mini trans-blot apparatus (Bio-Rad, Milan, Italy) according to manufacturer's instructions. The PVDF membrane was blocked in 5% w/v milk buffer (5% w/v non-fat dried milk, 50 mM Tris, 200 mM NaCl, 0.2% Tween 20) and incubated with primary antibodies diluted in 5% w/v milk or bovine serum albumin (BSA) buffer for 2 h at RT or overnight at 4 °C. The blots, washed three times with TTBS (Tris-buffered saline, 0.1% Tween), were incubated for 1 h at RT with HRP-conjugated secondary antibodies (Santa-Cruz biotechnology). The proteins were visualized by an enhanced chemiluminescence method (ECL, GE-Healthcare) and analyzed by Quantity One W software of ChemiDoc TM XRS system (Bio-Rad, Milan, Italy). For IP experiments, extracts were pre-cleared with 30 μ L of protein A-agarose (50% slurry; Roche, Mannheim, Germany), and incubated overnight at 4 °C with anti-YB-1 (3 μ g) or α -rabbit IgG (3 μ g). Whole extracts were separated by SDS-PAGE and subjected to immunoblot, as previously described.

2.9. Reactive oxygen species (ROS) generation assay

Intracellular ROS generation was measured by flow cytometry using 2'-7'-dichlorofluorescein diacetate (DCFDA), a non-fluorescent compound permeable to the cell membrane, which can be oxidized by ROS, giving a fluorescent compound. In brief, 3×10^5 cells were treated with different concentrations of *Uncaria tomentosa* (0.3 and 3 mg/ml), the medium was removed after 24 h and cells were washed with PBS. Fresh medium with DCFDA (1 mM) was added for 30 min, then DCFDA was removed by washing in PBS and the cells were harvested. The measurement of ROS was obtained using flow cytometry Accuri C6 (BD-biosciences, US) and for each sample at least 10,000 events were evaluated. The fluorescence emitted from the cells treated with DCFDA, compared to the untreated cells, was performed using the FL1-A

(530–533 nm) channel. The data obtained as mean fluorescence intensities were analyzed and converted into percentages of ROS by BD Accuri C6 Software.

2.10. Genomic DNA extraction

Uncaria tomentosa treated and untreated cells were harvested in lysis buffer (10 mM Tris pH 8.0, 50 mM NaCl, 20 μ g/ml di Proteasi K, 20 μ g/ml di RNasi) with 1% SDS. Samples were incubated 2 h at 55 °C and then treated with 1.5 M of NaCl. A 1:1 vol of chloroform was added and samples were incubated for 1 h on rotation at room temperature. Samples were centrifuged at 13,200 rpm for 3 min, then 0.7 vol (compared to volume of lysis buffer) of isopropanol was added to supernatants.

Samples were centrifuged for 3 min at 13,200 rpm, the white pellet was resuspended in TE solution. 20 microliters of each sample were loaded in 1.2% agarose gel in TAE buffer. Images were acquired after trans-UV irradiation and analyzed by Quantity One W software of ChemiDoc TM XRS system (Bio-Rad, Milan, Italy).

2.11. Comet assay

The glass slides were coated with 50 μ L of normal-melting-point agarose (0.7%). Then, 200 μ L of 1% agarose were applied and allowed to solidify at 4 °C. Then, 50 μ L of cell/agarose mixture, 25 μ L of 0.7% agarose plus 25 μ L of cell suspension (10^5 cells), was applied as a third layer. After 20 min in ice, 200 μ L of 0.7% agarose was applied as a cover layer of the microgel.

The slides were immersed in cold fresh lysis solution (2.5 M NaCl, 100 mM EDTA, 10 mM Tris) for 1.5 h at 4 °C and then placed for 20 min in electrophoresis buffer (300 mM NaOH, 1 mM EDTA, pH 13). The electrophoresis was performed at 25 V at room temperature for 30 min. The slides were then rinsed twice with the neutralization buffer (0.4 M Tris, pH 7.5) and stained with DAPI.

Images were acquired with Nikon Eclipse TE-2000U fluorescence microscope. Cells (100) were counted and those showing the comet were expressed as percentage of the total.

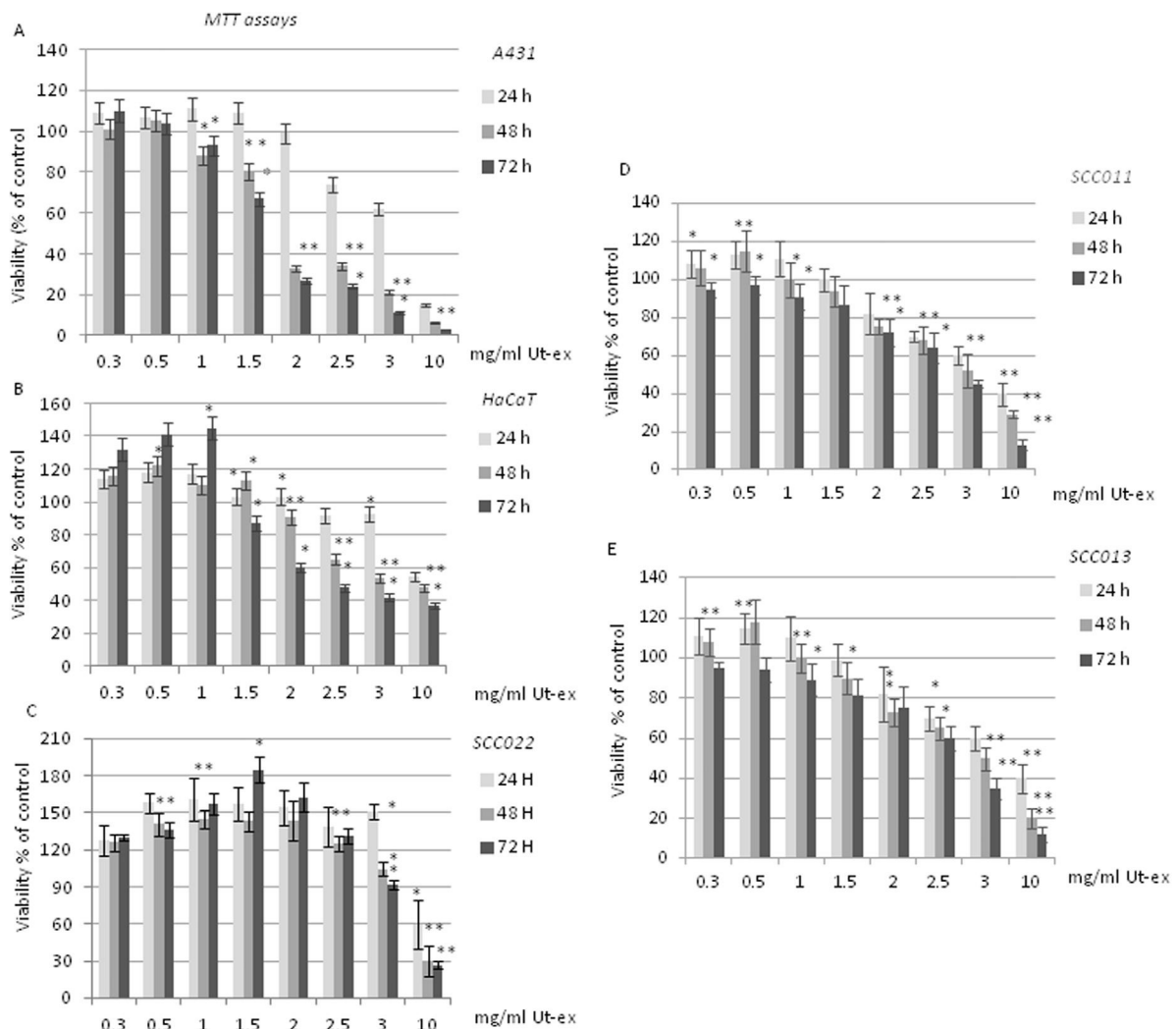


Fig. 2. (A–E) Percentage of viability of A431, HaCaT, SCC022, SCC011 and SCC013 cells after 24, 48 and 72 h of incubation with increasing doses of UT-ex (0.3, 0.5, 1, 1.5, 2, 2.5, 3.0 and 10 mg/ml). Cell viability was measured by the chromogenic MTT assay and is expressed as the percentage of viable cells compared to cells in the absence of the plant extract (mean \pm S.D. n = 6 technical replicates). ANOVA * p < 0.05, ** p < 0.005.

2.12. Statistical analysis

Statistical significance of difference in measured variables between control and treated groups was determined by *t*-test or one-way ANOVA. Difference was considered significant at $P < 0.05$ (*) and $P < 0.005$ (**).

2.13. General chemical procedures

Analytical and preparative TLC were performed on silica gel (Kieselgel 60, F_{254} , 0.20 and 0.5 mm respectively) and on reversed phase (Kieselgel 60 RP-18, F_{254} , 0.20 mm) plates (Merck, Darmstadt, Germany). The spots were visualized by exposure to UV radiation (254), or by spraying first with 10% H_2SO_4 in MeOH and then with 5% phosphomolybdic acid in EtOH, followed by heating at 110 °C for 10 min.

The HPLC system (HITACHI) consisted of a pump (5160) and a spectrophotometric detector (5410). The HPLC separation were performed using a Phenomenex LUNA (C18 (2) 5 μ 150 \times 4.6 mm). The mobile phase used to elute the samples was MeOH:H₂O, 0.1% TFA at a flow rate of 0.4 ml/min. The analysis was performed using a linear gradient starting from 30% of MeOH increased linearly to 50% MeOH in 10 min and holded this conditions for 25 min. The initial conditions were restored according to a linear gradient over 5 min and the column

was re-equilibrated under these conditions for 10 min before the next run. Detection was performed at 250 nm. Samples were injected using a 20- μ L loop and monitored for 30 min.

¹H NMR spectra were recorded at 400 or 500 MHz in CDCl₃ on Bruker (Karlsruhe, Germany) and Varian (Palo Alto, CA, USA). The same solvent was used as internal standard.

LC-TOF analysis were performed using the LC/MS TOF system (AGILENT 6230B, HPLC 1260 Infinity), using the same HPLC conditions.

Spectra/Por Dialysis Membrane (cut-off 3500 Da) were purchased from Sigma (Milan, Italy) and the dialyses carried out for two days against a large volume of distilled water.

3. Results

3.1. UT-ex cytotoxicity in squamous carcinoma cells

Human immortalized HaCaT keratinocytes and keratinocyte-derived squamous carcinoma cells (SCC013, SCC011, SCC022 and A431) were treated for 48 h with increasing doses of UT-ex, from 0.5 to 10 mg/ml, and cell viability was analyzed by MTT assay. The yellow tetrazolium salt 3-(4, 5-dimethylthiazol-2-yl)-2, 5-diphenyltetrazolium bromide (MTT) is widely used to determine cell viability in cell proliferation and cytotoxic assays. MTT is reduced by metabolically

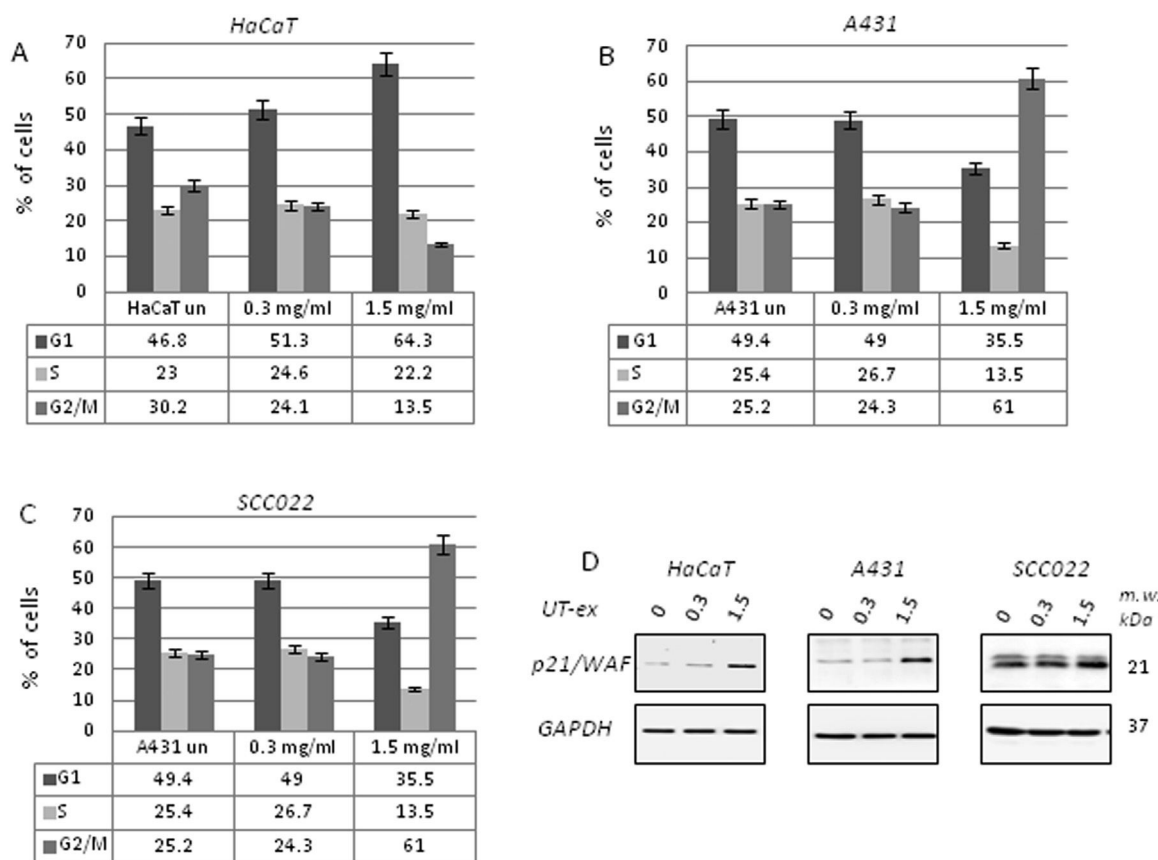


Fig. 3. Cell cycle analysis of HaCaT (A), A431 (B) and SCC022 (C) cells treated or not with 0.3 and 1.5 mg/ml of UT-ex. Each plot represents the percentage of cells in the different cell cycle phases. (D) Immunoblot analysis of extracts from HaCaT, A431 and SCC022 cells treated with 0.3 and 1.5 mg/ml of UT-ex for 24 h. Aliquots of extracts (25 µg) were loaded and subjected to SDS-PAGE and immunoblot analysis with p21-WAF and GAPDH antibodies.

active cells to form an insoluble purple formazan product that is quantifiable by spectrophotometry. At 0.5 mg/ml of UT-ex, immortalized HaCaT, highly metastatic SCC022, and non-metastatic SCC013 and SCC011 cells were more viable than control cells (ranging from 1.1 to 1.5 folds) (Fig. 1A). Vulvar epidermoid A431 cells remained almost unaffected by treatment with 0.5 mg/ml of UT-ex (Fig. 1A). At higher concentrations, UT-ex was clearly cytotoxic and exhibited a dose-dependent effects in all tested cell lines (Fig. 1A). Compared to untreated controls, epidermoid A431 cells were the most susceptible to UT-ex with a residual cell viability of less than 10% at 10 mg/ml of UT-ex (Fig. 1A).

Bright-field microscopy and imaging confirmed the major sensitivity of A431 cells compared to the other cell lines. However, upon treatment with 10 mg/ml of UT-ex, all tested cells exhibited a round morphology, a cytoplasmic vacuolization and loss of cell-cell contacts, indicating severe cell damage (Fig. 1B).

To better examine their different susceptibility, we performed a more detailed evaluation of UT-ex, cytotoxicity on squamous cancer cell lines compared to spontaneously immortalized HaCaT keratinocytes. We confirmed that A431 cells were the most sensitive to UT-ex with a half-maximal inhibitory concentration (IC₅₀) between 1.5 and 2.0 mg/ml at 48 h of treatment (Fig. 2A). HaCaT cell viability began to progressively decline at UT-ex concentration of 1.5 mg/ml of UT-ex, (Fig. 2B) while viability of SCC022, SCC011 and SCC013 cells dropped precipitously to 20–30% upon treatment with 10 mg/ml of UT-ex for 48 h (Fig. 2C–E). As shown in Fig. 2A–E, the reduction of cell viability was most pronounced at 48 and 72 h of treatment in all cell lines thus revealing a time-dependent toxicity of UT-ex. Remarkably, at 10 mg/ml of UT-ex, untransformed HaCaT keratinocytes were more resistant than all squamous carcinoma cell lines tested (Fig. 2A–E). Similar results were obtained by treating cells with the extract that was first

lyophilized, stored at –20 °C for 1 month and then reconstituted by re-adding water up to the initial volume (reUT-ex) (Fig. S1).

Using MTT assays, we detected an increase of cell viability at UT-ex concentrations ranging between 0.3 and 1.5 mg/ml, in all tested cell lines (Fig. 2A–E). With cell growth profiling, however, we found no increase in the rate of cell proliferation (Fig. S2 A–C).

Next, we focused our further studies on A431 and SCC022 carcinoma cells which are the most sensitive and the most resistant to UT-ex, respectively.

We investigated the effect of low doses of UT-ex (0.3 and 1.5 mg/ml) on cell cycle distribution by flow cytometry. As shown in Fig. 3A, B and C, there was a significant change in the cell number in the different cell cycle phases. Specifically, at 1.5 mg/ml of UT-ex, in HaCaT cells we observed accumulation of G1 arrested cells (3A) while the majority of A431 and SCC022 cells were arrested in the G2/M phase (Fig. 3B and C). The observed cell cycle arrest was associated with the induction of the cell cycle inhibitor p21/WAF protein (Fig. 3D).

The presence of cleaved Poly [ADP-ribose] polymerase 1 (PARP-1) is used diagnostically to detect apoptosis in many cell types (Gobeil et al., 2001). Thus, we analyzed PARP-1 proteolysis by immunoblot in HaCaT, A431 and SCC022 cells treated with 0.3, 3.0 and 10 mg/ml of UT-ex. Based on the MTT assays, at this concentration range, we expected to detect molecular evidence of UT-ex effects. In fact, at 0.3 mg/ml of UT-ex all cell lines showed a viability comparable to the control cells; at 3.0 mg/ml the most resistant cell line (SCC022) exhibited a clear response to the treatment; finally at 10 mg/ml, all cell lines were sensitive to UT-ex treatment and underwent cell death.

The appearance of the 89 kDa PARP-1 fragment generated by Caspase 3 cleavage (Fig. 4A, black arrows) along with the apoptotic DNA fragmentation pattern observed in UT-ex treated HaCaT cells suggested the occurrence of apoptosis (Fig. 4B). This was also

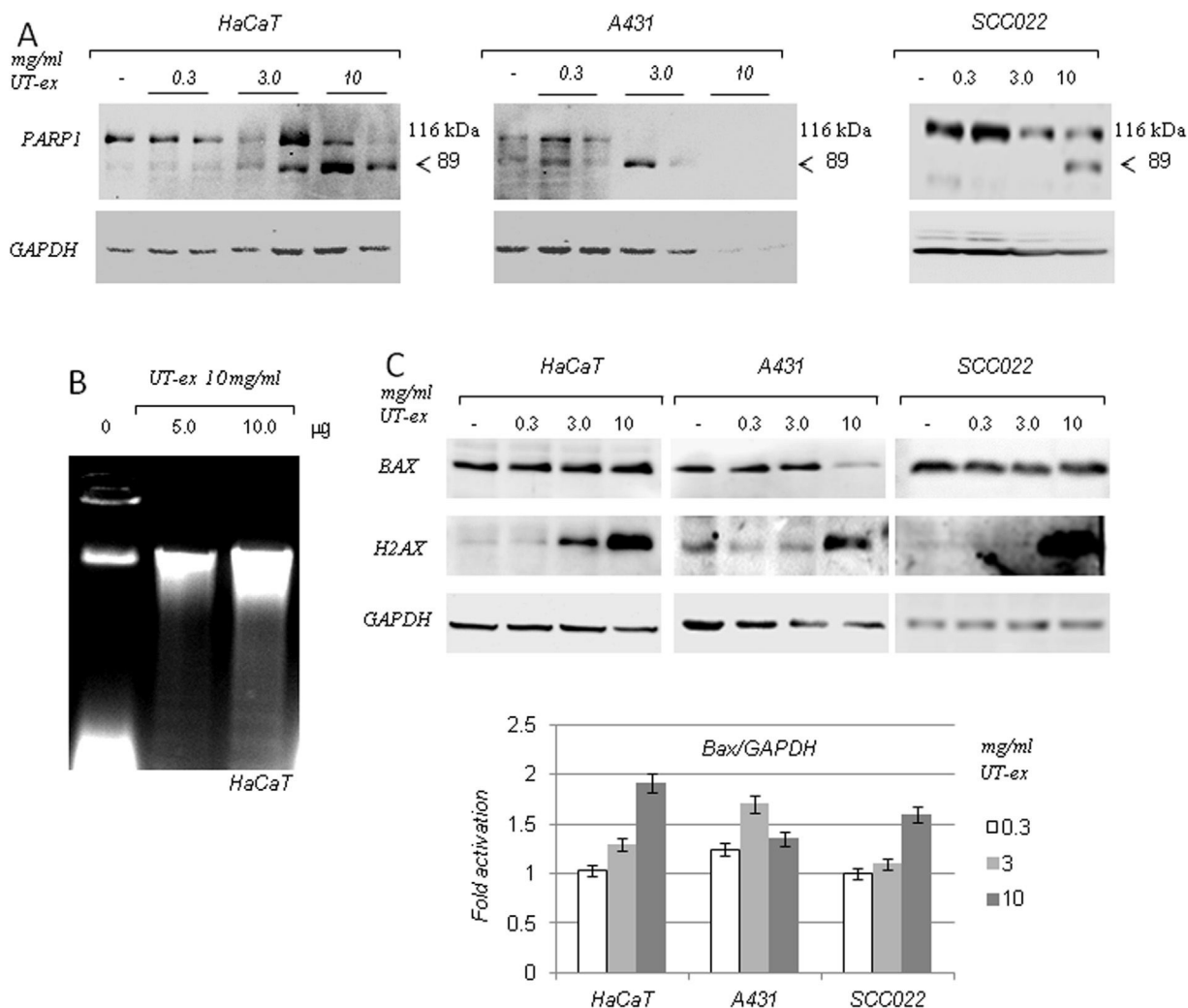


Fig. 4. (A) Representative immunoblot analyses of HaCaT, A431 and SCC022 cells after 48 h of treatment with the indicated doses of UT-ex (mg/ml). Equal aliquots of extracts (25 µg) were subjected to immunoblot analysis with PARP1 antibodies. (B) Electrophoresis on agarose gel (1.2%) of genomic DNA isolated from HaCaT cells treated or not with 10 mg/ml of UT-ex extract. (C) *upper panel* Representative immunoblot analyses of HaCaT, A431 and SCC022 cells after 48 h of treatment with the indicated doses of UT-ex (mg/ml). Equal aliquots of extracts (25 µg) were subjected to immunoblot analysis with Bax and H2AX antibodies. GAPDH antibodies were used as loading control; *lower panel* Densitometric analysis of Bax protein levels.

confirmed by the comet assay (Fig. S3) and induction of the proapoptotic Bax protein in HaCaT and SCC022 cells (Fig. 4C). Unfortunately, because of their high sensitivity to UT-ex, very limited amount of cell extract was recovered from A431 cells treated with 10 mg/ml of UT-ex. However, the strong induction of γ-H2AX histone protein indicated the occurrence of DNA damage in all tested cell lines (Fig. 4C).

3.2. UT-ex induces oxidative stress in HaCaT and A431 cells

Previous studies have shown that many natural products cause apoptosis in cancer cells through the production of Reactive Oxygen Species (ROS) (Martin-Cordero et al., 2012). Therefore, we tested whether apoptosis induced by UT-ex was ROS-dependent using flow cytometry after staining with 2'-7' dichlorofluorescein diacetate (DCFDA). Control cells were incubated for 30 min with DCFDA alone, while treated cells were incubated with UT-ex (0.3 or 3.0 mg/ml) for 24 h and subsequently with DCFDA for 30 min. The amount of ROS was normalized for a sample of cells without DCFDA. Compared to control cells, HaCaT and A431 cells treated with 0.3 mg/ml of UT-ex showed a moderate increase of intracellular ROS (Fig. 5). Treatment with 3 mg/ml of UT-ex, instead, resulted in a 28% and 70% increase in ROS

production in HaCaT and A431 cells, respectively (Fig. 5). These results strongly suggest that the observed cell death was ROS-dependent.

3.3. UT-ex influences YB-1 proteolytic cleavage

The multifunctional Y-box binding Protein-1 (YB-1 or YBX-1) provides cellular protection from oxidative stress and participates in DNA damage repair mechanisms by interacting with Mre11 and Rad50 complexes (Somasekharan et al., 2015; Kim et al., 2013). It was previously reported that YB-1 cleavage by the 20 S proteasome leads to the accumulation of a 36 kDa nuclear form which is recruited to DNA damage sites to participate in DNA repair (Kim et al., 2013).

We tested the effect of increasing the amount of UT-ex (from 0.3 to 10 mg/ml) on YB-1 using immunoblot analyses.

In untreated HaCaT cells, full length YB-1 (50 kDa) was largely predominant over the 36 kDa form (Fig. 6A, lane 1). However, the 36 kDa proteolytic fragment of YB-1 increased as a result of UT-ex treatment up to 3.0 mg/ml (Fig. 6A, lanes 2–5) and abruptly disappeared at 10 mg/ml of UT-ex (Fig. 6A, lane 6 and 7). Interestingly, in untreated SCC022 and A431 cells, the 50 and 36 kDa forms of YB-1 were almost equally represented in (Fig. 6B and C, lanes 1). However, similarly to what we observed in HaCaT, in SCC022 cells the 36 kDa

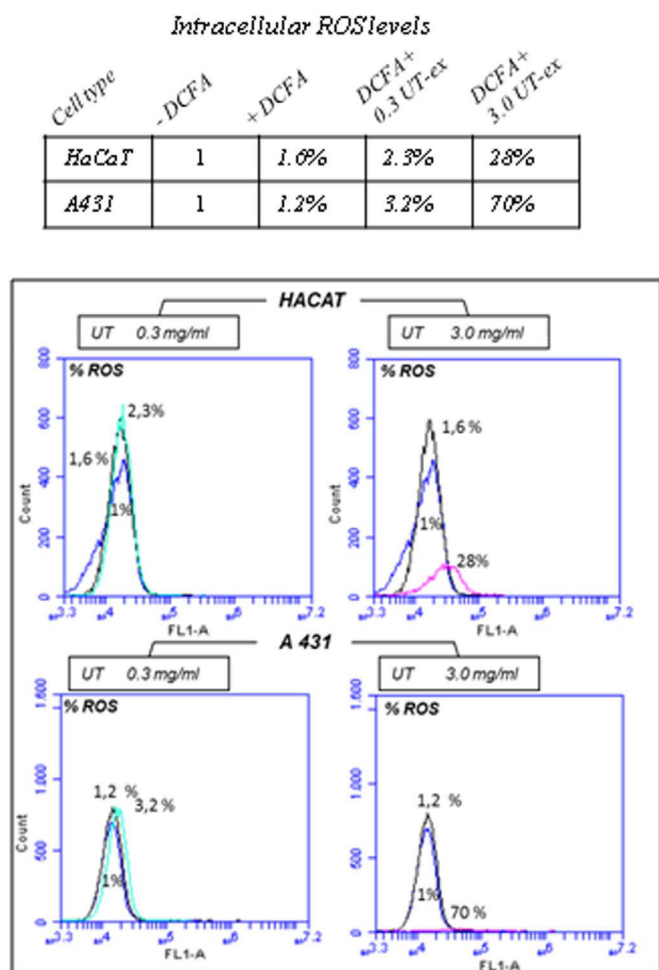


Fig. 5. Percentage of intracellular ROS levels in HaCaT and A431 cells treated with 0.3 or 3.0 mg/ml UT-ex. Data were analyzed and converted in percentage of ROS by BD Accuri C6 Software. Representative FACS-derived histograms showing increased ROS in HaCaT (upper panel) and A431 (lower panel) cells treated with UT-ex 0.3 mg/ml (left panel) or UT-ex 3.0 mg/ml (right panel) compared with control cells without DCFDA (% of ROS = 1) and untreated cells incubated with DCFDA. 20,000 events were evaluated. Data were analyzed and converted in percentage of ROS by BD Accuri C6 Software.

band of YB-1 was significantly reduced at 10 mg/ml of UT-ex (Fig. 6B, lane 4). In A431 cells, however, the 36 kDa YB-1 band disappeared in cells treated with 3.0 mg/ml of UT-ex (Fig. 6C, lanes 3 and 5). In contrast, the level of full length YB-1 appeared to be unaffected or even increased thereby suggesting that full length YB-1 was stabilized (Fig. 6A, B, C). However, it has to be noted that at 10 mg/ml of UT-ex both YB-1 and GAPDH were undetectable because of extensive cell death (Fig. 6C, lane 6). Strikingly, the level of hnRNPA1, a RNA-binding protein that is known to be degraded by caspase 3 (Back et al., 2002), was completely degraded in cells treated with UT-ex, in a dose-dependent manner (Fig. 6D, E and F).

We have previously shown that YB-1 is polyubiquitinated (Di Martino et al., 2016). Moreover, under DNA damage conditions, YB-1 undergoes a proteasome-dependent proteolytic cleavage, resulting in the YB-1 36 kDa form. Accumulation of full length YB-1, with the parallel disappearance of the YB-1 36 kDa, suggests an impairment of proteasome activity. Therefore, we investigated whether UT-ex caused an accumulation of protein ubiquitination. Immunoblot analysis of total protein extract from untreated and UT-ex treated cells clearly showed an increase of total ubi-conjugated proteins, thereby confirming a defective proteasomal degradation in the presence of UT-ex (Fig. 7A, B, C). Finally, we performed a specific immunoprecipitation of YB-1 protein. YB-1 immunocomplexes were then analyzed by immunoblot with

Ubiquitin (Ubi) antibodies. As shown in Fig. 7D, the signal obtained from cells treated with UT-ex was enhanced, thus confirming that Ubi-conjugated YB-1 was accumulated (Fig. 7D).

3.4. Preliminary chemical analysis of aqueous extract

The dried aqueous extract obtained from *Uncaria tomentosa* cell cultures was analyzed by TLC in different solvent mixtures: *i*-PrOH:H₂O 8:2, v/v; CHCl₃:*i*-PrOH 9:1, v/v; EtOAc:*n*-hexane 6:4, v/v that showed the presence of a mixtures of low and medium molecular weight compounds. The extract was dissolved in a minimal amount of ultrapure Milli-Q water and dialysed (cut-off 3500 Da). The tube content (IN) and the out fraction (OUT) were collected lyophilized, and re-suspended in the same initial volume. The fractions were separately tested for their cytotoxic activity against A431 cells by MTT assay as previously described. Remarkably, most of cytotoxic activity remained in the OUT fraction that contains hydrophilic low molecular weight metabolites (Fig. S4). Therefore, the OUT fraction was analyzed by HPLC, ¹H NMR and LC-TOF.

The HPLC profile of the OUT fraction of the dialyses (Fig. S5) showed the presence of several peaks. Its ¹H NMR (Fig. S6) showed the presence of two main anomeric protons at δ 5.4 and 5.1 ppm and complex signals in the region of the hydroxylated protons in the range of δ 4.1–3.2 ppm, suggesting the presence of saccharide mixtures. Complex signals were also present in the region of aliphatic protons at δ 2.0–1.5 ppm (Pretsch et al., 2000).

The LC-MS/TOF (Figs. S7 and 8) spectra showed eight main peaks detected in the molecular weight range of 350–570 *m/z* that could be consistent with the nature of metabolites suggested by HPLC and ¹H NMR analysis. In particular, four of them (Fig. S7) showed both the sodiated [M + Na]⁺ and the sodiated dimer [2M + Na]⁺ forms at *m/z* 383 and 743, 409 and 795, 428 and 833, 501 and 979, consistent with molecular weight of 360, 386, 405 and 478, respectively.

4. Discussion

Biological effects of complex mixtures of phytochemicals are difficult to predict from chemical analysis of individual constituents because they generally combine the advantage of targeting multiple molecular pathways that are involved in complex disorders with a considerable reduction in toxic side effects (Wagner et al., 1985b).

Cancer control may benefit from the potential in alternative therapies. Ideally, a phytochemical should possess anti-tumor properties, minimal, toxicity and a defined mechanism of action. The knowledge of the mechanism of action and the signaling pathways targeted by natural compounds can lead to understanding the molecular mechanisms involved in cancer progression and may indicate novel therapeutic approaches.

Induction of apoptosis is considered one of the most important markers of cytotoxicity for antitumor agents. Some natural compounds, including plant metabolites, are able to induce apoptotic pathways that, through various mechanisms are usually blocked in cancer cells.

We have presented evidence that an aqueous extract from *Uncaria tomentosa* barks affects viability of squamous carcinoma cells through a combination of *increased oxidative stress* and *impaired DNA repair*. Our data are in agreement with previous studies showing that *Uncaria tomentosa* extract is able to enhance chemotherapy-induced apoptosis, with an increase in caspase activities and DNA fragments in cultures of neoplastic cells (De Oliveira et al., 2014).

In our study, *Uncaria tomentosa* water extract exhibited dose-dependent cytotoxic and antimetabolic effects on human spontaneously immortalized HaCaT keratinocytes and squamous carcinoma cells. The inhibitory effect on cell viability was time and dose-dependent.

Remarkably, compared to the other tumor cell lines used in this study, the SCC022 cells exhibit a very different response to UT-ex treatment. However, in a previous work from our group (Troiano et al.,

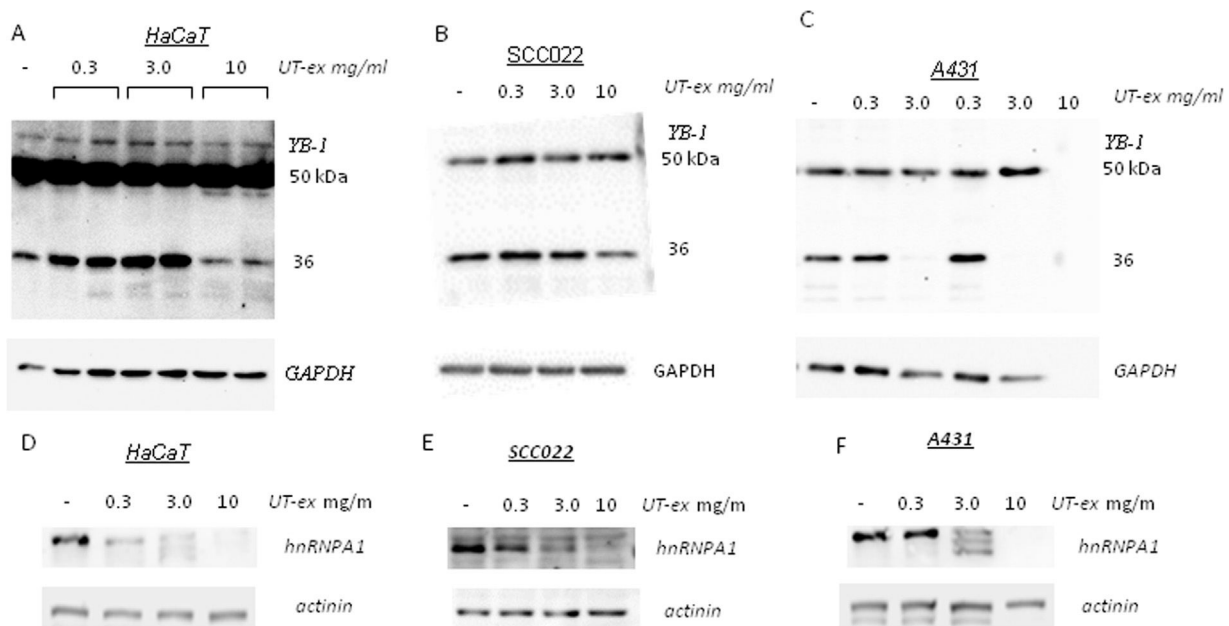


Fig. 6. (A–C) Immunoblot analysis of HaCaT, SCC022 and A431 cells treated with 0.3, 3.0 and 10 mg/ml of UT-ex for 48 h. Equal aliquots of extracts (25 µg) were loaded and subjected to SDS-PAGE and immunoblot analysis with YB-1 antibodies. GAPDH antibodies were used as loading control. (D–F) Immunoblot analysis of HaCaT, SCC022 and A431 cells treated with 0.3 and 3.0 and 10 mg/ml of UT-ex for 48 h. Equal aliquots of extracts (25 µg) were loaded and subjected to SDS-PAGE and immunoblot analysis with hnRNPA1 antibodies. Actinin antibodies were used as loading control.

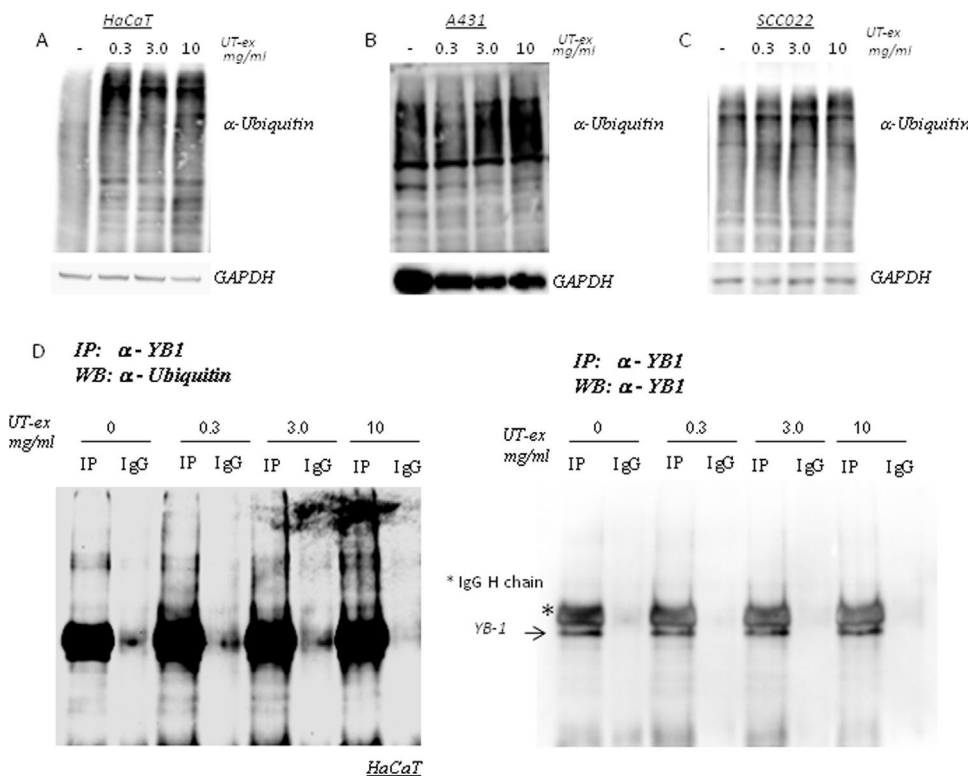


Fig. 7. (A–C) Immunoblot analysis of HaCaT, A431 and SCC022 cells treated with 0.3, 3.0 and 10 mg/ml of UT-ex for 48 h. Equal aliquots of extracts (25 µg) were loaded and subjected to SDS-PAGE and immunoblot analysis with Ubiquitin antibodies. GAPDH antibodies were used as loading control. (D) Equal aliquots of HaCaT cells treated with 0.3 and 3.0 and 10 mg/ml of UT-ex for 48 h shown in Fig. 7A were immunoprecipitated (IP) with anti-YB-1 or an irrelevant α-rabbit antibodies (IgG). Immunocomplexes were blotted and probed with Ubiquitin (left panel) or YB-1 (right panel) antibodies.

2015) we have shown that this cell line is PTEN-defective and therefore exhibits constitutive AKT_{Ser473} hyperphosphorylation that was even potentiated by YB-1 silencing. Constitutive activation of AKT survival pathway may be the likely explanation for the lower sensitivity of these cells to UT-ex treatment.

Morphological changes induced by UT-ex were associated with PARP1 cleavage, increase of BAX protein levels, and internucleosomal DNA fragmentation indicating apoptosis.

An important finding of our work is that Uncaria-induced

cytotoxicity was associated with ROS production. ROS are also a by-product of normal metabolism; short exposure of non-proliferating cells to relatively low doses of ROS was shown to activate signal transduction pathways comparable to the effects of mitogens (Deavall et al., 2012). This may be the most likely explanation for the increase of cell viability observed at low concentrations of UT-ex, in the majority of the cell lines tested in this work (HaCaT and SCCs). However, when the level of ROS exceeded the cellular antioxidant capacity, their reactive nature may otherwise cause damage to key cellular components and induce cell

death.

Because cancer cells are sensitive to oxidative stress, the mechanism of action for many cancer chemotherapeutic drugs involves ROS-mediated apoptosis (De Oliveira et al., 2014). Interestingly, after treatment with low doses of UT-ex, immortalized keratinocytes were still able to activate a G1/S cell cycle checkpoint, allowing them to repair DNA damage before DNA duplication. This could potentially explain their relative resistance to UT-ex induced apoptosis. Under the same conditions, A431 and SCC022 cancer cells showed a defective G1/S checkpoint with a consequent accumulation of G2/M arrested cells followed by massive apoptosis.

Exposure of non-proliferating cells to relatively low doses of ROS can activate mitogenic signals (Deavall et al., 2012). At low doses, UT-ex increased HaCaT and A431 cell viability; however, we found no significant increase in the rate of cell proliferation, thereby suggesting that, at the concentration tested, UT-ex could enhance cell metabolism rather than cell proliferation.

Our in vitro studies implicate the Y-Box-binding protein 1 (YB-1) in UT-ex induced apoptosis. YB-1 is a multifunctional protein participating in oncogenesis and is an oncomarker of breast, lung, liver, ovarian and squamous cell carcinoma (Lasham et al., 2013). We have previously identified YB-1 as a partner of Δ Np63 α , the predominant protein expressed in proliferative squamous epithelia, and demonstrated that YB-1 and Δ Np63 α interplay supports keratinocyte proliferation and protects keratinocytes from apoptosis under genotoxic stress (Di Martino et al., 2016; Di Costanzo et al., 2012). YB-1 is predominantly localized to cytoplasm, where it serves as a sensor of oxidative stress. Indeed, it was found to be implicated in translational repression and assembly of Stress Granules upon heat shock and oxidative stress (Kedersha et al., 2005). However, in response to severe genotoxic insults, UV, doxorubicin, cisplatin, etoposide and prolonged oxidative stress, YB-1 accumulates into the nucleus and participates in DNA damage repair (Kim et al., 2013). In particular, full length YB-1 (50 kDa) undergoes specific post-translational modifications and limited cleavage by the proteasome leading to the nuclear accumulation of the N-terminal YB-1 36 kDa fragment. YB-1 36 kDa form functionally interacts with BER factors (NEIL1, PARP1 and 2) and Double Strand Break (DSB) repair proteins MRE11 and Rad50 (Alemasova et al., 2016) and enhances cell survival (Kim et al., 2013). We believe that the relevance of this mechanism in cancer-cell chemo-resistance is still underestimated.

Strikingly, we found that treatment of cells with lethal doses of UT-ex were associated with the reduction/disappearance of the pro-survival YB-1 36 kDa form in HaCaT, SCC022 and A431 cells. Because the level of full length YB-1 was unaffected, or even increased, by UT-ex treatment, we postulate that UT-ex could have a proteasome-inhibitory activity. The increase of total protein ubiquitination and the accumulation of Ubiquitin-conjugated YB-1 confirmed our hypothesis. It is not hard to speculate that other proteasome inhibitors already in clinical practice such as Bortezomib (Crawford et al., 2011) can exert their anticancer effects by targeting YB-1, and their relative efficacy may partly depend upon on their effect on YB-1 proteolytic cleavage. Although not exhaustive, chemical analysis of UT-ex showed that beside a large amount of saccharides, it contained further low molecular weight metabolites. Previously, phytochemical investigations on *U. tomentosa* and related species suggested the presence of indole and oxindole alkaloids, triterpenes and polyphenols (Lock et al., 2016). However, further purification of the mixture is in progress in order to confirm the nature of these classes of compounds and identify those that are effective against squamous carcinoma cells.

5. Conclusion

Being at the interface between oxidative stress and molecular mechanisms controlling cell proliferation and DNA damage repair, the YB-1 protein might not only provide a survival advantage to error-prone cancer cells, but also protect them from chemotherapy-induced

apoptosis. We have clear evidence that *Uncaria tomentosa* water extracts contains bioactive molecules that interfere with the proteasome-mediated YB-1 proteolytic cleavage thus reducing the capacity of cells to effectively repair damaged DNA. Our study indicates that *Uncaria tomentosa* pro-apoptotic activity results from its ability to simultaneously induce oxidative DNA damage and antagonize the mechanisms of DNA repair relying on the activity of YB-1 36 kDa form. In light of our current knowledge about the pro-apoptotic effects of UT-ex in squamous cancer cells, we believe that this plant may have a high potential value as an effective agent for treatment of cancerous skin lesions.

Acknowledgments

We thank the company BIOPHARMA s.r.l. for constructive collaboration.

Funding

This work was supported by Regione Campania LR No 5/2007, Progetto DIMO POR-FESR Campania 2007–2013 Bando per la realizzazione delle reti biotecnologiche Campane and Programma Ricerca e Innovazione Smart Specialization Strategy (RIS3) Regione Campania.

Conflict of interest statement

None declared.

Appendix A. Supplementary material

Supplementary data associated with this article can be found in the online version at <http://dx.doi.org/10.1016/j.jep.2017.09.031>.

References

- Akesson, C., Lindgren, H., Pero, R.W., Leanderson, T., Ivars, F., 2003. An extract of *Uncaria tomentosa* inhibiting cell division and NF-kappa B activity without inducing cell death. *Int. Immunopharmacol.* 3, 1889–1900.
- Alemasova, E.E., Moor, N.A., Naumenko, K.N., Sukhanova, M.V., Pestryakov, P.E., Lavrik, O.I., 2016. Y-box-binding protein 1 as a non-canonical factor of base-excision repair. *Biochim. Biophys. Acta* 1864 (12), 1631–1640.
- Amoresano, A., Di Costanzo, A., Leo, G., Di Cunto, F., La Mantia, G., Guerrini, L., Calabrò, V., 2010. Identification of Δ Np63 α protein interactions by mass spectrometry. *J. Proteome Res.* 9 (4), 2042–2048.
- Back, S.H., Shin, S., Jang, S.K., 2002. Polypyrimidine tract-binding proteins are cleaved by Caspase-3 during apoptosis. *J. Biol. Chem.* 277, 27200–27209.
- Boukamp, P., 2005. Non-melanoma skin cancer: what drives tumor development and progression. *Carcinogenesis* 26, 1657–1667.
- Calabrò, V., Mansueto, G., Santoro, R., Gentilella, Pollice, A., Ghioni, P., Guerrini, L., La Mantia, G., 2004. Inhibition of p63 transcriptional activity by p14ARF: functional and physical link between human ARF tumor suppressor and a member of the p53 family. *Mol. Cell. Biol.* 24, 8529–8540.
- Ccahuana-Vasquez, R.A., Santos, S.S.F., Koga-Ito, C.Y., Jorge, A.O.C., 2007. Antimicrobial activity of *Uncaria tomentosa* against oral human pathogens. *Braz. Oral. Res.* 21 (1) ([Dx.doi.org/10.1590](http://dx.doi.org/10.1590)).
- Crawford, L.J., Walker, B., Irvine, A.E., 2011. Proteasome inhibitors in cancer therapy. *J. Cell Commun. Signal.* 5 (2), 101–110.
- De Oliveira, L.Z., Farias, I.L.G., Rigo, M.L., et al., 2014. Effect of *uncaria tomentosa* extract on apoptosis triggered by oxaliplatin exposure on HT29 cells. *Evid.-Based Complement. Altern. Med.: eCAM* 2014, 274786. <http://dx.doi.org/10.1155/2014/274786>.
- Deavall, D.G., Martin, E.A., Horner, J.M., 2012. Drug-induced oxidative stress and toxicity. *J. Toxicol.* 2012, 1–13.
- Di Costanzo, A., Festa, L., Roscigno, G., Vivo, M., Pollice, A., Morasso, M., La Mantia, G., Calabrò, V., 2011. A dominant mutation etiologic for human tricho-dento-osseous syndrome impairs the ability of DLX3 to downregulate Δ Np63 α . *J. Cell. Physiol.* 226 (8), 2189–2197.
- Di Costanzo, A., Troiano, A., Di Martino, O., Cacace, A., Natale, C.F., Ventre, M., Netti, P., Caserta, S., Pollice, A., La Mantia, G., Calabrò, V., 2012. The p63 protein isoforms Δ Np63 α modulates Y-box binding protein 1 in its subcellular distribution and regulation of cell survival and motility genes. *J. Biol. Chem.* 287 (36), 30170–30180.
- Di Martino, O., Troiano, A., Guarino, A.M., Pollice, A., Vivo, M., La Mantia, G., Calabrò, V., 2016. Δ Np63 α controls YB-1 protein stability: evidence on YB-1 as a new player in keratinocyte differentiation. *Genes Cells* 21, 648–660. <http://dx.doi.org/10.1111/gtc.12373>.

- Garcia Prado, E., Garcia Gimenez, M.D., De la Puerta Vazquez, R., 2007. Antiproliferative effects of mitraphylline, a pentacyclic oxindole alkaloid of *Uncaria tomentosa* on human glioma and neuroblastoma cell lines. *Phytomedicine* 14, 280–284.
- Gobeil, S., Boucher, C.C., Nadeau, D., Poirier, G.G., 2001. Characterization of the necrotic cleavage of poly(ADP-ribose) polymerase (PARP-1): implication of lysosomal proteases. *Cell Death Differ.* 8 (6), 588–594.
- Gurrola-Diaz, C.M., Garcia-Lopez, P.M., Gulewicz, K., Pilarski, R., Dihlmann, S., 2011. Inhibitory mechanisms of two *Uncaria tomentosa* extracts affecting the Wnt-signaling pathway. *Phytomedicine* 18 (8–9), 683–690.
- Heitzman, M.E., Neto, C.C., Winiarz, E., Vaisberg, A.J., Hammond, G.B., 2005. Ethnobotany, phytochemistry and pharmacology of *Uncaria Rubiaceae*. *Phytochemistry* 66, 5–29.
- Kaiser, S., Dietrich, F., de Resende, P.E., Verza, S.G., Moraes, R.C., Morrone, F.B., Batastini, A.M., Ortega, G.G., 2013. Cat's claw oxindole alkaloid isomerization induced by cell incubation and cytotoxic activity against T24 and RT4 human bladder cancer cell lines. *Planta Med.* 79, 1413–1420.
- Kedersha, N., Stoecklin, G., Ayodele, M., Yacono, P., Lykke-Andersen, J., Fritzler, M.J., Scheuner, D., Kaufman, R.J., Golan, D.E., Anderson, P., 2005. Stress granules and processing bodies are dynamically linked sites of mRNP remodeling. *J. Cell Biol.* 169 (6), 871–884.
- Keplinger, K., Laus, G., Wurm, M., Dierich, F., Teppner, H., 1998. *Uncaria tomentosa* (Wild) DC. – ethnomedicinal use and new pharmacological, toxicological and botanical results. *J. Ethnopharmacol.* 64 (1), 23–33.
- Kim, E.R., Selyutina, A.A., Buldakov, I.A., Evdokimova, V., Ovchinnikov, L.P., Sorokin, A.V., 2013. The proteolytic YB-1 fragment interacts with DNA repair machinery and enhances survival during DNA damaging stress. *Cell Cycle* 12, 3791–3803.
- Lasham, A., Print, C.G., Dunn, S.E., Braithwaite, A.W., 2013. YB-1 oncoprotein, prognostic marker and therapeutic target? *Biochem. J.* 449, 11–23.
- Lo Iacono, M., Di Costanzo, A., Calogero, R.A., Mansueto, G., Saviozzi, S., Crispi, S., Pollice, A., La Mantia, G., Calabrò, V., 2006. The hay wells syndrome-derived TAp63 α Q540L mutant has impaired transcriptional and cell growth regulatory activity. *Cell Cycle* 5 (1), 78–87.
- Lock, O., Perez, E., Villar, M., Flores, D., Rojas, R., 2016. Bioactive compounds from plants used in peruvian traditional medicine. *Nat. Prod. Comm.* 11 (3), 315–337.
- Mammone, T., Akesson, C., Gan, D., Giampapa, V., Pero, R.W., 2006. A water soluble extract from *Uncaria tomentosa* (Cat Claw's) is a potent enhancer of DNA repair in primary organ cultures of human skin. *Phytother. Res.* 20 (3), 178–183.
- Martin-Cordero, C., Martin-Cordero, C., Leon-Gonzalez, A.J., Calderon-Montano, J.M., Burgos-Moron, E., Lopez-Lazaro, M., 2012. Pro-oxidant natural products as anticancer agents. *Curr. Drug Targets* 13 (8), 1006–1028.
- Mentor, J.M., Etemadi, A., Patta, A.M., Scheinfeld, N., 2015. Topical AC-11 abates actinic keratoses and early squamous cell cancers in hairless mice exposed to Ultraviolet A (UVA) radiation. *Dermatol. Online J.* 21 (4) (pii:13030/qt5tr46141).
- Pretsch, E., Buhlmann, P., Affolter, C., 2000. Structure Determination of Organic Compounds – Tables of Spectral Data, 3rd ed. Springer-Verlag, Berlin, pp. 161–243.
- Resto, V.A., Burdick, M.M., Dagia, N.M., McCammon, S.D., Fennewald, S.M., Sackstein, R., 2008. L-selectin-mediated lymphocyte-cancer cell interactions under low fluid shear conditions. *J. Biol. Chem.* 283 (23), 15816–15824.
- Riva, L., Coradini, D., Di Fronzo, G., De Feo, V., De Tommasi, N., De Simone, F., Pizza, C., 2001. The antiproliferative effects of *Uncaria tomentosa* extracts and fractions on the growth of breast cancer cell line. *Anticancer Res.* 21 (4A), 2457–2461.
- Sapijaszko, M., Zloty, D., Bourcier, M., Poulin, Y., Janiszewski, P., Ashkenas, J., 2015. Non-melanoma skin cancer in Canada chapter 5: management of squamous cell carcinoma. *J. Cutan. Med. Surg.* 19, 249–259.
- Somasekharan, S.P., El-Naggar, A., Leprivier, G., Cheng, H., Hajee, S., Grunewald, T.G., Zhang, F., Ng, T., Delattre, O., Evdokimova, V., Wang, Y., Gleave, M., Sorensen, P.H., 2015. YB-1 regulates stress granule formation and tumor progression by translationally activating G3BP1. *J. Cell Biol.* 208, 913–929.
- Troiano, A., Lomoriello, I.S., di Martino, O., et al., 2015. Y-box binding protein 1 is part of a complex molecular network linking Δ Np63 α to the PI3K/Akt pathway in cutaneous squamous cell carcinoma. *J. Cell. Physiol.* 2015, 2067–2074.
- Wagner, H., Kreutzkamp, B., Jurcic, K., 1985a. The alkaloids of *Uncaria tomentosa* and their phagocytosis-stimulating action. *Planta Med.* 5, 419–423.
- Wagner, H., Kreutzkamp, B., Jurcic, K., 1985b. Die Alkaloide von *Uncaria tomentosa* und ihre Phagozytose-steigernde Wirkung. *Planta Med.* 51 (5), 419–423.

Manuscript 2

1 *Protective and therapeutic effects of Bacillus megaterium spores on gut oxidative stress*

2

3

4 Giuliana Donadio^{o1}, Arianna Mazzoli ^{o1,2}, Mariamichela Lanzilli¹, Andrea Maria Guarino¹, Miriam Rivetti,

5 Raffaella Crescenzo¹, Ezio Ricca¹, Susanna Iossa¹, Alessandra Pollice¹ and Rachele Istico^{1*}

6

7

8 ¹ Department of Biology, Federico II University, Naples, Italy

9 ² Wallenberg Laboratory, Department of Molecular and Clinical Medicine, University of Gothenburg,

10 Göteborg, Sweden

11

12

13

14

15 * corresponding author: Department of Biology
16 Federico II University
17 via Cinthia 21 - MSA
18 80126 Naples Italy
19 Ph. +39 081 679038
20 fax +39 081 679233
21 email isticato@unina.it
22

23

24

25 ^o These authors contributed equally to the work.

26

27

28

29

30 **Funding**

31 This work was supported by a grant (Star - 2014) from the Federico II University to R.I.

32

33

34

35

36

37

38 **Abstract**

39 **Background.** Endogenous reactive oxygen species (ROS) are by-products of the aerobic metabolism of cells
40 and have an important signalling role as secondary messengers in various physiological processes, including
41 cell growth and development. However, the excessive production of ROS as well as the exposure to
42 exogenous ROS, originated, for example, from xenobiotics or foods, can cause protein oxidation, lipid
43 peroxidation and DNA damages leading to cell damages and a number of health disorders. ROS accumulation
44 has been associated, for example, to neurodegenerative diseases, progression of arteriosclerosis and
45 inflammatory bowel diseases. A variety of molecules and live bacteria with antioxidant activity have been
46 proposed as food additives to avoid ROS accumulation.

47 **Objective.** Here we demonstrate that spores of SF185, a human isolate of *Bacillus megaterium*, have intrinsic
48 antioxidant activity and we analyse their effect *in vitro* and *in vivo*.

49 **Methods.** The antioxidant effects of SF185 spores were tested *in vitro* on Caco-2 cells measuring the ability
50 of spores to reduce the toxicity of hydrogen peroxide and *in vivo* in a murine model of dextran sodium sulfate
51 (DSS) -induced oxidative stress.

52 **Results.** *In vitro*, spores have a scavenging action reducing the amount of intracellular ROS and so inducing
53 a protected state in cells. Pre-dosing mice with spores before the treatment with DSS protects the animals
54 from the chemically-induced damages.

55 **Conclusions.** The consumption of spores-based products could prevent or reduce the damages caused by
56 oxidative stress. The human origin of SF185, its strong antioxidant activity, and its protective effects both *in*
57 *vitro* and *in vivo* led to propose the spore of this strain as a new probiotic for gut health.

58

59 **Introduction**

60 Reactive Oxygen Species, including hydrogen peroxide, superoxide and hydroxyl radicals, are common by-
61 products of the aerobic metabolism of all cells [1]. While at low intracellular concentrations ROS are critical
62 signalling molecules with a role in cell proliferation and survival [2], their accumulation severely damages DNA,
63 proteins and lipids leading to a variety of chronic diseases, including atherosclerosis, arthritis, diabetes,
64 neurodegenerative, cardiovascular problems and inflammatory bowel diseases [3-7]. All aerobic organisms
65 avoid ROS accumulation with a variety of enzymes (catalase, superoxide dismutase, glutathione peroxidase,
66 and glutathione reductase) and with non-enzymatic molecules with antioxidant activity (glutathione,
67 thioredoxin, Vitamin C, Vitamin E). The production of an excess of ROS induces the development of a state of
68 oxidative stress that has a crucial role in the development and perpetuation of an inflammatory status, thus
69 contributing to the pathophysiology of several diseases [8]. In particular, intestinal epithelial cells are
70 continuously exposed to ROS derived by their own metabolism, by the metabolism of the huge number of
71 microbes normally living in the animal gut and by ingested foods [9]. Antioxidant additives contribute to avoid
72 the accumulation of ROS and thus have a protective role against oxidative damages [10]. During years many
73 natural antioxidant additives have been proposed and tested. Examples include polyphenols (green tea),
74 flavones, ginsenosides and more recently carotenoids [11-12].

75 Intestinal bacteria have a clear role in protecting the animal body against oxidative damages. A study
76 performed with a rat model of diet-induced oxidative stress has shown that an antibiotic treatment, as well as
77 the replacement of the gut microbiota, was able to prevent the oxidative damages in liver and skeletal muscle
78 [13]. Therefore, it is not surprising that beneficial bacteria (probiotics) with strong antioxidant properties have
79 been proposed to prevent oxidation of cellular substrates [10]. Examples are species of the *Bifidobacterium*
80 and *Lactobacillus* genera, shown able to scavenge hydroxyl radicals and superoxide anions *in vitro* and to
81 enhance the action of antioxidant enzymes *in vivo* [14-16], or cells of a carotenoid-producing strain of *Bacillus*
82 *indicus*, shown to reduce oxidative markers in plasma and liver *in vivo* [17].

83 In addition to vegetative cells also bacterial spores have been shown to have antioxidant properties. Spores
84 are quiescent cell forms produced by over 1,000 bacterial species, mainly belonging to the *Clostridium* or
85 *Bacillus* genera [18]. These microorganisms respond to adverse environmental conditions by producing a
86 highly resistant spore, that can survive indefinitely in the absence of water and nutrient [19]. The dormant
87 spore can, however, germinate originating a vegetative cell able to grow when appropriate conditions are
88 encountered [19]. Spores of several *Bacillus* species are commonly used as probiotics and are known to have
89 beneficial properties [20, 21]. An *in vitro* study has recently shown that a pre-treatment with *Bacillus subtilis*

90 spores before a sodium arsenite-induced oxidative stress allows human keratinocytes to keep normal levels
91 of intracellular ROS, GSH and lipid peroxidation [22]. Spores have been proposed to contribute to cell
92 protection by inducing the expression of antioxidant enzymes by activating the nuclear translocation of the E2-
93 related factor 2 (Nrf2). In the nucleus, Nrf2 binds to *cis*-acting Antioxidant Response Elements, present in the
94 promoter region of genes coding for antioxidant/detoxifying enzymes, activating transcription initiation [3, 22].
95 Here, we report that spores of a human isolate of *Bacillus megaterium* have a strong antioxidant activity and
96 that a treatment with these spores protects Caco-2 cells from oxidative damages and reduces the DSS-induced
97 gut damages in mice.

98

99 **Methods**

100 **Bacterial strains**

101 Sporulation of *Bacillus megaterium* SF185 and QM B1551 strains was induced by the exhaustion method [23].
102 After 30 hours of growth in Difco Sporulation medium (DSM) at 37°C with vigorous shaking, spores were
103 collected, washed three times with distilled water and purified by gastrografin gradient as described before
104 [23]. Spore counts were determined by serial dilution and plate-counting.

105

106 **Cell culture conditions and MTT assay**

107 Human colon adenocarcinoma Caco-2 cells (ATCC HTB-37) were routinely cultured at 37°C in a humidified
108 5% CO₂ incubator in Dulbecco's Modified Eagle Medium (DMEM, Gibco) supplemented with 10% (v/v) FBS
109 (Gibco), 1% penicillin-streptomycin (Gibco), 1% L-glutamine (Gibco) [24]. Cell viability was assessed using the
110 MTT assay (Sigma-Aldrich). It is based on the reduction of the tetrazolium ring of 3-(4,5-dimethylthiazol-2-yl)-
111 2,5-diphenyltetrazolium bromide (MTT) by mitochondrial dehydrogenases, yielding a purple dye (formazan),
112 which can be measured spectrophotometrically; the amount of formazan produced is proportional to the
113 number of viable cells. Cells were incubated for 3 h at 37°C with a 1X MTT solution diluted in DMEM without
114 Phenol Red, supernatant was removed, and acidic isopropanol 0.01 N was added to each well to dissolve
115 insoluble formazan crystals formed. The absorbance of the samples was measured at a 570 nm using a
116 microplate reader (Multiskan spectrum, Thermo) [25].

117

118 **DPPH and Catalase Assays**

119 The α,α -diphenyl- β -picrylhydrazyl (DPPH) free radical scavenging method was used to evaluate the potential
120 antioxidant activity of spores [26]. Different concentrations of spores were incubated in a final volume of 1 ml

121 of 100% methanol containing 0.1 mM of freshly prepared DPPH (giving absorbance ≤ 1.0). The reaction was
122 allowed to proceed for a maximum time of 30 minutes at 25°C, in any case till completion, and followed at $\lambda =$
123 515nm. The DPPH free radical scavenging activity was calculated according to the following equation:

124
$$\text{DPPH radical scavenging activity (\%)} = \left(1 - \frac{A_{\text{samples}}}{A_{\text{control}}}\right) \times 100$$

125 where A_{sample} is the absorbance of the reacted mixture of DPPH with the with the extract sample, and A_{control}
126 is the absorbance of the DPPH solution.

127 Quantitative determination of catalase activity of spores was measured by the loss of absorbance at 240 nm
128 as previously described by Beers and Sizer [27]. Briefly, spores (5×10^8 or 1×10^9) were incubated for 30 min at
129 room temperature in 1ml of hydrogen peroxide solution [50mM Potassium Phosphate Buffer, pH 7.0; 0.036%
130 (w/w) H_2O_2]. Then, samples were centrifuged for 1 min at 13000 g to remove the spores and the hydrogen
131 peroxide concentration in solution was determined by measuring the absorbance at 240 nm. The percentage

132 of peroxide removed was calculated as follows:
$$\text{H}_2\text{O}_2 \text{ removed (\%)} = \left(1 - \frac{A_{\text{samples}}}{A_{\text{control}}}\right) \times 100$$

133 Where A_{control} is the absorbance of 1 ml of hydrogen peroxide solution.

134 For the pH-stability assay, spores were incubated at 37°C for 1 hour in following buffers: 0.1 M Glycine-HCl
135 pH 2.0; 0.1 M citrate-phosphate pH 4.0 and pH 6.0, or 0.1 M HEPES pH 7.0. The peroxidase activity of the
136 samples was measured following the protocol described above. For the intestinal-stability assay, spores were
137 incubated for 1 hour at 37°C in 100 μl of simulated gastric juice (SGF) [1 mg of pepsin (porcine stomach
138 mucosa; Sigma) per ml of 10mM HCl; pH 2.0] or small intestine fluid (SIF) [1 mg of pancreatin (porcine
139 pancreas; Sigma) per ml and 0.2% bile salts (50% sodium cholate-50% sodium deoxycholate; Sigma); pH
140 6.8]. To remove the proteases contained in SIF and SGF, after incubation, spores were washed, collected by
141 centrifugation (10 min at 13000xg) and then assayed for the peroxidase activity.

142

143 **Intracellular ROS evaluation**

144 Intracellular ROS levels were quantified by a DCFDA assay (Abcam), based on the cell permeant reagent
145 2',7'- dichlorofluorescein diacetate (DCFDA), a fluorogenic dye that measures reactive oxygen species activity
146 within the cell. After diffusion in to the cell, DCFDA is deacetylated by cellular esterase to a non-fluorescent
147 compound, which is later oxidized by ROS into 2', 7'-dichlorofluorescein (DCF). DCF is a highly fluorescent
148 compound which can be detected by fluorescence spectroscopy, and the fluorescence intensity is proportional
149 to intracellular ROS produced. DCFDA (25 μM) was added to cells that were then incubated for 45 min in the

150 dark at 37°C. Fluorescence intensity was measured at λ excitation and λ emission of 485 nm and 535 nm,
151 respectively, in a plate reader (Synergy 4, BioTek).

152

153 **Lipid peroxidation in Caco-2 cells**

154 Lipid peroxidation products [thiobarbituric acid reactive substances (TBARS) also known as malondialdehyde-
155 equivalents (MDA-equivalents)] from Caco-2 cells were measured by the thiobarbituric acid colorimetric assay,
156 according to Fernandes et al. [28]. Briefly, Caco-2 cells were preincubated for 24 hours with spores at 1:1 ratio
157 cells/spores and then subjected to oxidative stress with 100 μ M H₂O₂ for 2 hours. Then, the medium was
158 removed, and cells were washed with PBS, counted and centrifuged at 500 g for 5 min at 25 °C. After removal
159 of supernatant, 0.5 ml of ice-cold 40% trichloroacetic acid and 0.5 ml of 0.67% of aqueous thiobarbituric acid
160 were added to the pellet. The mixtures were heated at 90 °C for 15 min, then cooled in ice for 10 min, and
161 centrifuged at 800 g for 10 min. The supernatant fractions were collected, and lipid peroxidation estimated
162 spectrophotometrically at 530 nm. The amount of TBARS formed was calculated using a molar extinction
163 coefficient of 1.56 $\times 10^5$ /mol/cm and expressed as nmol TBARS/10⁶ cells.

164

165 **Mouse model and experimental design**

166 Eight-week-old C57BL-6 mice were housed in standard animal cages under specific pathogen-free conditions.
167 The mice were maintained in an environment of constant temperature and humidity with a 12-hours light-dark
168 cycle and were given free access to food and water. Treatment, housing, and euthanasia of the animals met
169 the guidelines set by the Italian Health Ministry. All experimental procedures involving animals were approved
170 by “Comitato Etico-Scientifico per la Sperimentazione Animale” of the University “Federico II” of Naples.
171 Experimental colitis was induced in the C57BL-6 mice by added DSS (2%, wt:vol) in drinking water ad libitum
172 from day 2 to day 6, followed by DSS-free water for 2 days. Mice were randomly allocated into the three
173 following groups (n = 6 per group): 1) untreated mice receiving placebo (Control group); 2) mice receiving DSS
174 in water (DSS group) for 5 days; 3) mice receiving DSS in water for 5 days and spores by gavage, starting
175 from two days before the DSS treatment, until two days after DSS treatment (DSS spores group). During the
176 treatments, body weight, food and water intake were monitored daily.

177

178

179

180

181 **Evaluation of experimental colitis**

182 After mice euthanasia, the macroscopic score was evaluated according to the scheme of table1.

183 The macroscopic score was determined by combining the scores from these 4 categories and dividing the
184 resulting number by 4.

185

186 **Lipid peroxidation in colon samples**

187 Protein extracts from distal colon were assayed for lipid peroxidation as described above. The amount of
188 TBARS formed was calculated using a molar extinction coefficient of 1.56×10^5 /mol/cm and expressed as
189 nmol TBARS/mg tissue.

190

191 **Determination of TNF- α , IL-12 and IL-10 in proximal colon samples**

192 TNF- α and IL-12/IL-10 concentrations in protein extracts from colon were determined using a rat specific
193 enzyme linked immunosorbent assay (R&D Systems, MN, USA and ThermoFisher Scientific, IL USA,
194 respectively) according to manufacturer instructions. Briefly, for TNF- α the wells of a microtitre plate were
195 coated with 100 μ l of mouse anti-rat TNF- α (4 μ g/ml) in PBS (137 mM NaCl; 2.7 mM KCl; 8.1 mM Na₂HPO₄; 1.5
196 mM KH₂PO₄, pH 7.4), and incubated overnight at room temperature. The antibody excess was then removed
197 by washing with Wash Buffer (containing 0.05% (v/v) Tween 20 in PBS, pH 7.4), and the remaining sites on
198 the plate were blocked with reagent diluent (PBS containing 1% BSA) (1 h, room temperature). After extensive
199 washing, 100 μ l of samples (1:2-1:10 dilution in reagent diluent) were added to the wells and incubated for 2
200 hours at room temperature. After further washing, the wells were incubated with biotinylated goat anti-rat TNF-
201 α (225 ng/ml in reagent diluent) followed by treatment with Streptavidin-HRP (1:200 dilution; 1h, room
202 temperature). For IL-12/IL-10 determination, 50 μ l of samples (1:2 dilution in reagent diluent for IL-12, undiluted
203 for IL-10) were added in the wells of a microtiter plate and incubated for 1 h at 20-25°C for IL-12 and for 3 h at
204 20-25° for IL-10. After 3 washing with Wash Buffer (provided by the kit), the wells were incubated with 100 μ L
205 for IL-12 and 50 μ L for IL-10 of Biotinylated Antibody Reagent (BAR) for 1 hours at 20-25°C. After 3 washing
206 with wash buffer, the wells were treated with Streptavidin-HRP (1:400 dilution; 30 minutes, 20-25°C). For both
207 TNF- α and IL-12/IL-10 determination, peroxidase-catalyzed color development from tetramethylbenzidine was
208 measured at 450 nm.

209

210 **Myeloperoxidase (MPO) activity in distal colon**

211 MPO activity was assessed in colon samples as previously described [29]. Briefly, tissue samples (100 mg)
212 were homogenized in 1 ml of hexadecyltrimethylammonium bromide (HTAB) buffer (0.5% HTAB in 50 mM
213 phosphate buffer, pH 6.0) and centrifuged at 13400 x g for 6 minutes at 4°C. MPO activity was measured
214 spectrophotometrically: 10 µl of supernatant were combined with 200 µl of 50 mM phosphate buffer, pH 6.0,
215 containing 0.167 mg/ml 0-dianisidine hydrochloride and 1.25% hydrogen peroxide. The change in absorbance
216 at 450 nm was measured and one unit of MPO activity was defined as that degrading 1 µmol of peroxide per
217 minute at 25°C.

218

219 **Statistical analysis**

220 All data are expressed as means of independent experiments ± standard errors (SE). The analysis of variance
221 was carried out by using One-way ANOVA or by two-tail unpaired t-test. The statistical analysis of *in vitro* and
222 *in vivo* experiments was performed with the use of Graph-Pad Prism (Graph-Pad Software).

223

224 **Results**

225 **Spores of *B. megaterium* have antioxidant activity**

226 Antioxidant activity of the spores of *B. megaterium* was assayed by two different methods, DPPH free radicals
227 and catalase assays. For both assays, different number of purified spores of the *B. megaterium* strains QM
228 B1551 (reference strain) or SF185 (isolated from human ileal biopsies [31, 32], were added to either 1 mL of
229 methanol containing 0.1 mM DPPH or of hydrogen peroxide solution (see methods section), for the DPPH and
230 the catalase assay, respectively. In both assays, spores of both strains showed the ability to scavenge DPPH
231 (Figure 1a) and H₂O₂ (Figure 1b) and in both cases the activity increased by increasing the number of spores
232 used in the assay. Results of Figure 1, thus indicated that spores of the two strains were characterized by
233 similar antioxidant activities. Based on this, we decided to perform all further experiments using only spores of
234 the human-isolated strain SF185.

235 While it is well-established that ingested spores safely transit through the stomach [33], it is not known whether
236 enzymes present on the spore surface remain active after the exposure to the low pH conditions typical of the
237 stomach. Therefore, we analysed the stability of the spore-associated catalase at various pH conditions and
238 after treatment with either simulated gastric or intestinal conditions. To this aim, 1.0 x10¹⁰ spores of SF185
239 were incubated for 1 hour either at various acidic conditions or at simulated gastric or simulated intestinal fluid
240 (SGF or SIF, respectively) and the catalase activity assayed as reported in the Methods section. As shown in
241 Figure 1C, spores were able to remove hydrogen peroxide at all the pH conditions tested. At pH 2.0 the spore-

242 associated catalase was still active and able to remove almost 80% of H₂O₂ (Figure 1c). Incubation of spores
243 in either SGF or SIF only slightly affected the catalase activity (Figure 1d).

244 245 **SF185 spores exert anti-oxidant activity and stimulate Caco-2 cell viability**

246 Measurement of the intracellular ROS levels was carried out on Caco-2 cells by using a well-established
247 method based on the compound DCFDA that, when administered to cells, becomes deacetylated by cellular
248 esterase and then oxidized by intracellular ROS into DCF, whose level of fluorescence can be used as an
249 indirect measurement of intracellular ROS production. We first verified that spores did not germinate when
250 incubated in standard culture conditions (DMEM +10%FBS) used to cultivate Caco-2 cells in the following
251 experiments. In agreement with what previously reported for *B. subtilis* spore [22], we observed that SF185
252 spores did not germinate after 24 hours of incubation in DMEM at 37°C under CO₂ pressure (not shown). Next,
253 we analysed the oxidative status of Caco-2 cells grown under physiological conditions, in the presence or
254 absence of *B. megaterium* spores at a 1:1 ratio spores to cells. As Figure 2a shows, while 2 hours of incubation
255 with spores caused only a slight reduction in ROS production (light grey bar), an overnight (ON) incubation
256 induced a drastic effect (dark grey bar), with over 10-fold reduction in ROS production (Figure 2a). The
257 protective effect exerted by spores was also observed when cells were subjected to oxidative stress by H₂O₂:
258 treatment of cells with 100mM H₂O₂ for 2 hours in the presence of 1:1 ratio spores/cells, induced a less
259 pronounced oxidative stress in terms of ROS production (Figure 2b). The effect was more pronounced when
260 Caco-2 cells were pre-incubated ON with spores, washed to eliminate the spores and then challenged with
261 H₂O₂ for 2 hours (Figure 2 c, dark grey bars). If spores were re-added during the H₂O₂ treatment following
262 the ON pre-incubation with spores, there is only a slight reduction of ROS, further indicating the preventive,
263 protective effect of spores (Figure 2c light grey bar).

264 Further, we analyzed ROS-induced oxidative damages through evaluation of lipid peroxidation of the Caco-2
265 cell membranes. To this purpose, cells were pre-incubated for 24 hours with a 1:1 ratio spores to cells, washed
266 and challenged with 100 µM H₂O₂ for 2 hours. The lipid peroxidation level was measured as described in
267 methods section. Briefly, the end products of lipid peroxidation are reactive aldehydes, such as
268 Malondialdehyde, whose levels can be quantified through a reaction with a chromogenic reagent, TBA (2-
269 thiobarbituric acid), which yield a chromophore with absorbance maximum at 532 nm. As shown in figure 3,
270 the TBARS levels, an indirect measurement of lipid peroxidation, was markedly reduced in samples pretreated
271 with spores with respect to not only H₂O₂-treated cells but also to control cells, confirming that spores have an
272 antioxidant activity against both exogenous and endogenous ROS.

273 To further analyze the effects of spores on Caco-2 cells, we asked whether they can affect cell viability.
274 Therefore, an MTT assay was conducted following a 24 hours incubation of Caco-2 cell with *B. megaterium*
275 SF185 spores at 1:1 ratio. Interestingly, cell viability increased about 1.5 folds with respect to the control when
276 cells were incubated with spores (Figure 4), confirming that spores are not only non-toxic for Caco-2 cells but,
277 instead, exert a beneficial effect.

278

279 ***In vivo* antioxidant activity of SF185 spores**

280 The antioxidant activity of SF185 spores was also tested *in vivo*, using a mouse model, in which colitis was
281 induced by DSS administration in drinking water [34]. DSS addition to drinking water did not influence food or
282 water intake, nor did the administration of spores (Figure 5a-b). Mice treated with DSS showed lower weight
283 gain, while those treated with DSS+spores exhibited weight gains similar to those of control mice (Figure 5c).
284 In addition, the induction of colitis by DSS treatment and the protective effect of SF185 spores were confirmed
285 by the determination of macroscopic score (Figure 5d), that revealed a strong disease activity index in DSS-
286 challenged mice but not in those pre- and post-treated with the spores. The antioxidant protective effect of
287 SF185 spores was also confirmed *in vivo* in colon samples of DSS-treated mice by evaluating lipid
288 peroxidation, MPO activity, the concentration of the inflammatory cytokine TNF α and the IL12/IL10 cytokines
289 ratio (Figure 6). As Figure 6a shows, lipid peroxidation increased in colon samples of mice treated with DSS
290 and was restored to levels similar to the control, in mice also treated with spores. Also, MPO activity, colonic
291 TNF α and IL12/IL10 ratio (two cytokines with inflammatory and anti-inflammatory activities, respectively),
292 common markers of inflammation [35, 36], are restored in spore treated mice (Figure 6 b, c, d, e). Overall
293 these *in vivo* experiments indicate that DSS treatment significantly increases all markers of inflammation in
294 the colon, while treatment with SF185 spores is able to exert a strong protective effect.

295

296 **Discussion**

297 Main conclusions of this work are that spores of *B. megaterium* have an intrinsic antioxidant activity and that
298 have protective effects *in vitro* on Caco-2 cells against exogenous ROS and *in vivo* on murine intestinal cells
299 against DSS-induced oxidative damages. The bacterial antioxidant activity is stable at low pH conditions or in
300 simulated gastric and intestinal conditions (Figure 1c, d), suggesting that SF185 spores are able to remove
301 H₂O₂ and act as antioxidants at the intestinal level upon the ingestion and transit through the gut.

302 The *in vitro* experiments clearly suggest that spores act as ROS scavengers reducing free oxidants outside
303 cells and tissues but also exerting a preventive effect on oxidative stress of the cells. Such scavenging effect

304 was also exerted against oxidants produced by the physiological metabolic activity of Caco-2 cells, as shown
305 by the increased viability of cells incubated with spore but not subjected to H₂O₂ insults.

306 Accordingly, a protective effect was also observed when spores were incubated with Caco-2 cells for 18 hours
307 and then removed before the treatment of cells with hydrogen peroxide. This indicates that a mechanism other
308 than ROS scavenging is also played by spores. One explanation is that spores are able to reduce oxidants or
309 catabolites produced by the cell's metabolism, thus conferring better conditions of growth as indicated by the
310 observed reduction of intracellular ROS in physiological conditions (Figure 2a). On the other hand, it has been
311 recently reported that spores of a different *Bacillus* species, *B. subtilis*, induce the nuclear translocation of the
312 Nrf-2 factor with the subsequent activation of stress response genes [22]. We have not investigated this aspect
313 and can only hypothesize that *B. megaterium* spores are also able to induce the activation of genes coding for
314 antioxidant/detoxifying enzymes, rendering the cells more resistant to a subsequent oxidative insult and
315 allowing us to conclude that spores protect cells against ROS *in vitro*.

316 In *in vivo* assays, the pre and post-dosing treatments with SF185 spores showed marked protective effects
317 against weight loss and colon damage, reducing inflammation and the oxidative stress damages. The exerted
318 protection against the DSS-induced colitis symptoms can be due to the scavenging mechanism, to the
319 activation of stress-response genes or to a combination of the two spore-mediated effects. While additional
320 experiments are needed to clarify the mechanism of action of spores, the presented experiments strongly
321 suggest that spores of *B. megaterium* SF185 represent a promising new probiotic with antioxidant activity and
322 that administration of spore-based products may have therapeutic and possibly preventive efficacy in human
323 colitis.

324

325 **Authors' contribution**

326 G.D. and A.M. conducted most of the experiments; M.L. contributed to spore production; M.R. and A.M.G.
327 contributed to *in vitro* experiments; S.I. and R.C. designed *in vivo* experiments and analysed data; ER -
328 contributed discussions and suggestions and manuscript writing; A.P. designed *in vitro* experiment and
329 analysed data; R.I. designed the experiments, wrote the paper and had primary responsibility for final content.
330 All authors read and approved the final manuscript.

331

332 **Conflict of Interest and Funding Disclosure**

333 The authors declare that they have no conflict of interest

334

335 **Ethical standards statement**

336 All experimental procedures involving animals were approved by “Comitato Etico-Scientifico per la
337 Sperimentazione Animale” of the University “Federico II” of Naples

338 **Funding**

339 This work was supported by a grant (Star - 2014) from the Federico II University to R.I.

340

341 **References**

- 342 1. Ames BN, Shigenaga MK, Hagen TM (1993) Oxidants, antioxidants, and the degenerative diseases of
343 aging. *Proc Natl Acad Sci USA* 90:7915–7922.
- 344 2. Ray PD, Huang BW, Tsuji Y (2012) Reactive oxygen species (ROS) homeostasis and redox regulation in
345 cellular signalling. *Cell Signal* 24:981-990.
- 346 3. Eftekharzadeh B, Maghsoudi N, Khodaghali F (2010) Stabilization of transcription factor Nrf2 by tBHQ
347 prevents oxidative stress-induced amyloid β formation in NT2N neurons. *Biochimie* 92:245–253.
- 348 4. Harrison D, Griendling KK, Landmesser U, Hornig B, Drexler H (2003) Role of oxidative stress in
349 atherosclerosis. *Am J Cardiol* 91:7–11.
- 350 5. Ostrakhovitch EA, Afanas'ev IB (2001) Oxidative stress in rheumatoid arthritis leukocytes: Suppression by
351 rutin and other antioxidants and chelators. *Biochem Pharmacol* 62:743–746.
- 352 6. Griendling KK, FitzGerald GA (2003) Oxidative stress and cardiovascular injury part I: Basic mechanisms
353 and in vivo monitoring of ROS. *Circulation* 108:1912–1916.
- 354 7. Ceriello A, Motz E (2004) Is oxidative stress the pathogenic mechanism underlying insulin resistance,
355 diabetes, and cardiovascular disease? The common soil hypothesis revisited. *Arterioscler Thromb Vasc*
356 *Biol* 24:816–823.
- 357 8. Lugin J, Rosenblatt-Velin N, Parapanov R, Liaudet L (2014) The role of oxidative stress during
358 inflammatory processes *Biol Chem* 395(2): 203–230.
- 359 9. Engler JA, Gupta A, Li L, Rao R K (1999) Inhibition of DNA synthesis in Caco-2 cells by oxidative stress.
360 Amelioration by epidermal growth factor. *Dig Dis Sci* 44:1902–1909.
- 361 10. Wang, Y, Wu Y, Wang Y, Xu H, Mei X, Yu D, Wang Y, Li W (2017) Antioxidant properties of probiotic
362 bacteria. *Nutrients* 9, 521.
- 363 11. Lü JM, Lin PH, Yao Q, Chen C (2010) Chemical and molecular mechanisms of antioxidants: experimental
364 approaches and model system. *Cell Mol Med* 14 (4): 840-860

- 365 12.Kaulmann A, Bohn T (2014) Carotenoids, inflammation, and oxidative stress--implications of cellular
366 signaling pathways and relation to chronic disease prevention. *Nutr Res.* 34(11):907-929.
- 367 13.Di Luccia B, Crescenzo R, Mazzoli A, Cigliano L, Venditti P, Walser J-C, Widmer A, Baccigalupi L, Ricca
368 E, Iossa S (2015) Rescue of Fructose-Induced Metabolic Syndrome by Antibiotics or Faecal
369 Transplantation in a Rat Model of Obesity. *PLoS ONE* 10(8): e0134893. doi:
370 10.1371/journal.pone.0134893.
- 371 14.Shen Q, Shang N, Li P (2011) *In vitro* and *in vivo* antioxidant activity of *Bifidobacterium animalis* isolated
372 from centenarians. *Curr Microbiol* 62:1097–1103.
- 373 15.Bao Y, Wang Z, Zhang Y, Wang L, Dong X, Su F, Yao G, Wang S, Zhang H. Effect of *Lactobacillus*
374 *plantarum* P-8 on lipid metabolism in hyperlipidemic rat model. *Eur J Lipid Sci Technol* 2012; 114:1230–
375 1236.
- 376 16.Martarelli D, Verdenelli M.C, Scuri S, Cocchioni M, Silvi S, Cecchini C, Pompei P (2011) Effect of a probiotic
377 intake on oxidant and antioxidant parameters in plasma of athletes during intense exercise training. *Curr*
378 *Microbiol* 62:1689–1696.
- 379 17.Crescenzo R, Mazzoli A, Cancelliere R, Bucci A, Naclerio G, Baccigalupi L, Cutting S.M, Ricca E, Iossa S
380 (2017) Beneficial effects of carotenoid-producing cells of *Bacillus indicus* HU16 in a rat model of diet-
381 induced metabolic syndrome. *Beneficial Microbes* 8(5):823-831.
- 382 18.Fritze D. Taxonomy and systematics of the aerobic endospore forming bacteria: *Bacillus* and related genera
383 (2004) In: E Ricca, AO Henriques, and SM Cutting (Eds.), *Bacterial Spore Formers*. Norfolk, UK: Horizon
384 Bioscience pp. 17–34.
- 385 19.Tan IS, Ramamurthi KS (2014) Spore formation in *Bacillus subtilis*. *Environ Microbiol Rep* 6(3):212-225.
- 386 20.Cutting SM. *Bacillus* probiotics. *Food Microbiology* 2011; 28: 214-220.
- 387 21.Cutting SM, Hong HA, Baccigalupi L, Ricca E (2009) Oral Vaccine Delivery by Recombinant Spore
388 Probiotics. *Inter Rev Immunol* 28:6, 487—505.
- 389 22.Petruk G, Donadio G, Lanzilli M, Isticato R, Monti DM (2018) Alternative use of *Bacillus subtilis* spores:
390 protection against environmental oxidative stress in human normal keratinocytes. *Sci Rep* 8(1):1745.
- 391 23.Nicholson WL, Setlow P. Sporulation, germination and out-growth(1990) *In* *Molecular biological methods*
392 *for Bacillus*. Edited by Harwood C, Cutting S. Chichester, United Kingdom: John Wiley and Sons 391–450.
- 393 24.Troiano A, Lomoriello IS, di Martino O, Fusco S, Pollice A, Vivo M, La Mantia G, Calabrò V (2015) Y-box
394 Binding Protein-1 Is Part of a Complex Molecular Network Linking Δ Np63 α to the PI3K/akt Pathway in
395 Cutaneous Squamous Cell Carcinoma. *J Cell Physiol.* 2015 Sep;230(9):2067-74.

- 396 25.Vivo M, Fontana R, Ranieri M, Capasso G, Angrisano T, Pollice A, Calabrò V, La Mantia G (2017) p14ARF
397 interacts with the focal adhesion kinase and protects cells from anoikis. *Oncogene*. doi:
398 10.1038/onc.2017.104
- 399 26.Kedare SB, Singh RP (2011) Genesis and development of DPPH method of antioxidant assay. *J Food Sci*
400 *Technol* 48: 412-422.
- 401 27.Beers R & Sizer I(1952) A spectrophotometric method for measuring the breakdown of hydrogen peroxide
402 by catalase. *J Biol Chem* 195: 133-140.
- 403 28.Fernandez J (1997) Thiobarbituric acid test for monitoring lipid oxidation in meat. *Food Chemistry*
404 59 (3): 345-353.
- 405 29.Kim JJ, Shajib MS, Manocha MM, Khan WI (2012) Investigating intestinal inflammation in DSS-induced
406 model of IBD. *J Vis Exp* 60. pii: 3678. doi: 10.3791/3678.
- 407 30.Vary PS (1994) Prime time for *Bacillus megaterium*. *Microbiology* 140:1001-1013
- 408 31.Di Luccia B, D'Apuzzo E, Varriale F, Baccigalupi L, Ricca E, Pollice, A (2016) *Bacillus megaterium* SF185
409 induces stress pathways and affects the cell cycle distribution of human intestinal epithelial cells. *Benef*
410 *Microbes* 7(4):609-20.
- 411 32.Fakhry S, Sorrentini I, Ricca E, De Felice M, Baccigalupi L (2008) Characterisation of spore forming Bacilli
412 isolated from the human gastrointestinal tract. *J. Applied Microbiology* 105:2178-2186.
- 413 33.Hoa TT, Duc LH, Isticato R, Baccigalupi L, Ricca E, Van PH, Cutting SM (2001). Fate and dissemination
414 of *Bacillus subtilis* spores in a murine model. *Appl Environ Microbiol* 67: 3819-3823.
- 415 34.Di Luccia B, Mazzoli, Cancelliere R, Crescenzo R, Ferrandino I, Monaco A, Bucci A, Naclerio G, Iossa S,
416 Ricca E, Baccigalupi L (2018) *Lactobacillus gasseri* A SF1183 protects the intestinal epithelium and
417 prevents colitis symptoms *in vivo*. *J Functional Food* 42: 195-202
- 418 35.Foligne B, Dessein R, Marceau M, Poiret S, Chamaillard M, Pot B, Simonet M, Daniel C (2007) Prevention
419 and treatment of colitis with *Lactococcus lactis* secreting the immunomodulatory Yersinia LcrV protein.
420 *Gastroenterology* 133(3):862-74.
- 421 36.Sokol H, Pigneur B, Watterlot L, Lakhdari O, Bermúdez-Humarán LG, Gratadoux JJ, Blugeon S,
422 Bridonneau C, Furet JP, Corthier G et al (2008) *Faecalibacterium prausnitzii* is an anti-
423 inflammatory commensal bacterium identified by gut microbiota analysis of Crohn disease patients. *Proc*
424 *Natl Acad Sci U S A* 105(43):16731-6.

The tumor-associated YB-1 protein: new player in the circadian control of cell proliferation

Cristina Pagano^{1,*}, Orsola di Martino^{2,*}, Gennaro Ruggiero¹, Andrea Maria Guarino², Nathalie Mueller¹, Rima Siauciunaite¹, Markus Reischl³, Nicholas Simon Foulkes¹, Daniela Vallone¹, Viola Calabro²

¹Institute of Toxicology and Genetics (ITG) Hermann-von-Helmholtz-Platz 1, 76344 Eggenstein-Leopoldshafen, Germany

²Department of Biology, University of Naples "Federico II", 80126 Naples, Italy

³Institute for Applied Computer Science (IAI) Karlsruhe Institute of Technology, Hermann-von-Helmholtz-Platz 1, 76344 Eggenstein-Leopoldshafen, Germany

*Co-first authors

Correspondence to: Daniela Vallone, **email:** daniela.vallone@kit.edu
Viola Calabro, **email:** vcalabro@unina.it

Keywords: circadian clock, cell proliferation, cell cycle, Y-box binding protein, SUMOylation

Received: May 20, 2016

Accepted: December 12, 2016

Published:

ABSTRACT

Correct spatial and temporal control of cell proliferation is of fundamental importance for tissue homeostasis. Its deregulation has been associated with several pathological conditions. In common with almost every aspect of plant and animal biology, cell proliferation is dominated by day-night rhythms generated by the circadian clock. However, our understanding of the crosstalk between the core clock and cell cycle control mechanisms remains incomplete. In this study, using zebrafish as a vertebrate model system, we show that the nuclear localization of the Y-box binding protein 1 (YB-1), a regulator of cyclin expression and a hallmark of certain cancers, is robustly regulated by the circadian clock. We implicate clock-controlled changes in YB-1 SUMOylation as one of the mechanisms regulating its periodic nuclear entry at the beginning of the light phase. Furthermore, we demonstrate that YB-1 nuclear protein is able to downregulate cyclin A2 mRNA expression in zebrafish via its direct interaction with the cyclin A2 promoter. Thus, by acting as a direct target of cyclic posttranslational regulatory mechanisms, YB-1 serves as one bridge between the circadian clock and its cell cycle control.

INTRODUCTION

The circadian clock generates day-night rhythms in most aspects of physiology and behaviour [1]. Central to the circadian timing system is a pacemaker that oscillates with a period of circa 24 hours and is reset on a daily basis by environmental signals such as light, food or temperature, via input pathways. In turn, the master clock regulates physiology and behavior via clock output pathways [1, 2].

At the core of the circadian clock mechanism is a transcription-translation feedback loop, which requires approximately 24 hours to complete one cycle. In vertebrates, the transcription factors CLOCK and BMAL activate expression of *Period (Per)* and *Cryptochrome (Cry)* genes, via binding to E-box enhancers in their promoters.

Per and *Cry* in turn inhibit their own transcription by blocking CLOCK/BMAL driven transcriptional activation [3]. Additional transcriptional regulatory loops stabilize the entire timing mechanism [4]. Furthermore, cyclic post translational modifications, protein turnover and changes in the sub-cellular localization of key clock components all combine to reinforce the core clock mechanism's timing function [5–7].

One key mechanism regulated by the circadian clock is the timing of cell proliferation and circadian clock disruption has been associated with several pathological conditions [8–10]. Clock components have been implicated in controlling the expression of cell cycle regulatory genes in order to “gate” critical cell cycle steps to times of day when there is a reduced exposure to damaging ultraviolet light. Thus, the expression of several

mammalian cell-cycle control genes such as *Wee-1* and *p21* has been found to be regulated in a circadian manner [11–13]. In addition, it has been shown that the clock has an impact on the cell cycle also through direct protein-protein interactions [14]. Other clock-controlled cell cycle regulators include *c-Myc*, *Mdm2*, the D1, A and B cyclins and the tumor suppressor *p53* [10]. There is also evidence that DNA damage can phase advance circadian rhythms via its effect on progression of the cell cycle [15]. Thus, the cell cycle can in turn also control the circadian clock. Therefore, understanding how these two key cellular oscillators, the clock and cell cycle, are inter-connected at the molecular level has become a major goal in the last few years.

The zebrafish (*Danio rerio*) has been established as one of the vertebrate model systems for studying the interplay between cell proliferation and the circadian timing system. In zebrafish, key cell cycle regulators, notably cyclins, are clock regulated and the circadian clock generates daily rhythms of S, as well as M phase by a cell-autonomous mechanism [16–19]. Most zebrafish tissues contain independent “peripheral” circadian clocks. However, while in mammals light entrainment of peripheral clocks occurs indirectly via the retina and the central clock of the suprachiasmatic nucleus (SCN) [20], zebrafish peripheral clocks are entrained by direct exposure to light [21]. In turn, direct exposure to light dark cycles result in high amplitude rhythms of cell proliferation in zebrafish cells and tissues.

One of the key regulators of cyclin expression during cell cycle progression [22] is the Y box binding protein 1 (YB-1, YBX-1). High YB-1 levels are typical of regenerating and proliferating cells and its abnormally elevated expression is a hallmark of cancer progression [23]. YB-1 is a DNA/RNA binding protein involved in almost all DNA and mRNA-dependent process, including DNA replication and repair, transcription, pre-mRNA splicing and translation. This protein is composed of three domains: a protein-protein interaction A/P rich N-terminal domain; a five stranded β -barrel CSD (Cold shock domain) [24] and a large C-terminal domain involved in controlling the subcellular localization of the protein [22, 25–27]. Although most YB-1 is located in the cytoplasm, recent evidence has shown that YB-1 can shuttle between the nucleus and the cytoplasm [28]. In the nucleus, YB-1 orchestrates expression of proliferation-related genes, whereas in the cytoplasm it associates with mRNA and directs translation. YB-1 relocalization from the cytoplasm to the nucleus at the G1/S phase transition has been associated with its function of regulating cyclin gene expression [22, 29, 30]. In this regard, in the nucleus YB-1 protein has been demonstrated to bind DNA as well as RNA, in a sequence-specific fashion to an inverted CCAAT box sequence (5'- CTGATTGGC/TC/TAA - 3'), termed the Y-box [31].

Here, using zebrafish as a model, we implicate YB-1 as one of the links between the circadian clock and the control of cell cycle progression. We reveal a circadian clock control of YB-1 sub-cellular nuclear localization involving cyclic changes in SUMOylation and that this regulation is, at least in part, responsible for circadian cell cycle regulation.

RESULTS

Clock regulation of nuclear zfYB-1

We have previously shown that the transcription of cell cycle control genes, including *zfcyclin A2* and *zfcyclin B1*, is regulated by the circadian clock in the adult zebrafish caudal fin [16]. Given the central role played by YB-1 in the control of the cell cycle, we wished to investigate its involvement in circadian clock-regulated cell proliferation in zebrafish. It is well documented that the regulation of gene expression exerted by the human YB-1 protein is mainly due to dynamic changes in its nuclear localization [22, 32]. Therefore, based on the high homology between human and zfYB-1 (Supplementary Figure S1), we performed immunohistochemical analysis of zebrafish caudal fins at two different times during the light-dark cycle (14:10) using three different antibodies raised against full length, the N-terminal and the C-terminal portions of the human YB-1 protein, named: α -YB-1 F, α -YB-1 N-ter and α -YB-1 C-ter, respectively (Figure 1 and Supplementary Figure S2A, S2B). With all three antibodies we observed an enriched nuclear localization at zeitgeber time (zt) 3 (day time) compared with zt 15 (night time), where zt 0 is defined as “lights on” and zt 14 “lights off” (Figure 1A, 1B and Supplementary Figure S2B, S2C). This daily change in zfYB-1 nuclear localization, was confirmed by western blot analysis of fin nuclear extracts harvested at 6 hourly intervals during 2 Light/Dark (LD) cycles (Figure 2). A statistically significant sinusoidal rhythm in the nuclear expression of immunoreactive zfYB-1 with a peak at zt 3 and a trough at zt 15 was observed (Figure 2A, 2B and Supplementary Table S1 for statistical analysis).

Consistent with previous studies where multiple YB-1 immunoreactive bands were associated with complex post translational modifications [27, 31, 33], we also observed differences in the number and molecular weight of immunoreactive bands depending on the antibody used (ranging between 45 and 60 kDa). In addition, the oscillation of nuclear YB-1 expression persisted under constant conditions (constant darkness, DD) showing a circadian clock regulation rather than simply a light-dependent YB-1 rhythmicity (Figure 2C and Supplementary Figure S2C and Supplementary Table S1). Then, using a combination of approaches based on siRNA, recombinant protein and immunoprecipitation assays, we confirmed that the immunoreactive bands observed using

the YB-1 antibodies, indeed correspond to zfYB-1 protein (Supplementary Figure S3A–S3D).

One frequently encountered feature of genes that serve to bridge the circadian clock with its output pathways is that their mRNA expression exhibits clock driven rhythms. We thus performed a high-resolution qRT-PCR analysis of *zfYb-1* mRNA levels in caudal fins prepared from zebrafish raised under LD cycles and then transferred to constant darkness (DD). At the RNA level, *zfYb-1* showed no significant circadian rhythm (Supplementary Figure S4A and Supplementary Table S1), unlike for *zfper1b* and *zfcyclin A2* which both show a predominant circadian clock regulation (Supplementary Figure S4B, S4C and Supplementary Table S1). However, basal *zfYb-1* mRNA levels did show a progressive increase after transfer to constant darkness implicating light in setting the levels *zfYb-1* mRNA expression (Supplementary Figure S4A and Supplementary Table S1).

Cell autonomous regulation of nuclear zfYB-1 by the circadian clock

Consistent with a cell autonomous clock-regulation, immunohistochemical and western blot analysis also revealed a robust oscillation of zfYB-1 nuclear protein in zebrafish PAC-2 cells (Figure 3A, 3B and Supplementary Figure S5A, S5B and Supplementary Table S1), although compared with fins, levels remained elevated in the nuclei for a longer period (peak zt3-9). We next wished to test whether the observed 24 h rhythmicity of nuclear zfYB-1 was directly driven by the core circadian clock mechanism or merely reflected clock-dependent rhythmicity of cell cycle progression. With this goal, we explored the effect of genetic clock disruption or cell proliferation arrest upon zfYB-1 nuclear rhythmicity. Specifically, in the first approach we employed PAC-2 cells stably expressing a dominant negative form of the CLOCK1 protein, *CLOCK1*

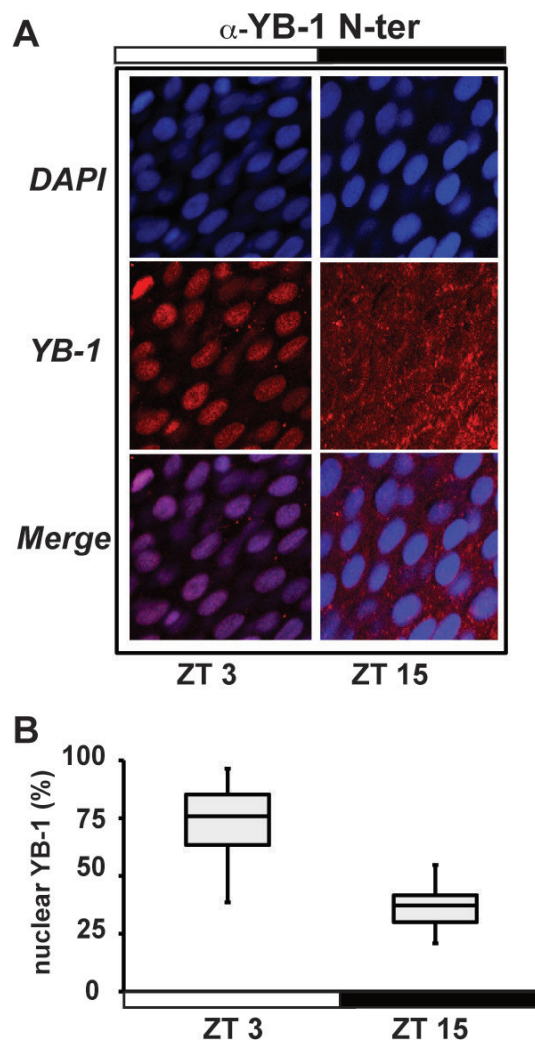


Figure 1: zfYB-1 cellular localization in zebrafish caudal fins. (A) Immunofluorescence analysis of zfYB-1 protein in the caudal fin at ZT3 (light phase) and ZT15 (dark phase) using α -YB-1 N-ter and α -YB-1 F antibodies. Panels also show DAPI staining and Merge, which combines both the DAPI and YB-1 signals. White and black bars above the panels indicate the corresponding lighting conditions. (B) Quantification of the panel A.

DN, which has been shown to disrupt core clock function (Supplementary Figure S5C–S5E) [34]. In *CLOCK1 DN* cells exposed to a LD cycle, we observed no significant rhythmicity in nuclear zFYB-1 protein (Figure 3C, 3D and Supplementary Table S1). In the second approach, we inhibited PAC-2 cell proliferation by serum deprivation at a high level of cell confluence. Under this condition, we observed rhythmicity of nuclear zFYB-1 levels under LD cycles, which also persisted on the second day following transfer to DD conditions (Supplementary Figure S5F). Together, these data confirm that rather than simply reflecting clock-dependent rhythmicity of cell cycle progression, zFYB-1 nuclear oscillation is a target of the CLOCK/BMAL-based core clock mechanism.

Given the importance of YB-1 function in mammalian cells, we also wished to explore whether this circadian clock regulation of YB-1 nuclear localization is an evolutionary conserved mechanism. Thus, we entrained the circadian clock in human HEK 293 cells via transient treatment with dexamethasone and then assayed nuclear YB-1 levels during the subsequent 48 h (Figure 4). In treated cells, clock synchronization was confirmed by circadian, antiphase rhythms of mRNA expression in two core clock genes, *hper2* and *hbm11* (Figure 4A, 4B and Supplementary Table S1). In these cells, we also observed a circa 24 h oscillation of nuclear YB-1 protein (Figure 4C, 4D and Supplementary Table S1). Therefore, all our results point to the cell-autonomous circadian clock finely tuning the nuclear localization of the zFYB-1 protein via an evolutionary conserved mechanism.

YB-1 SUMOylation in PAC-2 cells

How does the clock regulate zFYB-1 nuclear localization? One mechanism that has been implicated in clock-directed shuttling of proteins between the nucleus and cytoplasm is SUMOylation [5, 35]. SUMOylation has been documented to time the nuclear entry of the BMAL1 clock protein. Using GPS-SUMO 1.0 software we identified three potential conserved SUMOylation target sites in the zFYB-1 protein, one of which is a canonical inverted site (DSKA in position 287–290) and the other two are non-canonical sites (TKED 60–63 and EKRE 151–154) (Supplementary Figure S1). Extracts from PAC-2 cells immunoprecipitated (IP) at zt 3 with each of the three YB-1 antibodies independently, were subjected to immunoblotting for SUMO-1. Our results showed that the IP proteins from all three YB-1 antibodies were also recognized by the SUMO-1 antibody, consistent with the presence of SUMOylated YB-1 in zebrafish (Figure 5A). Furthermore, overexpression of the SUMO-conjugating enzyme UBC9 resulted in an increase in the overall quantity of zFYB-1 nuclear protein at zt 3 and also an increase in molecular weight observed at zt 15 (Figure 5B and Supplementary Figure S5B for comparison). To explore how the clock could regulate the YB-1 SUMOylation events, we next

investigated the possibility that the expression of a subset of genes involved in SUMOylation could also be clock regulated. Real time qRT-PCR analysis in PAC-2 cells exposed to a LD cycle followed by DD conditions revealed daily rhythmic expression of *zfunc9* (*zfube2ia*, *zfube2ib*), *zsumo1*, *zfsae1* (SUMO1 activating enzyme subunit 1) and *zfpias1* (E3 SUMO-protein ligase PIAS1) with a peak around the light–dark transition, which also persisted in most cases under DD conditions (Figure 5C, Supplementary Figure S6 and Supplementary Table S1). In addition, western blot analysis of PAC-2 cells for proteins covalently linked with SUMO-1 groups showed a day–night rhythm in the global levels of nuclear SUMOylated protein that is consistent with the timing of zFYB-1 nuclear localization (Figure 5D). Therefore, together these data point to a more general control of protein SUMOylation by the circadian clock rather than only YB-1.

Inhibition of *zfcyclin A2* expression by zFYB-1

Previous reports have demonstrated that YB-1 plays a key role in regulating cell proliferation. In the nucleus, YB-1 orchestrates expression of many proliferation-related genes. Therefore, we wished to explore the functional consequences of changes in nuclear YB-1 levels in zebrafish cells. FACS analysis of PAC-2 cells over expressing zFYB-1 and exposed to a LD cycle assayed at 6 hourly intervals during 24 h showed a loss of cell cycle rhythmicity with an elevation in the proportion of cells in S and G2/M phase and a reduction in G0/G1 cells (Supplementary Figure S7A and Supplementary Table S1). Therefore, YB-1 has an impact on the dynamics of cell cycle progression in zebrafish cells.

It has been previously shown that the mRNA expression of cyclins in zebrafish tissues is clock regulated [16, 18, 19]. Consistently, we confirmed the clock regulation of *zfcyclin A2* mRNA expression in PAC-2 cells (Supplementary Figure S7B). To address the role of zFYB-1 in cell cycle control we analyzed the contribution of zFYB-1 to the regulation of *zfcyclin A2* mRNA expression. Thus, we cloned a 447 bp fragment of the *zfcyclin A2* promoter including its 5'-UTR region, upstream of a luciferase reporter (*zfcyclin A2 pr.*). This region contains 4 putative YB-1 binding sites, 3 of them in the promoter and 1 in the 5'UTR region (Supplementary Figure S7C). Expression of this reporter construct in cells exposed to LD cycles increases progressively over the course of the assay but at a significantly higher rate during the dark phase (Figure 6A and Supplementary Figure S7D). Consistent with this reflecting regulation by the circadian clock, in transfected *CLOCK1 DN* cells this rhythmicity was not observed (Figure 6A). The higher cyclin A2 reporter gene expression during the dark period correlates with lower nuclear levels of zFYB-1 protein (see Figure 4A, 4B). In support of zFYB-1 playing a negative regulatory role, we observed a dose dependent inhibition

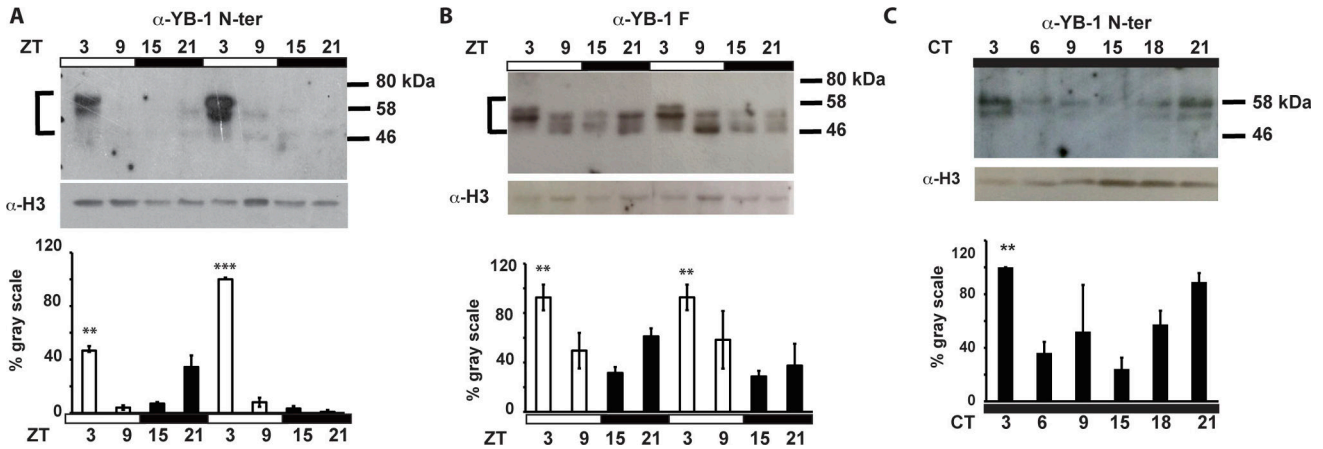


Figure 2: zfYB-1 protein expression in caudal fins. Western blot analysis and quantification of zfYB-1 levels in nuclear extracts under LD cycles (A, B) or during the second day in constant darkness, DD (C). The specific antibody used to detect YB-1 protein is indicated above each panel. An α -H3 antibody was used to provide a loading control. Vertical “brackets” on the left side of the panels A and B demarcate the YB-1 immunoreactive bands that were quantified using Image Lab™ Software. Quantification was expressed as % of gray scale relative to the highest peak of expression and is plotted on the Y-axes. Statistical significance between peak and trough points is indicated by asterisks where $p < 0.05$, $p < 0.001$ and $p < 0.0001$ are represented by *, ** and *** respectively. Results of the CircWave analysis are represented in Supplementary Table S1.

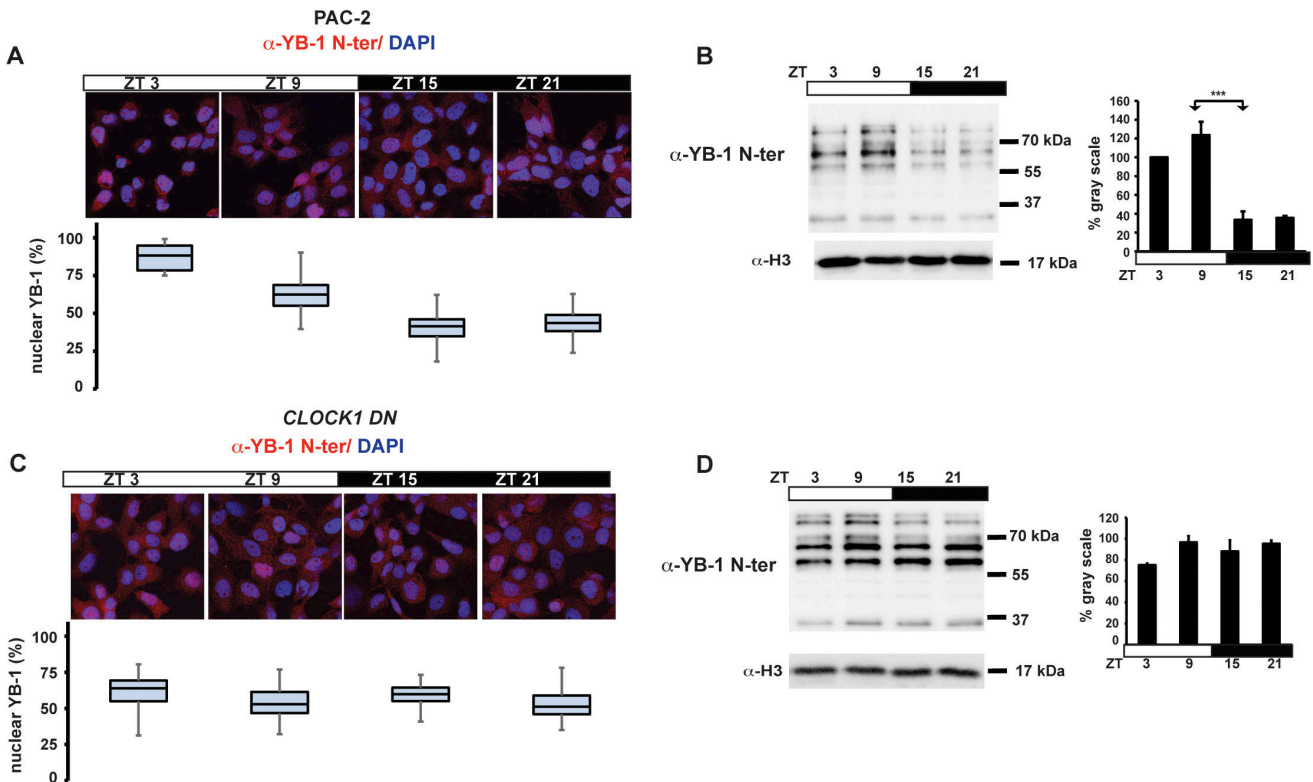


Figure 3: Nuclear zfYB-1 expression in PAC-2 and CLOCK1 DN cells. (A, C) Immunofluorescence analysis and quantification of nuclear levels of immunoreactive zfYB-1 in PAC-2 (A) and CLOCK1 DN (C) cells using the α -YB-1 N-ter antibody. Cells maintained under an LD cycle were fixed at 4 time points (ZT). A Merge of the DAPI and YB-1 staining images are shown. (B, D) Western blot analysis (right) and quantification (left) of α -YB-1 levels in fin nuclear extracts in PAC-2 (C) and CLOCK1 DN (D) cells under LD conditions and normalized for H3 expression (α -H3). Quantification was expressed as % of gray scale relative to the highest peak time point (ZT 9) and is plotted on the y-axis. ZT times are plotted on the x-axis. Statistically significant differences between peak and trough points are indicated by asterisks (*). Results of the CircWave analysis are represented in Supplementary Table S1.

of *zfcyclin A2* promoter expression after co-transfection with the expression constructs for zebrafish YB-1 (5'Myc-tag or 3'GFP-tag *zfYB-1*) and human YB-1 (3'GFP-tag *hYB-1*) (Figure 6B, 6C and Supplementary Figure S3D for controls) in PAC-2 cells. Finally, using a chromatin immunoprecipitation (ChIP) assay, we revealed a direct interaction between *zfYB-1* and the *zfcyclin A2* promoter (Figure 6D and Supplementary Figure S7E). Therefore, together our results are consistent with a role of *zfYB-1* in the circadian clock control of *cyclin A2* expression.

DISCUSSION

Circadian rhythmicity is one of the defining features of normal cell cycle progression in many highly proliferative tissues *in vivo*. Furthermore, frequent disruption of the circadian clock has been linked with an increased risk of many pathologies including cancer. For this reason, a major goal is to understand the links between the core clock mechanism and key cell cycle control systems. Here, using the zebrafish as a model, we have implicated YB-1 as one such element. The sub-cellular localization of this protein changes significantly with the time of day and high nuclear levels are associated with the early day period. These dynamic changes in YB-1 location are driven by the cell autonomous circadian clock

mechanism and involve SUMOylation, a post-translational modification already implicated in core clock function [5]. We show that in the nucleus, YB-1 physically associates with the *cyclin A2* gene 5' regulatory region and down-regulates its expression.

Previous findings have pointed to considerable complexity in YB-1 function consistent with a central role in the regulation of cell proliferation. However, the majority of these studies have focused on the role of YB-1 in tumorigenesis with comparatively little attention being applied to its normal physiological function. Although most YB-1 is located in the cytoplasm, recent evidence has shown that YB-1 can shuttle between the nucleus and the cytoplasm [28]. In the nucleus, YB-1 orchestrates expression of proliferation-related genes, whereas in the cytoplasm it associates with mRNA and regulates translation. Here we present data linking high nuclear levels of YB-1 with repression of *cyclin A2* expression. Cyclin A2 is synthesized at the onset of S-phase and then localizes to the nucleus where it is implicated in the initiation and progression of DNA synthesis. Our findings are consistent with previous results implicating YB-1 as a cell cycle stage-specific transcription factor [22] present in the nucleus at the boundary between G1 and S phase of the cell cycle. However, the precise manner whereby YB-1 regulates *cyclin A2* gene expression remains

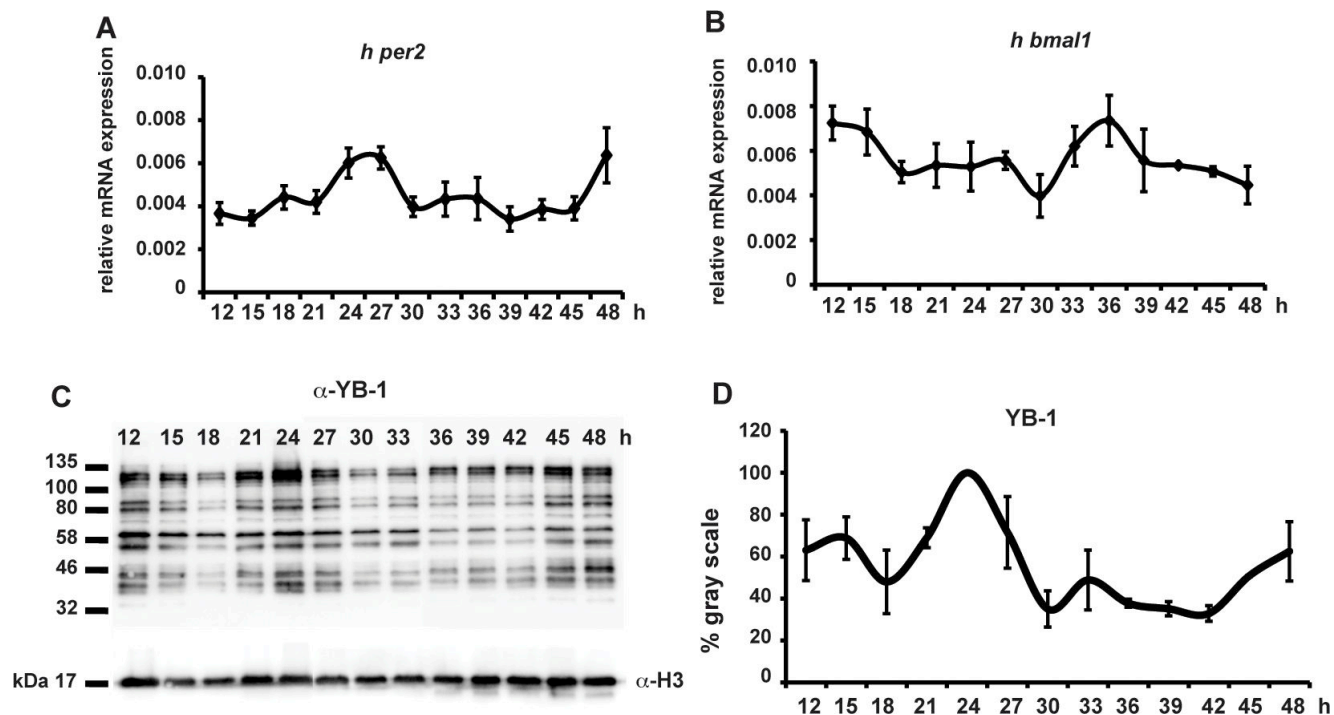


Figure 4: hYB-1 expression in clock synchronized HEK293 cells. (A, B) Real time qRT-PCR analysis of *hper2* and *hbm1* expression in HEK293 cells during 48 hours following transient treatment with 100 nM of Dexamethazone. Relative mRNA levels are plotted on the y-axis. Times after DEX treatment are plotted on the x-axis. Levels of *h-gapdh* mRNA were used for normalization. Results of the CircWave analysis are represented in Supplementary Table S1. (C) Western blot analysis using the α -YB-1 C-ter antibody in HEK293 cell nuclear extracts prepared after DEX treatment. H3 expression was used as a loading control. (D) Quantification analysis of panel (C). Quantification was expressed as % of gray scale relative to the highest peak time point (24 hrs) and plotted on the y-axis. Times after DEX treatment are plotted on the x-axis. The result of the CircWave analysis is represented in Supplementary Table S1.

uncertain. Nevertheless, it is tempting to speculate that the clock control of YB-1 might serve as part of a more general mechanism to restrict DNA replication to a specific temporal window to minimize the impact of UV light-induced DNA damage. However, given the multiple cellular mechanisms which involve YB-1, this clock related function is almost certainly not the only role played by the YB-1 protein.

Many lines of evidence also point to tight control of the timing of DNA repair processes during the day-night cycle. Thus, robust circadian rhythmicity of DNA replication which is anti-phase to that of DNA repair has been reported [36]. Furthermore, in zebrafish the expression of many genes involved in DNA repair is strongly induced by light, thus leading to an increase in DNA repair capacity during periods of maximum sunlight-induced DNA damage. In addition, DNA damage itself has been shown to constitute a zeitgeber for the circadian clock [15]. Thus, circadian clock gating of the cell cycle may also optimally time DNA damage repair. In this

respect, it is interesting to note that nuclear YB-1 has been demonstrated to have anti-apoptotic properties based on its ability to coordinate DNA excision repair function and protect cells against damaging agents [37]. Furthermore, various forms of stress, including oxidative, genotoxic stress and hyperthermia induce nuclear translocation of YB-1 [31, 38] implicating YB-1 in stress and DNA damage responses.

Cell autonomous, circadian clock control of cellular processes frequently occurs at the level of transcription initiation. Circadian rhythms in the expression of many clock-controlled genes (ccgs) are directed by circadian E-box enhancer promoter elements that represent the regulatory targets of the core clock proteins CLOCK and BMAL1. However, a host of other proteins, including kinases and phosphatases [39], chromatin modifiers [40] and RNA-binding factors [41] in turn play essential roles in conferring robustness on the core circadian clock mechanism. YB-1 is constitutively expressed in proliferating tissues and performs a multitude of cellular

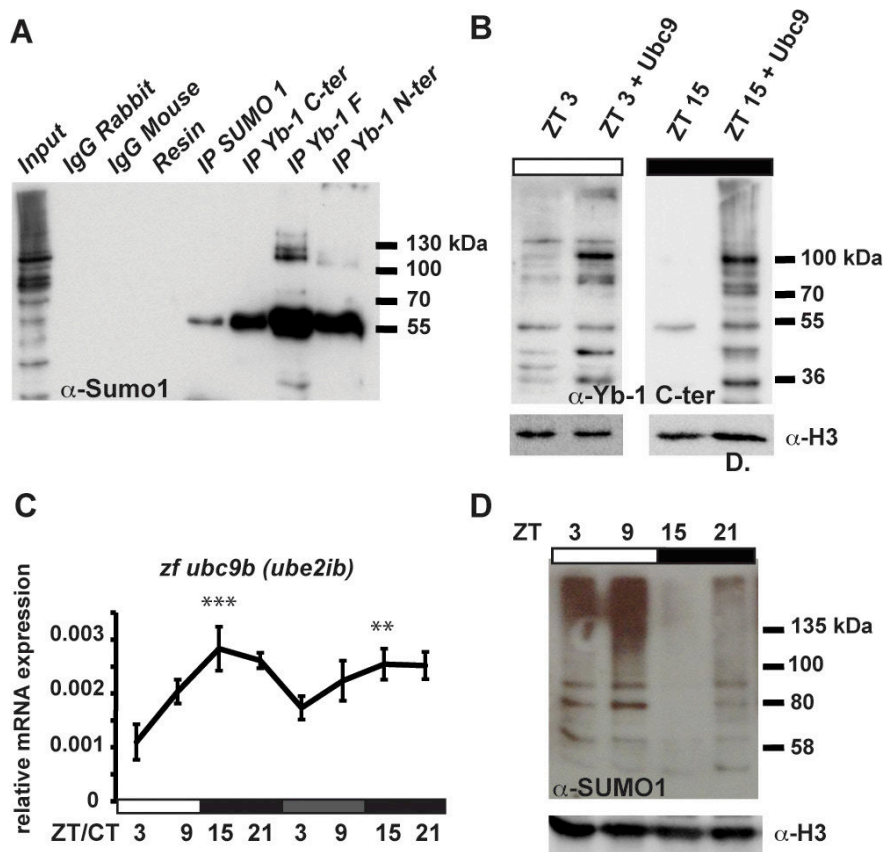


Figure 5: zfYB-1 SUMOylation. (A) Western blot analysis with the α -SUMO-1 antibody of IPs prepared from total cell extracts using each of the three α -YB-1 antibodies. Input and negative controls are indicated. (B) Western blot analysis using the α -YB-1 C-ter antibody in PAC-2 cell nuclear extracts prepared at ZT3 and ZT15 under an LD cycle in the absence or presence of over-expressed SUMO-conjugating enzyme UBC9 (+Ubc9). H3 expression was used as a loading control. (C) Real time qRT-PCR analysis of *zfubc9b* expression during exposure to a LD cycle followed by transfer to DD. Relative mRNA levels are plotted on the y-axis. ZT and CT times are plotted on the x-axis. β -actin mRNA was used for normalization. Statistical significance between peak and trough values in LD and in DD are indicated by asterisks. (D) Western blot analysis of SUMO-1 immunoreactive proteins in nuclear extracts prepared from cells under LD cycles. H3 expression was used as a loading control. Results of the CircWave analysis are represented in Supplementary Table S1.

functions, thus it is predictable that certain YB-1 functions are regulated by reversible post-translational modifications (PTM) rather than transcriptional mechanisms. In this regard, our results implicate SUMOylation in the clock-controlled translocation of YB-1 into the nucleus. Interestingly, circadian rhythmicity in the SUMOylation of the core clock protein, BMAL1, that is mediated by CLOCK, has been implicated in the regulation of nuclear entry [42]. Furthermore, our data point to general circadian rhythmicity in the mechanisms controlling SUMOylation. Thus, we speculate that YB-1 is the target of a cycling SUMOylation mechanism that relays timing information both within and outwards from the core clock mechanism.

Among the hallmarks of cancer, genome instability and mutations in cell cycle genes are recurring enabling factors [10]. Indeed mutations in cell cycle genes have been encountered in 90% of human cancers [43]. However, disruption of normal circadian clock function has also been

linked with tumorigenesis [44]. At an epidemiological level, shift work, chronic jet lag and other environmental factors impacting on circadian clock function are also linked with increased cancer development and disrupted cell proliferation. Many human cancer cell lines that by definition exhibit abnormal cell cycle progression, also display abnormal circadian clock gene expression [9, 10]. Furthermore, mouse knock out lines affecting certain core clock genes show an increased susceptibility to tumor formation [45, 46]. While expression of YB-1 protein is frequently elevated in tumors, its precise role in tumorigenesis is still poorly understood. In human tumors, such as breast, lung and prostate cancer, elevated YB-1 protein levels and nuclear localization [47] appear to be prognostic, indicating poor clinical outcome. Furthermore, the accumulation of YB-1 protein in the nucleus is associated with increased cell survival and multidrug resistance [31, 48]. However, YB-1 over-expression has

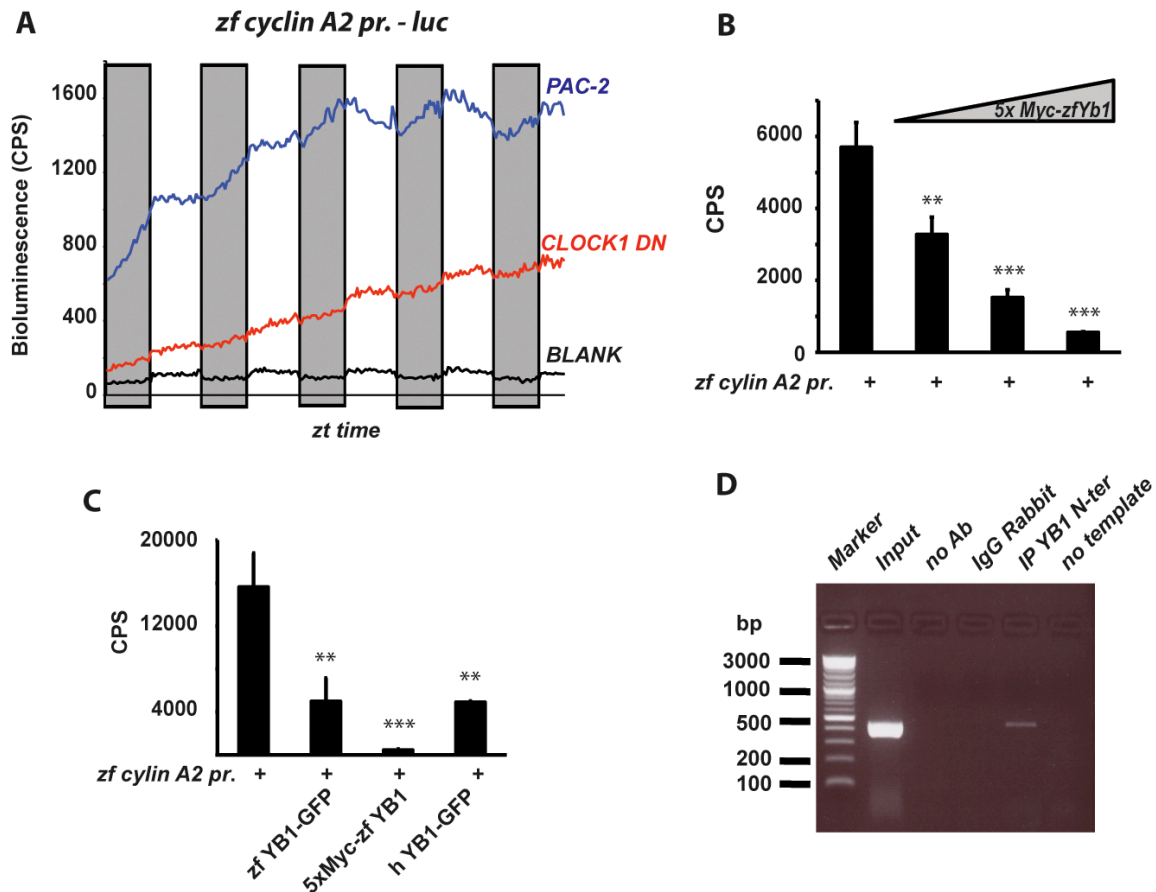


Figure 6: Regulation of *zf Cyclin A2* expression by *zfYB-1*. (A) Graphical representation of the real time bioluminescence assay results from PAC-2 (blue trace) and CLOCK1 DN cells (red trace) transfected with the *cyclin A2 pr.* luciferase reporter. The black trace (BLANK) represents the luminescence background of the cell plate. The bioluminescence in counts per second (CPS) is plotted on the y-axis and the ZT times on the x-axis. Results are plotted as the mean of 4 independent transfections. Gray bars indicate the corresponding dark periods. (B–C) *In vitro* luciferase assays in cells co-transfected with the *cyclin A2 -pr.* reporter and (B) 25, 50 and 100 ng of the 5xMyc-zfYB-1 expression vector or (C) with 50 ng of the zfYB-1-GFP, 5xMyc-zfYB-1 or the hYB-1-GFP expression vectors. Data are represented as means of triplicate samples +/- SD. At least three independent experiments were analyzed. Data were standardized for transfection efficiency using a β -galactosidase assay. Statistical significance is indicated above the graph by asterisks (*). (D) Agarose gel showing the 447 bp DNA promoter product amplified from ChIP assays using primers shown in Supplementary Table S2. Input and negative controls are indicated.

also been reported to block oncogenic transformation [49]. These apparently contradictory results may be the consequence of differential sub-cellular localization. Specifically, in the cytoplasm YB-1 may interfere with oncogenic transformation as a result of its function in translational control [25, 50]. YB-1 regulates the expression of several tumor-associated genes [51, 52]. As a result, elevated levels of YB-1 may play a role in facilitating tumor cell invasion and metastasis, as well as enhancing cell growth and resistance to chemotherapeutic agents. Thus, it is tempting to speculate that disruption of normal circadian rhythmicity of YB-1 function may serve as a key link with tumorigenesis.

MATERIALS AND METHODS

Fish care, treatment and ethical statements

Zebrafish (*D. rerio*) were maintained according to standard procedures [53] in a re-circulating water system at 28°C and under 14:10 light : dark cycles. For each experiment 6–12 months old zebrafish males or females were used. Under constant darkness, the fish were fed twice daily at random time points using automatic feeders. The caudal fins were amputated using razor blades following anesthesia with 0.02% w/v MS222 (3-aminobenzoate methanesulfonic acid, Sigma Aldrich). All zebrafish husbandry and experimental procedures were performed in accordance with the German animal protection standards (Animal Protection Law, BGBl. I, 1934 (2010)) and were approved by the Local Government of Baden-Württemberg, Karlsruhe, Germany (Az.: 35-9185.81/G-130/12 and 35-9185.81/G-131/16). General license for fish maintenance and breeding: Az.: 35-9185.64).

Quantitative RT-PCRs

Total RNA was extracted with Trizol Reagent (Gibco, BRL) according to the manufacturer's instructions. Reverse transcription was performed using Superscript III RT (Invitrogen). A StepOnePlus Real-Time qRT-PCR System (Applied Biosystems) and SYBR Green I fluorescent dye (Promega) were used. Expression levels were normalized using *zf β-actin* and *gapdh* mRNA expression for zebrafish and human HEK cells, respectively. The relative levels of mRNA were calculated using the $2^{-\Delta\Delta CT}$ method. For each gene, primer sequences are presented in Supplementary Table S2.

RNA interference

zfYB-1, NM_001126457, transient silencing was carried out in PAC-2 cells with increasing concentrations of IBONI YB-1 siRNA (RIBOXX GmbH, Germany) and FuGene HD reagent (Promega) according to the manufacturers' recommendations. iBONi siRNA Negative Control was provided by Riboxx as a pool of 3 different

siRNA. In Supplementary Table S3, all the siRNA sequences utilized are presented.

Protein analysis

Nuclear and cytoplasmic protein extracts were obtained using the NP40 lysis buffer protocol as described elsewhere [54]. Total protein extracts were also prepared by directly adding 200 μl of 1X Laemmli buffer (6% SDS, 20% glycerol, 125 mM TrispH6.8, 0.01% bromophenol blue, 100 mM DTT) including 1× cocktails of protease and phosphatase inhibitors (Sigma Aldrich) to the fin tissue or the cells. Gel electrophoresis was performed in a SDS polyacrylamide gel and proteins transferred to a Hybond-P membrane (Millipore). Binding of each antibody was visualized using the ECL detection system (Biorad). All images were acquired and analyzed with Image Lab™ Software (Bio Rad, USA) or with X-Ray films (Kodak). Then, images were quantified using the Scion Image software (NIH, <http://rsb.info.nih.gov/nihimage/>). A list of the primary and secondary antibodies used is shown in Supplementary Table S4. YB-1 immunofluorescence analysis of fins was performed after overnight fixation of fin-clips in Carnoy's solution (60% ethanol, 30% chloroform, 10% acetic acid) at 4°C followed by an incubation overnight in 100% Methanol and sequential rehydration steps in 100%, 66% and 33% methanol in PBTX (1XPBS, 0.3% Triton X100). Instead, adherent cells (1.2×10^5) were fixed overnight at 4°C in 4% PFA in 1× PBS and then transferred to PBST (1X PBS plus 0.1% Tween 20). At this stage, fins and cells were pre-incubated in blocking solution (PBTX and PBST, respectively plus 1% BSA (GE healthcare) for 3 hrs. Then the primary antibody was added and the samples were incubated at 4°C overnight. After several washes, the samples were incubated at 4°C with the secondary fluorescent antibody (Supplementary Table S4) for 2 hours (cells) or overnight (fins). DAPI staining was used for visualization of nuclei. The samples were mounting on glass slides and photographed using a Confocal Microscope SPE (Leica) with a 40X oil immersion objective and the quantification of nuclear and cytoplasmic signals was calculated using Image Lab™ Software (Bio Rad, USA). Co-Immunoprecipitations (Co-IPs) were performed as previously described [32]. The antibody concentrations used in each IPs and for western blotting analysis were chosen according to the manufacturers' recommendations.

Cell cultures and clock entrainment

The zebrafish cell line PAC-2 [55] was propagated as previously described [56].

The zebrafish *CLOCK1 DN* cells were a kind gift of David Whitmore and were propagated as previously described (Tamai et al., 2012 ref). The HEK293 (human embryonic kidney derived) cell line was cultured at 37°C with 5% CO₂ in Dulbecco's Modified Eagle's Medium

(DMEM) containing 10% heat inactivated fetal calf serum (FCS), 2 mM L-glutamine, 50 µg/ml penicillin and 50 µg/ml streptomycin.

The circadian clock in zebrafish cells was entrained by direct exposure of the cells to light–dark cycles at a constant temperature of 25°C using white light emitting diodes (LED, Kopa 440 nm–690 nm) adjusted to deliver a photon flux of $1.42 \times 10^{18} \pm 0,04 \times 10^{18}$ photons/s/m².

The clock entrainment in the HEK293 cells was performed by plating the cells at a concentration of 2.5×10^6 in DMEM medium (Sigma-Aldrich) in the presence of 10% serum. At 80% confluence, the concentration of serum was reduced to 2%. After 24 h, the cultures were treated with 100 nM water-soluble dexamethasone (Sigma-Aldrich) to synchronize the cells (time = 0 h), and after 2 h of incubation the medium was replaced with DMEM culture medium containing 2% serum. All cultures were incubated at 37°C in a humidified 5% CO₂ atmosphere until harvesting at specific time points after dexamethasone treatment (from 12 h to 48 h) according to the specific analysis.

FACS analysis for flow cytometry

Cells were trypsinized, collected and washed two times in cold 1x PBS via centrifugation at 1200 rpm for 4 minutes at 4°C. Next, the cell pellets were resuspended in 0.5 ml of ice-cold 100% methanol and incubated on ice for 20 minutes. After centrifugation at 1200 rpm for 4 minutes at 4°C, the pellets were resuspended again in cold 1x PBS and incubated on ice for 30 minutes prior to centrifugation and final resuspension in 0.5 ml of 1x PBS in the presence of RNAase at a final concentration of 100 µg/ml. After 20 minutes of incubation in RNAase at room temperature, the samples were finally stained with 50 µg/ml of Propidium iodide (PI) (Sigma) for 30 minutes on ice and in darkness. Data acquisition and analysis of the cell cycle phases were performed using a BD Accury C6 cytometer and software from BD Biosciences. Each time point was analyzed in triplicate, 40.000 events were analyzed for each sample.

Luciferase assays

Cell transfections were performed using FuGene HD (Promega) or ScreenFect (S-4001 InCella) reagents according to the manufacturers' protocols. β-galactosidase expression was used to normalize for transfection efficiency using a standard protocol [57]. Luciferase activity was measured using the Luciferase Assay System kit (Promega) and a VICTOR Multilabel Plate Reader (Perkin Elmer). The real-time bioluminescence assays were performed and analyzed as described previously [56, 58]. Bioluminescence was assayed with a Topcount NXT automatic scintillation counter (Perkin Elmer). Data were imported into Microsoft Excel using the "Import and Analysis" macro (S. Kay, Scripps Research Institute).

Constructs

The expression constructs 5xMyc-zfYB-1 and zfYB-1–GFP and the *zfcyclin* A2 promoter were cloned by PCR amplification of PAC-2 cell DNA using pfu polymerase (Promega) and then subcloned into the pCS2-MTK 5xMyc (Invitrogen), pcDNA6-V5/HisB GFP (ThermoFisher) and pGL3 basic-Luc (Promega) expression vectors (see Supplementary Table S4 for details). The hYB-1-GFP expression vector was previously described (24). The p3259 pCMV hUBC 9 mt HA was a gift from Peter Howley ADDGENE (14439) [59].

Chromatin immunoprecipitation (ChIP)

The ChIP assay was performed as described previously [60] with some minor changes described below. In brief, 1×10^6 cells were seeded and then, after 24 hours were fixed for 15 min. at room temperature in 1x formaldehyde solution (HCOH 1%, NaCl 10 mM, EDTA 0.1 mM, EGTA 0.05 mM, Hepes 5 mM in L-15 cell medium). After cell lysis in buffer L1 (Tris-HCl 50 mM pH 8.0, EDTA 0.2 mM pH 8.0, NP40 0.1%, Glycerol 10% including a 1x cocktail of protease and phosphatase inhibitors (Sigma Aldrich)), the nuclei were recovered by centrifugation (5 min. at 4°C at 3000 rpm) and resuspended in lysis buffer L2 (Tris-HCl 50 mM pH 8.0, EDTA 5 mM, SDS 1%). The sonicated chromatin (8 × 5s pulses) solution was diluted to a final volume of 3 ml with DB buffer (Tris-HCl 50 mM pH 8.0, EDTA 5 mM, NaCl 200 mM, NP40 0.5%). For each test (α-YB-1, no antibody (Ab) and α-IgG controls), 1 ml of chromatin solution was used. Immunoprecipitation was performed at 4°C over-night on a rotating platform. The antibody concentration was chosen according to the manufacturer's instructions. To recover the immunocomplexes (antibody plus chromatin) we used magnetic beads (Dyna beads Protein G, ref. 1004D, Novex Life-Technology). After extensive washing, bound DNA fragments were eluted and subsequently analyzed by PCR. PCR primers are reported in Supplementary Table S1. The 150 bp or 450 bp PCR products were visualized by 2% Agarose Gel Electrophoresis.

Statistical analysis

CircWaveBatch 3.3 (by courtesy of Dr. Roelof Hut, <http://www.euclock.org/component/zoo/item/deliverables.html>) was used to identify sinusoidal differential expression during the 24-hour cycle. This statistical algorithm tests each expression profile against a harmonic curve by varying the phase and period length. A F-test was used to measure the goodness-of-fit and the transcript was considered rhythmic when the harmonic regression was statistically significant ($p < 0.05$). Results of the CircWave analysis are represented in Supplementary Table S1. One-way analysis of variance (ANOVA) followed by

Bonferroni's multiple comparison tests was also performed using GraphPad Prism 4.0 (<http://www.graphpad.com>).

Statistical analysis of the real time bioluminescence data from the cyclin A2 luciferase reporter construct was performed using the MATLAB R2015b software as follows: Each night/day cycle was processed separately. A regression routine of order one delivered a mean slope per cycle. Equal cycles were averaged per well. To obtain cycle changes between night and day, the mean slope of all cycles was subtracted. A *t*-test for differences was analysed (see Supplementary Table S1).

All the statistical results are expressed as means \pm SD of three biological replicates where for each *in vivo* experiment a minimum of $n = 3$ fish were used per timepoint. In the statistical tests $p < 0.05$ was considered statistically significant. In each figure, $p < 0.05$, $p < 0.001$ and $p < 0.0001$ are represented by *, ** and *** respectively.

ACKNOWLEDGMENTS

We thank O. Kassel, R. M. Ceinos and J. Voegelé for support and discussion and M. Rastetter and T. Liepert for excellent technical assistance. We thank Prof. P. Mertens for providing us the hYB-1-GFP plasmid. We thank David Whitmore for the kind gift of the CLOCK1 DN zebrafish cell line and Professor Veronique Orian-Rousseau and Giuseppina Pace for kind help with the mammalian cells.

CONFLICTS OF INTEREST

The authors declare no conflicts of interest in the work presented.

GRANT SUPPORT

This research was funded through the Helmholtz funding programme BIFTM for D. Vallone and N.S. Foulkes; the BMBF project MIE for C. Pagano; By grants awarded to V. Calabro' from PO FESR 2007–2013 “DiMo” and Progetto “Campania Research in Experimental Medicine” (CREME), POR Campania FSE 2007–2013. We thank EMBO for a Short-term Fellowship grant awarded to O. di Martino. We acknowledge support by the Deutsche Forschungsgemeinschaft and the open access publishing fund of Karlsruhe Institute of Technology.

REFERENCES

1. Pittendrigh CS. Temporal organization: reflections of a Darwinian clock-watcher. *Annu Rev Physiol.* 1993; 55:16–54.
2. Wager-Smith K, Kay SA. Circadian rhythm genetics: from flies to mice to humans. *Nat Genet.* 2000; 26:23–27.
3. Reppert SM, Weaver DR. Molecular analysis of mammalian circadian rhythms. *Annu Rev Physiol.* 2001; 63:647–676.

4. Preitner N, Damiola F, Lopez-Molina L, Zakany J, Duboule D, Albrecht U, Schibler U. The orphan nuclear receptor REV-ERB α controls circadian transcription within the positive limb of the mammalian circadian oscillator. *Cell.* 2002; 110:251–260.
5. Cardone L, Hirayama J, Giordano F, Tamaru T, Palvimo JJ, Sassone-Corsi P. Circadian clock control by SUMOylation of BMAL1. *Science.* 2005; 309:1390–1394.
6. Lee C, Etchegaray JP, Cagampang FR, Loudon AS, Reppert SM. Posttranslational mechanisms regulate the mammalian circadian clock. *Cell.* 2001; 107:855–867.
7. Miyazaki K, Nagase T, Mesaki M, Narukawa J, Ohara O, Ishida N. Phosphorylation of clock protein PER1 regulates its circadian degradation in normal human fibroblasts. *Biochem J.* 2004; 380:95–103.
8. Savvidis C, Koutsilieris M. Circadian rhythm disruption in cancer biology. *Mol Med.* 2012; 18:1249–1260.
9. Fu L, Kettner NM. The circadian clock in cancer development and therapy. *Prog Mol Biol Transl Sci.* 2013; 119:221–282.
10. Feillet C, van der Horst GT, Levi F, Rand DA, Delaunay F. Coupling between the Circadian Clock and Cell Cycle Oscillators: Implication for Healthy Cells and Malignant Growth. *Front Neurol.* 2015; 6:96.
11. Matsuo T, Yamaguchi S, Mitsui S, Emi A, Shimoda F, Okamura H. Control mechanism of the circadian clock for timing of cell division *in vivo*. *Science.* 2003; 302:255–259.
12. Hirayama J, Cardone L, Doi M, Sassone-Corsi P. Common pathways in circadian and cell cycle clocks: light-dependent activation of Fos/AP-1 in zebrafish controls CRY-1a and WEE-1. *Proc Natl Acad Sci USA.* 2005; 102:10194–10199.
13. Grechez-Cassiau A, Rayet B, Guillaumond F, Teboul M, Delaunay F. The circadian clock component BMAL1 is a critical regulator of p21WAF1/CIP1 expression and hepatocyte proliferation. *J Biol Chem.* 2008; 283:4535–4542.
14. Hunt T, Sassone-Corsi P. Riding tandem: circadian clocks and the cell cycle. *Cell.* 2007; 129:461–464.
15. Oklejewicz M, Destici E, Tamanini F, Hut RA, Janssens R and van der Horst GT. Phase resetting of the mammalian circadian clock by DNA damage. *Curr Biol.* 2008; 18:286–291.
16. Idda ML, Kage E, Lopez-Olmeda JF, Mracek P, Foulkes NS, Vallone D. Circadian timing of injury-induced cell proliferation in zebrafish. *PLoS One.* 2012; 7:e34203.
17. Dekens MP, Santoriello C, Vallone D, Grassi G, Whitmore D, Foulkes NS. Light regulates the cell cycle in zebrafish. *Curr Biol.* 2003; 13:2051–2057.
18. Laranjeiro R, Tamai TK, Peyric E, Krusche P, Ott S, Whitmore D. Cyclin-dependent kinase inhibitor p20 controls circadian cell-cycle timing. *Proc Natl Acad Sci USA.* 2013; 110:6835–6840.
19. Peyric E, Moore HA, Whitmore D. Circadian clock regulation of the cell cycle in the zebrafish intestine. *PLoS One.* 2013; 8:e73209.

20. Bailes HJ, Lucas RJ. Melanopsin and inner retinal photoreception. *Cell Mol Life Sci.* 2010; 67:99–111.
21. Whitmore D, Foulkes NS, Sassone-Corsi P. Light acts directly on organs and cells in culture to set the vertebrate circadian clock. *Nature.* 2000; 404:87–91.
22. Jurchott K, Bergmann S, Stein U, Walther W, Janz M, Manni I, Piaggio G, Fietze E, Dietel M, Royer HD. YB-1 as a cell cycle-regulated transcription factor facilitating cyclin A and cyclin B1 gene expression. *J Biol Chem.* 2003; 278:27988–27996.
23. Basaki Y, Taguchi K, Izumi H, Murakami Y, Kubo T, Hosoi F, Watari K, Nakano K, Kawaguchi H, Ohno S, Kohno K, Ono M, Kuwano M. Y-box binding protein-1 (YB-1) promotes cell cycle progression through CDC6-dependent pathway in human cancer cells. *Eur J Cancer.* 2010; 46:954–965.
24. Matsumoto K, Wolffe AP. Gene regulation by Y-box proteins: coupling control of transcription and translation. *Trends Cell Biol.* 1998; 8:318–323.
25. Bader AG, Vogt PK. Inhibition of protein synthesis by Y box-binding protein 1 blocks oncogenic cell transformation. *Mol Cell Biol.* 2005; 25:2095–2106.
26. En-Nia A, Yilmaz E, Klinge U, Lovett DH, Stefanidis I, Mertens PR. Transcription factor YB-1 mediates DNA polymerase alpha gene expression. *J Biol Chem.* 2005; 280:7702–7711.
27. Evdokimova V, Ruzanov P, Anglesio MS, Sorokin AV, Ovchinnikov LP, Buckley J, Triche TJ, Sonenberg N, Sorensen PH. Akt-mediated YB-1 phosphorylation activates translation of silent mRNA species. *Mol Cell Biol.* 2006; 26:277–292.
28. Raffetseder U, Frye B, Rauen T, Jurchott K, Royer HD, Jansen PL, Mertens PR. Splicing factor SRp30c interaction with Y-box protein-1 confers nuclear YB-1 shuttling and alternative splice site selection. *J Biol Chem.* 2003; 278:18241–18248.
29. Basaki Y, Hosoi F, Oda Y, Fotovati A, Maruyama Y, Oie S, Ono M, Izumi H, Kohno K, Sakai K, Shimoyama T, Nishio K, Kuwano M. Akt-dependent nuclear localization of Y-box-binding protein 1 in acquisition of malignant characteristics by human ovarian cancer cells. *Oncogene.* 2007; 26:2736–2746.
30. Mertens PR, Harendza S, Pollock AS, Lovett DH. Glomerular mesangial cell-specific transactivation of matrix metalloproteinase 2 transcription is mediated by YB-1. *J Biol Chem.* 1997; 272:22905–22912.
31. Kohno K, Izumi H, Uchiumi T, Ashizuka M, Kuwano M. The pleiotropic functions of the Y-box-binding protein, YB-1. *Bioessays.* 2003; 25:691–698.
32. Di Costanzo A, Troiano A, di Martino O, Cacace A, Natale CF, Ventre M, Netti P, Caserta S, Pollice A, La Mantia G, Calabro V. The p63 protein isoform DeltaNp63alpha modulates Y-box binding protein 1 in its subcellular distribution and regulation of cell survival and motility genes. *J Biol Chem.* 2012; 287:30170–30180.
33. di Martino O, Troiano A, Guarino AM, Pollice A, Vivo M, La Mantia G, Calabro V. ΔNp63α controls YB-1 protein stability: evidence on YB-1 as a new player in keratinocyte differentiation. *Genes to Cells.* 2016 in press.
34. Tamai TK, Young LC, Cox CA, Whitmore D. Light acts on the zebrafish circadian clock to suppress rhythmic mitosis and cell proliferation. *J Biol Rhythms.* 2012; 27:226–236.
35. Abad-Morales V, Domenech EB, Garanto A, Marfany G. mRNA expression analysis of the SUMO pathway genes in the adult mouse retina. *Biol Open.* 2015; 4:224–232.
36. Chen Z, McKnight SL. A conserved DNA damage response pathway responsible for coupling the cell division cycle to the circadian and metabolic cycles. *Cell Cycle.* 2007; 6:2906–2912.
37. Fomina EE, Pestryakov PE, Maltseva EA, Petrusheva IO, Kretov DA, Ovchinnikov LP, Lavrik OI. Y-box binding protein 1 (YB-1) promotes detection of DNA bulky lesions by XPC-HR23B factor. *Biochemistry (Mosc).* 2015; 80:219–227.
38. Ohga T, Uchiumi T, Makino Y, Koike K, Wada M, Kuwano M, Kohno K. Direct involvement of the Y-box binding protein YB-1 in genotoxic stress-induced activation of the human multidrug resistance 1 gene. *J Biol Chem.* 1998; 273:5997–6000.
39. Reischl S, Kramer A. Kinases and phosphatases in the mammalian circadian clock. *FEBS Lett.* 2011; 585:1393–1399.
40. Sahar S, Sassone-Corsi P. The epigenetic language of circadian clocks. *Handb Exp Pharmacol.* 2013; :29–44.
41. Kowalska E, Ripperger JA, Hoegger DC, Bruegger P, Buch T, Birchler T, Mueller A, Albrecht U, Contaldo C, Brown SA. NONO couples the circadian clock to the cell cycle. *Proc Natl Acad Sci USA.* 2013; 110:1592–1599.
42. Stojkovic K, Wing SS, Cermakian N. A central role for ubiquitination within a circadian clock protein modification code. *Front Mol Neurosci.* 2014; 7:69.
43. Bonelli P, Tuccillo FM, Borrelli A, Schiattarella A, Buonaguro FM. CDK/CCN and CDKI alterations for cancer prognosis and therapeutic predictivity. *Biomed Res Int.* 2014; 2014:361020.
44. Parent ME, El-Zein M, Rousseau MC, Pintos J, Siemiatycki J. Night work and the risk of cancer among men. *Am J Epidemiol.* 2012; 176:751–759.
45. Fu L, Pelicano H, Liu J, Huang P, Lee C. The circadian gene *Period2* plays an important role in tumor suppression and DNA damage response *in vivo*. *Cell.* 2002; 111:41–50.
46. Lee S, Donehower LA, Herron AJ, Moore DD, Fu L. Disrupting circadian homeostasis of sympathetic signaling promotes tumor development in mice. *PLoS One.* 2010; 5:e10995.
47. Shibahara K, Sugio K, Osaki T, Uchiumi T, Maehara Y, Kohno K, Yasumoto K, Sugimachi K, Kuwano M. Nuclear expression of the Y-box binding protein, YB-1, as a novel marker of disease progression in non-small cell lung cancer. *Clin Cancer Res.* 2001; 7:3151–3155.

48. Sorokin AV, Selyutina AA, Skabkin MA, Guryanov SG, Nazimov IV, Richard C, Th'ng J, Yau J, Sorensen PH, Ovchinnikov LP, Evdokimova V. Proteasome-mediated cleavage of the Y-box-binding protein 1 is linked to DNA-damage stress response. *EMBO J.* 2005; 24:3602–3612.
49. Bader AG, Felts KA, Jiang N, Chang HW, Vogt PK. Y box-binding protein 1 induces resistance to oncogenic transformation by the phosphatidylinositol 3-kinase pathway. *Proc Natl Acad Sci USA.* 2003; 100:12384–12389.
50. Bader AG, Vogt PK. An essential role for protein synthesis in oncogenic cellular transformation. *Oncogene.* 2004; 23:3145–3150.
51. Lasham A, Lindridge E, Rudert F, Onrust R, Watson J. Regulation of the human fas promoter by YB-1, Puralpha and AP-1 transcription factors. *Gene.* 2000; 252:1–13.
52. Mertens PR, Alfonso-Jaume MA, Steinmann K, Lovett DH. A synergistic interaction of transcription factors AP2 and YB-1 regulates gelatinase A enhancer-dependent transcription. *J Biol Chem.* 1998; 273:32957–32965.
53. Nüsslein-Volhard C, Dahm R. *Zebrafish : a practical approach.* (Oxford: Oxford University Press). 2002
54. Kassel O, Schneider S, Heilbock C, Litfin M, Gottlicher M, Herrlich P. A nuclear isoform of the focal adhesion LIM-domain protein Trip6 integrates activating and repressing signals at AP-1- and NF-kappaB-regulated promoters. *Genes Dev.* 2004; 18:2518–2528.
55. Lin S, Gaiano N, Culp P, Burns JC, Friedmann T, Yee JK, Hopkins N. Integration and germ-line transmission of a pseudotyped retroviral vector in zebrafish. *Science.* 1994; 265:666–669.
56. Vatine G, Vallone D, Appelbaum L, Mracek P, Ben-Moshe Z, Lahiri K, Gothilf Y, Foulkes NS. Light directs zebrafish period2 expression via conserved D and E boxes. *PLoS Biol.* 2009; 7:e1000223.
57. Sambrook J, Fritsch EF, Maniatis T. (1989). *Molecular cloning : a laboratory manual.* (Cold Spring Harbor: Cold Spring Harbor Laboratory Press).
58. Vallone D, Gondi SB, Whitmore D, Foulkes NS. E-box function in a period gene repressed by light. *Proc Natl Acad Sci USA.* 2004; 101:4106–4111.
59. Yasugi T, Howley PM. Identification of the structural and functional human homolog of the yeast ubiquitin conjugating enzyme UBC9. *Nucleic Acids Res.* 1996; 24:2005–2010.
60. Wells J, Boyd KE, Fry CJ, Bartley SM, Farnham PJ. Target gene specificity of E2F and pocket protein family members in living cells. *Mol Cell Biol.* 2000; 20:5797–5807.

Modulation of DNA Repair Systems in Blind Cavefish during Evolution in Constant Darkness

Haiyu Zhao,¹ Giuseppe Di Mauro,^{1,2} Sebastian Lungu-Mitea,^{1,3,6} Pietro Negrini,^{1,2} Andrea Maria Guarino,^{1,5} Elena Frigato,² Thomas Braunbeck,³ Hongju Ma,⁴ Tilman Lamparter,⁴ Daniela Vallone,¹ Cristiano Bertolucci,² and Nicholas S. Foulkes^{1,7,*}

¹Institute of Toxicology and Genetics, Karlsruhe Institute of Technology, Hermann-von-Helmholtz Platz 1, 76344 Eggenstein-Leopoldshafen, Germany

²Department of Life Science and Biotechnology, University of Ferrara, Via Luigi Borsari 46, 44121 Ferrara, Italy

³Aquatic Ecology and Toxicology, Centre for Organismal Studies, University of Heidelberg, Im Neuenheimer Feld, 69120 Heidelberg, Germany

⁴Botanical Institute, Karlsruhe Institute of Technology, 76128 Karlsruhe, Germany

⁵Department of Biology, University of Naples "Federico II," 80126 Naples, Italy

⁶Department of Biomedical Sciences and Veterinary Public Health, Swedish University of Agricultural Sciences, 75007 Uppsala, Sweden

⁷Lead Contact

*Correspondence: nicholas.foulkes@kit.edu

<https://doi.org/10.1016/j.cub.2018.08.039>

SUMMARY

How the environment shapes the function and evolution of DNA repair systems is poorly understood. In a comparative study using zebrafish and the Somalian blind cavefish, *Phreatichthys andruzzii*, we reveal that during evolution for millions of years in continuous darkness, photoreactivation DNA repair function has been lost in *P. andruzzii*. We demonstrate that this loss results in part from loss-of-function mutations in pivotal DNA-repair genes. Specifically, C-terminal truncations in *P. andruzzii* DASH and 6-4 photolyase render these proteins predominantly cytoplasmic, with consequent loss in their functionality. In addition, we reveal a general absence of light-, UV-, and ROS-induced expression of *P. andruzzii* DNA-repair genes. This results from a loss of function of the D-box enhancer element, which coordinates and enhances DNA repair in response to sunlight. Our results point to *P. andruzzii* being the only species described, apart from placental mammals, that lacks the highly evolutionary conserved photoreactivation function. We predict that in the DNA repair systems of *P. andruzzii*, we may be witnessing the first stages in a process that previously occurred in the ancestors of placental mammals during the Mesozoic era.

INTRODUCTION

DNA stability is of utmost importance for the maintenance of normal cellular function. However, it is subject to sustained assault from the environment. Ultraviolet (UV) radiation from sun-

light is the most common and powerful factor that can induce mutagenic and cytotoxic lesions in DNA, such as cyclobutane-pyrimidine dimers (CPDs), 6-4 photoproducts (6-4PPs), and their Dewar valence isomers [1–3]. Such damage must be rapidly removed to ensure complete and accurate DNA replication and transcription, so organisms have developed a battery of DNA-repair mechanisms [4].

Photoreactivation serves as one of the most important and ubiquitous DNA-repair systems, enzymatically repairing UV-induced DNA lesions using the energy from violet/blue light [5–8]. This light-dependent reaction is catalyzed by photolyases. These represent a highly conserved class of flavoproteins where the flavin adenine dinucleotide (FAD) molecule serves as a key light-harvesting cofactor, together with a second antenna chromophore that differs between photolyases and species [2, 6]. Photolyases are subdivided into CPDs and 6-4 photolyases based on their different substrates (CPDs and 6-4PPs, respectively) [6], while cryptochrome-DASH selectively repairs CPDs in single-stranded DNA and RNA [9–11]. Nucleotide excision repair (NER) and base excision repair (BER) are other major DNA repair mechanisms found in nearly all organisms. NER removes a wide variety of DNA-distorting lesions, including UV-induced CPDs and 6-4PPs [4, 12, 13], while BER represents the predominant pathway repairing lesions arising from ionizing radiation and reactive oxygen species (ROS) generated by metabolism or by UV radiation [14–18]. These excision repair pathways remove DNA lesions by a sequential, multistep process ranging from damage recognition to DNA resynthesis and ligation [13, 15, 19]. Lesion recognition, in the case of NER, is performed by a complex incorporating XPC and DDB2 (p48), while the DNA glycosylase Neil1 initiates this first step in BER. Interestingly, expression of XPC and Neil1 has been reported to be transcriptionally regulated by UV radiation in mammals [20]. Furthermore, visible light exposure upregulates photolyase expression in non-mammalian vertebrates [21, 22]. Thus, specific transcriptional activation of key DNA-repair genes appears

to represent part of a strategy whereby DNA repair activity is enhanced in response to sunlight to counter the detrimental effects of UV-induced DNA damage. However, the mechanisms whereby sunlight regulates the expression of DNA repair genes remain poorly understood.

One key, unanswered question concerns how the environment influences the evolution of DNA-repair systems. For example, photolyases are phylogenetically ancient enzymes that are present in animals, plants, unicellular organisms, and even bacteria. However, curiously, humans and other placental mammals lack photolyases and photoreactivation, relying instead on the more complex and less efficient NER mechanism [23]. Might a particular set of environmental conditions, experienced during the early evolution of placental mammals, have led to the eventual loss of photoreactivation?

In this manuscript, we aim to investigate how sunlight affects the evolution of DNA repair systems. Specifically, we address the consequence of evolution under extreme aphotic conditions for DNA repair in the Somalian blind cavefish *Phreatichthys andruzzii*. This species has evolved in the complete absence of light and UV-induced DNA damage for millions of years [24] and so represents a powerful model for exploring the influence of sunlight on DNA repair function over an evolutionary timescale. Cave-dwelling organisms share a set of striking phenotypes—so-called “troglomorphisms,” including notably complete loss of the eyes and body pigmentation. In certain cases, alterations in DNA repair function have also been reported [25–27]. For example, enhanced DNA repair has been encountered in blind cave forms of *Astyanax mexicanus* [25]. Our chosen cavefish model, *P. andruzzii*, shows a more extreme troglomorphic phenotype than *A. mexicanus*, even to the extent of lacking photic regulation of the circadian clock [28, 29]. In order to study DNA repair function in this species, we compare it with a more genetically accessible epigeal sighted species: the zebrafish, *Danio rerio*. The zebrafish contains nearly all the genes involved in DNA repair pathways in eukaryotes, including the photolyases, and so represents an ideal model for gaining mechanistic insight into DNA repair systems [30].

Using this comparative approach, we find that *P. andruzzii* represents the only species described, apart from placental mammals, that lacks the highly evolutionary conserved photoreactivation function. The loss of photoreactivation is associated with mutations in photolyase genes, as well as impaired light-, UV-, and ROS-induced transcription of DNA-repair genes resulting from loss of D-box enhancer element function.

RESULTS

Loss of Light-Driven DNA Repair in Somalian Cavefish

Following UV irradiation, exposure to a light/dark (LD) cycle enhances survival of zebrafish embryos [31]. Is this property conserved during evolution for millions of years in the complete absence of sunlight? *P. andruzzii* (PA) and zebrafish (ZF) embryos raised in complete darkness until 3 days post fertilization (dpf) were exposed to different doses of UV-C radiation ranging from 53 to 424 J/m². Embryo mortality was then assessed daily under either LD cycle or constant darkness (DD) conditions (Figure 1A). Under both conditions, we observed a UV-dose-dependent increase in mortality in the embryos of

each species (Figures 1B–1E and S1A). However, a generally lower cavefish embryo survival compared with the zebrafish indicates species-specific differences in sensitivity to UV damage. Importantly, consistent with previous findings [31], zebrafish embryos exposed to a LD cycle exhibited a significantly lower mortality compared with the DD group following UV exposure (Figures 1B–1E and S1A and Table S1). In contrast, the presence of a LD cycle did not significantly enhance cavefish survival (Figures 1B–1E and S1A and Table S1). These results point to a loss of the protecting effect of LD cycles in *P. andruzzii*.

As a first step toward exploring this loss of the protective effect of visible light in *P. andruzzii*, we next tested whether the same phenomenon exists at the cell culture level. *P. andruzzii* cell lines, derived from embryos (EPA) [32] and adult fin clips (CF1) [28], as well as zebrafish embryo-derived (PAC-2) [33] and adult fin-derived (AB9) [34] cell lines, were irradiated with a range of UV-C doses and subsequently exposed to either LD or DD conditions. Cell viability was then assessed using a 3-(4,5-dimethylthiazol-2-yl)-2,5-diphenyl tetrazolium bromide (MTT) assay (Figures 1F–1J). Consistent with our *in vivo* experiments, cell survival was significantly enhanced by the presence of LD cycles in zebrafish cells, but not in cavefish cells (Figures 1F–1J and Table S1). We have previously reported that exposure of zebrafish cells to LD cycles results in entrainment of the endogenous circadian clock [35]. However, zebrafish cell survival was also enhanced under constant light (LL) following UV radiation (Figures S1B–S1F and Table S1), arguing against clock entrainment being responsible for the protective effect of light.

Then, to address whether the loss of the protective effect of light in this cavefish reflects abnormalities in DNA repair, we assayed DNA repair in cavefish and zebrafish cells under light (LL or LD) or dark (DD) conditions following UV exposure. We chose to specifically test the effects of blue light exposure, given its documented importance in DNA repair system function [36] (Figures 2 and S2). We first tested the formation of DNA strand breaks, which are generated during NER- and BER-based DNA repair, by measuring Histone H2AX phosphorylation at Ser 139 (γ -H2AX) [37–40]. Consistent with our cell viability assay results, UV-induced H2AX phosphorylation was significantly reduced upon exposure to light (LD or LL) in zebrafish cells, but not in *P. andruzzii* cells (Figures 2B, 2C, and S2B–S2D and Table S1). We then performed a single-cell electrophoresis assay, the comet assay, which also detects the presence of DNA strand breaks [41, 42]. Control zebrafish cells kept under blue light showed significantly lower levels of fragmented DNA following UV treatment than cells maintained in darkness (Figures 2D, S2E, and S2F). In contrast, in cavefish cells, the levels of fragmented DNA were again comparable under LD and DD lighting conditions (Figures 2E, S2G, and S2H).

Since CPD photoproducts account for more than 75% of UV-induced DNA lesions in the genome [1, 43], we then used an ELISA assay to directly assay the levels of UV-induced CPD photoproducts in the zebrafish (ZF-CPD) and cavefish (PA-CPD) cell lines during exposure to 9 hr of blue light or darkness. Our results showed that the levels of CPDs in zebrafish were significantly reduced upon illumination, while no significant difference between the illuminated and dark groups was observed in the

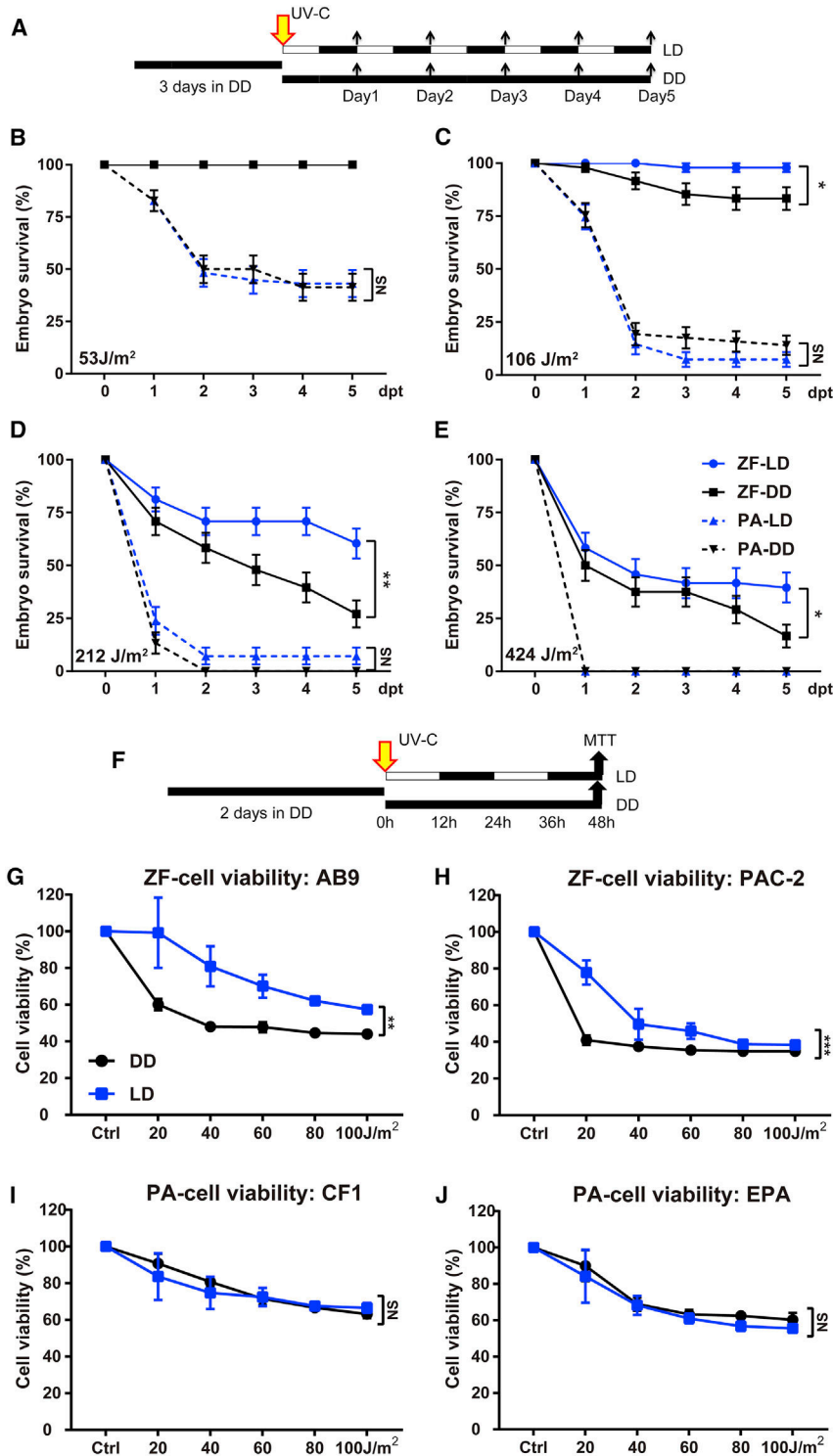


Figure 1. UV-Induced Mortality in Larvae and Cells

(A) Experimental design for data presented in (B)–(E). (B–E) Survival of Zebrafish (ZF) and *P. andruzzii* (PA) embryos irradiated with different doses of UV-C (B, 53 J/m²; C, 106 J/m²; D, 212 J/m²; E, 424 J/m²) and subsequently transferred to light (LD) cycles or constant darkness (DD). Survival rates (%) during the following 5 days are plotted against time (dpt, days post treatment). For untreated controls, see Figure S1. Statistical analysis (log rank [Mantel-Cox] and Gehan-Breslow-Wilcoxon tests) and the number of animals analyzed are reported in Table S1.

(F) Experimental design for data presented in panels (G)–(J).

(G–J) 3-(4,5-dimethylthiazol-2-yl)-2,5-diphenyl tetrazolium bromide (MTT) cell viability assay in (G and H) ZF and (I and J) PA cell lines after UV irradiation and subsequently exposure for 48 hr to DD or LD cycles. UV-C doses are plotted on the x axes, while cell viability (%) ± SEM (n = 4) with respect to untreated cells is plotted on the y axes.

Each experiment was repeated independently three times. Two-way ANOVA followed by Sidak's multiple comparisons test results are reported in Table S1. Significant differences are indicated by asterisks (**p < 0.01, *p < 0.05; NS, no significance). See also Figure S1.

Loss-of-Function Mutations in Cavefish Photolyase Genes

We next explored the molecular basis of this loss of light-responsive DNA repair function. Photolyases are central to the ability of light to enhance DNA repair [5–8]. Does *P. andruzzii* retain normal photolyase function? We cloned and sequenced the cavefish photolyase genes in order to search for loss-of-function mutations. Based on RNA sequencing (RNA-seq) and RT-PCR using RNA extracted from a range of cavefish tissues and cells and consistent with other published teleost genome sequences [44], we identified three different photolyase genes in *P. andruzzii* (*pa 6-4phr*, *pa DASHphr*, and *pa CPDphr*) (Figure 3A and Table S2). In the case of the *pa 6-4phr* gene, we identified one cDNA encoding a full-length form (*pa 6-4phr*), sharing high homology (88.8%) with the zebrafish ortholog, and two additional cDNAs encoding C-terminally truncated proteins (*pa 6-4phr-MT1* and *pa 6-4phr-MT2*) (Figures 3A and S3A). Given that apart

from these mutations, the nucleotide sequences of the three *pa 6-4phr* cDNAs were identical, and the fact that our original RNA samples were derived from pools of individuals, this points to the existence of multiple *pa 6-4phr* gene alleles in the *P. andruzzii* population. In the case of the *pa DASHphr* gene, only two cDNAs encoding C-terminally

truncated proteins (*pa 6-4phr-MT1* and *pa 6-4phr-MT2*) (Figures 3A and S3A). Given that apart from these mutations, the nucleotide sequences of the three *pa 6-4phr* cDNAs were identical, and the fact that our original RNA samples were derived from pools of individuals, this points to the existence of multiple *pa 6-4phr* gene alleles in the *P. andruzzii* population. In the case of the *pa DASHphr* gene, only two cDNAs encoding C-terminally

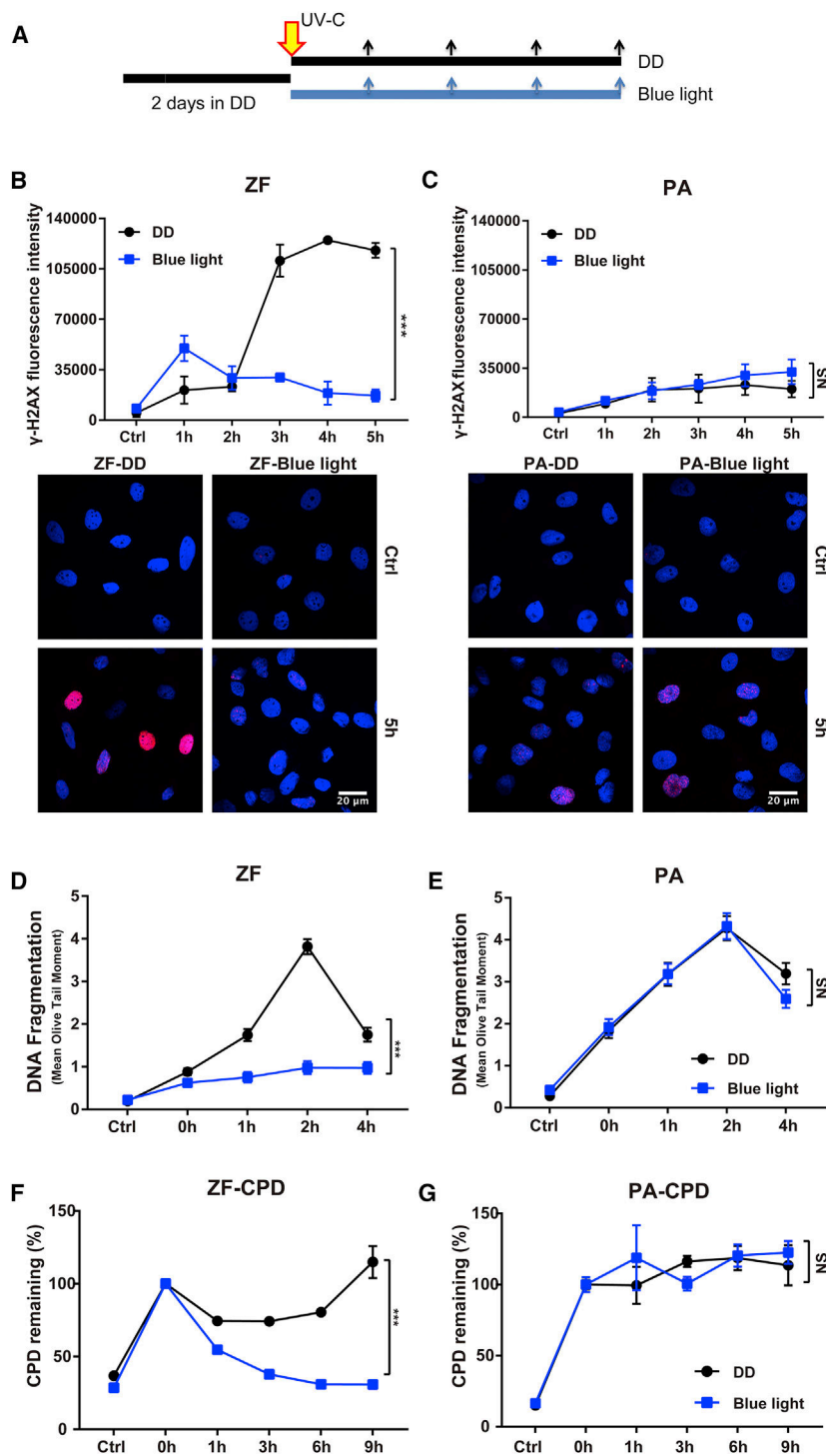


Figure 2. Effect of Blue Light on DNA Repair

(A) Experimental design: cells were maintained in darkness for 48 hr and then exposed to a 40 J/m^2 UV-C pulse followed by DD or blue light prior to harvesting. (B and C) Immunofluorescence analysis of γ -H2AX in (B) ZF and (C) PA. On the y axes is fluorescence intensity ($n = 200$) \pm SEM, while times after irradiation are indicated on the x axes. Representative images of stained cells are presented below, where nuclei are blue (DAPI) and γ -H2AX is red.

(D and E) Comet assay results from (D) ZF and (E) PA cells. Times after UV treatment are plotted on the x axes. On the y axes are indicated the levels of DNA strand breaks ($n = 300$) \pm SEM expressed as mean Olive tail moment.

(F and G) Representative ELISA assay results of UV-induced CPD levels in (F) ZF and (G) PA cell lines exposed to a 20 J/m^2 UV-C pulse and then maintained in DD or blue light. CPD abundance (%) \pm SEM ($n = 3$) is indicated on the y axes, while times after treatment are plotted on the x axes.

Each experiment was repeated independently three times. For each panel, two-way ANOVA followed by Sidak's multiple comparisons test results are reported in Table S1. Significant differences are indicated by asterisks (***) $p < 0.001$, ** $p < 0.01$, * $p < 0.05$; NS, no significance). See also Figure S2.

Since the integrity of the C terminus in the closely related cryptochrome proteins is critical for nuclear localization [45, 46], we tested the subcellular localization of our C-terminally truncated *P. andruzzii* photolyase proteins. N-terminally Myc-tagged versions of all the photolyase proteins were ectopically expressed in zebrafish or *P. andruzzii* cells. Immunofluorescence staining revealed that full-length pa 6-4pnr, as well as the zebrafish zf 6-4pnr and zf DASHpnr proteins, exhibited nuclear localization. In contrast, all the truncated cavefish photolyases were predominantly cytoplasmic (Figures 3B and 3C). A bioinformatics search for candidate nuclear localization signal (NLS) sequences [47] revealed that two putative NLS sequences (KKNILRMKAAYAKRSPEDKTINK GEKRKASPSIKEMFQKKAKR) and GPSSSK GRKGSSYTARQHKDR) present in the C-terminal portion of the zf 6-4pnr and zf DASHpnr proteins, respectively, were deleted in the truncated cavefish pa 6-4pnr and pa DASHpnr orthologs. Thus, the mutant cavefish photolyases, which lack a significant portion of their light-harvesting FAD binding domains, are restricted to the cytoplasmic compartment and so are unlikely to contribute directly to nuclear photoreactivation function.

truncated proteins lacking a major portion of the FAD binding domain were identified, both resulting from aberrant mRNA splicing (Figures 3A and S3B). Interestingly, in contrast to the situation observed for these two cavefish photolyase genes, we only encountered cDNAs encoding a single form of *P. andruzzii* CPD photolyase (pa CPDpnr) with all predicted functional domains intact and bearing high homology (84.5%) with the zebrafish ortholog (Figure 3A and Table S2).

Interestingly, pa CPDpnr, like its zebrafish ortholog, contains a predicted NLS sequence (PDSAGGKQPKLTGGKGRESGWLL KEVTKLRKAA) at the N terminus of the protein and is localized predominantly in the nucleus (Figures 3B and 3C). However, to

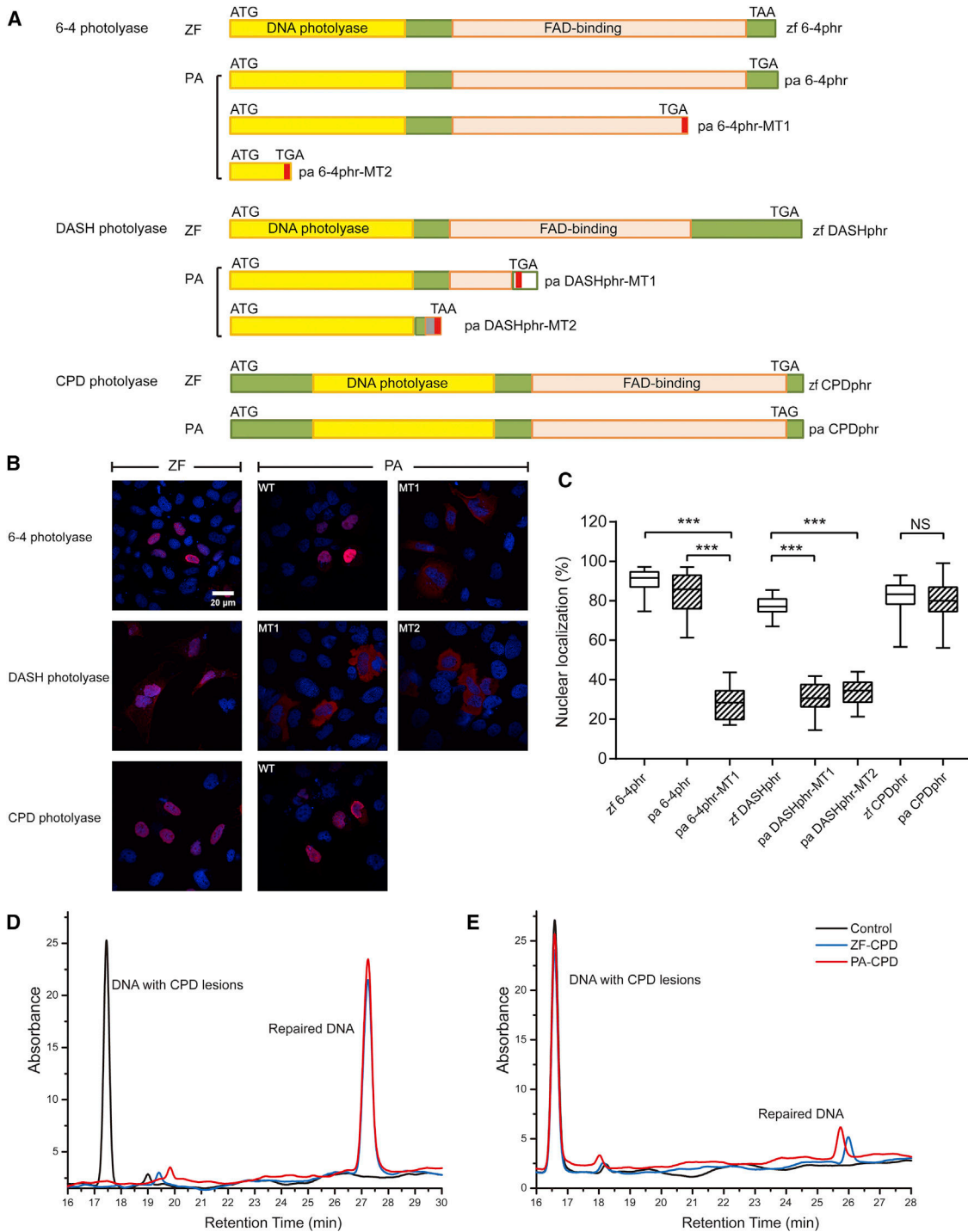


Figure 3. Cavefish Photolyase Characterization

(A) Predicted photolyase proteins from ZF and PA. The conserved N-terminal photolyase domain (yellow) and C-terminal FAD binding domain (pink) are indicated. Premature termination codons are indicated as red boxes (see also Figure S3 and Table S2).

(B) Immunofluorescence images for myc-tagged PA and ZF photolyase proteins (red) expressed in PAC-2 cells, with nuclei stained using DAPI (blue).

(C) Quantitative analysis of the data in (B) presented as box-and-whisker plots. The nuclear localization (%) ($n = 30$) is indicated on the y axis. The boxes indicate the degree of dispersion of the data. The horizontal lines within the boxes indicate the median values, and the whiskers represent the 25th and 75th percentiles. The results of Student's *t* test (unpaired, two tailed) statistical analysis are represented by asterisks (***) ($p < 0.001$) and reported in Table S1. NS, no significance.

(D and E) HPLC detection of DNA repair mediated by (D) 10 μ M or (E) 1 μ M CPD photolyase from ZF-CPD and PA-CPD *in vitro*. A synthetic CPD lesion-containing oligonucleotide (Control) was incubated with the photolyase proteins and irradiated with blue light ($\lambda_{\text{max}} = 400 \text{ nm}$, $250 \mu\text{mol m}^{-2} \text{ s}^{-1}$) for 10 min. HPLC analysis was performed using a detection wavelength of 264 nm. Levels of absorbance are plotted on the y axes and retention time from the HPLC column on the x axes.

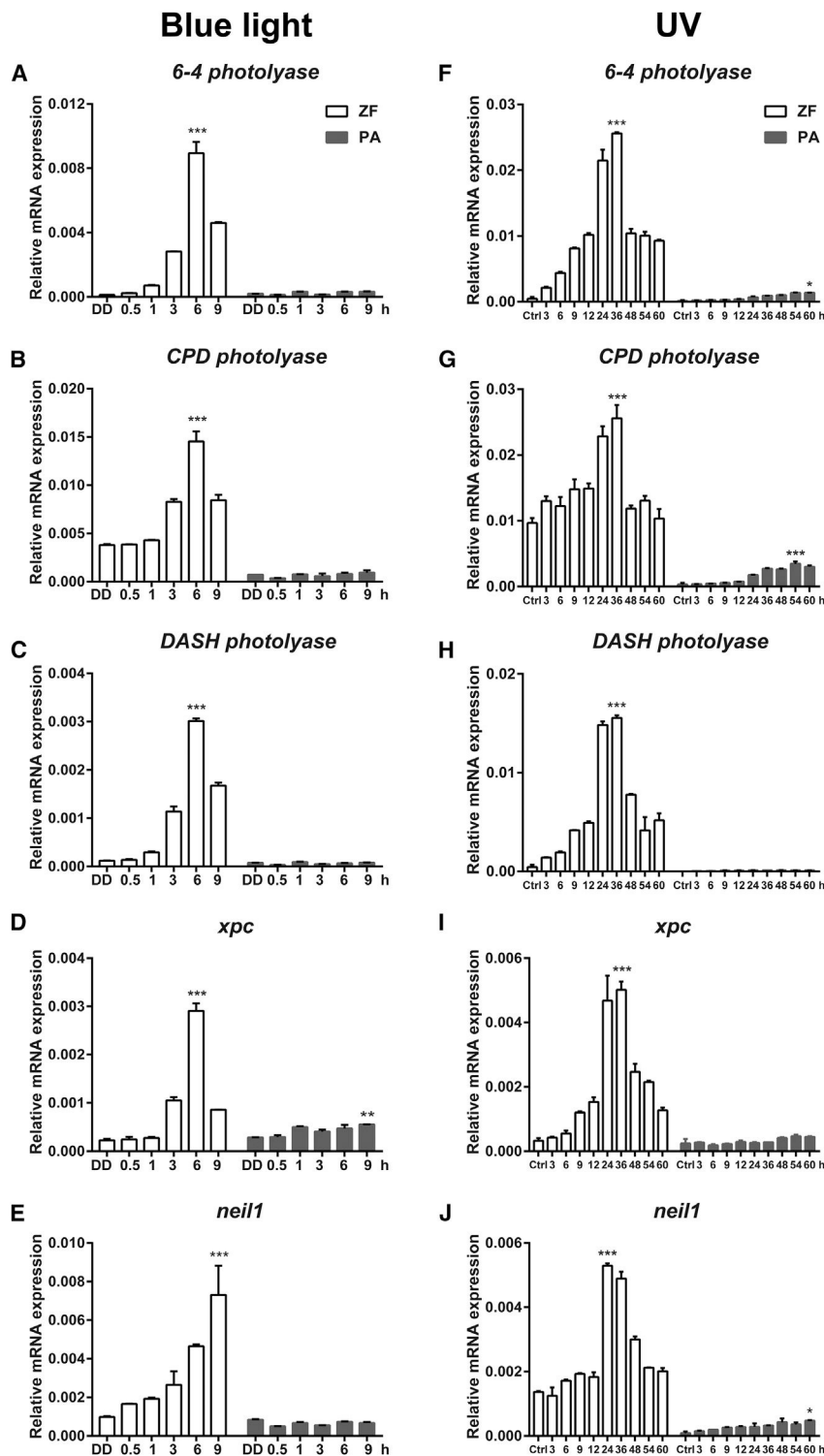


Figure 4. DNA-Repair Gene Expression

(A–E) qRT-PCR analysis of gene expression (A, *6-4 photolyase*; B, *CPD photolyase*; C, *DASH photolyase*; D *xpc*; E, *neil1*) in PAC-2 (ZF, white) and EPA (PA, gray) cells during 9 hr of blue-light exposure.

(F–J) Comparable qRT-PCR analysis of gene expression (F, *6-4 photolyase*; G, *CPD photolyase*; H, *DASH photolyase*; I, *xpc*; J, *neil1*) in cells during a 60 hr period in DD following exposure to a short UV-C pulse (20 J/m²).

In each panel, relative mRNA expression levels are plotted on the y axes as means ± SEM (n = 3) and times (h) are plotted on the x axes. Two-way ANOVA followed by Sidak’s multiple comparisons test results are reported in [Table S1](#). Significant differences between peak points of expression and the control untreated (DD) samples are indicated by asterisks (**p < 0.001, *p < 0.01, *p < 0.05). See also [Figure S4](#) for the light spectrum.

High-performance liquid chromatography (HPLC) analysis showed that 10 μM and 1 μM *P. andruzzii* CPD photolyase repairs CPD photo-lesions efficiently (100% and 12.15%, respectively) in an equivalent manner to the zebrafish protein ([Figures 3D and 3E](#)).

Loss of Light-Inducible DNA-Repair Gene Expression in Cavefish

We have revealed that a subset of cavefish photolyases has lost its nuclear function as a result of coding sequence mutations. However, CPD photolyase, which makes a major contribution to photoreactivation function [1, 43], exhibits normal enzymatic activity and nuclear localization in cavefish. These findings contrast with the observed loss of photoreactivation function in this cavefish species. Many genes implicated in DNA repair, including the photolyase genes, have been shown in zebrafish to be transcriptionally activated by visible light. Without this light-dependent induction, animals appear to have reduced tolerance of environmental stress and increased mortality [31]. We therefore reasoned that the loss of light-enhanced DNA repair in *P. andruzzii* might involve abnormalities in the light-inducible expression of DNA repair genes. qRT-PCR analysis of DNA repair gene expression in PAC-2 and EPA cell

lines upon exposure to blue light reveals a reduction (*xpc*) or complete absence (all photolyase genes and *neil1*) of light-inducible gene expression in cavefish cells compared to the robust induction of all genes observed in zebrafish cells ([Figures 4A–4E and Table S1](#); see also [Figure S4](#) for the blue light spectrum).

test whether the cavefish CPD photolyase is able to catalyze the photoreactivation of CPD photoproducts, we performed an *in vitro* DNA repair assay. The cavefish and zebrafish CPD photolyase proteins were expressed in bacteria, purified by Ni affinity chromatography, and then incubated with synthetic DNA incorporating CPD photoproducts during 10 min of blue-light illumina-

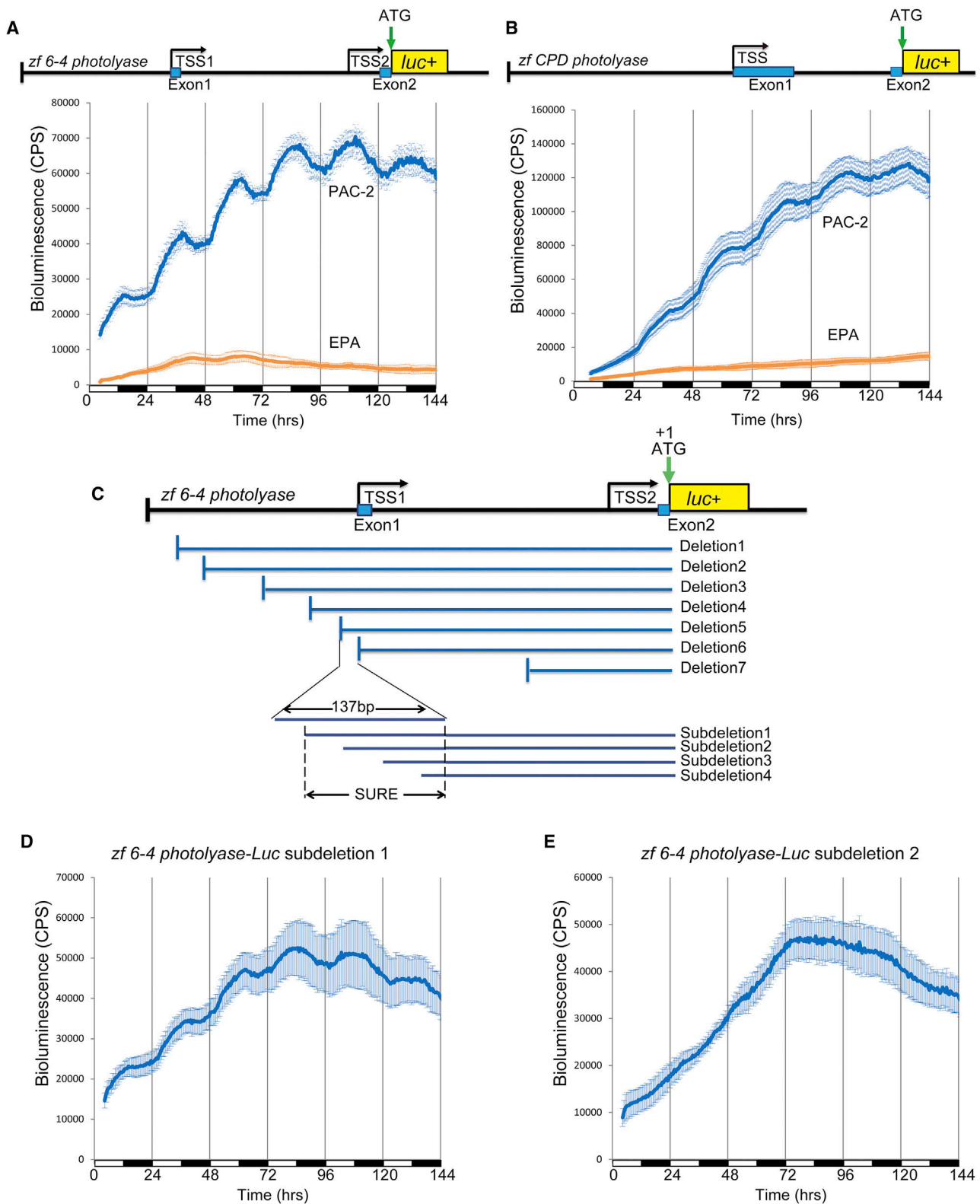


Figure 5. Light-Responsive Region of the *zf 6-4phr* Promoter

(A and B) Upper sections: schematic representation of the (A) *zf 6-4 photolyase-Luc* and (B) *zf CPD photolyase-Luc* promoter reporter constructs. Transcription start sites (TSSs) and the luciferase reporter gene (*luc+*) are indicated. Lower sections: representative real-time bioluminescence assays in PAC-2 or EPA cells

(legend continued on next page)

It has previously been reported that pre-exposure to UV light enhances resistance to subsequent UV-induced DNA damage [48, 49]. We therefore wondered whether the exposure to UV radiation, as well as generating DNA damage, might also influence the expression of DNA repair-associated genes. qRT-PCR analysis of DNA-repair gene expression in zebrafish and *P. andruzzii* cell lines following acute exposure to a UV pulse revealed that all zebrafish genes were strongly induced (Figures 4F–4J and Table S1; see also Figure S4 for the UV spectrum). Interestingly, UV-induced gene expression in zebrafish showed a significantly prolonged induction compared to the response triggered by blue light (peaks at circa 36 hr and 6 hr, respectively). In contrast, in the case of cavefish DNA-repair genes, we observed an absence (*DASHphr* and *xpc*) or a significant reduction (*6-4phr* and *neil1*) in the amplitude of UV-induced expression (Figures 4F–4J and Table S1). For *CPDphr*, although the amplitude of UV-induced expression was comparable to that in zebrafish, the basal levels of expression were considerably reduced. Thus, our results point to a general impairment of the DNA-repair gene expression response to both visible light and UV in *P. andruzzii*.

Loss of D-Box-Regulated Transcription in *P. andruzzii*

To explore the origin of the loss of visible and UV light-induced expression of cavefish DNA-repair genes, we cloned 4029 bp and 894 bp promoter regions for the zebrafish *6-4* and *CPD photolyase* genes, respectively, into a luciferase reporter vector. Transient transfection of both reporter constructs into zebrafish PAC-2 cells followed by exposure to alternating periods of light and darkness revealed a light-driven induction of bioluminescence in zebrafish cells, but not in *P. andruzzii* cells (Figures 5A and 5B). To pinpoint precisely the light-responsive region of the *zf 6-4phr* promoter, we prepared a series of overlapping promoter deletion and subdeletion constructs (Figure 5C), which were tested for light-induced expression in PAC-2 cells. We identified a promoter region (termed SURE for “sunlight responsive” region) that is sufficient to confer light-inducible reporter gene expression. This region contains two palindromic D-boxes, two E-boxes and one AP1/CREB binding site (Figures 5C–5E, 6A, and S5).

Systematic deletion of each individual element in the SURE region within the context of *zf 6-4 photolyase SURE-Luc* (Figure 6A) revealed that the presence of the two palindromic D-box elements is crucial for the photic regulation of the zebrafish *6-4phr* gene (Figures 6A–6C and S5M–S5U). Specifically, deletion of the two E-boxes together with the AP1/CREB binding site did not significantly affect the kinetics of light-driven, SURE-regulated expression. On the contrary, deletion of both D-boxes resulted in a classical circadian clock-regulated pattern of expression, with an induction in bioluminescence occurring prior to the light onset. This clock-regulated behavior correlates with the presence of the E-box elements in the D-box-mutated SURE constructs (see also Figures S5M–S5U). The importance

of the D-box enhancer element in shaping *zf 6-4phr* expression was confirmed by the lack of light inducibility and reduced basal levels of expression from the full-length promoter containing mutations in both D-box elements (*zf 6-4 photolyase (D-box mut)-Luc*) (Figure S5V, orange trace).

Transfection of the *SURE* mutant 8 reporter construct, retaining only the D-box enhancers (renamed as *D-box_{6-4phr}-Luc*), into cavefish EPA cells showed no light responsiveness compared with the robust light-driven pattern observed in zebrafish cells (Figure 6D). Considering the complete conservation of D-box enhancer sequences between the zebrafish and *P. andruzzii 6-4phr* promoters (Figure 6F), these results indicate that the absence of light-induced photolyase gene expression in cavefish is due to a loss of function of the light-regulated mechanisms that control transcription via D-box enhancers.

Expression of the *6-4phr* gene is induced in zebrafish by UV light, and this response is impaired in *P. andruzzii* (Figure 4). Therefore, to address whether the D-box enhancer may also represent a nuclear target for UV, we studied the expression of the *D-box_{6-4phr}-Luc* reporter in zebrafish PAC-2 and cavefish EPA cells following UV exposure. In zebrafish cells, UV treatment induced bioluminescence with similar kinetics to those of the endogenous gene, revealing that the palindromic D-box elements in the *SURE* region are also sufficient for directing UV-induced expression (Figure 6E). Furthermore, similar to the pattern observed for endogenous gene expression (Figure 4F) in transfected EPA cells, UV-C treatment failed to activate expression of the *D-box_{6-4phr}-Luc* reporter (Figure 6E). These results reveal that the D-box serves as the convergence point for the mechanisms mediating visible and UV light-induced gene expression and that this integrating function is absent in *P. andruzzii*.

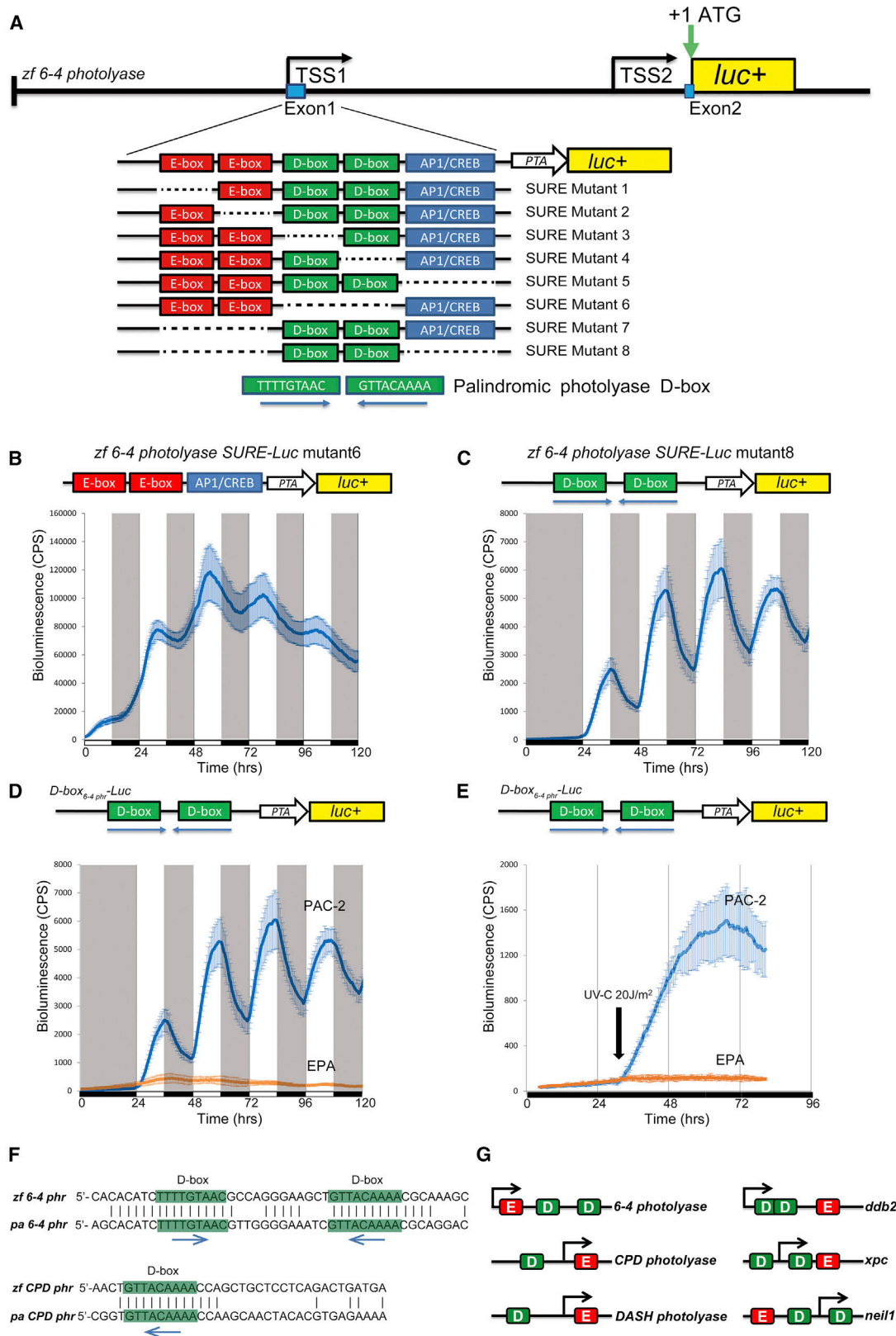
Given the central role played by the D-box in the regulation and evolution of *6-4phr* gene function, we searched the promoter sequences of other light-induced DNA-repair genes for this enhancer element in zebrafish, as well as a broad range of fish genome sequences (*Oryzias latipes*, *Astyanax mexicanus*, *Poecilia Formosa*, etc.; see Table S3). Our analysis revealed that the 5'-TTTTGTAAC-3' D-box enhancer element is present in many other DNA-repair genes (*CPD* and *DASH photolyase*, as well as *ddb2*, *xpc*, and *neil1*), in close proximity to their transcription start sites, and canonical E-box elements (5'-CACGTG-3') (Figure 6G and Table S3). While the E-boxes potentially represent binding sites for the core circadian clock factors CLOCK and BMAL, robust circadian rhythms of photolyase gene expression were not observed following transfer of zebrafish cells from LD to DD conditions (Figures S6A–S6C). Furthermore, cells transfected with the wild-type *6-4phr* gene promoter reporter construct showed an immediate attenuation of rhythmicity following transfer from LD to DD (Figure S6D, blue trace). In addition, cells transfected with the D-box-mutated *6-4phr* reporter construct, where the E-boxes are still intact, failed to show

transfected with each luciferase reporter. Bioluminescence, counts per second (cps), is plotted against time (hr). Black and white bars along the x axes show dark and light periods. Each time point represents the mean of $n = 8 \pm$ SEM.

(C) Schematic representation of *zf 6-4 photolyase-Luc* and its deletion and subdeletion constructs. The position of the 120 bp *zf 6-4phr* sunlight responsive region (SURE) is indicated by horizontal arrowheads.

(D and E) Bioluminescence analysis of cells transfected with (D) *zf 6-4 photolyase-Luc* subdeletion 1 and (E) subdeletion 2.

See also Figure S5 for the complete promoter analysis.



(legend on next page)

rhythmicity either in LD or DD (Figure S6D, orange trace). Together, these results point to the D-box, rather than the E-box, playing a highly conserved, coordinating role in the DNA repair response.

What is the origin of this loss of light- and UV-regulated D-box enhancer function in *P. andruzzii*? UV and light exposure both increase intracellular ROS [32, 50–52]. We have recently reported that elevated levels of ROS are crucial for light-induced clock gene expression via the D-box [32]. Consistent with ROS also serving as a key coordinating signal for photolyase genes, pretreatment of zebrafish cells with N-acetylcysteine (NAC), a general ROS scavenger, efficiently blocked UV-induced, as well as blue-light-induced, photolyase gene expression (Figures 7A–7C). Furthermore, the expression of photolyase genes and the 6-4 photolyase D-box reporter are all induced by ROS (300 μ M H₂O₂) in zebrafish cells (Figures 7D–7G). In contrast, ROS treatment failed to significantly induce photolyase or D-box reporter expression in EPA cells (Figures 7D–7G), pointing to loss of function in ROS-dependent signaling pathways in *P. andruzzii*. The MAP kinase (MAPK) signaling pathway plays a key role in bridging oxidative stress and DNA damage with a range of cellular responses [53, 54]. By western blot analysis using phospho-specific MAPK antibodies, we revealed a significant attenuation of the levels of phosphorylated (activated) forms of ERK, JNK, and p38 in cavefish cells following UV exposure compared with the robust induction observed in zebrafish cells (Figures 7H–7J and S7). Thus, our data reveal fundamental differences in the signaling pathways triggered by UV exposure between cavefish and zebrafish.

DISCUSSION

Here, by comparing the blind cavefish, *P. andruzzii*, with the zebrafish, we have explored how sunlight shapes the evolution of DNA repair systems. We have revealed that both the integrity of photolyase genes, as well as transcriptional control mechanisms regulating the expression of DNA-repair genes in response to sunlight, have been targeted by evolutionary mechanisms operating under extreme aphotic conditions.

Loss of Photolyase Function in *P. andruzzii*

We have revealed the presence of mutations in the 6-4 and DASH photolyase gene coding sequences, which result in C-terminally truncated, cytoplasmic proteins unable to perform DNA repair. However, the contribution of these mutations to the observed lack of photoreactivation is unclear given the gen-

eral loss of sunlight-induced photolyase transcription in cavefish cells.

Curiously, despite the absence of photoreactivation DNA repair, the *pa* CPDp_{hr} coding sequence carries no apparent loss-of-function mutations. This may reflect the persistence of an additional, photoreactivation-independent function for this photolyase gene in *P. andruzzii* that continues to confer a selective advantage during evolution in DD. Indeed, CPD photolyase has been reported to bind to sites of DNA damage in the absence of light and subsequently recruit DNA repair proteins [8, 55]. Another possible function of CPD photolyase relates to its similarity with the cryptochrome proteins [6, 56]. The cryptochrome/photolyase flavoprotein family share a “core” domain that contains the binding sites for FAD and a second antenna chromophore cofactor. This domain has been conserved during evolution from an ancestral CPD photolyase gene but with diversification of the N-terminal and C-terminal portions of the protein [57]. In the case of the cryptochrome proteins, an extended C-terminal portion confers additional functional diversity and is associated with loss of photoreactivation function. While cryptochromes serve as blue-light photoreceptors in plants and *Drosophila*, in vertebrates, they act as negative elements within the core circadian clock mechanism [58, 59]. Recent studies have shown that CPD photolyase, when ectopically expressed in mammalian cells, can interact directly with the CLOCK protein to reduce CLOCK/BMAL-dependent transactivation and thereby, like the cryptochromes, serve as a clock component [60]. This indicates that the highly conserved cryptochrome/photolyase core domain also directly contributes to circadian clock function. Interestingly, changes in CPD photolyase expression in cavefish are encountered together with abnormalities in the circadian clock. Thus, in cave forms of *A. mexicanus* where CPD photolyase expression is upregulated, many light-regulated clock genes show constitutively elevated expression, reminiscent of the clock’s response to constant light exposure [25]. In contrast, in *P. andruzzii*, which exhibits a loss of the sunlight-dependent transcriptional control mechanisms for CPD photolyase, the circadian clock lacks photic entrainment [28].

An alternative explanation for the retention of CPD photolyase function in cavefish may relate to the length of time that evolution has occurred in the dark cave environment. In support of this interpretation, recent microsatellite polymorphism analysis has suggested that surface and cave populations of *Astyanax* that may have diverged less than 20,000 years ago [61] carry no mutations in the photolyase coding sequences ([25] and AstMex102 database in ENSEMBL vs92). In contrast, geological evidence

Figure 6. Transcriptional Control of the *zf* 6-4p_{hr} Gene via D-Box Enhancers

(A) Schematic representation of SURE and the *zf* 6-4 photolyase SURE-Luc mutation constructs 1–8. The two E-boxes, the palindromic D-boxes, and the AP1/CREB binding sites are indicated.

(B and C) Representative real-time bioluminescence assays from PAC-2 cells transfected with (B) *zf* 6-4 photolyase SURE-Luc mutant 6 and (C) *zf* 6-4 photolyase SURE-Luc mutant 8 (also see Figure S5).

(D and E) Bioluminescence results from PAC-2 (blue) and EPA (orange) cells transfected with the *zf* 6-4 photolyase SURE-Luc mutant 8 (renamed D-box_{6-4p_{hr}}-Luc) reporter construct. This construct is represented graphically above the panels. After transfection, cells were exposed either (D) to alternating periods of light and dark or (E) to DD following a short pulse of UV-C (black arrow, 20 J/m²).

(B–E) Mean bioluminescence ($n = 8$) \pm SEM is expressed as counts per second (cps) and is plotted against time (hr).

(F) Sequence alignment of the ZF and PA D-box enhancer element sequences within the 6-4p_{hr} SURE and CPDp_{hr} promoter region.

(G) Schematic representation of the D-box and E-box elements present in the promoters of DNA-repair genes in the ZF (*Danio rerio*). These elements are conserved in a broad range of fish species (see Table S3 for accession numbers).

See also Figure S6.

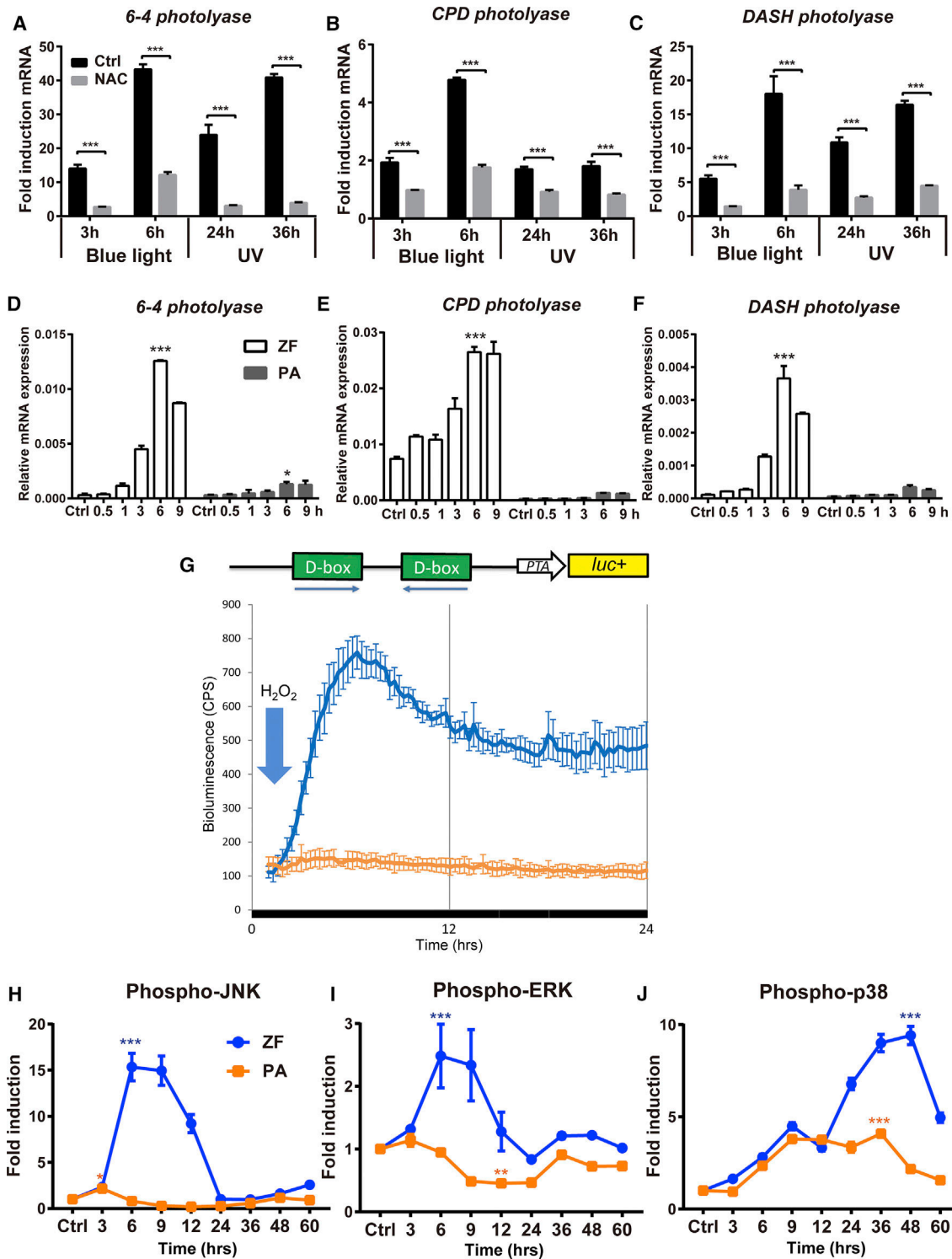


Figure 7. D-Box Regulation via ROS Signaling

(A–C) qRT-PCR analysis of gene expression (A, *6-4 photolyase*; B, *CPD photolyase*; C, *DASH photolyase*) in ZF cells treated with 6 mM NAC (gray) or vehicle (Ctrl, black), following 3 or 6 hr exposure to blue light or 24 hr and 36 hr following a short UV-C pulse (20 J/m^2). On the y axes are plotted the fold induction (\pm SEM) of expression with respect to samples subjected to identical treatment but maintained under DD. Times and treatments are indicated on the x axes. Statistical analysis results (Student's t test [unpaired, two tailed]) are represented by asterisks (***) $p < 0.001$ and reported in Table S1.

(D–F) qRT-PCR analysis of gene expression (D, *6-4 photolyase*; E, *CPD photolyase*; F, *DASH photolyase*) in ZF PAC-2 (white) and cavefish EPA (gray) cells after $300 \mu\text{M H}_2\text{O}_2$ treatment. Relative mRNA expression are plotted on the y axes as mean ($n = 3$) \pm SEM. Times (hr) are plotted on the x axes. Two-way ANOVA

(legend continued on next page)

suggests that *P. andruzzii* has been completely isolated from sunlit surface water for at least 3 million years [24, 29], with the elimination of any remaining surface populations by desertification [62, 63]. In this hypogean species, mutations have already affected the 6-4 and DASH photolyases, and over a sufficient evolutionary timescale, all the photolyase genes might eventually suffer loss of function or even be lost as in the case of placental mammals.

Flexibility in D-Box Enhancer Function during Vertebrate Evolution

In *P. andruzzii*, we show that the lack of photoreactivation originates primarily from a loss of D-box enhancer function. We have identified the D-box in zebrafish as being a central player in coordinating the transcriptional response to visible light, UV, and ROS [32, 64, 65]. By upregulating the expression of key elements involved in photoreactivation and NER and BER DNA repair, this promoter element specifically enhances the capacity of cells to resolve DNA damage generated by exposure to these cellular stressors. The D-box elements identified in the light responsive DNA repair genes reported here are highly conserved in nearly all published fish genome sequences. Interestingly, circadian E-box enhancer elements are frequently encountered in close proximity to the D-boxes, although our data do not support a strong functional link between the circadian clock and DNA-repair gene transcriptional regulation. Interaction between a D-box and E-box enhancer is crucial for light-induced expression of the *period 2* clock gene [64], but the D-box sequence in the *period 2* promoter differs slightly from those identified here in the DNA-repair gene promoters. Together, our results point to specific regulatory properties of these 5'- TTTTGTAAAC -3' D-box elements being linked with DNA repair function. A family of six bZip/PAR factors, as well as six E4BP4-related transcription factors, can bind to D-box enhancer elements in homo- and heterodimeric combinations [66]. Differences in the consensus D-box sequence may therefore lead to differential binding of factors eliciting different transcriptional responses. Interestingly, previous evidence points to considerable plasticity in D-box function over the course of vertebrate evolution. While in fish, the D-box serves as a light input pathway component for the entrainment of the circadian clock, in mammals, the D-box is strictly clock regulated and acts within clock output pathways [67]. Furthermore, in mammals, the D-box is neither light nor ROS inducible and is targeted by a smaller family of three bZip/PAR and one E4BP4 factors [32, 68, 69]. Finally, D-box enhancer sequences are not encountered in the promoters of the mammalian DNA-repair gene orthologs such as *neil1*, *xpc*, and *ddb2*. Taken together, our results point to the occurrence of major changes in D-box enhancer function during vertebrate evolution.

Evolution of DNA Repair Systems in Extreme Aphotic Environments

Does the absence of UV damage and visible light represent the only feature in the cave environment influencing the evolution of DNA repair systems? Alternatively, do additional genotoxic stressors exist, specific to these subterranean aquatic environments? Elevated levels of *CPD photolyase* and *ddb2* expression in blind cave forms of *A. mexicanus* have been speculated to provide a selective advantage in repairing different types of DNA damage experienced in the cave environment [25]. For example, life in the hypoxic and slightly acidic water locked inside these cave systems may lead to an increase of intracellular oxidative stress [70]. This may be exacerbated in certain caves (e.g., Cueva Chica and El Pachón) that serve as roosting sites for large numbers of bats that bring organic materials (guano and dead bodies) into the water on a daily basis [25, 70]. Interestingly, an enhancement of DNA repair capacity has also been identified in the blind mole rat, *Spalax carmeli*, linked with its hypoxia tolerance [26]. An additional feature of certain cave systems that might cause elevated DNA damage is the natural radioactive gas, radon ^{222}Rn , which is released from certain rocks and concentrated in caves [71]. This source of radioactivity has been linked with an increase in the rate of deletion of satellite DNA sequences at the whole-genome level in *Dolichopoda* cave crickets [72].

Photoreactivation is a highly conserved DNA repair mechanism encountered in most animal, plant, and unicellular species, with the curious and unique exception of placental mammals [73]. Based on the results of this study, we can now add the blind cavefish *P. andruzzii* to this small group of exceptions. Why placental mammals lost this DNA repair function remains a mystery. Taking into account palaeontological data, one theory that has been proposed is termed the “nocturnal bottleneck” [74, 75]. This predicts that the ancestors of modern mammals that lived during the dinosaurs’ domination of the Earth avoided predation by becoming exclusively nocturnal [74, 76]. It is predicted that adaptation to this ecological niche may explain many features of present-day mammals. These include a general loss of extraretinal photoreception, as well as adaptations in the eye and retina to facilitate vision under low-lighting conditions [74, 76]. Interestingly, adaptation to a nocturnal life style is also predicted to have entailed a general loss of UV protection mechanisms. These include changes in lens composition, resulting in a more efficient penetration of UV light to the retina, as well as the loss of photolyase genes and photoreactivation function [74, 77]. However, the mammalian ancestors retained NER systems in order to repair the limited UV-induced DNA damage they experienced in their nocturnal environment. Following the extinction of dinosaurs, mammals subsequently diversified and occupied new surface habitats but still carried relics of their

followed by Sidak’s multiple comparisons test results are reported in Table S1. Significant differences between peak points of expression and the control untreated samples are indicated by asterisks (** $p < 0.001$, * $p < 0.01$, $p < 0.05$).

(G) Real-time bioluminescence assays from ZF PAC-2 (blue) and cavefish EPA (orange) cells transfected with the 6-4 photolyase D-box reporter represented above the panel and treated in DD with 300 μM H_2O_2 at the time point indicated by the blue arrow.

(H–J) Western blot quantification of (H) P-JNK, (I) P-ERK, and (J) P-p38 levels in zebrafish PAC-2 and cavefish EPA cells during a 60 hr period in DD following exposure to a short UV-C pulse (20 J/m^2). Fold induction \pm SEM ($n = 3$) is plotted on the y axis and time (hr) on the x axis. Two-way ANOVA followed by Sidak’s multiple comparisons test results are reported in Table S1. Significant differences between peak points of expression and the control samples are indicated by asterisks (** $p < 0.001$, * $p < 0.01$, $p < 0.05$). Original western blots are presented in Figure S7.

dark-adapted past existence. It is tempting to speculate that in the DNA repair systems of the blind cavefish, *P. andruzzii*, we may be witnessing the first stages in a process that previously occurred in the ancestors of placental mammals during the Mesozoic era.

STAR★METHODS

Detailed methods are provided in the online version of this paper and include the following:

- **KEY RESOURCES TABLE**
- **CONTACT FOR REAGENT AND RESOURCE SHARING**
- **EXPERIMENTAL MODEL AND SUBJECT DETAILS**
 - in vivo animal studies
 - Cell lines
- **METHOD DETAILS**
 - Cell Viability Assay
 - “Comet Assay”: the single cell gel electrophoresis assay
 - CPD quantitation ELISA assay
 - Cloning and gene expression analysis
 - Protein expression analysis
 - in vitro DNA repair assay
 - Real-time bioluminescence assay
 - Light sources
- **QUANTIFICATION AND STATISTICAL ANALYSIS**
- **DATA AND SOFTWARE AVAILABILITY**

SUPPLEMENTAL INFORMATION

Supplemental Information includes seven figures and six tables and can be found with this article online at <https://doi.org/10.1016/j.cub.2018.08.039>.

ACKNOWLEDGMENTS

We thank J. Wittbrodt, F. Loosli, M. Reischl, S. Fuselli, O. Armant, and O. Kasel for support and discussion and N. Geyer and M. Rastetter for excellent technical assistance. We are also grateful to Donato Vincenzi and Micol Boschetti (Dipartimento di Fisica e Scienze della Terra, Università di Ferrara) for light spectrum measurements. This research was funded through the Helmholtz Association funding programme BIFTM for N.S.F. and D.V. and the CSC (China Scholarship Council) scholarship (2014–2018) for H.Z. We acknowledge support by the Deutsche Forschungsgemeinschaft and the open-access publishing fund of Karlsruhe Institute of Technology. C.B., G.D.M., and E.F. are supported by research grants from the University of Ferrara (FAR 2015–2017); G.D.M. is supported by the Istituto Studi Superiori (IUSS) of the University of Ferrara (PhD mobility grant, 2017). A.M.G. is supported by 31st PhD program in biotechnology at the University of Naples, Federico II (2016–2019–MIUR). N.S.F. and C.B. are also supported by the MIUR-DAAD Joint Mobility Program 2018.

AUTHOR CONTRIBUTIONS

N.S.F., H.Z., C.B., and D.V. conceived and designed the experiments. H.Z., S.L.-M., G.D.M., E.F., P.N., A.M.G., and H.M. performed the experiments. N.S.F., H.Z., T.L., D.V., T.B., and C.B. analyzed the data. T.B., T.L., C.B., and N.S.F. contributed reagents, materials, and analysis tools. N.S.F., H.Z., C.B., and D.V. wrote the manuscript.

DECLARATION OF INTERESTS

The authors declare no competing interests.

Received: April 8, 2018

Revised: July 19, 2018

Accepted: August 16, 2018

Published: October 11, 2018

REFERENCES

1. Sinha, R.P., and Häder, D.-P. (2002). UV-induced DNA damage and repair: a review. *Photochem. Photobiol. Sci.* **1**, 225–236.
2. Sancar, A. (2016). Mechanisms of DNA Repair by Photolyase and Excision Nuclease (Nobel Lecture). *Angew. Chem. Int. Ed. Engl.* **55**, 8502–8527.
3. Essen, L.O., and Klar, T. (2006). Light-driven DNA repair by photolyases. *Cell. Mol. Life Sci.* **63**, 1266–1277.
4. Cline, S.D., and Hanawalt, P.C. (2003). Who’s on first in the cellular response to DNA damage? *Nat. Rev. Mol. Cell Biol.* **4**, 361–372.
5. Kim, S.T., Malhotra, K., Smith, C.A., Taylor, J.S., and Sancar, A. (1994). Characterization of (6-4) photoproduct DNA photolyase. *J. Biol. Chem.* **269**, 8535–8540.
6. Sancar, A. (2004). Photolyase and cryptochrome blue-light photoreceptors. *Adv. Protein Chem.* **69**, 73–100.
7. Sancar, A. (1996). No “End of History” for photolyases. *Science* **272**, 48–49.
8. Thoma, F. (1999). Light and dark in chromatin repair: repair of UV-induced DNA lesions by photolyase and nucleotide excision repair. *EMBO J.* **18**, 6585–6598.
9. Selby, C.P., and Sancar, A. (2006). A cryptochrome/photolyase class of enzymes with single-stranded DNA-specific photolyase activity. *Proc. Natl. Acad. Sci. USA* **103**, 17696–17700.
10. Chaves, I., Pokorny, R., Byrdin, M., Hoang, N., Ritz, T., Brettel, K., Essen, L.-O., van der Horst, G.T.J., Batschauer, A., and Ahmad, M. (2011). The cryptochromes: blue light photoreceptors in plants and animals. *Annu. Rev. Plant Biol.* **62**, 335–364.
11. Daiyasu, H., Ishikawa, T., Kuma, K., Iwai, S., Todo, T., and Toh, H. (2004). Identification of cryptochrome DASH from vertebrates. *Genes Cells* **9**, 479–495.
12. de Laat, W.L., Jaspers, N.G.J., and Hoeijmakers, J.H.J. (1999). Molecular mechanism of nucleotide excision repair. *Genes Dev.* **13**, 768–785.
13. Costa, R.M.A., Chiganças, V., Galhardo, Rda.S., Carvalho, H., and Menck, C.F.M. (2003). The eukaryotic nucleotide excision repair pathway. *Biochimie* **85**, 1083–1099.
14. Seeberg, E., Eide, L., and Bjørås, M. (1995). The base excision repair pathway. *Trends Biochem. Sci.* **20**, 391–397.
15. Hitomi, K., Iwai, S., and Tainer, J.A. (2007). The intricate structural chemistry of base excision repair machinery: implications for DNA damage recognition, removal, and repair. *DNA Repair (Amst.)* **6**, 410–428.
16. Houtgraaf, J.H., Versmissen, J., and van der Giessen, W.J. (2006). A concise review of DNA damage checkpoints and repair in mammalian cells. *Cardiovasc. Revasc. Med.* **7**, 165–172.
17. Almeida, K.H., and Sobol, R.W. (2007). A unified view of base excision repair: lesion-dependent protein complexes regulated by post-translational modification. *DNA Repair (Amst.)* **6**, 695–711.
18. Robertson, A.B., Klungland, A., Rognes, T., and Leiros, I. (2009). DNA repair in mammalian cells: Base excision repair: the long and short of it. *Cell. Mol. Life Sci.* **66**, 981–993.
19. Nospikel, T. (2009). DNA repair in mammalian cells: Nucleotide excision repair: variations on versatility. *Cell. Mol. Life Sci.* **66**, 994–1009.
20. Christmann, M., and Kaina, B. (2013). Transcriptional regulation of human DNA repair genes following genotoxic stress: trigger mechanisms, inducible responses and genotoxic adaptation. *Nucleic Acids Res.* **41**, 8403–8420.
21. Weger, B.D., Sahinbas, M., Otto, G.W., Mracek, P., Armant, O., Dolle, D., Lahiri, K., Vallone, D., Ettwiller, L., Geisler, R., et al. (2011). The light responsive transcriptome of the zebrafish: function and regulation. *PLoS ONE* **6**, e17080.

22. Gavriouchkina, D., Fischer, S., Ivacevic, T., Stolte, J., Benes, V., and Dekens, M.P.S. (2010). Thyrotroph embryonic factor regulates light-induced transcription of repair genes in zebrafish embryonic cells. *PLoS ONE* 5, e12542.
23. Lucas-Lledó, J.I., and Lynch, M. (2009). Evolution of mutation rates: phylogenomic analysis of the photolyase/cryptochrome family. *Mol. Biol. Evol.* 26, 1143–1153.
24. Colli, L., Paglianti, A., Berti, R., Gandolfi, G., and Tagliavini, J. (2009). Molecular phylogeny of the blind cavefish *Phreatichthys andruzzii* and *Garra barreimiae* within the family Cyprinidae. *Environ. Biol. Fishes* 84, 95–107.
25. Beale, A., Guibal, C., Tamai, T.K., Klotz, L., Cowen, S., Peyric, E., Reynoso, V.H., Yamamoto, Y., and Whitmore, D. (2013). Circadian rhythms in Mexican blind cavefish *Astyanax mexicanus* in the lab and in the field. *Nat. Commun.* 4, 2769.
26. Domankevich, V., Eddini, H., Odeh, A., and Shams, I. (2018). Resistance to DNA damage and enhanced DNA repair capacity in the hypoxia-tolerant blind mole rat *Spalax carmeli*. *J. Exp. Biol.* 221, jeb174540.
27. Carlini, D.B., and Fong, D.W. (2017). The transcriptomes of cave and surface populations of *Gammarus minus* (Crustacea: Amphipoda) provide evidence for positive selection on cave downregulated transcripts. *PLoS ONE* 12, e0186173.
28. Cavallari, N., Frigato, E., Vallone, D., Fröhlich, N., Lopez-Olmeda, J.F., Foà, A., Berti, R., Sánchez-Vázquez, F.J., Bertolucci, C., and Foulkes, N.S. (2011). A blind circadian clock in cavefish reveals that opsins mediate peripheral clock photoreception. *PLoS Biol.* 9, e1001142.
29. Calderoni, L., Rota-Stabelli, O., Frigato, E., Panziera, A., Kirchner, S., Foulkes, N.S., Kruckenhauser, L., Bertolucci, C., and Fuselli, S. (2016). Relaxed selective constraints drove functional modifications in peripheral photoreception of the cavefish *P. andruzzii* and provide insight into the time of cave colonization. *Heredity (Edinb.)* 117, 383–392.
30. Pei, D.-S., and Strauss, P.R. (2013). Zebrafish as a model system to study DNA damage and repair. *Mutat. Res.* 743–744, 151–159.
31. Tamai, T.K., Vardhanabhuti, V., Foulkes, N.S., and Whitmore, D. (2004). Early embryonic light detection improves survival. *Curr. Biol.* 14, R104–R105.
32. Pagano, C., Siauicunaita, R., Idda, M.L., Ruggiero, G., Ceinos, R.M., Pagano, M., Frigato, E., Bertolucci, C., Foulkes, N.S., and Vallone, D. (2018). Evolution shapes the responsiveness of the D-box enhancer element to light and reactive oxygen species in vertebrates. *Sci. Rep.* 8, 13180.
33. Lin, S., Gaiano, N., Culp, P., Burns, J.C., Friedmann, T., Yee, J.K., and Hopkins, N. (1994). Integration and germ-line transmission of a pseudotyped retroviral vector in zebrafish. *Science* 265, 666–669.
34. Hukriede, N.A., Joly, L., Tsang, M., Miles, J., Tellis, P., Epstein, J.A., Barbazuk, W.B., Li, F.N., Paw, B., Postlethwait, J.H., et al. (1999). Radiation hybrid mapping of the zebrafish genome. *Proc. Natl. Acad. Sci. USA* 96, 9745–9750.
35. Vallone, D., Gondi, S.B., Whitmore, D., and Foulkes, N.S. (2004). E-box function in a period gene repressed by light. *Proc. Natl. Acad. Sci. USA* 101, 4106–4111.
36. Weber, S. (2005). Light-driven enzymatic catalysis of DNA repair: a review of recent biophysical studies on photolyase. *Biochim. Biophys. Acta.* 1707, 1–23.
37. Rogakou, E.P., Pilch, D.R., Orr, A.H., Ivanova, V.S., and Bonner, W.M. (1998). DNA double-stranded breaks induce histone H2AX phosphorylation on serine 139. *J. Biol. Chem.* 273, 5858–5868.
38. Banáth, J.P., and Olive, P.L. (2003). Expression of phosphorylated histone H2AX as a surrogate of cell killing by drugs that create DNA double-strand breaks. *Cancer Res.* 63, 4347–4350.
39. Nakamura, A.J., Rao, V.A., Pommier, Y., and Bonner, W.M. (2010). The complexity of phosphorylated H2AX foci formation and DNA repair assembly at DNA double-strand breaks. *Cell Cycle* 9, 389–397.
40. Sharma, A., Singh, K., and Almasan, A. (2012). Histone H2AX phosphorylation: a marker for DNA damage. *Methods Mol. Biol.* 920, 613–626.
41. Singh, N.P., McCoy, M.T., Tice, R.R., and Schneider, E.L. (1988). A simple technique for quantitation of low levels of DNA damage in individual cells. *Exp. Cell Res.* 175, 184–191.
42. Schnurstein, A., and Braunbeck, T. (2001). Tail moment versus tail length—application of an in vitro version of the comet assay in biomonitoring for genotoxicity in native surface waters using primary hepatocytes and gill cells from zebrafish (*Danio rerio*). *Ecotoxicol. Environ. Saf.* 49, 187–196.
43. Mitchell, D.L. (1988). The relative cytotoxicity of (6-4) photoproducts and cyclobutane dimers in mammalian cells. *Photochem. Photobiol.* 48, 51–57.
44. Oliveri, P., Fortunato, A.E., Petrone, L., Ishikawa-Fujiwara, T., Kobayashi, Y., Todo, T., Antonova, O., Arboleda, E., Zantke, J., Tessmar-Raible, K., and Falciatore, A. (2014). The Cryptochrome/Photolyase Family in aquatic organisms. *Mar. Genomics* 14, 23–37.
45. Liu, C., Hu, J., Qu, C., Wang, L., Huang, G., Niu, P., Zhong, Z., Hong, F., Wang, G., Postlethwait, J.H., and Wang, H. (2015). Molecular evolution and functional divergence of zebrafish (*Danio rerio*) cryptochrome genes. *Sci. Rep.* 5, 8113.
46. Hirayama, J., Nakamura, H., Ishikawa, T., Kobayashi, Y., and Todo, T. (2003). Functional and structural analyses of cryptochrome. Vertebrate CRY regions responsible for interaction with the CLOCK:BMAL1 heterodimer and its nuclear localization. *J. Biol. Chem.* 278, 35620–35628.
47. Nguyen Ba, A.N., Pogoutse, A., Provart, N., and Moses, A.M. (2009). NLStradamus: a simple Hidden Markov Model for nuclear localization signal prediction. *BMC Bioinformatics* 10, 202.
48. Dimova, E.G., Bryant, P.E., and Chankova, S.G. (2008). “Adaptive response” - some underlying mechanisms and open questions. *Genet. Mol. Biol.* 31, 396–408.
49. Tomcic, M.T., Reischmann, P., Rasenberger, B., Meise, R., Kaina, B., and Christmann, M. (2011). Delayed c-Fos activation in human cells triggers XPF induction and an adaptive response to UVC-induced DNA damage and cytotoxicity. *Cell. Mol. Life Sci.* 68, 1785–1798.
50. Widel, M., Krzywon, A., Gajda, K., Skonieczna, M., and Rzeszowska-Wolny, J. (2014). Induction of bystander effects by UVA, UVB, and UVC radiation in human fibroblasts and the implication of reactive oxygen species. *Free Radic. Biol. Med.* 68, 278–287.
51. Allen, R.G., and Tresini, M. (2000). Oxidative stress and gene regulation. *Free Radic. Biol. Med.* 28, 463–499.
52. Valacchi, G., Sticozzi, C., Pecorelli, A., Cervellati, F., Cervellati, C., and Maioli, E. (2012). Cutaneous responses to environmental stressors. *Ann. N Y Acad. Sci.* 1271, 75–81.
53. Son, Y., Kim, S., Chung, H.-T., and Pae, H.-O. (2013). Reactive oxygen species in the activation of MAP kinases. In *Methods in Enzymology* (Elsevier Inc.), pp. 27–48.
54. Son, Y., Cheong, Y.-K., Kim, N.-H., Chung, H.-T., Kang, D.G., and Pae, H.-O. (2011). Mitogen-Activated Protein Kinases and Reactive Oxygen Species: How Can ROS Activate MAPK Pathways? *J. Signal Transduct.* 2011, 792639.
55. Ozer, Z., Reardon, J.T., Hsu, D.S., Malhotra, K., and Sancar, A. (1995). The other function of DNA photolyase: stimulation of excision repair of chemical damage to DNA. *Biochemistry* 34, 15886–15889.
56. Green, C.B. (2004). Cryptochromes: tail-ored for distinct functions. *Curr. Biol.* 14, R847–R849.
57. Kanai, S., Kikuno, R., Toh, H., Ryo, H., and Todo, T. (1997). Molecular evolution of the photolyase-blue-light photoreceptor family. *J. Mol. Evol.* 45, 535–548.
58. van der Horst, G.T.J., Muijtjens, M., Kobayashi, K., Takano, R., Kanno, S., Takao, M., de Wit, J., Verkerk, A., Eker, A.P.M., van Leenen, D., et al. (1999). Mammalian Cry1 and Cry2 are essential for maintenance of circadian rhythms. *Nature* 398, 627–630.
59. Kume, K., Zylka, M.J., Sriram, S., Shearman, L.P., Weaver, D.R., Jin, X., Maywood, E.S., Hastings, M.H., and Reppert, S.M. (1999). mCRY1 and

- mCRY2 are essential components of the negative limb of the circadian clock feedback loop. *Cell* 98, 193–205.
60. Chaves, I., Nijman, R.M., Biernat, M.A., Bajek, M.I., Brand, K., da Silva, A.C., Saito, S., Yagita, K., Eker, A.P.M., and van der Horst, G.T.J. (2011). The Potorous CPD photolyase rescues a cryptochrome-deficient mammalian circadian clock. *PLoS ONE* 6, e23447.
 61. Fumey, J., Hinaux, H., Noirot, C., Thermes, C., Rétaux, S., and Casane, D. (2018). Evidence for late Pleistocene origin of *Astyanax mexicanus* cavefish. *BMC Evol. Biol.* 18, 43.
 62. deMenocal, P.B. (1995). Plio-Pleistocene African climate. *Science* 270, 53–59.
 63. Levin, N.E., Quade, J., Simpson, S.W., Semaw, S., and Rogers, M. (2004). Isotopic evidence for Plio- Pleistocene environmental change at Gona, Ethiopia. *Earth Planet. Sci. Lett.* 219, 93–110.
 64. Vatine, G., Vallone, D., Appelbaum, L., Mracek, P., Ben-Moshe, Z., Lahiri, K., Gothilf, Y., and Foulkes, N.S. (2009). Light directs zebrafish period2 expression via conserved D and E boxes. *PLoS Biol.* 7, e1000223.
 65. Mracek, P., Santoriello, C., Idda, M.L., Pagano, C., Ben-Moshe, Z., Gothilf, Y., Vallone, D., and Foulkes, N.S. (2012). Regulation of per and cry genes reveals a central role for the D-box enhancer in light-dependent gene expression. *PLoS ONE* 7, e51278.
 66. Ben-Moshe, Z., Vatine, G., Alon, S., Toviv, A., Mracek, P., Foulkes, N.S., and Gothilf, Y. (2010). Multiple PAR and E4BP4 bZIP transcription factors in zebrafish: diverse spatial and temporal expression patterns. *Chronobiol. Int.* 27, 1509–1531.
 67. Ueda, H.R., Hayashi, S., Chen, W., Sano, M., Machida, M., Shigeyoshi, Y., Iino, M., and Hashimoto, S. (2005). System-level identification of transcriptional circuits underlying mammalian circadian clocks. *Nat. Genet.* 37, 187–192.
 68. Gachon, F., Olela, F.F., Schaad, O., Descombes, P., and Schibler, U. (2006). The circadian PAR-domain basic leucine zipper transcription factors DBP, TEF, and HLF modulate basal and inducible xenobiotic detoxification. *Cell Metab.* 4, 25–36.
 69. Mitsui, S., Yamaguchi, S., Matsuo, T., Ishida, Y., and Okamura, H. (2001). Antagonistic role of E4BP4 and PAR proteins in the circadian oscillatory mechanism. *Genes Dev.* 15, 995–1006.
 70. Beale, A. (2013). The circadian clock of the Mexican blind cavefish, *Astyanax mexicanus*. PhD thesis (UCL, London)
 71. Jostes, R.F. (1996). Genetic, cytogenetic, and carcinogenic effects of radon: a review. *Mutat. Res.* 340, 125–139.
 72. Allegrucci, G., Sbordoni, V., and Cesaroni, D. (2015). Is radon emission in caves causing deletions in satellite DNA sequences of cave-dwelling crickets? *PLoS ONE* 10, e0122456.
 73. Menck, C.F.M. (2002). Shining a light on photolyases. *Nat. Genet.* 32, 338–339.
 74. Gerkema, M.P., Davies, W.I., Foster, R.G., Menaker, M., and Hut, R.A. (2013). The nocturnal bottleneck and the evolution of activity patterns in mammals. *Proc. Biol. Sci.* 280, 20130508.
 75. Maor, R., Dayan, T., Ferguson-Gow, H., and Jones, K.E. (2017). Temporal niche expansion in mammals from a nocturnal ancestor after dinosaur extinction. *Nat Ecol Evol* 1, 1889–1895.
 76. Heesy, C.P., and Hall, M.I. (2010). The nocturnal bottleneck and the evolution of mammalian vision. *Brain Behav. Evol.* 75, 195–203.
 77. Ringvold, A. (2018). Aqueous humour and ultraviolet radiation. *Acta Ophthalmol.* 58, 69–82.
 78. Nüsslein-Volhard, C., and Dahm, R. (2002). Zebrafish: A Practical Approach (Oxford University Press).
 79. Stemmer, M., Schuhmacher, L.-N., Foulkes, N.S., Bertolucci, C., and Wittbrodt, J. (2015). Cavefish eye loss in response to an early block in retinal differentiation progression. *Development* 142, 743–752.
 80. Vallone, D., Santoriello, C., Gondi, S.B., and Foulkes, N.S. (2007). Basic Protocols for Zebrafish Cell Lines. In *Circadian Rhythms: Methods and Protocols*, E. Rosato, ed. (Totowa, NJ: Humana Press), pp. 429–441.
 81. Mosmann, T. (1983). Rapid colorimetric assay for cellular growth and survival: application to proliferation and cytotoxicity assays. *J. Immunol. Methods* 65, 55–63.
 82. Olive, P.L., and Banáth, J.P. (1993). Detection of DNA double-strand breaks through the cell cycle after exposure to X-rays, bleomycin, etoposide and 125I dUrd. *Int. J. Radiat. Biol.* 64, 349–358.
 83. Yu, Y., Zhu, W., Diao, H., Zhou, C., Chen, F.F., and Yang, J. (2006). A comparative study of using comet assay and gammaH2AX foci formation in the detection of N-methyl-N'-nitro-N-nitrosoguanidine-induced DNA damage. *Toxicol. In Vitro* 20, 959–965.
 84. Muslimovic, A., Johansson, P., and Hammarsten, O. (2012). Measurement of H2AX Phosphorylation as a Marker of Ionizing Radiation Induced Cell Damage. In *Current Topics in Ionizing Radiation Research*.
 85. Graf, D., Wesslowski, J., Ma, H., Scheerer, P., Krauß, N., Oberpichler, I., Zhang, F., and Lamparter, T. (2015). Key amino acids in the bacterial (6-4) photolyase PhrB from *Agrobacterium fabrum*. *PLoS ONE* 10, e0140955.
 86. Zhang, F., Scheerer, P., Oberpichler, I., Lamparter, T., and Krauß, N. (2013). Crystal structure of a prokaryotic (6-4) photolyase with an Fe-S cluster and a 6,7-dimethyl-8-ribityllumazine antenna chromophore. *Proc. Natl. Acad. Sci. USA* 110, 7217–7222.



A novel approach to quantify the wound closure dynamic



Flora Ascione^a, Andrea Maria Guarino^b, Viola Calabro^b, Stefano Guido^{a,c,d,*}, Sergio Caserta^{a,c,d}

^a Dipartimento di Ingegneria Chimica dei Materiali e della Produzione Industriale (DICMAPI) Università di Napoli Federico II, P.le Tecchio, 80, 80125 Napoli, Italy

^b Dipartimento di Biologia, Università di Napoli Federico II, Via Cintia 21 - Complesso Monte S. Angelo, 80126 Napoli, Italy

^c CEINGE Biotecnologie Avanzate, Via Sergio Pansini, 5, 80131 Napoli, Italy

^d Consorzio Interuniversitario Nazionale per la Scienza e Tecnologia dei Materiali (INSTM), UDR INSTM Napoli Federico II, P.le Tecchio, 80, 80125 Napoli, Italy

ARTICLE INFO

Keywords:

Wound Healing
Cell Migration
Cell Proliferation
Diffusion
Mathematical modeling
Time-lapse Microscopy
Image Analysis
Transport Phenomena
Breast Cancer

ABSTRACT

The Wound Healing (WH) assay is widely used to investigate cell migration *in vitro*, in order to reach a better understanding of many physiological and pathological phenomena.

Several experimental factors, such as uneven cell density among different samples, can affect the reproducibility and reliability of this assay, leading to a discrepancy in the wound closure kinetics among data sets corresponding to the same cell sample. We observed a linear relationship between the wound closure velocity and cell density, and suggested a novel methodological approach, based on transport phenomena concepts, to overcome this source of error on the analysis of the Wound Healing assay. In particular, we propose a simple scaling of the experimental data, based on the interpretation of the wound closure as a diffusion-reaction process. We applied our methodology to the MDA-MB-231 breast cancer cells, whose motility was perturbed by silencing or over-expressing genes involved in the control of cell migration. Our methodological approach leads to a significant improvement in the reproducibility and reliability in the *in vitro* WH assay.

1. Introduction

Cell migration and proliferation play pivotal roles in a variety of physiological and pathological processes. These include morphogenesis, angiogenesis, inflammation, tissue repair, and tumor invasion [1,2]. Therefore, it is of great interest and potential therapeutic importance to understand the mechanisms driving cell dynamic behavior, which are still far from being fully understood [3,4].

The wide range of *in vitro* assays to quantitatively evaluate cell motility, invasion and chemotaxis include straightforward and economical ones, such as the Boyden Chamber assay [5], or more expensive, time-consuming and technically demanding as the cell random motility assay [6,7]. This last one enables the investigation of cell motility at the level of both individual cells and entire cell population. The choice of one or the other method depends on the specific research question and cell type under investigation [8].

One of the most popular, widely used, and straightforward methods to characterize and quantify cell dynamic behavior *in vitro* is the Wound Healing (WH) assay [8], because of its low cost and simplicity to set-up [9]. Recently, it was proved the results from WH assay can be used to estimate single cell motility parameters [10],

such as random motility coefficient, typically measured by time consuming random motility assay. In the conventional WH assay, also known as scratch test, cells are seeded on a planar surface, allowed to attach, spread and proliferate until they reach confluency. An artificial “wound” is then made by dragging a sterile pipette tip or needle across the cell monolayer [11,12]. Then cells are washed with an appropriate medium to remove debris and floating cells. Recently, novel non-mechanical techniques have been developed to achieve wounding without mechanically disrupting the cell layer [13–19]. After the wounding, the cells on the edges of the newly created gap loose the cell-cell contact inhibition and, stimulated by the availability of free space, start to move and proliferate until new cell-cell contacts are re-established and the wound is closed [20]. Contact inhibition is a property of normal somatic cells and a key anticancer mechanism that arrests cell division when cells reach a high density. Cancerous cells typically lose this property and thus grow in an uncontrolled manner even when in contact with neighboring cells. Loss of contact-inhibition has important implications for cancer invasion and metastasis [21,22].

Two different experimental approaches can be followed to monitor the wound closure process; microscope images within the sample can

* Corresponding author at: Dipartimento di Ingegneria Chimica dei Materiali e della Produzione Industriale (DICMAPI) Università di Napoli Federico II, P.le Tecchio, 80, 80125 Napoli, Italy.

E-mail address: stefano.guido@unina.it (S. Guido).

<http://dx.doi.org/10.1016/j.yexcr.2017.01.005>

Received 4 August 2016; Received in revised form 11 January 2017; Accepted 17 January 2017

Available online 28 January 2017

0014-4827/ © 2017 Elsevier Inc. All rights reserved.

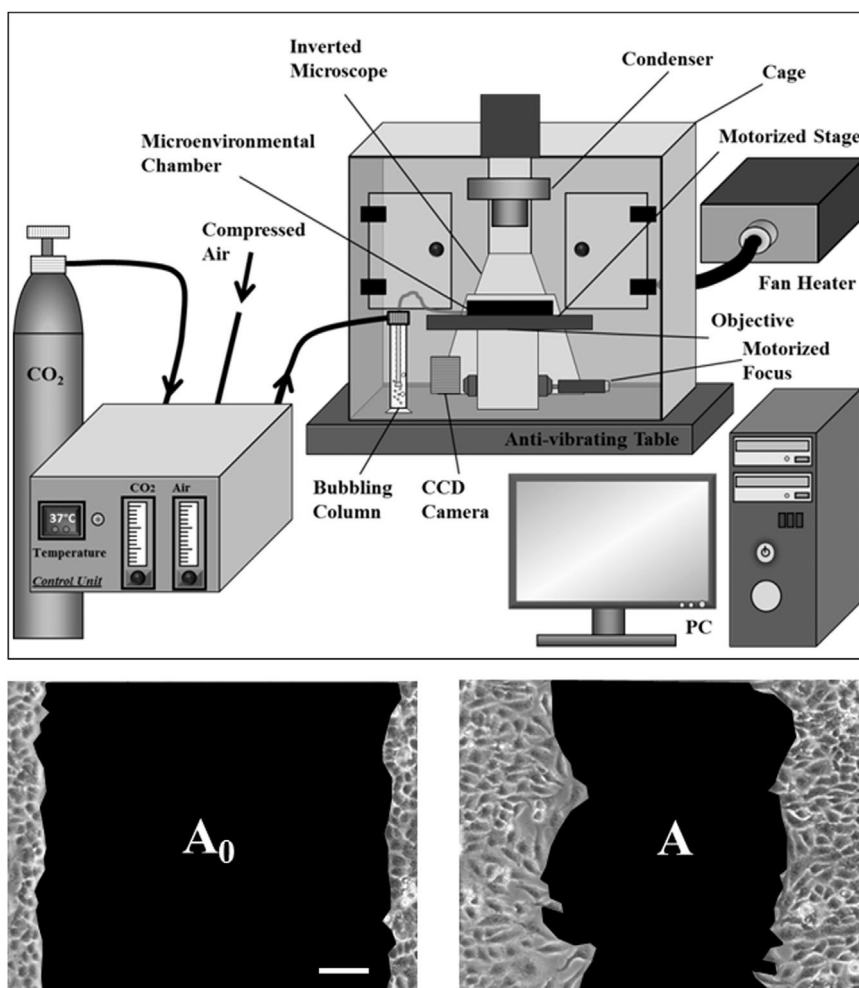


Fig. 1. Image acquisition technique. Scheme of the time-lapse microscopy workstation on the top. In the bottom, two typical images acquired during a WH experiment, corresponding to $t=0$ h (left) where the initial wound size A_0 is measured, and a generic $t > 0$ h (right), where the wound size is reduced to A . The cell-free area at $t=0$ (A_0) and at $t > 0$ (A) is shown in black. Scale bar= $100 \mu\text{m}$.

and grown on micro cover glasses (BDH). After 24 h cells were transfected with $\Delta\text{Np63}\alpha$ plasmid (mock) or YB-1 siRNA oligos. 24 h after transfection cells were washed with cold phosphate-buffered saline (PBS) and fixed with 4% paraformaldehyde (PFA) (Sigma-Aldrich, St. Louis, MO) for 10 min at room temperature. Cells were permeabilized with 0.5% Triton-

PBS for 5 min, blocked with a solution of 3% BSA at room temperature for 20 min, washed with PBS and incubated with YB-1 (Ab12148) antibody (1:300 dilution). After washing in PBS, samples were incubated with conjugated anti-rabbit IgGs (Green-Alexa Fluor 488, ThermoFisher) at room temperature for 45 min. Nuclei were detected by incubating cells

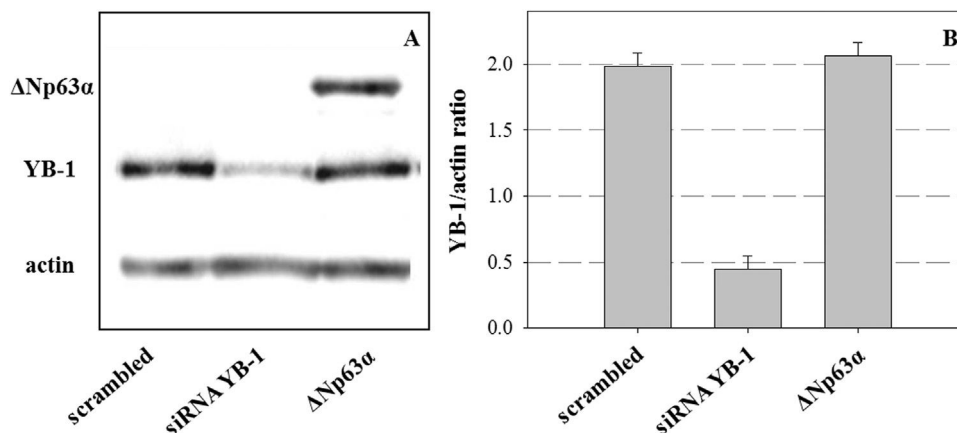


Fig. 2. A representative immunoblot showing the expression level of $\Delta\text{Np63}\alpha$ and YB-1 in equal aliquots of MDA-MB-231 cell extracts. MDA-MB-231 cells were transfected with scrambled oligos, YB-1 oligos or $\Delta\text{Np63}\alpha$ encoding vector. After 24 h total protein extracts were prepared and quantified. Equal aliquots of extracts were loaded on SDS/PAGE gel and subjected to immunoblot with anti-YB-1, anti-p63, and anti- β -actin antibodies. B. Histograms presenting the ratio of YB-1 over β -actin signals from immunoblot analysis (mean values and standard deviations were calculated from biological triplicates).

with Hoechst 33342 (2'-[4-ethoxyphenyl]-5-[4-methyl-1-piperazinyl]-2,5'-bi-1H-benzimidazole trihydrochloride trihydrate) (Thermo Scientific) for 5 min. Actin bundles were stained with Rhodamine conjugated phalloidin (Sigma) in PBS for 30 min at room temperature. Images were digitally acquired using Nikon TE Eclipse E1000 microscope (40x) and processed using ImageJ Software.

2.7. Time-lapse microscopy

Time-lapse Microscopy (TLM) image acquisition was performed using an automated workstation [46] based on an inverted microscope (Zeiss Axiovert 200, Carl Zeiss, Jena Germany) enclosed in a homemade incubator that allows to keep the sample at constant temperature (37 ± 0.1 °C) and under 5% CO₂, 100% humidified atmosphere. A scheme of the workstation is reported in Fig. 1. Sample images were iteratively acquired by a high-resolution high-sensitivity monochromatic CCD video camera (Hamamatsu Orca AG, Japan) using a long working distance 10x objective in phase contrast (CP Achromat Ph1). The microscope was also equipped with motorized stage and focus control (Prior, Cambridge, UK) for automated positioning. The workstation was controlled by homemade control software in Labview. For each cell sample, several independent fields of view were selected in different wells of the multiwell culture plate. The delay time between consecutive image acquisitions was 15 min, and the whole experiment length was about 50 h.

2.8. Image and data analysis

For each cell sample, overall at least five fields of view from three independent experimental campaigns were analyzed and compared.

The wound closure dynamics was quantified by measuring the size of the cell-free area for each time step (A), normalized respect to its value at time 0 (A_0). A homemade automated image analysis software, based on the analysis of image variance, was used to identify the wound edge as the boundary of the scattering cells. The result of this segmentation is reported in Fig. 1, which shows two images corresponding to $t=0$ h and $t>0$ h; the black area represents the cell-free region, as measured by image analysis. The curves describing the evolution of the wound area over time showed a linear trend. The wound closure velocity was determined as the slope of the linear fit of experimental data (α , h^{-1}).

Cell density at time 0 was measured for each field of view by manually counting the cells on the left and right wound edge in the image acquired at time 0. The density value was calculated dividing the number of cells by the area covered, measured by drawing manually the cell covered area contour using an image analysis software (Image Pro Plus).

3. Results and discussion

Y Box binding protein 1 (YB-1 or YBX-1) and $\Delta Np63\alpha$ are interacting partners involved in the control of cell adhesion and migration [47]. In particular, $\Delta Np63\alpha$ is a marker of epithelial basal cells that provides inhibitory signals for cell motility and spread [48]. To define the role of YB-1 and $\Delta Np63\alpha$ in the control of cell movements, we set out WH assays in MDA-MB-231 cells. MDA-MB-231 cells lack endogenous $\Delta Np63\alpha$ expression and express high level of YB-1. Cells transfected with $\Delta Np63\alpha$ plasmid or depleted of endogenous YB-1 by short interfering RNA (siRNA) were used for WH assays to compare their behavior to control cells. Immunoblot analysis of total cell extract was performed to confirm efficient YB-1 knockdown and $\Delta Np63\alpha$ transfection (Fig. 2).

Continuous cell monolayers were manually wounded in order to induce the cells to cover the cell-free region. Wound closure dynamics was captured by imaging the samples through TLM acquisition. Data sets from three independent WH experiments were collected and compared.

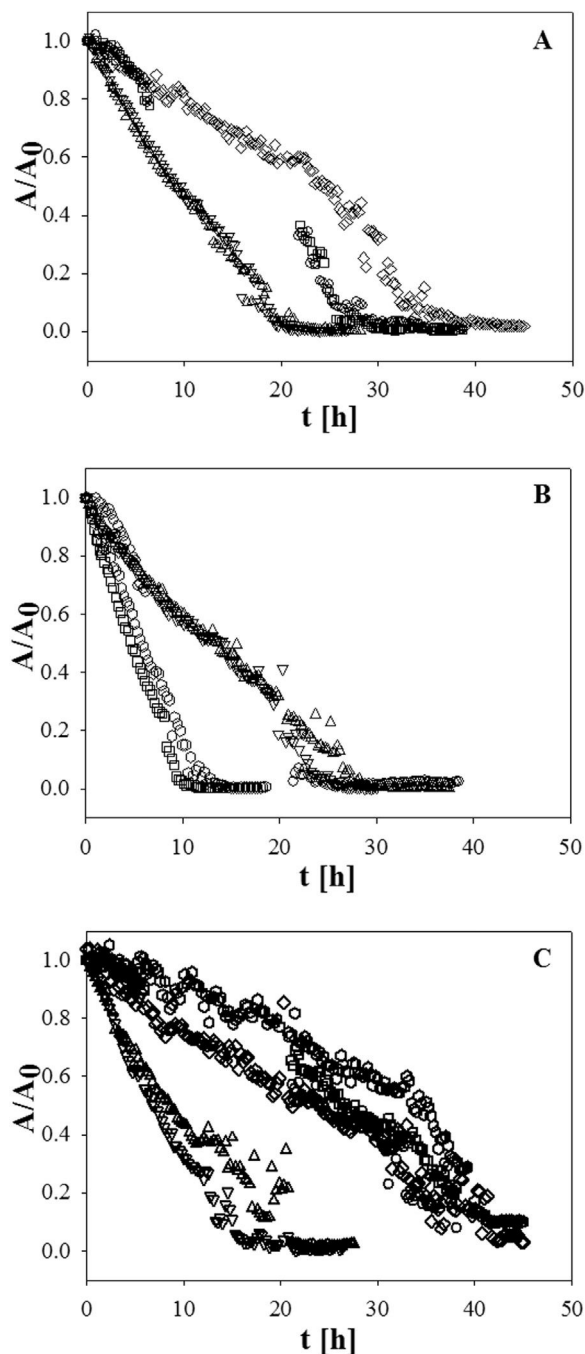


Fig. 3. Evolution in time of the wound area A , normalized to the value A_0 at time 0, for MDA-MB-231 control cells (A, 6 data series), cells silenced for YB-1 expression (B, 8 data series) and cells transfected with $\Delta Np63\alpha$ (C, 8 data series).

The wound closure process was quantified measuring by image analysis the reduction of wound area over time, as described in the Material and Methods section. In Fig. 3, the evolution of wound area, normalized respect to the value at time 0 (A/A_0), is reported as a function of time for the control sample (Fig. 3(A)) and the two cell treatments (Figs. 3(B) and 3(C)). For each of the three distinct experimental settings (control, YB-1 silenced and $\Delta Np63\alpha$ transfected cells), we produced at least five data sets and plotted them as independent data series. The obtained profiles, all starting from $A/A_0=1$ and describing the temporal evolution of the wound area (wound closure kinetics), exhibited a linear trend until complete wound closure was reached ($A/A_0 \approx 0$). This suggests that the wound healing process occurs at a constant velocity, in agreement with the prediction of the

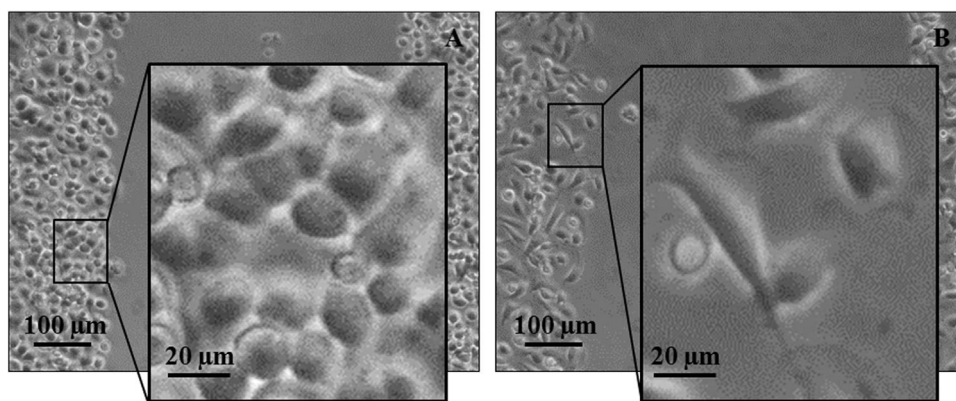


Fig. 4. Images acquired during a WH experiment at time $t=0$ for two cell samples silenced for YB-1 expression.

Fisher-Kolmogoroff equation model [20] that describes the process as wave of the cell density function traveling at constant velocity, after a short transient phase. The initial lag time can be neglected in our case, on the time scale of our interest. The slope of the linear fit of experimental data (α , h^{-1}) can be considered as a direct measurement of wound closure velocity, and is directly related to the speed of the propagating cell front (v , $\mu\text{m}/\text{h}$), predicted by the Fischer-Kolmogoroff model. In particular, $v = \alpha \cdot b/2$, where b is the width of the wound at time 0, in μm .

Surprisingly, as shown in Fig. 3, within each experimental setting we found a strong discrepancy among the data sets although the samples were technical replicates of a single experiment. In fact, different wound closure times, corresponding to different wound closure velocities, can be observed for each cell sample, including the control cells. For example, in Fig. 3(B) two different trends can be distinguished; in one case the wound closure was achieved in about 10 h (two data sets), whereas in the other case more than 20 h were required (three data sets). Similar discrepancies were visible also for the other samples.

Although unexpected, inconsistency in data from WH statistical replicates are common in the literature and can lead to results difficult to interpret, compare or integrate [43,49].

To explore the possible reasons for data discrepancies, the images acquired at time 0 for each data set were visually inspected and found to be substantially different in cell density. Fig. 4 shows the images acquired at time 0 for two samples corresponding to cells silenced for YB-1 expression (Fig. 3(B)). In particular, Fig. 4(A) is relative to a cell sample where the complete closure of the wound region required 10 h, while Fig. 4(B) corresponds to a sample where the wound closure required about 30 h. Magnification of selected regions on the wound edge highlights the difference in cell density between the two samples. A different cell density might reasonably explain variations in wound closure kinetics, being all the other conditions the same. Videos of the wound healing process for these two cell samples are available as Supporting Information (Video 1 and Video 2, referring to the samples in Figs. 4(A) and 4(B) respectively).

Supplementary material related to this article can be found online at doi:10.1016/j.yexcr.2017.01.005.

Pharmacological treatment and widely used methods in cell biology research to modulate gene expression, such as lipofection and electroporation, may trigger cellular stress and determine unwanted detachment of a certain amount of cells from the cell monolayer [49,50]. Moreover, static seeding techniques, poor plate quality and uneven adhesion can lead to non-uniform spatial spreading of the cells in the culture dish after plating so that fluctuations in cell population density can also occur in control samples thereby limiting the reproducibility of the measurements in WH assays.

Our set of experiments was designed to compare the wound healing

kinetic of MDA-MB-231 cells with that of the same cells subjected to YB-1 silencing by RNA interference or $\Delta\text{Np}63\alpha$ over-expression by lipofection.

According to the Fisher-Kolmogoroff model, the wound closure process can be described as the evolution of cell density in space and time, due to two mechanisms, i.e., cell motility and proliferation, that are both involved in the spatial spreading of the cells in the wound region [39]. Cell motility, mathematically described as diffusion, is driven by a gradient of cell density generated between the cell monolayer and the wound area. Cell proliferation, described as a logistic growth, depends on the local cell density on the wound edge. Both the motility and the proliferation term of the Fisher-Kolmogoroff are related to the cell density, in first approximation in a linear way, thus suggesting that the wound closure velocity is linearly dependent with the cell density.

We investigated a possible relationship between the wound closure velocity and the initial cell density (u) of the samples, as measured from images acquired at time 0 for each data series (see Material and Methods section). In order to determine the wound closure velocity, each data set in Fig. 3 for the three samples under investigation was fitted assuming a linear trend; the slopes of the lines fitting the curves of A/A_0 versus time (starting from $A/A_0=1$ and stopping at a value around 0) represent the wound closure velocity for each specific sample. In Fig. 5, the so determined wound closure velocity (α) is reported as a function of the corresponding cell density (u). A linear relationship can be observed between v and u for each cell sample, suggesting the dependence of the wound closure kinetics on the cell

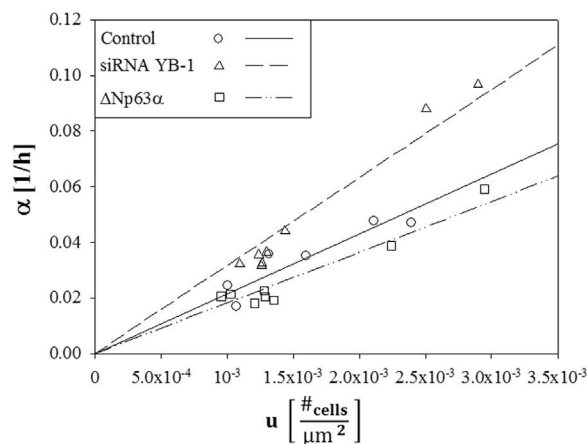


Fig. 5. The wound closure velocity (α) is reported as a function of the cell density at time 0 (u) for the three cell samples under investigation. A linear fit is reported, $R^2=0.83, 0.95$ and 0.93 , for MDA-MB-231 control cells, cells silenced for YB-1 expression and cells transfected with $\Delta\text{Np}63\alpha$, respectively.

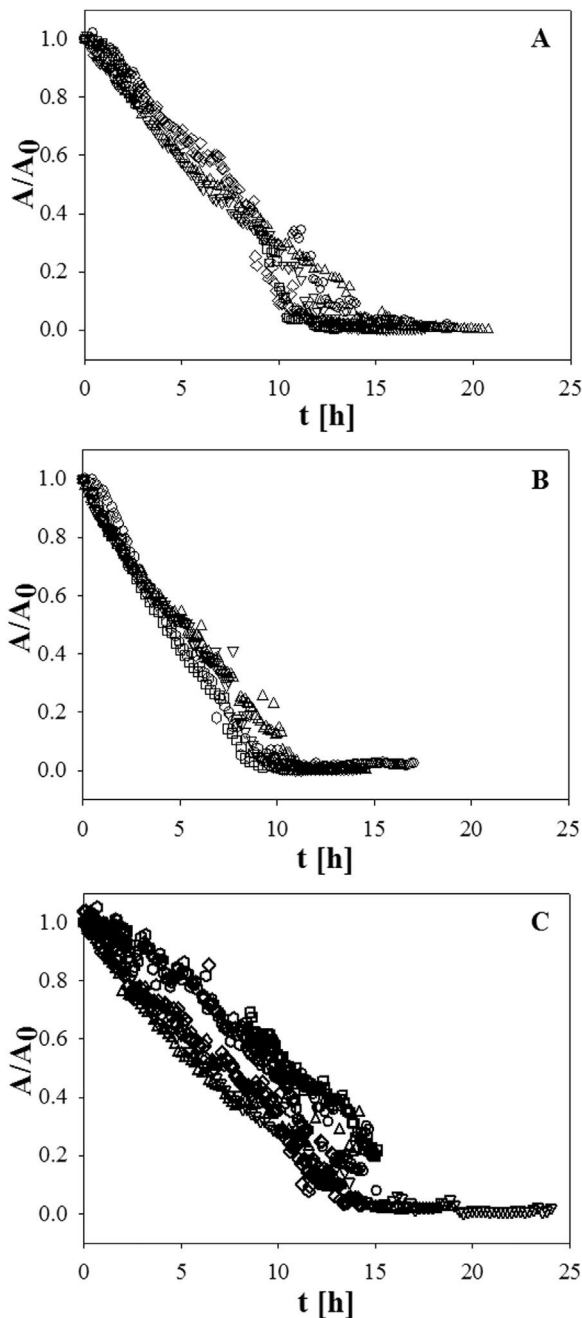


Fig. 6. Evolution in time of the wound area A , normalized to the value A_0 at time 0, after data scaling for MDA-MB-231 control cells (A), cells silenced for YB-1 expression (B) and cells transfected with $\Delta Np63\alpha$ (C). The symbols are in agreement with the legend in Fig. 3.

density. This result is in agreement with the dependence of the proliferation and migration mechanisms on the cell density, as suggested by Fisher-Kolmogoroff equation.

We propose a phenomenological scaling of the experimental data, which considers the differences we measured in the cell densities at time 0, and minimizes the differences in wound closure time we observed in Fig. 3 which are unexpected for technical replicates. The scaling is described in details in the Supplementary Materials section. Briefly, the calculation is based on the linear relationship between A/A_0 and the time, and between the wound closure velocity v and the cell density u . The scaling consists in the calculation, for each data series, of corrected time values t_c , obtained multiplying the experimental time t of each experimental point by a scaling factor, according to Eq. (2). The

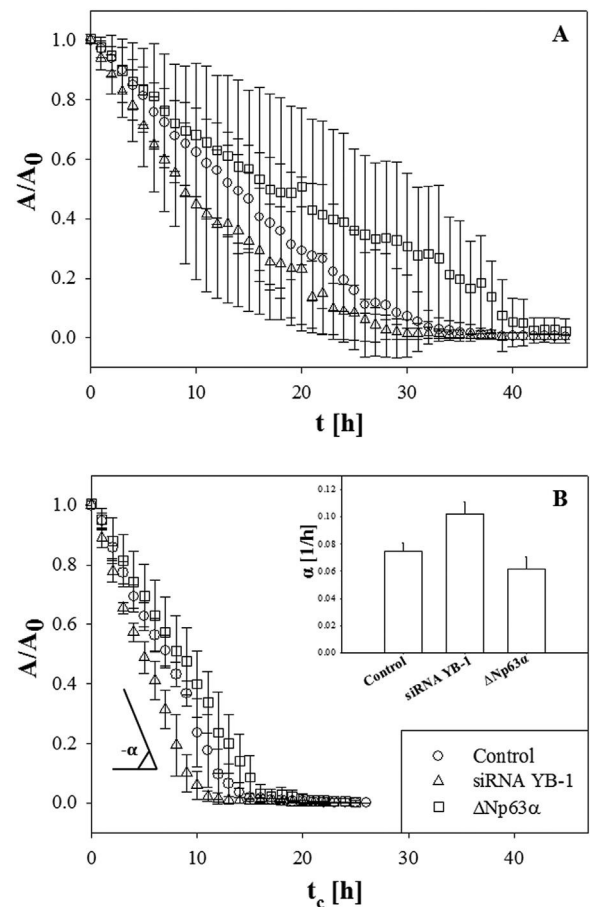


Fig. 7. Comparison of wound closure dynamics before (A) and after (B) data scaling for the three cell samples under investigation. In each graph the wound area A , normalized with respect to the initial value A_0 , is reported as function of time. Each curve is relative to a specific cell sample. Each data point of the curve represents the average of all the measurements reported in Figs. 3 and 6, respectively; the standard deviation is reported as error bars. The inset in B reports the wound closure velocity, reported as the slope of the normalized wound area reduction over time.

scaling factor is the ratio between the cell density at time 0 of the sample considered (u_i) and a reference value of the cell density (u_R), in principle also arbitrarily chosen:

$$t_c = \frac{u_i}{u_R} * t \quad (2)$$

Reasonable values of u_R are close to the cell density at confluency. A wider description of the calculation of the scaling is reported in the Supplementary Materials (Fig. S1).

We applied this simple mathematical scaling to each data set reported in Fig. 3. In Fig. 6, we report the evolution in time of the cell-free area (A/A_0) after data scaling for the control sample (Fig. 6(A)) and the two cell treatments (Figs. 6(B) and 6(C)) we considered. A direct comparison between Fig. 3 and Fig. 6 clearly shows that after the scaling we applied the profiles are significantly closer to each other.

Fig. 7 provides a direct comparison between the experimental data before (Fig. 7(A)) and after (Fig. 7(B)) the scaling. Each data series reported in the chart is calculated as the average of all the available measurements taken for each cell sample, in agreement with the typical data processing methods used in the literature to compare different cell treatments. The reproducibility error can be estimated calculating different parameters such as standard error of the mean or confidence intervals, that are all related to the standard deviation [51]. We reported the value of the standard deviation as error bar in Fig. 7. It is evident that a relevant improvement of the experimental reprodu-

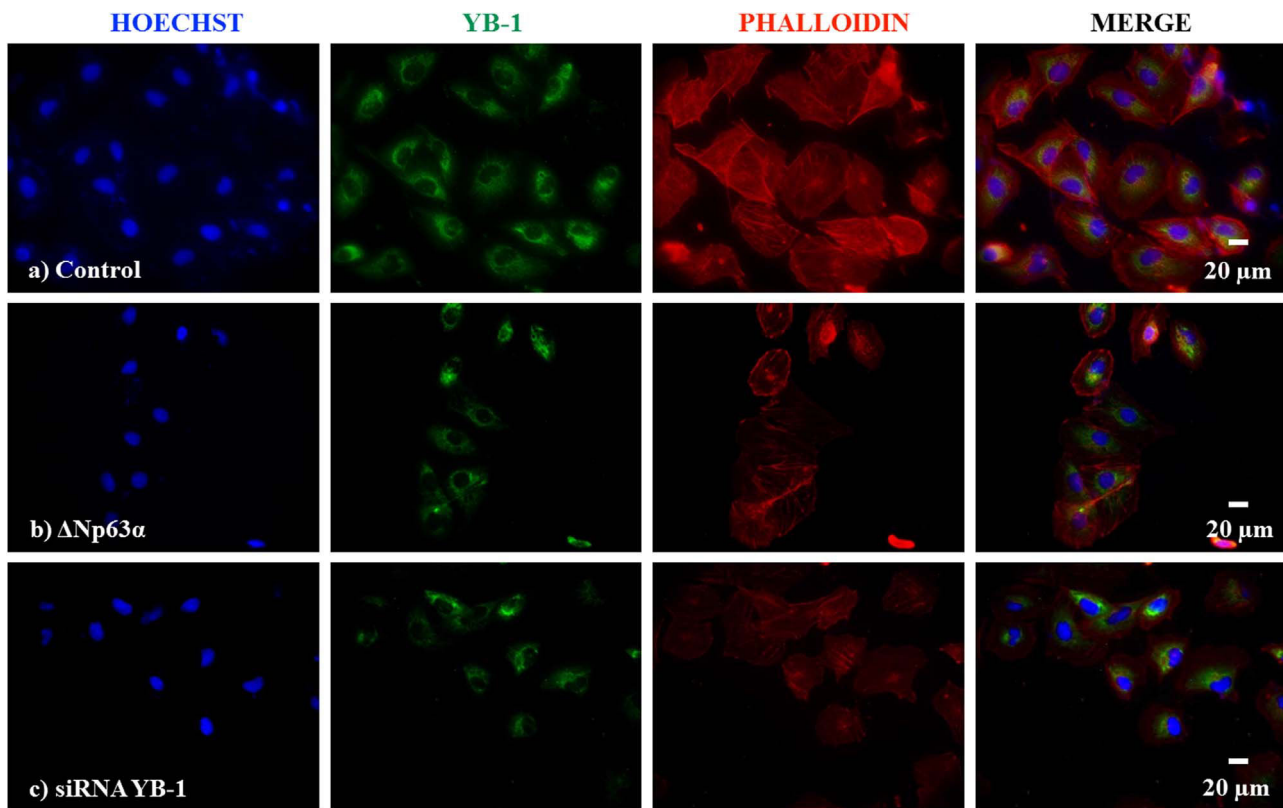


Fig. 8. MDA-MB-231 a) control, b) Δ Np63 α transfected and c) YB-1 silenced cells were stained for YB-1 (green), Rhodamine Phalloidin (red), nuclei were stained with HOECHST. F-actin fibers (red) appear altered in panel b) and c) compared to control.

cibility is achieved after the scaling, as suggested by the shorter error bars in Fig. 7(B) compared to Fig. 7(A). Such improvement also highlights the fact that cell density is one of the major factor responsible for data variability in WH assays.

As shown in Fig. 7(B), cells silenced for YB-1 expression close the wound region faster than control cells, while cells transfected with Δ Np63 α cover the wound area slower than control cells. Remarkably, the scaling procedure does not change the result of the experiment but it makes easier and reliable the comparison of data. In the inset of Fig. 7(B) the wound closure velocity α , calculated as the slope of the normalized wound area curves vs time, is reported for the three samples. The differences in wound closure kinetic between YB-1 silenced cells and Δ Np63 α transfected cell and the relative controls, measured as average of all the samples reported in Fig. 6, can be considered statistically significant, being the p-values 0.0005 and 0.023, respectively.

According to Fisher-Kolmogoroff model, these differences can be ascribed to either a change in cell proliferation rate, or to an influence over cell migration. In fact, the wound closure velocity is related to the speed of the cell front propagation, that according to Fisher-Kolmogoroff model is $v = \sqrt{\frac{4D\ln(2)}{\tau}}$ [38], where τ is the cell doubling time, and D is the random motility coefficient, analogous of a diffusion coefficient. Starting from the measurement of the wound closure velocity α (Fig. 7(B), inset), this equation can be used to estimate the ratio between doubling time τ and the cell random motility coefficient D , in order to make direct comparison between the values obtained for different cell samples. In our case, the speed of the cell front propagation v is 18.7 ± 3.6 , 26.1 ± 4.6 , and 15.5 ± 2.0 $\mu\text{m}/\text{h}$ for control cells, cells silenced for YB-1 expression and cells transfected with Δ Np63 α , respectively. The doubling time of the three cell populations was estimated by direct cell counting (see Materials and Methods). Δ Np63 α transfected cells showed a proliferation rate slightly lower than MDA-MB-231 control cells, with a duplication time about 10%

higher; given the differences we measured in v , this suggests that the cells transfected with Δ Np63 α show a random motility coefficient D about 30% lower than control cells. On the other hand, cells silenced for YB-1 showed a duplication time about 40% lower than control cells, thus suggesting a random motility coefficient about 37% higher than the control sample. We should mention that the proliferation measurements showed some scattering, and hence we can consider them only as indicative of a qualitative trend. However, at least in relative terms, all our measurements are consistent.

As a summary, the WH assays here performed suggest that cells silenced for YB-1 exhibit higher motility than MDA-MB-231 control cells, while the cells transfected with Δ Np63 α show a lower motility compared to control cells.

Finally, we imaged cell samples staining actin fibers using Phalloidin, a high-affinity F-actin probe. As shown in Fig. 8, control and Δ Np63 α transfected cells show a typical flattened epithelial-like morphology with well-defined cell margins and a regular network of cytoskeletal F-actin. According to our data, YB-1 depleted cells, instead, showed an altered retracted morphology with F-actin puncta and bundles, suggesting a loss of cell-cell contacts and an increase in cell motility. This result is in agreement with previous data showing that YB-1 is essential for organizing and stabilizing F-actin fibers [52].

4. Conclusions

In this work, we proposed a novel methodological approach to quantify the wound closure dynamic in the classical *in vitro* WH assay. Although particularly suitable to investigate and compare cell dynamic behavior *in vitro* under different experimental conditions, this assay is influenced by several factors that can produce misleading results, thus hindering experimental reproducibility and reliability. In particular, homogeneous cell density among samples is challenging to achieve and reproduce, due to inaccuracy in cell counting, uneven cell spatial

spreading and because of invasive treatments cells can be subjected to before the WH assay. This can make it difficult to compare the dynamic behavior of cell samples undergoing different biological treatments.

The conventional quantitative analysis of this assay typically neglects the influence of cell density on the wound closure kinetics *in vitro*. The focus of our work has been to assess how the density of cell samples can affect the healing process. In particular, we proposed a methodology of analysis based on transport phenomena concepts, mainly addressed to overcome the influence of cell density on the process. As a case study, we applied our methodological approach to the comparison of the wound healing kinetic of MDA-MB-231 breast cancer cells with that of the same cells whose motility was perturbed by depletion of YB-1 or overexpression of $\Delta Np63\alpha$. We found a linear relationship between the wound closure velocity of the cell samples under investigation and cell density. Moreover, we observed a strong discrepancy in the wound closure among data sets for each cell sample, including control cells, although they were technical replicates of a single experiment. The different cell density of the samples can explain the variation we observed in wound closure kinetics, being all the other conditions the same. This result is in agreement with Fisher-Kolmogoroff model that describes the wound healing as a diffusion-reaction process, in which the evolution of cell density in time and space is dependent on cell motility and proliferation mechanisms. Inspired by the Fisher-Kolmogoroff model, we proposed a phenomenological scaling of the experimental data, according to which the wound closure time of a sample with a given density is scaled to the closure time relative to a reference density. We applied this methodology to the investigation of MDA-MB-231 breast cancer cells whose motility was perturbed by depletion or over-expression of genes involved in the control of cell adhesion and migration. Our results, supported also by visualization of actin fibers morphology, are that YB-1 depleted cells show an increase in their migration ability, while $\Delta Np63\alpha$ transfected cells have a lower motility compared to control cells.

The methodological approach here proposed, based on transport phenomena concepts, can improve reproducibility and reliability in the WH assay, thus allowing the comparison between different experimental conditions or different sample types. Furthermore, the model proposed in this work can be used to estimate the relative contributions of cell motility and cell proliferation in WH assays, comparing the characteristic time of cell diffusion and the duplication time of the cell population.

Acknowledgements

This study was conducted under the umbrella of the European network action COST MP1106 “Smart and green interfaces - from single bubbles and drops to industrial, environmental and biomedical applications” and COST Action MP1305 “Flowing Matter”, supported by COST (European Cooperation in Science and Technology).

Appendix A. Supporting information

Supplementary data associated with this article can be found in the online version at doi:10.1016/j.yexcr.2017.01.005.

References

- [1] F. Ziebert, I.S. Aranson, Effects of adhesion dynamics and substrate compliance on the shape and motility of crawling cells, *PLoS One* 8 (2013) e64511.
- [2] R. Horwitz, D. Webb, Cell migration, *Curr. Biol.* 13 (2003) R756–R759.
- [3] D. Lauffenburger, A simple-model for the effects of receptor-mediated cell-substratum adhesion on cell-migration, *Chem. Eng. Sci.* 44 (1989) 1903–1914.
- [4] D. Veltman, Actin dynamics: cell migration takes a new turn with arpin, *Curr. Biol.* 24 (2014) R31–R33.
- [5] S. Boyden, The chemotactic effect of mixtures of antibody and antigen on polymorphonuclear leucocytes, *J. Exp. Med.* 115 (1962) 453–466.
- [6] R. Dickinson, R. Tranquillo, Optimal estimation of cell movement indexes from the statistical analysis of cell tracking data, *Aiche J.* 39 (1993) 1995–2010.
- [7] S. Vedel, S. Tay, D.M. Johnston, H. Bruus, S.R. Quake, Migration of cells in a social context, *Proc. Natl. Acad. Sci. USA* 110 (2013) 129–134.
- [8] N. Kramer, A. Walz, C. Unger, M. Rosner, G. Krupitza, M. Hengstschlaeger, H. Dolznig, In vitro cell migration and invasion assays, *Mutat. Res.-Rev. Mutat. Res.* 752 (2013) 10–24.
- [9] M. Bindschadler, J.L. McGrath, Sheet migration by wounded monolayers as an emergent property of single-cell dynamics, *J. Cell Sci.* 120 (2007) 876–884.
- [10] F. Ascione, A. Vasaturo, S. Caserta, V. D’Esposito, P. Formisano, S. Guido, Comparison between fibroblast wound healing and cell random migration assays in vitro, *Exp. Cell Res* (2016).
- [11] L.G. Rodriguez, X. Wu, J.L. Guan, Wound-healing assay, *Methods Mol. Biol.* 294 (2005) 23–29.
- [12] J. Yarrow, Z. Perlman, N. Westwood, T. Mitchison, A high-throughput cell migration assay using scratch wound healing, a comparison of image-based readout methods, *BMC Biotechnol.* 4 (2004).
- [13] R. van Horsen, T. ten Hagen, Crossing barriers: the new dimension of 2D cell migration assays, *J. Cell. Physiol.* 226 (2011) 288–290.
- [14] K. Hunt, H. Wingate, T. Yokota, Y. Liu, G. Mills, F. Zhang, B. Fang, C. Su, M. Zhang, M. Yi, K. Keyomarsi, Elafin, an inhibitor of elastase, is a prognostic indicator in breast cancer, *Breast Cancer Res.* 15 (2013).
- [15] C. Keese, J. Wegener, S. Walker, L. Giaeveer, Electrical wound-healing assay for cells in vitro, *Proc. Natl. Acad. Sci. U.S.A.* 101 (2004) 1554–1559.
- [16] M. Zordan, C. Mill, D. Riese, J. Leary, A. High Throughput, Interactive imaging, bright-field wound healing assay, *Cytom. Part A* 79A (2011) 227–232.
- [17] D. Kiehart, C. Galbraith, K. Edwards, W. Rickoll, R. Montague, Multiple forces contribute to cell sheet morphogenesis for dorsal closure in *Drosophila*, *J. Cell Biol.* 149 (2000) 471–490.
- [18] F. Nie, M. Yamada, J. Kobayashi, M. Yamato, A. Kikuchi, T. Okano, On-chip cell migration assay using microfluidic channels, *Biomaterials* 28 (2007) 4017–4022.
- [19] E. Anon, X. Serra-Picamal, P. Hersen, N.C. Gauthier, M.P. Sheetz, X. Trepat, B. Ladoux, Cell crawling mediates collective cell migration to close undamaged epithelial gaps, *Proc. Natl. Acad. Sci. USA* 109 (2012) 10891–10896.
- [20] A. Tremel, A. Cai, N. Tirtaatmadja, B.D. Hughes, G.W. Stevens, K.A. Landman, A.J. O’Connor, Cell migration and proliferation during monolayer formation and wound healing, *Chem. Eng. Sci.* 64 (2009) 247–253.
- [21] Y. Takai, J. Miyoshi, W. Ikeda, H. Ogita, Nectins and nectin-like molecules: roles in contact inhibition of cell movement and proliferation, *Nat. Rev. Mol. Cell Biol.* 9 (2008) 603–615.
- [22] R. Mayor, C. Carmona-Fontaine, Keeping in touch with contact inhibition of locomotion, *Trends Cell Biol.* 20 (2010) 319–328.
- [23] S. Kanazawa, T. Fujiwara, S. Matsuzaki, K. Shingaki, M. Taniguchi, S. Miyata, M. Tohyama, Y. Sakai, K. Yano, K. Hosokawa, T. Kubo, bFGF regulates PI3-kinase-Rac1-JNK pathway and promotes fibroblast migration in wound healing, *PLoS One* 5 (2010) e12228.
- [24] S. Lucena, E.E. Sanchez, J.C. Perez, Anti-metastatic activity of the recombinant disintegrin, r-mojastin 1, from the Mohave rattlesnake, *Toxicol.* 57 (2011) 794–802.
- [25] P. Yue, E. Leung, N. Mak, R. Wong, A simplified method for Quantifying cell migration/wound healing in 96-well plates, *J. Biomol. Screen.* 15 (2010) 427–433.
- [26] R. Sumagin, A.Z. Robin, A. Nusrat, C.A. Parkos, Activation of PKC β II by PMA facilitates enhanced epithelial wound repair through increased cell spreading and migration, *PLoS One* 8 (2013) e55775.
- [27] C. Wong, A.A. Chen, B. Behr, S. Shen, Time-lapse microscopy and image analysis in basic and clinical embryo development research, *Reprod. Biomed. Online* 26 (2013) 120–129.
- [28] I. Andújar, J.L. Ríos, R.M. Giner, M.C. Recio, Shikonin promotes intestinal wound healing in vitro via induction of TGF- β release in IEC-18 cells, *Eur. J. Pharm. Sci.* 49 (2013) 637–641.
- [29] M. Tsai, H. Huang, J. Hsu, Y. Lai, Y. Hsiao, F. Lu, H. Chang, Topical N-Acetylcysteine accelerates wound healing in vitro and in vivo via the PKC/Stat3 pathway, *Int. J. Mol. Sci.* 15 (2014) 7563–7578.
- [30] M. Poujade, E. Grasland-Mongrain, A. Hertzog, J. Jouanneau, P. Chavrier, B. Ladoux, A. Buguin, P. Silberzan, Collective migration of an epithelial monolayer in response to a model wound, *Proc. Natl. Acad. Sci. USA* 104 (2007) 15988–15993.
- [31] P. Vitorino, T. Meyer, Modular control of endothelial sheet migration, *Genes Dev.* 22 (2008) 3268–3281.
- [32] C.-C. Liang, A.Y. Park, J.-L. Guan, In vitro scratch assay: a convenient and inexpensive method for analysis of cell migration in vitro, *Nat. Protoc.* 2 (2007) 329–333.
- [33] P. Rørth, Collective cell migration, *Annu Rev. Cell Dev. Biol.* 25 (2009) 407–429.
- [34] J. Arnold, J. Adam, A simplified model of wound healing - II: the critical size defect in two dimensions, *Math. Comput. Model.* 30 (1999) 47–60.
- [35] J.A. Sherratt, J.D. Murray, Models of epidermal wound healing, *Proc. Biol. Sci.* 241 (1990) 29–36.
- [36] S. Johnston, M. Simpson, D. McElwain, How much information can be obtained from tracking the position of the leading edge in a scratch assay?, *J. R. Soc. Interface* 11 (2014).
- [37] A.Q. Cai, K.A. Landman, B.D. Hughes, Multi-scale modeling of a wound-healing cell migration assay, *J. Theor. Biol.* 245 (2007) 576–594.
- [38] P.K. Maini, D.L.S. McElwain, D.I. Leavesley, Traveling wave model to interpret a wound-healing cell migration assay for human peritoneal mesothelial cells, *Tissue Eng.* 10 (2004) 475–482.
- [39] P.K. Maini, D.L.S. McElwain, D. Leavesley, Travelling waves in a wound healing assay, *Appl. Math. Lett.* 17 (2004) 575–580.

- [40] M. Zhang, H. Li, H. Ma, J. Qin, A simple microfluidic strategy for cell migration assay in an in vitro wound-healing model, *Wound Repair Regen.* 21 (2013) 897–903.
- [41] L. Chou, J. Firth, V. Uitto, D. Brunette, Substratum surface-topography alters cell-shape and regulates fibronectin messenger-RNA level, messenger-RNA stability, secretion and assembly in human fibroblasts, *J. Cell Sci.* 108 (1995) 1563–1573.
- [42] O. Cochet-Escartin, J. Ranft, P. Silberzan, P. Marcq, Border forces and friction control epithelial closure dynamics, *Biophys. J.* 106 (2014) 65–73.
- [43] M. Doran, R. Mills, A. Parker, K. Landman, J. Cooper-White, A cell migration device that maintains a defined surface with no cellular damage during wound edge generation, *Lab a Chip* 9 (2009) 2364–2369.
- [44] A. Di Costanzo, L. Festa, O. Duverger, M. Vivo, L. Guerrini, G. La Mantia, M.I. Morasso, V. Calabrò, Homeodomain protein Dlx3 induces phosphorylation-dependent p63 degradation, *Cell Cycle* 8 (2009) 1185–1195.
- [45] M. Vivo, M. Ranieri, F. Sansone, C. Santoriello, R.A. Calogero, V. Calabro, A. Pollice, G. La Mantia, Mimicking p14ARF phosphorylation influences its ability to restrain cell proliferation, *PLoS One* 8 (2013) e53631.
- [46] A. Di Costanzo, A. Troiano, O. di Martino, A. Cacace, C.F. Natale, M. Ventre, P. Netti, S. Caserta, A. Pollice, G. La Mantia, V. Calabrò, The p63 protein isoform $\Delta Np63\alpha$ modulates Y-box binding protein 1 in its subcellular distribution and regulation of cell survival and motility genes, *J. Biol. Chem.* 287 (2012) 30170–30180.
- [47] A. Vasaturo, S. Caserta, I. Russo, V. Preziosi, C. Ciacci, S. Guido, A novel chemotaxis assay in 3-D collagen gels by time-lapse microscopy, *PLoS One* 7 (2012) e52251.
- [48] J.R. Olsen, A.M. Oyan, K. Rostad, M.R. Hellem, J. Liu, L. Li, D.R. Micklem, H. Haugen, J.B. Lorens, V. Rotter, X.S. Ke, B. Lin, K.H. Kalland, p63 attenuates epithelial to mesenchymal potential in an experimental prostate cell model, *PLoS One* 8 (2013) e62547.
- [49] Y. Kam, C. Guess, L. Estrada, B. Weidow, V. Quaranta, A novel circular invasion assay mimics in vivo invasive behavior of cancer cell lines and distinguishes single-cell motility in vitro, *Bmc Cancer* 8 (2008).
- [50] M.S. Al-Dosari, X. Gao, Nonviral gene delivery: principle, limitations, and recent progress, *AAPS J.* 11 (2009) 671–681.
- [51] G. Cumming, F. Fidler, D.L. Vaux, Error bars in experimental biology, *J. Cell Biol.* 177 (2007) 7–11.
- [52] T. Uchiumi, A. Fotovati, T. Sasaguri, K. Shibahara, T. Shimada, T. Fukuda, T. Nakamura, H. Izumi, T. Tsuzuki, M. Kuwano, K. Kohno, YB-1 is important for an early stage embryonic development: neural tube formation and cell proliferation, *J. Biol. Chem.* 281 (2006) 40440–40449.



Karlsruhe Institute of Technology

KIT-Campus North | P.O.Box 3640 | 76021 Karlsruhe, Germany

Institute of Toxicology and Genetics

Head: Prof. Dr. Uwe Strähle
Prof. Dr. Stefan Bräse

Hermann-von-Helmholtz-Platz 1
76344 Eggenstein-Leopoldshafen, Germany

Prof. Dr. Nicholas S. Foulkes

Phone: +49 721 6082- 3394
Fax: +49 721 6082- 3354
Email: nicholas.foulkes@kit.edu
Web: <http://www.kit.edu>

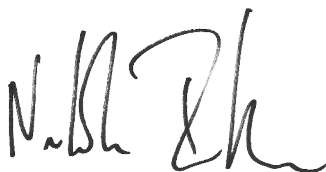
Our reference:

Date: 7th March 2018

To Whom it May Concern

I hereby confirm that according to plan, Andrea Maria Guarino has now (on Friday 2nd March) just completed his stay in my laboratory at the Institute of Toxicology and Genetics, Karlsruhe Institute of Technology, Eggenstein-Leopoldshafen, Germany. He first joined my laboratory on 4th September 2017 and has done some really great work. We are now preparing a manuscript incorporating the data he obtained during this period. I am extremely happy with his progress!

Yours sincerely,

A handwritten signature in black ink, appearing to read 'N. S. Foulkes'.

Nicholas S. Foulkes